Universidad Autónoma De Madrid
Facultad De Ciencias
Departamento De Biología Molecular

Modulación del comportamiento de las células B en respuesta a estimulación por quimioquinas y antígeno: mecanismos moleculares

Tesis doctoral

Memoria doctoral presentada por
Julia Sáez de Guinoa Corral
Para optar al título de doctor

Madrid, Marzo de 2013

El trabajo presentado en esta memoria se realizó en el Departamento de Inmunología y Oncología del Centro Nacional de Biotecnología (CNB)-CSIC, bajo la dirección de la Dra. Yolanda Rodríguez Carrasco.

La realización de esta tesis ha sido posible gracias a un contrato de Personal Investigador de Apoyo de la Comunidad de Madrid

A mi madre,
gracias por sobrevivir

ÍNDICE

1. SUMMARY

B lymphocytes, also known as B cells, encounter cognate antigen at the follicles of secondary lymphoid organs. B cells actively migrate within follicles, assisted by the chemokine CXCL13 and its receptor CXCR5. Antigen recognition through the B cell receptor (BCR) drives the B cell to stop and to establish the Immune Synapse (IS) with the antigen-presenting cell. Therefore, in this context B cells receive two distinct signals, a CXCL13/CXCR5-induced GO signal (motility) and a BCR/antigen-mediated STOP signal. Our goal is to study how the crosstalk between CXCR5 and the BCR fine-tunes B cell dynamics and its consequences for B cell antigen encounter and B cell activation.

We established an experimental system to study real-time B cell dynamics in response to distinct stimuli (chemokines, antigen, integrin ligands). CXCL13 induced B cell polarization in the absence of integrin ligands; however, the presence of a critical density of these ligands was necessary for the B cells to migrate. Integrin ligand type and density modulate B cell migration; we recreated *in vivo* data on B cell migration at the follicles. The presence of tethered antigen at the membrane promoted a heterogeneous B cell behaviour depending on BCR signalling strength. CXCL13/CXCR5 signalling did not impair the ability of B cells to form the IS; however it enhanced BCR-triggered B cell activation by affecting LFA-1 mediated adhesions. In IS forming B cells, CXCL13 assisted antigen gathering at the synapse by promoting membrane ruffling and LFA-1-supported adhesion; in motile B cells, CXCL13 allowed BCR signalling integration through the assembly of LFA-1 supported migratory junctions. Both dynamic states were dependent on the actomyosin cytoskeleton function.

We explored the molecular mechanisms implicated in B cell halt. Soluble antigen-BCR signalling did not avoid chemokine-mediated B cell motility, only slow down migration speed. The IS structure was necessary for arresting motile B cells. We demonstrated that the scaffold protein vinculin was recruited to the IS and localized in the F-actin and LFA-1-rich domain of the IS; when B cells encounter antigen in a soluble form however vinculin did not localize to the contact site. The recruitment of vinculin might be mediated by the local production of phosphatidylinositol 4,5-bisphosphate (PIP_2), product of type I phosphatidylinositol 4-phosphate 5-kinase gamma (PIPKIγ). Impairment of vinculin location at the IS allowed CXCL13-induced B cell migration. The activities of Spleen tyrosine kinase (Syk) and the non-muscle motor protein Myosin II were essential for vinculin recruitment and maintenance at the IS.
So far, data suggested that the motile B cell arrest upon antigen encounter on a target membrane is due to local BCR signalling, which drives vinculin recruitment and thus, IS stabilization and firm adhesion.

2. INTRODUCCIÓN

2.1.La respuesta inmunológica adaptativa humoral

2.1.1. Una visión global de la respuesta inmunológica humoral

El Sistema Inmunológico tiene como función principal la defensa del organismo contra los distintos patógenos a los que está expuesto como son virus, bacterias y parásitos. Tras la entrada de un patógeno a un tejido se genera un foco de infección, que es inicialmente controlado por el sistema inmunológico innato. Durante este periodo, se activan los mecanismos de respuesta del sistema inmunológico adaptativo, más tardíos pero de alta especificidad y eficiencia, que eliminarán los patógenos mediante la acción de los linfocitos efectores y la producción de anticuerpos.

Dentro de los mecanismos del sistema inmunológico adaptativo, los linfocitos B son los responsables de la respuesta inmunológica humoral. Los linfocitos B, también llamados células B, recorren activamente los órganos linfoides secundarios (OLS) en busca del antígeno para el cual su receptor de antígeno (*B Cell Receptor*, BCR) es específico (Cyster, 2005). El reconocimiento de antígeno a través del BCR junto con otro tipo de señales co-estimuladoras como la ayuda recibida por parte de los linfocitos T, proporcionan las señales necesarias para que las células B se activen, proliferen y se diferencien a células B efectoras productoras de anticuerpos (células plasmáticas y plasmablastos) y células B de memoria. En una fase temprana de la respuesta inmunológica humoral, se generan plasmablastos extrafoliculares para una primera producción rápida de anticuerpos (Ab) (Manz et al, 2002). Por otro lado, las células B activadas por antígeno dan lugar a la formación de los Centros Germinales (GC) en los OLS; en estas estructuras tienen lugar los procesos de cambio de isotipo e hipermutación somática en los genes que codifican para las cadenas de inmunoglobulinas del BCR, y la selección positiva de aquellas células B que expresan un BCR de alta afinidad por el antígeno (Shlomchik & Weisel, 2012). Las células B seleccionadas se diferencian a células plasmáticas que secretan Ab de alta afinidad, y a células B de memoria, que responderán con mayor rapidez y eficiencia a re-infecciones por el mismo patógeno (McHeyzer-Williams, 2003).

Los Ab producidos por plasmablastos y células plasmáticas neutralizan a los patógenos y sus toxinas mediante su unión a los mismos; activan el sistema del complemento para los procesos de citotoxicidad dependiente de Ab; también promueven la fagocitosis de los patógenos por células del sistema inmunológico innato mediante la opsonización de los mismos (Desjarlais & Lazar, 2011).

2.1.1.1. Diferenciación de las células B a partir de precursores hematopoyéticos

En el organismo adulto, las células B se originan en la médula ósea a partir de células madre hematopoyéticas. Las células estromales de la médula ósea proporcionan el ambiente y las señales necesarias para el desarrollo de células B, pasando por diferentes estadios de diferenciación según se va formando el BCR (Fig. 1). En el estadio de células B inmaduras, donde ya expresan la inmunoglobulina (Ig) de isotipo M como BCR, las células B sufren un proceso de selección negativa en el cual las células B auto-reactivas son eliminadas. Las células B no auto-reactivas, se diferencian a células B maduras, caracterizadas por la co-expresión en su membrana de dos isotipos de BCR, IgM e IgD. Esta población de células B maduras sale de la médula ósea y recircula por el organismo, entrando en los OLS en para terminar su diferenciación y buscar antígeno específico (Cariappa et al, 2007).

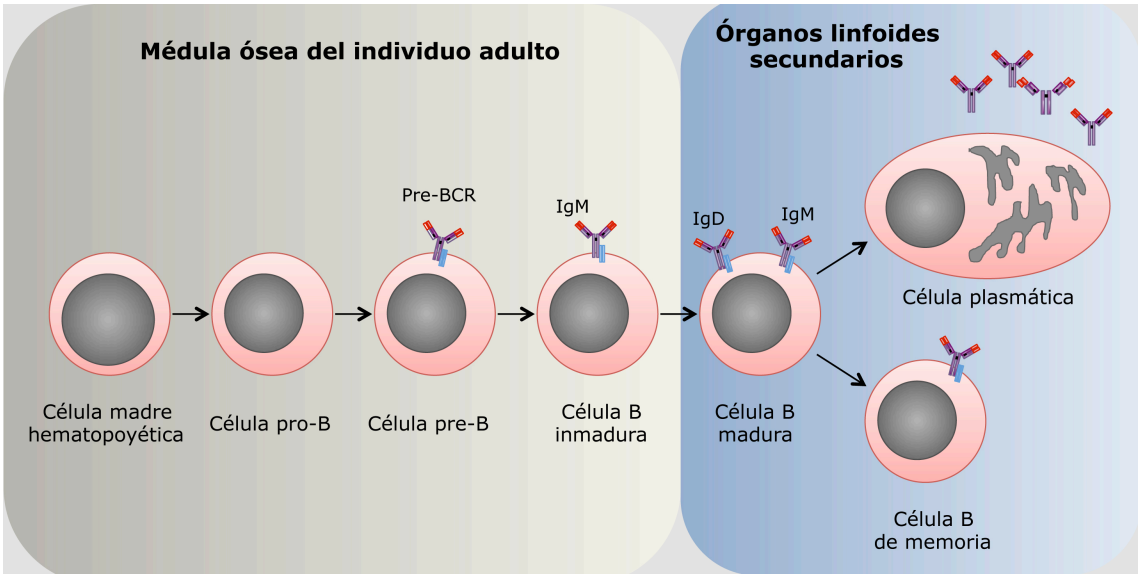

Figura 1. Estadios en el desarrollo, maduración y diferenciación de la célula B.

2.1.1.2. Sub-poblaciones de células B

Existen diferentes sub-poblaciones de células B (Fig. 2) (Allman & Pillai, 2008). Las células B-B1 son de origen embrionario, se localizan fundamentalmente en las cavidades peritoneal y pleural, y producen Ab IgM frente a antígenos T-independientes. Las células B Transicionales se encuentran en el bazo, corresponden a estadios intermedios de maduración de las células B, y se caracterizan por la expresión de un patrón específico de marcadores en superficie así como por tener determinadas propiedades funcionales. Las células B de la zona

marginal se diferencian en el bazo a partir de las células B transicionales; se localizan cerca de los senos marginales del bazo, responden fundamentalmente a antígenos T-independientes proteicos y lipídicos, y son capaces de transportar antígenos en forma de inmunocomplejos a los folículos del bazo mediante receptores de complemento (Cinamon et al, 2008). Las células B foliculares, se localizan en los folículos de los OLS y son las responsables de la respuesta inmunológica a antígenos T-dependientes. Las células B foliculares y de la zona marginal se conocen como células B-B2, y son la población objeto de estudio en esta tesis doctoral.

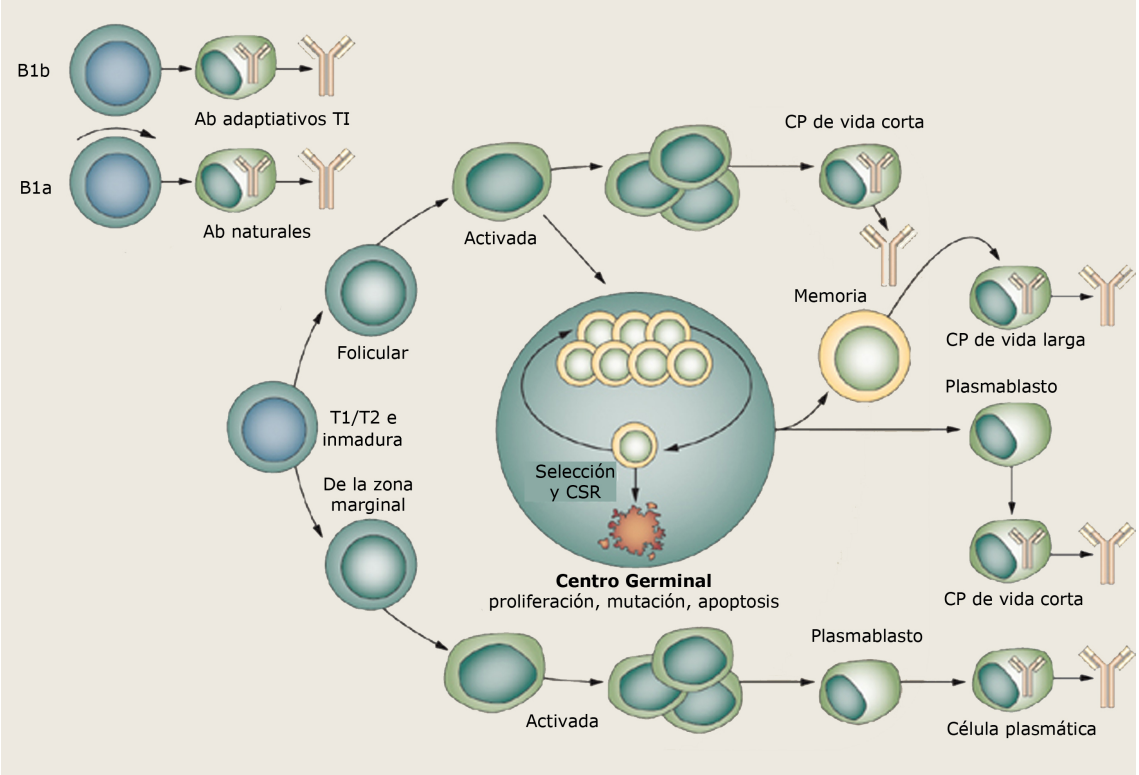

Figura 2. Sub-poblaciones de células B en periferia y diferenciación a células efectoras y de memoria. TI: respuesta T-independiente; T1/T2 células B transicionales de tipo 1 y 2; CP: célula plasmática; Ab: anticuerpo; CSR: cambio de isotipo por recombinación. Adaptada de (Tedder, 2009).

2.1.2. Las células B encuentran el antígeno

2.1.2.1. Los órganos linfoides secundarios, lugares de interacción con el antígeno

Existe una gran cantidad de patógenos potenciales que pueden infectar a un individuo; sin embargo, cada célula B expresa en su membrana muchas copias de un BCR con una única especificidad. Por tanto, la probabilidad de que una célula B encuentre el antígeno para el que es específico es muy baja. Para maximizar esta

probabilidad, el encuentro de la células B con el antígeno se produce en órganos especializados denominados OLS. Los OLS se distribuyen por todo el cuerpo (Fig. 3) e incluyen a los ganglios linfáticos, el bazo y los tejidos linfoides asociados a mucosas. Al igual que los otros OLS, los ganglios linfáticos poseen una estructura muy organizada y compartimentalizada (Nolte et al, 2003; Sixt et al, 2005) (Fig. 4). Están rodeados por una cápsula de tejido conectivo rico en colágeno, que penetra hacia el interior del ganglio formando trabéculas. La linfa llega al ganglio linfático a través de los vasos aferentes linfáticos que desembocan en el seno sub-capsular (*SubCapsular Sinus*, SCS), el cual, a su vez, se comunica con el seno medular a través de los senos corticales (Gretz et al, 2000). En la zona subyacente al seno sub-capsular se encuentra el córtex, formado por los folículos primarios, donde se localizan y concentran las células B y donde se generan los CG tras el encuentro con antígeno. Rodeando a los folículos por la parte interior del ganglio, se encuentra el paracórtex o zona T, donde se sitúan los linfocitos T. Las vénulas de endotelio alto (*High Endothelial venules*, HEV) se localizan en zonas interfoliculares y paracortex, y son lugar de entrada de los linfocitos B procedentes de la sangre. Más internamente al paracortex se localiza la médula, compuesta por el seno medular y los cordones medulares. De aquí parte el vaso eferente linfático que termina desembocando en la circulación sanguínea. Los ganglios linfáticos son órganos densamente empaquetados por células estromales y matriz extracelular. Las células estromales mayoritarias de la zona T son las células fibroblásticas reticulares (*Fibroblastic Reticular Cell*, FRC), mientras que en la zona B encontramos principalmente células foliculares dendríticas (*Follicular Dendritic Cell*, FDC) (Fig. 5) y FRC en menor número (Cyster et al, 2000; Katakai et al, 2004).

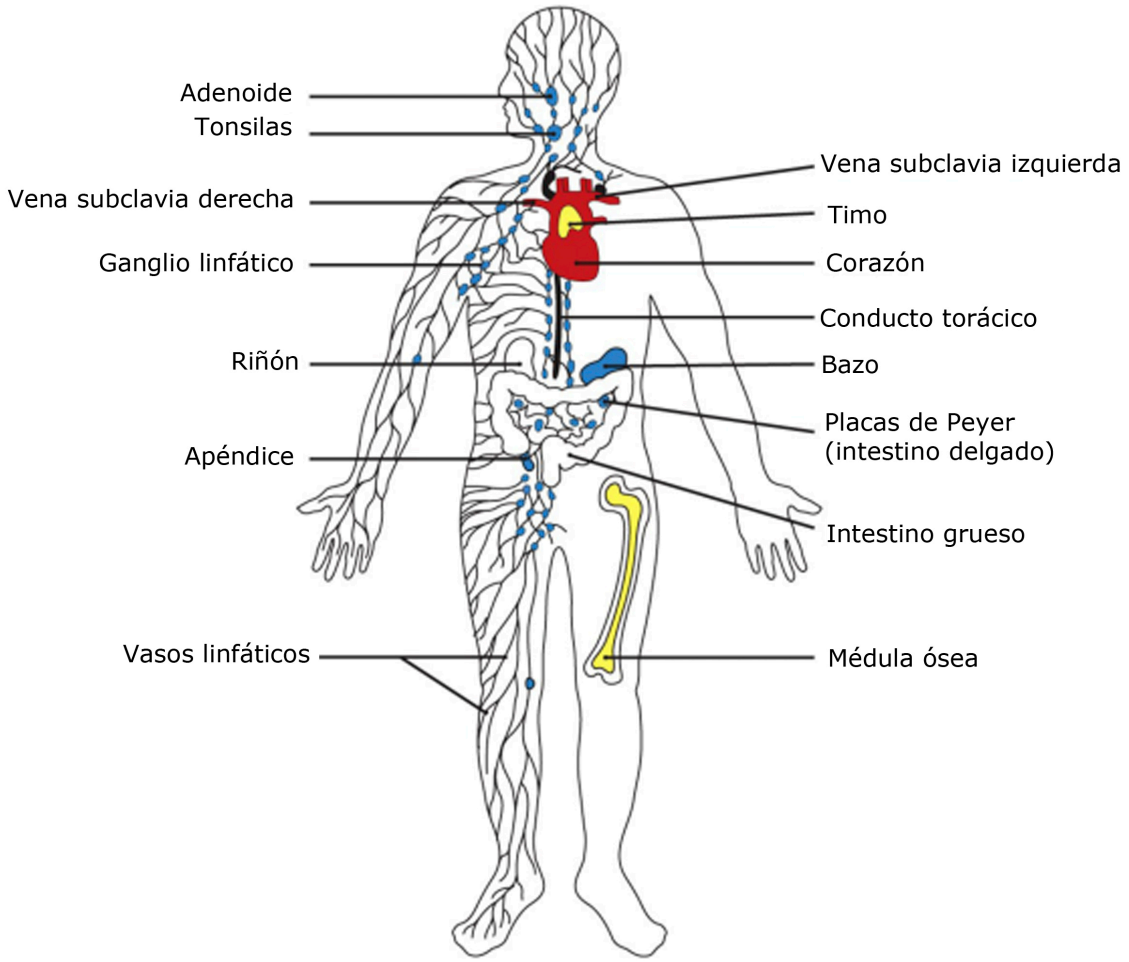

Figura 3. Distribución en el cuerpo humano de los órganos y tejidos linfoides primarios (amarillo) y secundarios (azul). Adaptada de (Murphy K, 2008)

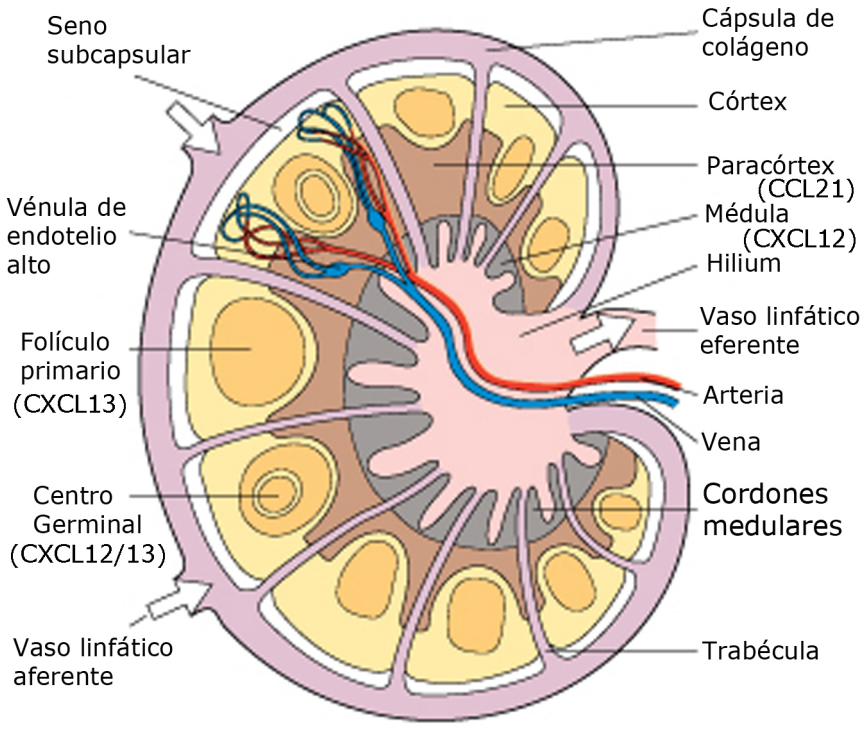

Figura 4. Estructura del ganglio linfático. Adaptada de (Drake R, 2009)**.**

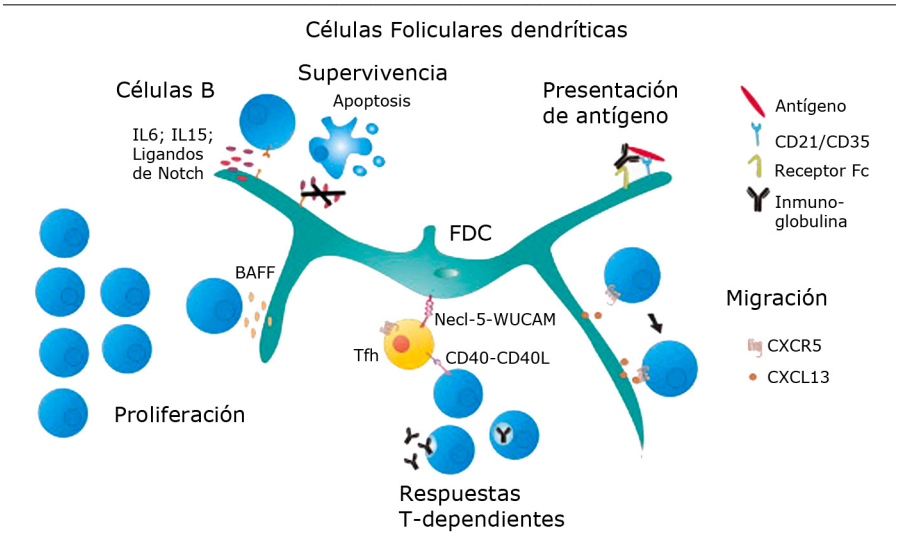

Figura 5. Funciones de las células foliculares dendríticas. 1) Soporte de migración para células B mediante la producción de CXCL13; 2) Mediación de respuestas T-dependientes mediante la interacción con células T foliculares cooperadoras (Tfh, *T follicular helper cell*) 3) Producción de factores solubles que promueven la proliferación y supervivencia de las células B; 4) Presentación de antígeno a través de receptores Fc y de complemento (CD21 y CD35). Adaptada de (Buettner et al, 2010).

2.1.2.2. La llegada del antígeno a los ganglios linfáticos y su acceso a los folículos

Existen diferentes rutas de acceso de los antígenos a los ganglios linfáticos (Fig. 6). Pueden ser transportados desde su lugar de entrada en los tejidos periféricos a las ganglios linfáticos de forma pasiva a través de la linfa; los vasos linfáticos aferentes los liberan en el SCS. Los antígenos de bajo peso molecular accederán desde el SCS al interior del folículo a través de pequeños poros que dan acceso al sistema de conductos de colágeno producido por las FRC (Fig. 6b) (Roozendaal et al, 2009), donde podrían ser capturados por FDC y presentados en su superficie (Bajenoff & Germain, 2009). Por otro lado, los macrófagos situados cerca del SCS capturan los antígenos a través de proyecciones de su membrana hacia el lumen del SCS, y los transfieren hacia el folículo donde pueden presentarlos a células B (Carrasco & Batista, 2007; Junt et al, 2007; Phan et al, 2007). Las células B pueden transportar antígenos desde la superficie de estos macrófagos a las FDC del folículo mediante un mecanismo dependiente de receptores del complemento (Fig. 6a) (Phan et al, 2007). Las FDC presentan el antígeno en su superficie principalmente en forma de inmunocomplejos unidos a receptores de Fc o del complemento (Haberman & Shlomchik, 2003; Kosco-Vilbois, 2003). Por último, los antígenos pueden ser capturados en los tejidos periféricos por células dendríticas (DC) y transportados de forma activa hasta los ganglios linfáticos; estas DC bien se localizan cerca de las HEV o migran al interior de los folículos, y pueden presentar antígeno a las células B (Fig. 6c) (Balazs et al, 2002; Berney et al, 1999; Colino et al, 2002; Qi et al, 2006; Wykes et al, 1998).

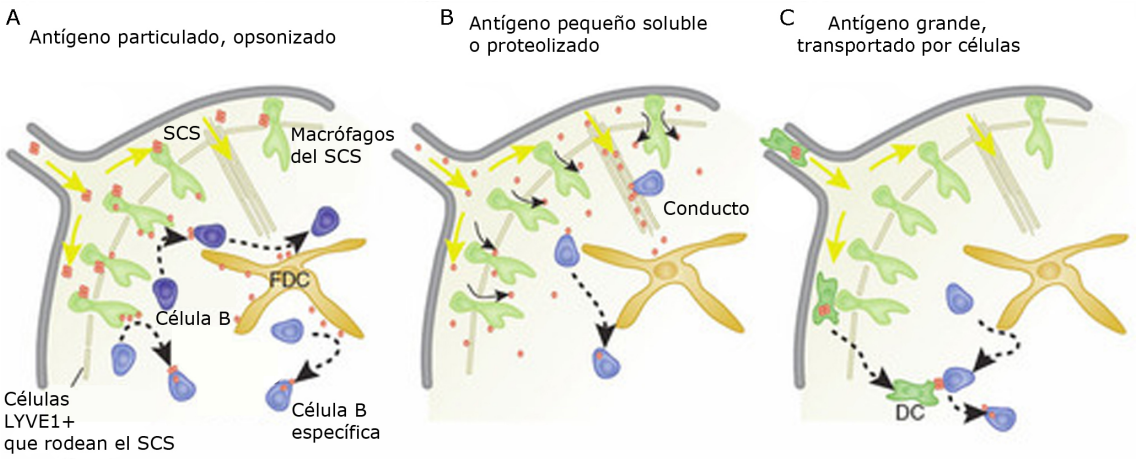

Figura 6. Rutas de acceso de antígenos a los folículos. (A) Los macrófagos del seno subcapsular captan antígenos particulados. (B) Los antígenos pequeños y solubles (que pueden haber sido proteolizados) utilizan los conductos de colágeno producidos por las células estromales. (C) Los antígenos grandes son transportados desde los tejidos periféricos por células dendríticas. Adaptada de (Cyster, 2010).

2.2.El comportamiento o dinámica de las células B

2.2.1. Migración

2.2.1.1. Las células B migran en los folículos de los OLS

La migración es un requisito necesario para que las células B puedan ejercer su función. Las células B procedentes de la sangre entran en los ganglios linfáticos a través de las HEV y migran a los folículos primarios (Bajenoff et al, 2006). Una vez allí, exploran activamente todo el volumen folicular en busca de antígeno, desplazándose sobre la red de FDC y mostrando una morfología muy polarizada, trayectorias aleatorias y una velocidad media de migración de 6 μm/min (Miller et al, 2002; Okada et al, 2005). Se ha estimado que las células B pueden permanecer hasta 24h dentro de un mismo OLS realizando este rastreo (Revisado en (Cyster, 2005). La activación por antígeno resulta en la migración de la célula B a la zona fronteriza entre el folículo y el paracortex, donde presenta péptidos antigénicos a células T para recibir señales co-estimulatorias (Garside et al, 1998; Okada et al, 2005). A continuación, la célula B activada se dirige a zonas interfoliculares donde prolifera activamente (Coffey et al, 2009). Por último, migra al centro del folículo para formar los CG, donde tienen lugar los procesos de maduración de la afinidad. En los CG las células B no permanecen estáticas sino que continúan migrando dentro de dicha estructura (Allen et al, 2007). El movimiento es por tanto intrínseco a la biología de las células B, y es promovido por distintos miembros de la familia de las quimioquinas.

2.2.1.2. Las quimioquinas dirigen el movimiento de las células B

Las quimioquinas son proteínas quimioatrayentes de bajo peso molecular. La mayoría son secretadas y presentan un carácter básico que les permite unirse a proteínas sulfatadas y proteoglicanos de la matriz extracelular (de Paz et al, 2007). Señalizan a través de receptores con siete dominios transmembrana acoplados a proteínas G (*G Protein-Couple Receptor*, GPCR). Las quimioquinas denominadas homeostáticas se expresan de forma constitutiva en los OLS y están implicadas en la compartimentalización y función de los mismos; las más destacadas son CXCL13 (cuyo receptor es CXCR5), CXCL12 (con su receptor CXCR4), y CCL19/CCL21 (que comparten el receptor CCR7). CXCL13 es principalmente producida y expuesta en la superficie de las FDC (Cyster, 2005); está implicada en la organización de los folículos de células B, y media la motilidad de las células B en los mismos. CXCL12 se encuentra a bajos niveles en las zonas B y T de los OLS, y tiene un papel importante en la organización y el movimiento de las células B en los CG (Allen et al, 2004; Cyster, 2005). Por último, CCL19 y CCL21 son producidas y se localizan sobre la superficie de las FRC de la zona T (Fig. 4) (Bajenoff et al, 2006).

2.2.1.3. Las células B presentan una migración de tipo ameboide

La señalización resultante de la unión de la quimioquina a su receptor induce la polarización de la célula, necesaria para que ésta pueda migrar (Nieto et al, 1997; Vicente-Manzanares et al, 2007). Al igual que otros leucocitos, las células B presentan una migración de tipo ameboide, que fue inicialmente caracterizada en la ameba *Dictyostelium discoideum (Devreotes & Zigmond, 1988)*. En el movimiento ameboide se alternan ciclos de expansión y contracción morfológicas dependientes de la dinámica del citoesqueleto de actina (Friedl et al, 2001). Además, se caracteriza por ser más rápido que otros tipos de movimiento celular y por no precisar de adhesiones fuertes al sustrato. En este tipo de movimiento, la célula emite una extensión de membrana o lamelipodio en el extremo anterior, dependiente de un flujo de polimerización de actina, el cual hace contacto con el sustrato a través de moléculas de adhesión tales como integrinas (Fig. 7). A continuación se produce una contracción en el cuerpo celular mediada por la actividad de la proteína motora no muscular Miosina-II sobre el citoesqueleto de actina, que empuja la célula hacia delante y genera en el extremo posterior de la célula el urópodo. Este tipo de movimiento permite a las células captar e integrar las señales que proceden del entorno de forma rápida y eficaz (Friedl & Weigelin, 2008), algo que es fundamental para que las células B puedan rastrear el folículo en busca de antígeno.

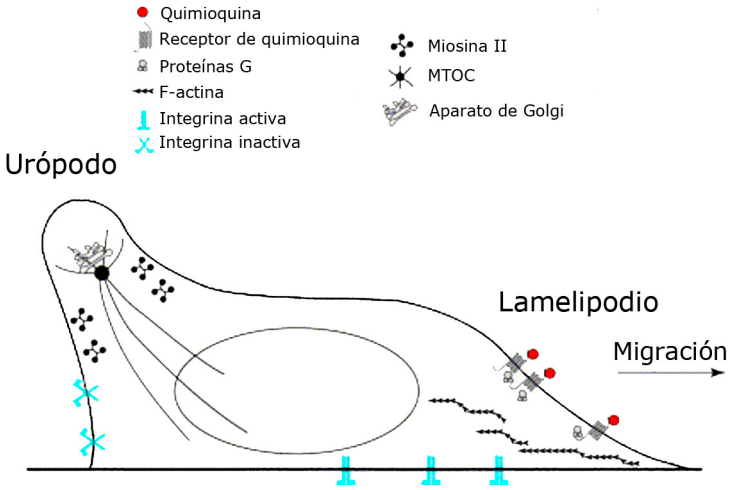

Figura 7. El movimiento ameboide. Esquema de un linfocito migrando con morfología ameboide en respuesta a quimioquinas. El lamelipodio, en la parte anterior, es rico en actina. El urópodo, en la parte posterior, incluye los orgánulos celulares, el centro organizador de microtúbulos (MTOC) y la miosina. La adhesión al sustrato de migración está mediada por integrinas. Adaptada de (Serrador et al, 1999).

2.2.2. El establecimiento de la sinapsis inmunológica

Las células B reconocen antígenos en su conformación nativa a través del BCR. Ello las hace capaces de responder *in vitro* a antígeno en forma soluble; sin embargo, la alta compartimentalización de los OLS así como la captura y presentación de antígenos por parte de distintos tipos celulares en el folículo (FDC, macrófagos, DC) indica que *in vivo* las células B encuentran el antígeno expuesto en la superficie de células presentadoras (APC) (Carrasco, 2010). El reconocimiento de antígeno a través del BCR desencadena un proceso de expansión morfológica (*spreading*) de la célula B sobre la superficie de la APC, seguido de una fase de contracción (*contraction*) (Fig. 8A) (Fleire et al, 2006). Durante estos procesos, el BCR recolecta y agrega el antígeno en un dominio central. Se forma así una estructura de reconocimiento de antígeno denominada Sinapsis Inmunológica (SI), caracterizada por la segregación de receptores en dominios de activación supramoleculares (*SupraMolecular Activation Clusters*, SMAC), y la adhesión estable de la célula B a la APC (Batista et al, 2001; Carrasco et al, 2004). La SI fue inicialmente descrita en células T (Grakoui et al, 1999; Monks et al, 1998) y células NK (Davis et al, 1999).

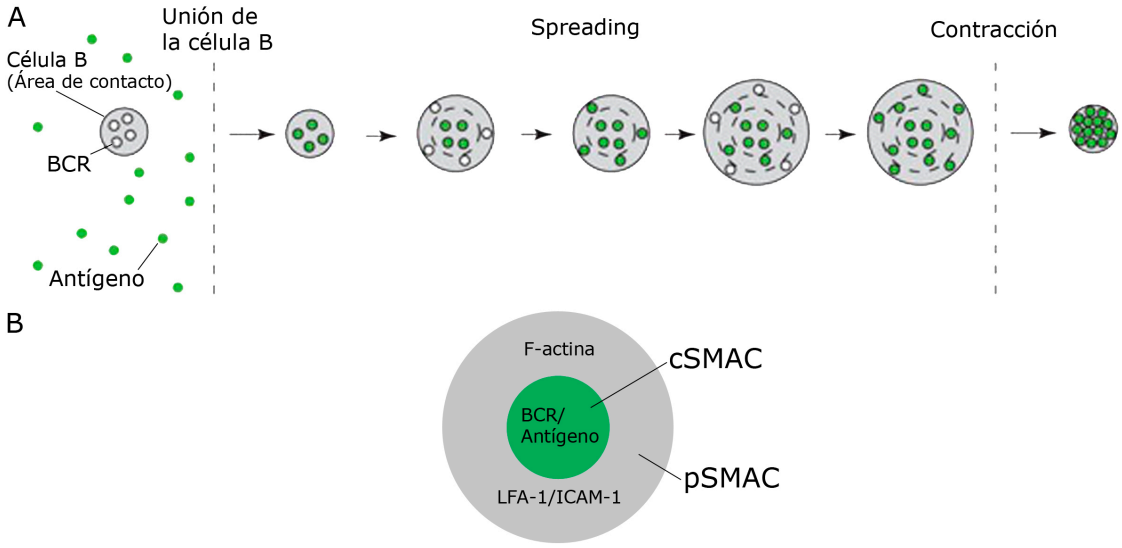

Figura 8. La sinapsis inmunológica de la célula B. (A) Fases de expansión (*spreading*) y contracción de una célula B durante la formación de la sinapsis inmunológica. (B) Complejos de activación supramolecular (SMAC) descritos en la sinapsis de la célula B. cSMAC: SMAC central; pSMAC: SMAC periférico. Adaptada de (Fleire et al, 2006).

La SI madura de las células B presenta un SMAC central (cSMAC), donde se acumula el par BCR/antígeno, y un SMAC periférico (pSMAC), caracterizado por la presencia de las integrinas LFA-1 (*Lymphocyte Function-associated Antigen 1*) y

VLA-4 (*Very Late Antigen 4*), y cuyos ligandos, ICAM-1 (*InterCellular Adhesion Molecule 1*) y VCAM-1 (*Vascular Cell-Adhesion Molecule 1*), respectivamente, se expresan en la membrana de las APC (Fig. 8B) (Carrasco & Batista, 2006; Carrasco et al, 2004). Se ha descrito que la SI de las células B excluye del cSMAC a la fosfatasa CD45 (Batista et al, 2001), lo que sugiere que en estas células podría existir un SMAC distal (dSMAC) similar al descrito en la SI de células T (Dustin, 2008).

El establecimiento de la SI es crítico para la activación de la célula B en condiciones limitantes de abundancia de antígeno, para la extracción de antígeno y su posterior presentación a las células T, así como para discriminar la afinidad del BCR por el antígeno (Batista et al, 2001; Carrasco et al, 2004; Fleire et al, 2006). La formación de la SI en células B ha sido observada in vivo por técnicas de microscopía multifotón (Carrasco & Batista, 2007). Estudios publicados durante el desarrollo de esta tesis doctoral también han confirmado en modelos *in vivo* la relevancia de la SI para la activación de la célula B y la respuesta humoral (Randall et al, 2009).

2.2.3. Señal de migración (*GO signal*) *versus* señal de parada (*STOP signal*)

Las células B se mueven activamente en los folículos de los OLS, con el fin de escanear la superficie de las APCs en busca de antígeno. Este movimiento está regido fundamentalmente por la quimioquina CXCL13, producida por las FDC (Bajenoff et al, 2006; Cyster, 2005). El reconocimiento específico del antígeno a través del BCR supone un cambio drástico en el comportamiento o dinámica de la célula B: detiene su migración y establece la SI. Por lo tanto, las FDC proporcionan en el mismo contexto molecular dos tipos de ligandos, CXCL13 y antígeno, que desencadenan a través de sus receptores CXCR5 y BCR, respectivamente, respuestas opuestas en las células B: migración (*GO signal*) versus parada (*STOP signal*). Además, estudios *in viv*o indican que la célula B establece SI con varias APC en el folículo antes de activarse y migrar al paracortex (Carrasco & Batista, 2007); ello implica la existencia de ciclos de migración-parada/SI en las células B. La regulación del comportamiento de la célula B en presencia de ambos estímulos y por tanto, la interrelación entre la señalización mediada por CXCR5 y por BCR se desconocía al inicio de este trabajo.

2.3. Componentes moleculares implicados en migración y adhesión celular

2.3.1. La señalización a través de los receptores de quimioquinas

Los receptores de quimioquinas (*ChemoKine Receptors*, CKR) pertenecen al grupo de los GPCR, y activan a proteínas G heterotriméricas (αβγ). La unión de la quimioquina promueve la asociación de la proteína G al CKR, y el GDP unido a la subunidad α del receptor es sustituido por GTP, con la consecuente disociación de las subunidades de la proteína G; α permanece unida al receptor mientras que el complejo βγ queda asociado a la membrana. Dependiendo de la naturaleza de la subunidad Gα, existen 4 grupos principales de proteínas G: Gαi, Gαs, Gαq y Gα12, cada una de las cuales activa rutas de señalización diferentes (Oldham & Hamm, 2008). La señalización por quimioquinas es mediada fundamentalmente por αi, subunidad sensible al tratamiento por la toxina de *Pertusis* (Simon et al, 1991). αi activa canales de calcio y potasio e inhibe la acción de la adenilato ciclasa (Fig. 9) (Kehrl, 1998); también puede activar la vía de señalización de las MAPK (*Mitogen-Activated Protein Kinase*).

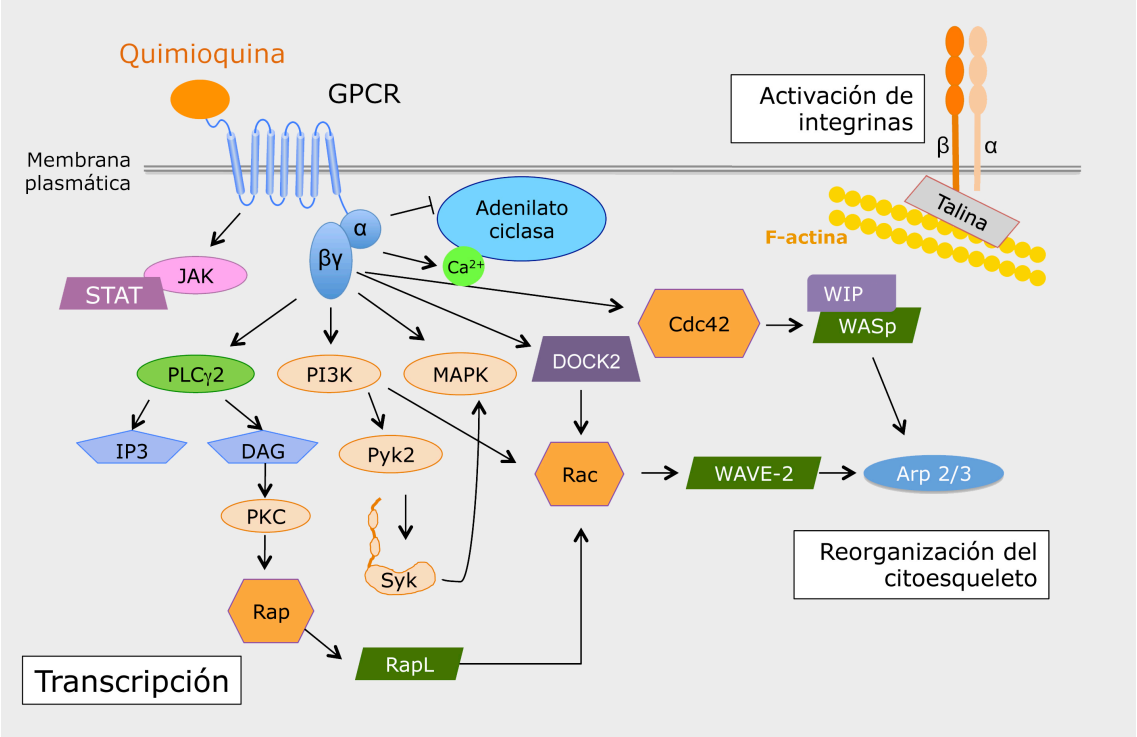

Figura 9. Señalización a través del receptor de quimioquina. La unión de la quimioquina al receptor desencadena una serie de cascadas de señalización que modulan proteínas GTP-asas, que actúan a nivel de reorganización del citoesqueleto y activación de integrinas, regulando los procesos de adhesión y migración.

El complejo βγ actúa sobre diferentes rutas de señalización, como son la de la fosfolipasa C (PLC), la fosfatidil-inositol 3 quinasa (PI3K) o la vía de las MAPK. La PLCβ hidroliza el fosfatidil inositol 4,5-bifosfato (PIP_2) de la membrana plasmática en inositol 1,4,5-trifosfato (IP_3) y en diacilglicerol (DAG), que promueven señales de calcio y la activación de la proteína quinasas C (PKC), respectivamente. PI3Kγ/δ actúa sobre Pyk2 (Proline-rich tyrosine kinase 2), dando lugar a la activación de Src quinasas (Syk, Lyn, Btk) y de la ruta de las MAPK (Thelen, 2001). Además de la activación de factores de transcripción, estas y otras vías de señalización se relacionan con la activación de las proteínas GTPasas pequeñas de la subfamilia de Rho (Rho, Rac, Cdc42). Estas proteínas actúan como interruptores moleculares que regulan los procesos de adhesión y migración celular inducidos por quimioquinas, mediante la reorganización del citoesqueleto de actina y la activación de integrinas. Se ha descrito que Rac promueve la polimerización de actina y la formación de lamelipodios, fundamentales para la migración celular (Mor et al, 2007). Rac puede ser activada directamente por DOCK2 (Fukui, 2002), o indirectamente por la ruta de Rap, Cdc42 y el complejo Par3/Par6/PKCz/Tiam (Gerard et al, 2007). Tanto Rap1 como Rap2, pertenecientes a otra subfamilia de GTPasas, son activados por CXCR4 y CXCR5 en células B a través de RapL y/o Pyk2, median la activación de integrinas y promueven migración (Durand et al, 2006; McLeod et al, 2004). Rho regula la función de miosina-II a través de su efector ROCK (Smith et al, 2003). Las proteínas tirosina quinasa Janus (JAK) también se asocian a algunos CKR unidos a ligando de manera independiente a αi, promoviendo la unión y activación de factores de transcripción de la familia STAT (*Signal Transducers and Activators of Transcription*) (Rodriguez-Frade et al, 2001).

Distintos mecanismos regulan la señalización a través del CKR. Las proteínas RGS (*Regulator of G protein Signalling*) se unen a la subunidad α y promueven su actividad GTPasa; α unida a GDP se vuelve a unir al complejo βγ, quedando la proteína G inactiva . Además, las proteínas quinasa del receptor de proteínas G (GRK) fosforilan al CKR activo en serina y treonina para promover la unión de arrestinas, que impiden la unión de otras proteínas G y favorecen la endocitosis mediada por clatrina (Neitzel & Hepler, 2006).

2.3.2. La señalización a través del BCR

El BCR es una Ig de membrana (mIg) compuesta por dos cadenas pesadas unidas entre si por puentes di-sulfuro, y dos cadenas ligeras unidas a las cadenas pesadas por puentes di-sulfuro. Las cadenas pesadas se anclan en la membrana plasmática y presentan unas colas citoplasmáticas muy cortas incapaces de señalizar; están asociadas de forma no covalente a un heterodímero de mIg, Igα-

Igβ, que poseen en sus tallos intracelulares motivos de activación basados en tirosina (*Immunoreceptor Tyrosine-based Activaton Motif*, ITAM). El BCR inactivo puede asociar a proteínas quinasas de la familia Src como Fyn y Lyn (Fig. 10) (Reth & Wienands, 1997).

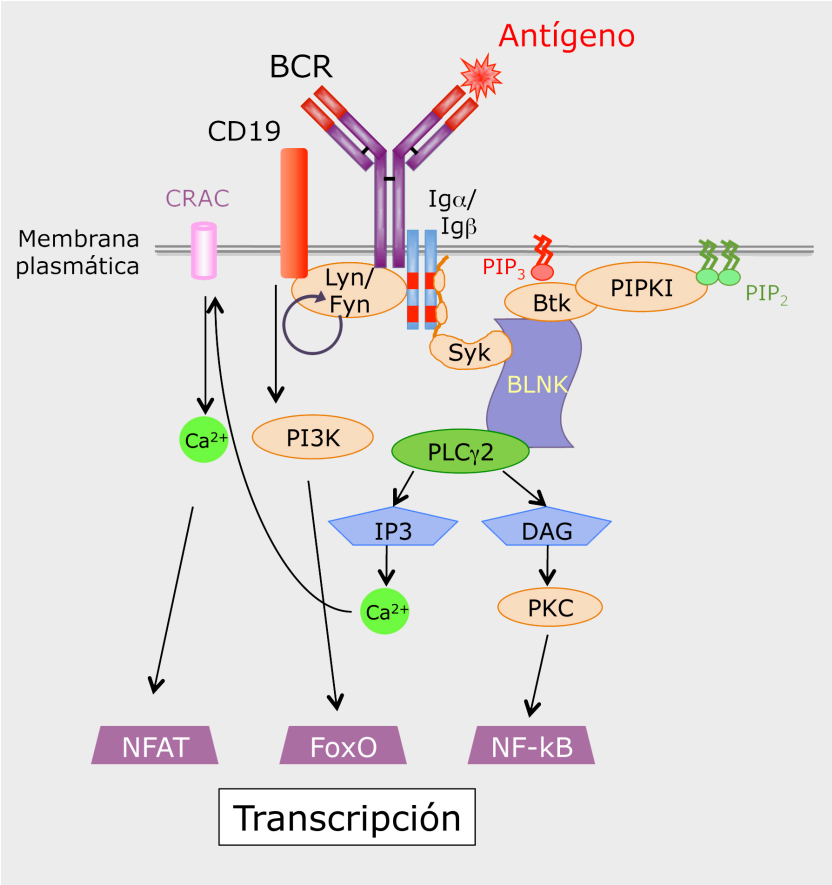

Figura 10. Señalización a través del BCR (I). La unión del antígeno al BCR desencadena la señalización que activa distintos factores de transcripción implicados en la activación y diferenciación de la célula B.

La unión de antígeno induce la fosforilación de los motivos ITAM de Igα-Igβ por las Src quinasas. La tirosina quinasa Syk es reclutada a los ITAM fosforilados a través de su dominio SH2 donde es activada por autofosforilación; Syk fosforila a la proteína adaptadora BLNK (B-cell linker protein), también llamada SLP-65 (*SH2 domain-containing Leukocyte Protein of 65 KDa*) (Kurosaki, 2002; Kurosaki & Hikida, 2009). La proteína quinasa Btk es reclutada a la membrana por la unión de su dominio PH (*Pleckstrin Homology*) al fosfatidilinositol 3,4,5-trifosfato (PIP_3) y a BLNK fosforilado. La activación de Btk requiere una fase inicial de fosforilación mediada por Lyn y una fase sostenida mediada por Syk (Kurosaki & Hikida, 2009). Btk se asocia y participa en el reclutamiento de la fosfatidilinositol 4-fosfato 5

quinasa (PIPKI) que producirá de manera local PIP_2 (Saito et al, 2003). BLNK también recluta a PLCγ2 a la membrana plasmática, y su activación por Btk produce IP_3 y DAG. El IP_3 libera calcio del retículo endoplasmático lo que conlleva la apertura de los canales CRAC (*Calcium Release-Activated Calcium Channels*) de la membrana plasmática y la activación de los factores de transcripción NFAT (*Nuclear Factor of Activated T cells*) mediante la acción de la fosfatasa calcineurina. El DAG permanece en la membrana y da lugar a la activación de los factores de transcripción NF-κB (*Nuclear Factor-kappa B*) a través de PKC (Kurosaki, 2011). La interacción BCR/antígeno también resulta en la fosforilación de la cola citoplasmática de CD19 por Lyn; ello permite la unión de la subunidad p85 de PI3K, vav y Lyn (Kurosaki & Hikida, 2009). PI3K activa Akt que inhibe al factor de transcripción FoxO, induciendo la supervivencia celular (Hess et al, 2004).

La acción de Syk y PLCγ2 también activa a miembros de la familia de las Rho-GTPasas, responsables de la reorganización del citoesqueleto de actina y activación de las integrinas por BCR (Fig. 11) (Arana et al, 2008; Lin et al, 2008; Weber et al, 2008). La activación de las Src quinasas y de PI3K promueve la activación de vav1 y vav2, activadores de Rho GTPasas. Rac2 junto con la GTPasa Rap1 son fundamentales en la activación de LFA-1 y la regulación del citoesqueleto de células B (Arana et al, 2008; Lin et al, 2008). Se postula que Rap1 recluta a Tiam1 y a Vav2, los cuales activan a Cdc42 y a Rac2, respectivamente (Arthur et al, 2004). Alternativamente, Rap1 induciría la formación de un complejo activador de integrinas que contendría al efector de Rap1 RIAM (*Rap1-GTP Interacting Adaptor Molecule*) y a la proteína del citoesqueleto talina (Critchley & Gingras, 2008).

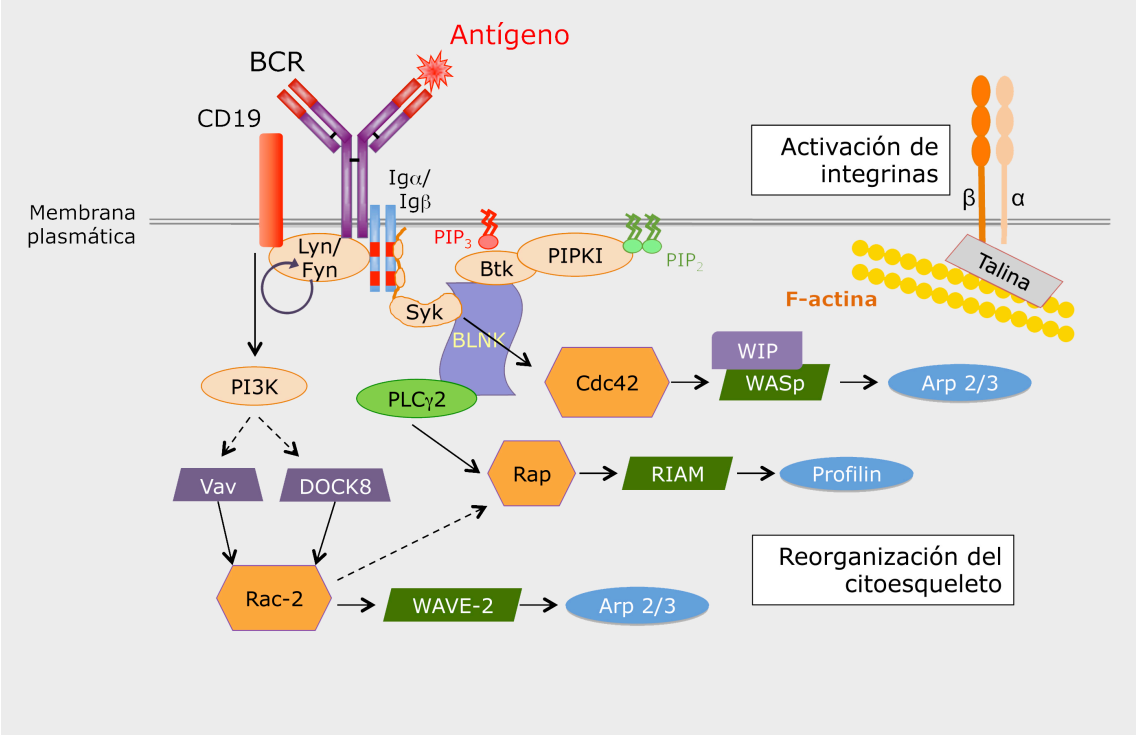

Figura 11. Señalización a través del BCR (II). El antígeno, mediante su unión al BCR, promueve la reorganización del citoesqueleto de actina y la activación de integrinas, necesarios para la formación de la sinapsis inmunológica de la célula B.

2.3.3. El citoesqueleto de actina

El citoesqueleto de actina es fundamental para la dinámica de la célula B. Esta implicado en la formación de filopodios y lamelipodios (Westerberg et al, 2001), y también en el establecimiento de la SI (Fleire et al, 2006; Harwood & Batista, 2008). Además, es necesario para el tráfico y el procesamiento de antígeno internalizado a través del BCR (Vascotto et al, 2007).

La formación de los filamentos de actina (F-actina) requiere de la acción de nucleadores de actina. Uno de ellos es el complejo Arp2/3, que se localiza en el extremo anterior de células en migración, donde alarga filamentos de actina ramificados preexistentes mediante la adición de monómeros de actina glomerular (G-actina) (Le Clainche & Carlier, 2008). La reorganización del citoesqueleto de actina es regulado por Rho-GTPasas (Fig. 9 y 11); Rac1, Cdc42 y RhoA inducen la formación de lamelipodios, filopodios y fibras de estrés, respectivamente (Mor et al, 2007). En células B activadas, Cdc42 y Rac1 inducen la formación de filopodios y lamelipodios (Westerberg et al, 2001). La familia de proteínas asociadas con el síndrome de Wiskott-Aldrich (WASP) incluye efectores de Cdc42 y Rac que activan el complejo Arp2/3 (Monypenny et al, 2010). Entre sus miembros encontramos a WASP, que se expresa sólo en células hematopoyéticas, N-WASP (*neural*-WASP),

de expresión ubicua, y SCAR (*suppressor of cAMP repector*)/WAVE (WASP-*family verprolin homology protein*).

N-WASP y WAVE, efectores de Cdc42 y Rac1, respectivamente, participan en la migración de distintos tipos celulares (Le Clainche & Carlier, 2008). WASP regula el citosqueleto de actina de células B; está implicado en la formación de los microvili así como en los procesos de adhesión, migración y homing (Westerberg et al, 2001; Westerberg et al, 2005). Cdc42, que promueve la polimerización de actina a través de WASP, es esencial en el desarrollo de células B y en su activación (Guo et al, 2009). WASP es fundamental para la homeostasis de las células B, en parte debido a una alteración en la función de las integrinas; también se le ha implicado en la formación del pSMAC de la SI en células B (Meyer-Bahlburg et al, 2008). La regulación de la actividad de las Rho-GTPasas a través de la señalización por CXCR5 y el BCR va a determinar los cambios necesarios en el citoesqueleto de actina para promover migración o bien la formación de la SI.

2.3.4. Las integrinas, piezas clave en la migración y la formación de la SI

Las integrinas son receptores de la superficie celular que median adhesión a otras células o bien a la matriz extracelular. Son heterodímeros con dos subunidades α y β, cada una de las cuales contiene un dominio extracelular grande, un dominio transmembrana y una cola citoplasmática corta (Luo et al, 2007).

Los linfocitos en respuesta a quimioquinas o antígeno son capaces de interaccionar con otras células mediante la activación de integrinas. Para ello, las integrinas cambian su avidez por el ligando a través de un proceso de señalización conocido como *inside-out signaling* (Dustin, 2007; Hogg et al, 2002). Este proceso supone un cambio en la afinidad de las integrinas por sus ligandos, pero también un aumento de la capacidad de las integrinas para difundir por la superficie celular y agregarse (*clustering*) (Fig. 12). La afinidad de la integrina por su ligando depende de la conformación de los dominios extracelulares de las subunidades: conformación doblada (*bent*), de baja afinidad por el ligando, conformación de extensión intermedia, y conformación extendida, de afinidad máxima por el ligando (Luo et al, 2007). Por otro lado, la agregación de integrinas resulta del reclutamiento de otras moleculas a sus dominios citoplasmáticos (Critchley, 2009; Yu et al), por la homodimerización de sus dominios transmembrana (Li et al, 2003) y/o mediante la liberación de las integrinas de su anclaje al citosqueleto (Ni et al, 2003).

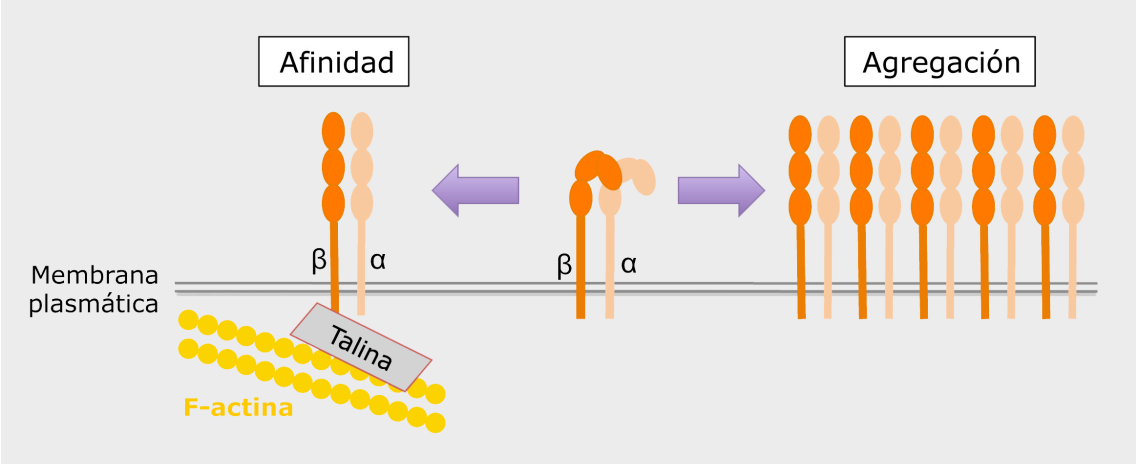

Figura 12. Activación de integrinas. La activación de integrinas supone un cambio de conformación (afinidad) y su agregación en la membrana plasmática (*clustering*)**.**

La activación de las integrinas requiere de la unión de la proteína Talina a la cola citoplasmática de la subunidad β (Simonson et al, 2006; Tadokoro et al, 2003), que desestabiliza la interacción de las subunidades α y β (Vinogradova et al, 2002). Talina además se une a F-actina y a otras proteínas como Vinculina, conectando así el citosqueleto de actina con las integrinas en la membrana de la célula (Critchley & Gingras, 2008). La ruta de Rap1/TIAM puede reclutar y activar a talina a la membrana, donde se encuentran las integrinas para su activación (Kinashi, 2005). RIAM también puede servir de adaptador para conectar Ras GTPasas a talina-1, reclutándola a la membrana y activando integrinas (Watanabe et al, 2008).

Las células B expresan las integrinas LFA-1 ($\alpha_L\beta_2$) y VLA-4 ($\alpha_4\beta_1$), cuyos principales ligandos son ICAM-1 y y VCAM-1, respectivamente. Ambas integrinas participan en la adhesión estable de la célula B a la APC y el establecimiento de la SI. LFA-1/ICAM-1 forma parte del pSMAC y reduce el umbral de antígeno necesario para activar a la célula B (Carrasco et al, 2004). VLA-4/VCAM-1 también facilita la activación de la célula B en condiciones limitantes de antígeno al promover su interacción con la APC (Carrasco & Batista, 2006). El papel de las integrinas en la migración intersticial es controvertido. Las células B se mueven sobre la red de FDC y otras células estromales en los folículos, donde encuentran CXCL13 en un contexto molecular que incluye ICAM-1 y VCAM-1 (Bajenoff et al, 2006); la señalización a través de CKR activa integrinas y por tanto su interacción con ligando. DC derivadas de ratones deficientes para todas las integrinas sin embargo son capaces de migrar en el interior de los OLS, proponiéndose que el movimiento ameboide es dependiente del flujo de polimerización de actina y no requiere de integrinas (Lammermann et al, 2008). En el transcurso de este trabajo, se ha reportado la preferencia de los leucocitos para moverse sobre superficies que

contienen ligandos de integrinas y quimioquina en comparación a un movimiento en ausencia de adhesión promovido por un gradiente soluble de quimioquina (Schumann et al, 2010).

2.3.5. Mecanismos moleculares implicados en migración versus SI en células B

Tanto la señalización a través del BCR como por CXCR5 provoca una reorganización del citoesqueleto celular y la activación de integrinas. Según el receptor activado, la célula B responde con dos estados dinámicos diferentes y opuestos: migración por CXCR5/CXCL13 y parada/formación de SI en respuesta a BCR/antígeno. Ambos receptores comparten rutas de señalización que dan lugar a fenómenos similares, pero de consecuencias opuestas. Al inicio de este estudio se desconocían los mecanismos moleculares que determinan el estado dinámico de las células B en presencia de antígeno y quimioquina.

3. OBJETIVOS

1. Establecimiento de un sistema experimental *in vitro* para el estudio del comportamiento o dinámica de células B primarias en respuesta a estimulación por quimioquinas y antígeno en tiempo real.

2. Estudio de la regulación de la dinámica de células B primarias en presencia simultánea de quimioquinas y antígeno.

3. Estudio de los mecanismos moleculares implicados en determinar la migración *versus* la parada y formación de la sinapsis inmunológica de las células B en respuesta a estimulación por quimioquina y antígeno.

4. MATERIAL Y MÉTODOS

4.1.Aislamiento de células B primarias de ratón y líneas de celulas B

Células B *naïve* primarias *wild type* (WT; C57BL/6 y BALB/c) y genéticamente modificadas fueron aisladas del bazo de ratones BCR-transgénicos MD4 (Goodnow et al, 1988), BCR-transgénicos 3-83 (Russell et al, 1991), CXCR5 deficientes (Forster et al, 1996) y WIP deficientes (Anton et al, 2002), mediante selección negativa (pureza >95%), como se ha descrito previamente (Carrasco et al, 2004). Brevemente, tras sacrificar al animal (4-6 meses) mediante inhalación de CO_2, se extrajo el bazo y se homogeneizó a través de un separador de células de nylon de 40 μm de diámetro de poro (BD Falcon). Las células mononucleares se separaron mediante centrifugación en un gradiente de densidad de *Lympholite* (Cedarlane Laboratories, Ontario, Canada). A continuación, se lisaron los eritrocitos contaminantes con una solución de cloruro amónico al 0,75 %. Los linfocitos B se purificaron utilizando un sistema de selección negativa (Dynabeads® Mouse pan T (Thy1.2), Invitrogen Dynal AS). Para aumentar el grado de pureza, las células se dejaron a 37ºC durante al menos 1h, permitiendo así la unión de células adherentes al plástico de la placa de cultivo. El medio de cultivo empleado durante todo el proceso de aislamiento y para el cultivo posterior de las células B fue RPMI suplementado con 10% de suero (*Fetal Calf Serum*; FCS), 10mM Hepes, 2 mM L-Glutamina, y 50 μM β-mercaptoetanol.

La línea de células B de ratón A20 fueron transfectadas de forma transitoria por electroporación (2 x 10^6 células, 10-20μgs vector; condiciones 250mV, 960μF) y analizadas 20h después mediante microscopía en tiempo real. La construcciones utilizadas fueron: 1) PIPKIγ_{665}-GFP (obtenida de la Dra. Rosana Lacalle; (Lacalle et al, 2007)), 2) la sonda para PIP_2 PLCδ-PH-GFP (obtenida de la Dra. Isabel Mérida; (Falasca et al, 1998)), 3) vinculina-GFP (suministrada por el Dr. Miguel Vicente-Manzanares; (Shen et al, 2011)), 4) la sonda para F-actina LifeAct-RFP (obtenida del Dr. Mario Mellado; (Riedl et al, 2008)), y 5) vectores lentivirales GIPZ shARNmir de raton (clones V2LMM_45006, V2LMM_56452, V2LMM_437636, que codifican para shARN específico de vinculina de ratón, y un vector control GIPZ shARNmir que no silencia; Thermo Scientific). La construcción CXCR5-GFP fue generada en el laboratorio; células B A20 fueron transfectadas por electroporación y cultivadas en presencia de G418 (1 mg/ml; GIBCO) para la obtención de clones que expresaran CXCR5-GFP de forma estable.

4.2.Anticuerpos y otros reactivos

Tabla I. Anticuerpos primarios. CF: citometría de flujo; IF: inmunofluorescencia; WB: western blot.

Anticuerpo	Descripción	Uso	Dilución	Procedencia
anti- B220-PE	clon RA3 rata	CF	1/200	Coulter
anti-CD11a-PE	clon 2D7 rata	CF	1/100	BD Pharmingen
anti-CD19-PE	clon 6D5 rata	CF	1/200	Coulter
anti-CD49d	clon JMPS/2 rata	CF	1/100	-
anti-CD69-FITC	clon H1.2F3 hamster	CF	1/200	BD Bioscience
anti-CD86-PE	clon GL1 rata	CF	1/200	BioLegend
anti-CXCR5-biotina	monoclonal rata	CF IF	1/100	BD Pharmingen
anti-fosfo-MLC2(T18/S19)	policlonal conejo	IF	1/200	Cell Signaling
anti-fosfo-p44/42 MAPK (T202/Y204)	policlonal conejo	WB	1/1000	Cell Signaling
anti-fosfo-ZAP70(Tyr319)/Syk(Tyr352)	policlonal conejo	IF WB	1/500 1/1000	Cell Signaling
anti-IgD-FITC	monoclonal rata	CF	1/200	Southern Biotechnology
anti-IgM-Cy5	policlonal cabra	CF	1/1000	Jackson Immunoresearch
anti-Syk	policlonal conejo	WB	1/1000	Cell Signaling
anti-talina	clon 8d4 ratón	IF	1/100	Sigma
anti-vinculina	clon hVIN-1 ratón	IF WB	1/200	Sigma
anti-WASP	policlonal conejo	IF	1/200	SC Biotecnology
anti-α-tubulina	clon DM1A ratón	WB	1/5000	Sigma
anti-β-actina	monoclonal ratón	WB	1/1000	Sigma
Faloidina Alexa Fluor 647	-	IF	1/250	Molecular Probes

Tabla II. Reactivos y anticuerpos secundarios. CF: citometría de flujo; IF: inmunofluorescencia; WB: western blot.

Anticuerpo	Descripción	Uso	Dilución	Procedencia
anti-Ig Conejo-HRP	policlonal cabra	WB	1/2000	Dako
anti-Ig Ratón-HRP	policlonal cabra	WB	1/2000	Dako
anti-IgG conejo- Alexa Fluor 488	policlonal cabra	IF	1/1000	Southern Biotechnology
anti-IgG rata- Alexa Fluor 488	policonal cabra	IF	1/500	Molecular Probes
anti-IgG1 ratón-FITC	policlonal cabra	IF	1/500	BD Bioscience
anti-μ(HC) ratón-Cy5	policonal cabra	IF	1/1000	Jackson Immunoresearch
Estreptavidina Alexa Fluor 488	-	CF	1/1000	Molecular Probes

4.3.Construcción de CXCR5-GFP

El ARN mensajero de CXCR5 de ratón fue amplificado por RT-PCR utilizando ADN complementario obtenido de células B de bazo. El cebador directo fue 5'-CCAAGCTTCAGAGCTGCAGCTATGAATCTA-3' y el indirecto fue 5'-CGGGATCCGAGCCTCCTGAGAAGGTGGTGAGGGAAGTAG-3'. El producto de la PCR fue clonado en los sitios de restricción HindIII/BamHI del vector de expresión pEGFP-N1 (Invitrogen), y secuenciado.

4.4.Citometría de flujo

Las células B fueron incubadas con los anticuerpos primarios a las diluciones correspondientes durante 20 minutos a 4ºC y, cuando así se requirió, tras un lavado, se incubaron con los anticuerpos o reactivos secundarios durante 20 minutos a 4ºC. El medio empleado para las incubaciones y los lavados fue PBS con albúmina de suero bovino (*Bovine Serum Albumin*; BSA) al 1%, FCS al 1% y NaN_3 10mM. Las muestras se analizaron en un citómetro de flujo FACSCalibur (Becton Dickinson, Mountain View, CA) utilizando el programa Cell Quest Pro y el programa FlowJo 8.0.

4.5.Ensayos de migración en transwell

Los ensayos de migración en *transwell* se realizaron en placas de 24 pocillos (Transwell® Permeable Supports) con membranas de policarbonato de 6.5 mm de diámetro, con un tamaño de poro de 3 μm. Sobre los insertos, se sembraron 250.000 células B primarias en 100 μl de medio de depleción (RPMI con 0.1% de BSA) en ausencia o en presencia de estímulo. Los estímulos empleados fueron $F(ab')_2$ anti-IgM (1 μg/ml; Jackson Immunoresearch Laboratories) o HEL (Hen Egg Lysozyme; Sigma) a las concentraciones indicadas. Cada inserto fue transferido a un pocillo con 600 μl de medio de depleción en ausencia o en presencia de estímulo (a la misma concentración que en el inserto correspondiente) y con o sin quimioquina (CXCL12 y CXCL13, ambas recombinantes de ratón; Peprotech) a las concentraciones indicadas. Tras un periodo de 2h 30min a 37ºC, se recolectó la totalidad del medio del compartimento inferior y se contaron las células que habían migrado mediante técnicas de citometría de flujo. El porcentaje de células migradas se estimó como el número de células que pasan por el citómetro a flujo alto durante un minuto, respecto al número de células de las que se partió inicialmente en el inserto, y contadas de la misma manera. Cada experimento se realizó por duplicado.

4.6. Ensayos de activación de células B

Brevemente, $1x10^6$ células B MD4 fueron puestas en cultivo en presencia de HEL a las concentraciones indicadas en pocillos de placas p48; tras un periodo de 20 h las células fueron recogidas. Los ensayos de activación sobre membranas artificiales se realizaron como se ha descrito previamente (Carrasco et al, 2004); brevemente, $2.5x10^5$ células B WT o MD4 fueron cultivadas sobre bicapas lipídicas formadas en cubreobjetos de 6 mm de diámetro (Multiwell chambered coverslips; Molecular Probes); las membranas artificiales contenían GPI-ICAM-1 (150 molec/μm^2), antígeno a las densidades indicadas, y fueron tapizadas o no con CXCL13 (100nM). Tras una incubación de 20 h a 37ºC, las células fueron recolectadas. En ambos tipos de ensayos, la activación de las células B se analizó mediante la detección de los niveles de expresión para los marcadores de activación CD69 y CD86 en la superficie de las células B por técnicas de citometría de flujo.

4.7. Ensayos de microscopía en tiempo real en bicapas lipídicas artificiales planas

Los ensayos de migración y formación de SI en dos-dimensiones (2D) se llevaron a cabo sobre bicapas lipídicas artificiales planas, formadas como se ha descrito previamente (Carrasco et al, 2004) en cámaras de flujo cerradas FCS2 (Bioptechs). Brevemente, se mezclaron liposomas de 1,2-dioleoyl-fosfatidil-colina (DOPC) (Avanti Polar Lipids, Inc.) con liposomas de DOPC que contenían ICAM-1 o VCAM-1 de ratón anclados por glicosil-fosfatidil-inositol (GPI) y con liposomas de DOPC que contenían lípidos biotinilados (Avanti Polar Lipids, Inc.), a los ratios necesarios para conseguir las densidades especificadas en cada caso. Las membranas artificiales planas se ensamblaron sobre cristales previamente tratados con solución sulfocrómica (20 min, *Room Temperature*, RT), y se bloquearon con PBS al 2% de FCS (1h, RT). El antígeno se unió a las membranas mediante una incubación con estreptavidina Alexa Fluor 647 o Alexa Fluor 555 (Molecular Probes), seguida bien del péptido p31 monobiotinilado para las células B 3-83, bien del anticuerpo monoclonal (mAb) anti-HEL F10 monobiotinilado más HEL (1μg/ml) o HEL biotinilada (1μg/ml) para las células B MD4, o bien del mAb anti-cadena ligera κ monobiotinilado (BD Bioscience) para las células B WT, deficientes en CXCR5, deficientes en WIP y la línea de células B A20. Finalmente, las membranas se incubaron con CXCL12 o CXCL13 (100nM, salvo otra indicación; 30min a RT), justo antes de la adquisición de imágenes. Se inyectaron $5x10^6$/ml de células B primarias o $3x10^6$/ml de células B A20 no marcadas o previamente marcadas con CFSE o SNARF (0.1 μg/ml, 10min 37ºC en PBS; Molecular Probes) en las cámaras

precalentadas, y éste se consideró como tiempo cero (0 min). Se tomaron series de imágenes de fluorescencia confocal, DIC (*Differential Interference Contrast*) e IRM (*Interference Refelction Microscopy)* cada 10 segundos durante 25 min o bien cada 30 segundos durante 20 min. Cuando así se indica, se inyectó en las cámaras FCS2 latrunculina A (0.5 μM; Calbiochem), blebistatina (50 μM; Calbiochem) o wiskostatina (5 μM; Calbiochem) y, seguidamente o pasados 10 min, se tomaron imágenes en tiempo real. El tratamiento con el inhibidor químico BAY 61-3606 (Calbiochem; 30 min a 37ºC) a las dosis indicadas de las células B primarias se realizó previamente a su inyección en las cámaras FSC2. Todos los ensayos sobre membranas artificiales en tiempo real se realizaron a 37ºC en PBS al 0.5% de FCS, 2 mM de Cl_2Mg, 0.5 m Cl_2Ca y 0.5 g/l de D- glucosa.

Las imágenes fueron adquiridas en un microscopio invertido Zeiss Axiovert LSM 510-META con un objetivo de inmersión 40x/NA1.2 y analizadas con los programas LSM 510 (Zeiss) e Imaris 7.0 (Bitplane).

4.8. Estudios cuantitativos en las membranas artificiales y en la superficie celular

El área de contacto de las células B con las membranas, detectada por IRM, se estimó utilizando el programa Image-J (NIH). El número de moléculas/μm^2 de ICAM-1-GPI, VCAM-1-GPI y antígeno en las bicapas lipídicas artificiales planas fue estimado mediante ensayos inmunofluorométricos utilizando mAb anti-ICAM-1, anti-VCAM-1 o anti IgG (para F10 o anti-κ), respectivamente; los valores estándar se obtuvieron a partir de microesferas calibradas con diferentes capacidades de unión a IgG (Bangs Laboratories).

El número de moléculas de antígeno presentes en la SI se estimó como sigue:

La densidad de moléculas ICAM-1 y VCAM-1 expresada en la superficie de los esplenocitos sin estimular o estimulados con TNFα (10 ng/ml; 20h, 37ºC; Peprotech) fue estimada por citometría de flujo como se detalla anteriormente, utilizando las microesferas calibradas como valores estándar.

4.9. Ensayos de inmunofluorescencia

Células B 3-83 se co-cultivaron durante 30 min a 37ºC con APC (línea de células L de ratón transfectadas establemente con ICAM-1-GFP; Carrasco, 2004) previamente crecidas sobre cubreobjetos (24h). A continuación, las células se fijaron con para-formaldehido (PFA) al 4% durante 10 min, se bloquearon con PBS al 2% de FCS y al 2% de BSA y se tiñeron con los anticuerpos primarios y, posteriormente, secundarios indicados durante 1h a RT en cada caso. Los cubreobjetos fueron montados con Fluoromount-G (Southern Biotechnology).

Alternativamente, células B primarias en contacto durante 30 min con bicapas lipídicas artificiales planas que contenían ICAM-1-GPI, tapizadas con CXCL13, y en ausencia o presencia de sAg ($F(ab')_2$ anti-IgM, 1 μg/ml; Jackson Immunoresearch Laboratories) o tAg, como se ha descrito anteriormente, se fijaron con PFA al 4% (10 min, 37ºC) en el interior de las cámaras FCS2. Tras permeabilizar con PBS con 0.1% de Triton–X100 (5 min, RT), se bloquearon con PBS al 2% de FCS y al 2% de BSA (4ºC, 20h), y se tiñeron con Alexa Fluor 647-Faloidina y los anticuerpos primarios y secundarios indicados en cada caso (30 min, RT). Seguidamente fueron analizadas mediante microscopía de fluorescencia confocal con un microscopio invertido Axiovert LSM 510-META (Zeiss), como se ha citado anteriormente.

Los análisis cualitativos y cuantitativos de la fluorescencia en distintos planos de la célula y en todo el volumen celular para las proteínas indicadas se realizaron utilizando el softwarer Imaris 7.0 (Bitplane). La fluorescencia relativa se obtuvo relativizando los valores de fluorescencia medidos a lo largo de una línea que trazada a lo largo de una célula en un plano, respecto al valor más alto de fluorescencia en dicha línea; dichos valores se obtuvieron con el programa Image J (N.I.H). Los ratios de fluorescencia se obtuvieron dividiendo la fluorescencia total de la proteína indicada en la SI o el plano de contacto entre la fluorescencia total en el plano medio de la célula. Los valores de fluorescencia total en el volumen completo celular se obtuvieron a partir de imágenes consecutivas en el plano (x,y), tomadas cada 1 μm a lo largo del eje z, utilizando el programa Imaris 7.0.

4.10. Ensayos de Calcio

Células B MD4 fueron marcadas con la sonda fluorescente Fluo-4FF (1 μM, 30 min, RT; Molecular Probes) e inmediatamente inyectadas en las cámaras FSC2 precalentadas. Seguidamente, se inició la adquisición de imágenes (256x256 pixels) cada 10 segundos durante 15 o 30 min utilizando un microscopio invertido Zeiss Axiovert LSM 510-META con un objetivo de inmersión 40x/NA1.2 . El flujo de calcio intracelular se midió en las imágenes de fluorescencia de Fluo-4FF utilizando los softwares de análisis LSM 510 (Zeiss) e Imaris 7.0 (Bitplane).

4.11. Infección de células B con partículas lentivirales

Los stocks de partículas lentivirales recombinates se obtuvieron de células HEK 293T co-transfectadas con el vector que codifica para el shARN (ARN *short hairpin*; pLKO.1, pGIPZ), el vector de la envuelta pMD.2G y el vector de empaquetamiento pCMVR8.91 (Zufferey et al, 1997). Se utilizaron dos tipos de vectores codificantes de shARN: 1) vectores lentivirales GIPZ shARNmir de raton (clones V2LMM_45006, V2LMM_56452, V2LMM_437636, que codifican para shARN específico de vinculina

de ratón y un vector control GIPZ shARNmir que no silencia; Thermo Scientific) y 2) shRNA de vinculina de ratón en vectores pLKO.1 (clones NM_009502.3-3466s1c1, NM_009502.3-1331s1c1, NM_009502.3-3154s1c1; Mission shRNA, Sigma). Brevemente, $2x10^6$ células HEK 293T fueron cultivadas en placas p150 durante 48h, y transfectadas con 2 μg de vector de envuelta, 5 μg de vector de empaquetamiento y 7 μg del vector que codifica el shARN, previamente acomplejados con JetPEI (0.1 mM, 30 min a RT; Polyplus transfection) en OPTIMEM (Gibco). Tras 4h a 37ºC el medio fue cambiado por medio fresco, DMEM al 2% de FCS; las partículas lentivirales fueron recogidas 48 o 72h después de la transfección. La suspensión de partículas se filtró (tamaño de poro de 0.45μm) y se concentró por ultracentrifugación (23.000 rpm, 2h, 4ºC). El precipitado se resuspendió en RPMI y se almacenó a -80ºC.

Se infectaron $2x10^6$ de células B primarias con las partículas lentivirales concentradas (MOI 1-10) en RPMI al 10% de FCS, en ausencia o presencia de IL-4 recombinante de ratón (50 ng/ml; Peprotech), CpG (1 μg/ml; Invivogen) o LPS (2.5 μg/ml; Sigma) durante 6h a 37ºC. El medio fue sustituido por medio fresco, RPMI 10% FCS, y las células se cultivaron en ausencia o presencia del estímulo indicado durante 48h para permitir la expresión del shARN y del gen reportero GFP. Los niveles de expresión de vinculina y GFP se determinaron por western blot.

4.12. Análisis de la expresión de proteínas por western blot

Se incubaron 5 $x10^6$ de células B primarias en medio de depleción (RPMI al 0.5% de FCS; 1h, 37ºC), y seguidamente se estimularon (30 min, 37ºC) con $F(ab')_2$ anti-IgM (1 μg/ml; con agitación) o con membranas artificiales que contenían ICAM-1, CXCL13 y/o tAg, según se indique. Se añadió PBS frío para parar la reacción, las células B se centrifugaron (2000 rpm, 5 min 4ºC) y se lisaron (30 min, 4ºC) en el tampón de lisis RIPA (50mM Tris HCl pH 8, 150 mM NaCl, 1% NP-40, 0.5% desoxicolato sódico, 0.1% SDS) con inhibidores de proteasas y fosfatasas (Roche). Los lisados se centrifugaron (14.000 rpm, 30 min, 4ºC); los sobrenadantes se almacenaron a -80ºC. Los lisados de células B infectadas con partículas lentivirales se obtuvieron de manera similar. La cantidad de proteína total en los lisados se cuantificó con el kit comercial *Micro BCA Protein assay* (Thermo Scientific). Las proteínas se separaron por electroforesis en geles de acrilamida con SDS y se transfirieron a membranas de PVDF (*polyvinyl difluoride*; BioRad); las membranas se bloquearon con BSA al 2% disuelto en TBS-T (10mM Tris-HCl pH 8, 150 mM NaCl, 0.1% Tween-20) (1h, RT) y se incubaron durante 20 h a 4ºC o durante 1 h a RT con los anticuerpos primarios indicados. Las membranas se incubaron durante

1h a RT con anticuerpos secundarios conjugados con peroxidasa (*HorseRadish Peroxidase*; HRP); la señal de HRP fue detectada con un sistema de detección de quimioluminescencia (ECL; GE Healthcare). La cuantificación de la señal para p-Erk y vinculina se realizó utilizando el software ImageJ (NIH); los valores obtenidos se normalizaron con los valores de tubulina o β-actina, y se relativizaron al control en cada caso.

4.13. Análisis Estadísticos

Las graficas y análisis estadísticos se realizaron con el software Prims 4.0 (GraphPad). Se aplicó *two-tailed unpaired Student t-test* para datos no apareados. *, $p<0.05$; **, $p<0.001$; ***, $p<0.0001$.

5. RESULTADOS

5.1.Caracterización de células B primarias de ratón

Para abordar los objetivos propuestos en este trabajo, utilizamos células B primarias aisladas del bazo de ratones *wild type* (WT) o genéticamente modificados (BCR-transgénicos; deficientes para determinadas moléculas) como modelo experimental. Purificamos células B mediante un proceso de selección negativa (ver métodos) y analizamos su pureza, fenotipo y estado de activación mediante citometría de flujo. La población celular obtenida mostró altos niveles de expresión en membrana para los marcadores distintivos de células B CD45R/B220 y CD19, con una pureza >95%; así mismo, encontramos niveles variables de BCR/IgM (Fig. 13A), característico de una población de células B maduras (Allman & Pillai, 2008). Los niveles detectados para los marcadores de activación celular CD86 y CD69 ($CD86^{low}$ $CD69^{-}$) indicaron que la población aislada no estaba activada (Fig. 13A). Salvo indicación, todos los ensayos de este trabajo se realizaron con células B primarias no activadas (*naïve)*.

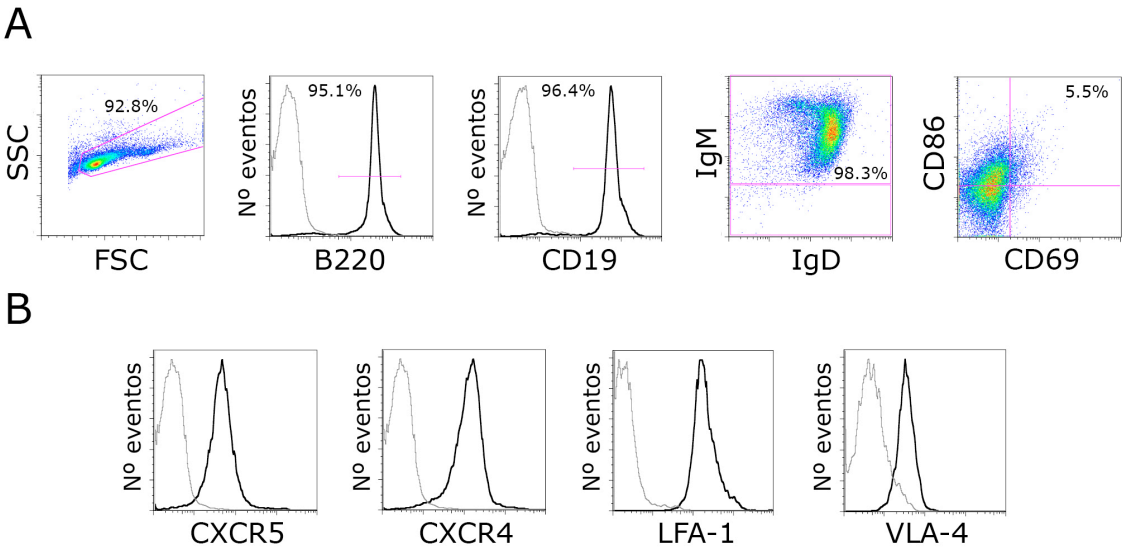

Figura 13. Caracterización de la población de células B primarias aislada de bazo de ratón. (A) Perfiles de expresión en membrana de CD45/B220 y CD19, y diagramas de dispersión de IgM/ IgD y CD69/CD86 en la población de células B primarias mostrada en el diagrama FSC-SSC. (B) Perfiles de expresión de los receptores de quimioquinas CXCR5 y CXCR4, y de las integrinas LFA-1 y VLA-4 en la membrana de las células B primarias; línea discontinua, control de isotipo.

Analizamos la expresión de los receptores de quimioquinas CXCR4 y CXCR5, así como de las integrinas LFA-1 y VLA-4, implicados en los procesos de migración y formación de la sinapsis inmunológica en células B y, por tanto, relevantes para el desarrollo de este estudio. La población de células B aisladas expresaba en su membrana niveles homogéneos para CXCR4, CXCR5, LFA-1 y VLA-4 (Fig. 13B).

5.2. Estudio de la capacidad de migración de las células B en respuesta a las quimioquinas CXCL13 Y CXCL12

Para estudiar el efecto de la señalización por BCR sobre la migración de las células B en respuesta a CXCL13 y CXCL12, utilizamos inicialmente ensayos *in vitro* de migración en *transwell*. Este ensayo permite analizar la migración de las células B a través de poros más pequeños que su tamaño, que pudieran simular el paso por los espacios más estrechos de la red de FDC presente en los folículos, y en respuesta a un gradiente de quimioquinas. Utilizamos *transwell* de tamaño de poro de 3 μm, inferior al diámetro de una célula B primaria (5 μm).

La capacidad de migración de las células B en ausencia de quimioquina fue muy baja (<5%), incrementándose notablemente en presencia de CXCL13 o CXCL12. Dicho aumento fue dependiente de la dosis y del tipo de quimioquina empleada. Sólo altas dosis de CXCL13 (500 nM) promovieron un aumento significativo de la frecuencia de migración de las células B (Fig. 14A). El máximo de migración en respuesta a CXCL12 se observó a dosis de 50 nM (Fig. 14B); el uso de dosis más altas reducía estos valores máximos, posiblemente debido al proceso de desensibilización de CXCR4. Además, la migración en respuesta a CXCL13 (37%) fue mayor que a CXCL12 (12%). Teniendo en cuenta estos resultados, en los siguientes experimentos utilizamos los dosis más óptimas de CXCL13 y CXCL12 (500 nM y 50 nM, respectivamente) para promover migración de células B.

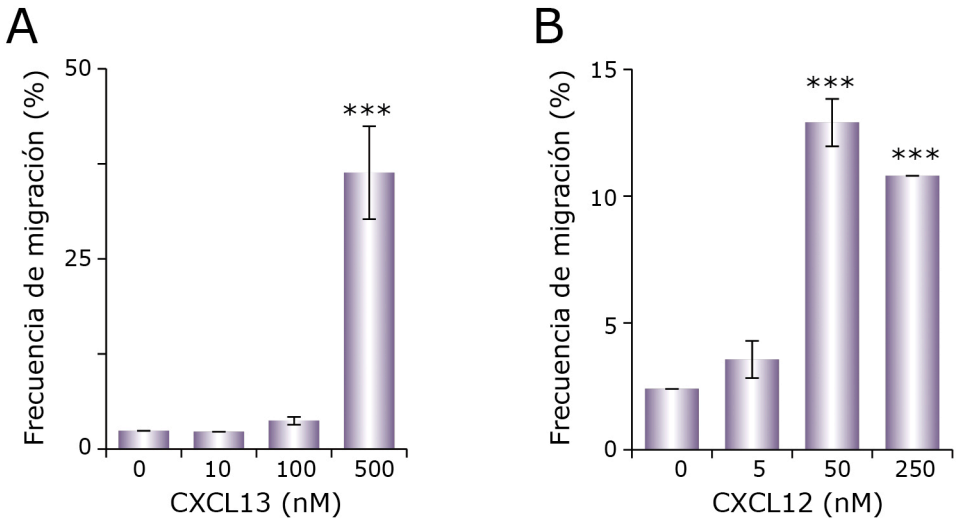

Figura 14. Migración de células B primarias en respuesta a gradientes de CXCL13 y CXCL12. Frecuencia de migración de células B en respuesta a las dosis indicadas de CXCL13 (A) o de CXCL12 (B) en ensayos de transwell. Los datos mostrados corresponden a un experimento representativo (n=3).

5.3.Efecto de la activación por antígeno en la migración de las células B

Realizamos dos tipos de ensayos: 1) pusimos a migrar células B en presencia simultánea de estimulación por BCR (anticuerpos anti-IgM, 1μg/ml) y de un gradiente de CXCL13; 2) pre-tratamos las células B con anticuerpos anti-IgM durante 2 h (fase de *priming*) para después ponerlas a migrar en presencia de CXCL13. La presencia de estimulación por BCR disminuyó la frecuencia de migración en un 50% (Fig. 159A). Sin embargo, tras la fase de *priming*, la migración de células B alcanzó valores comparables a la situación control (no anti-IgM) (Fig. 15A). Este mismo experimento se realizó en presencia de CXCL12, obteniéndose resultados análogos (Fig. 15B).

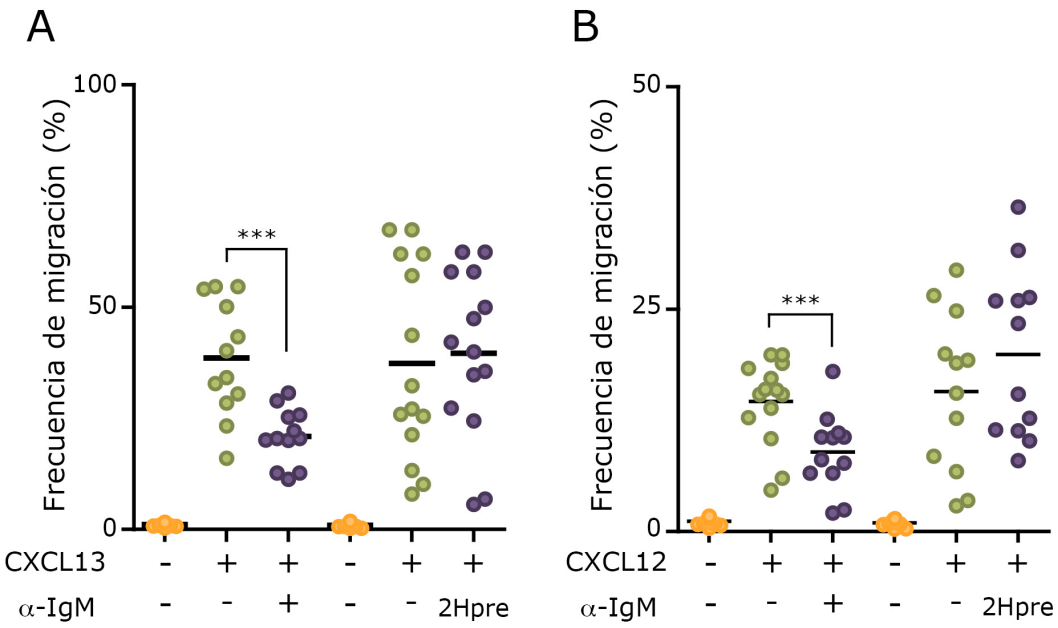

Figura 15 Efecto de la estimulación del BCR sobre la migración de células B en respuesta a CXCL13 y CXCL12. Frecuencia de migración en respuesta a CXCL13 (A) o CXCL12 (B) de células B primarias en ausencia o presencia de anticuerpos anti-IgM durante el ensayo, o pre-tratadas durante 2h (2Hpre) a 37ºC en ausencia o presencia de anticuerpos anti-IgM y luego puestas a migrar. Cada punto corresponde a un experimento individual.

Los datos indicaban que la estimulación por BCR interfiere con la señalización a través de CXCR5 y CXCR4, lo que se traduce en una menor capacidad migratoria de las células B en respuesta a CXCL13 o CXCL12. No obstante, la recuperación de la capacidad migratoria tras un periodo de *priming* sugería dos posibilidades, bien que es necesaria la presencia constante de señalización por BCR para interferir con la señal de migración del receptor de quimioquina, o bien que la alteración de la migración mediada por el BCR es transitoria.

5.4. Efecto dosis-dependiente de la estimulación por antígeno sobre la migración de las células B

A continuación analizamos cómo la intensidad de la señalización por BCR modula la capacidad de migración de las células B en respuesta a CXCL13 o CXCL12, mediante el uso de distintas dosis de antígeno. Para ello, utilizamos ratones BCR-transgénicos MD4, cuyas células B expresan un BCR que reconoce la proteína lisozima (*Hen Egg Lysozyme*, HEL) con una alta afinidad (Ka = $5x10^{10}$ M^{-1}). Las células B MD4 mostraron un comportamiento similar al de células B WT en ensayos de transwell en respuesta a diferentes dosis de CXCL13 y CXCL12 (Fig. 16A y B); por tanto, utilizamos igualmente las dosis de 500 nM para CXCL13 y de 50 nM para CXCL12 en los siguientes ensayos.

Realizamos ensayos de migración de células B MD4 en respuesta a CXCL13 y en ausencia o presencia de HEL a concentraciones decrecientes (desde 100 μM a 0.1 pM). Concentraciones de 100 μM a 10 nM de HEL inhibieron casi totalmente la migración, mientras que dosis de 1 nM e inferiores no tuvieron efecto (Fig. 16C). Analizamos la capacidad de las dosis de HEL utilizadas para inducir activación de las células B, determinando los niveles de expresión de CD69 y CD86 tras un período de estimulación de 20 h (Fig. 16C). Las dosis de antígeno que inhibían la migración celular, activaron completamente las células B (>90%); concentraciones de HEL que no afectaban a la migración, no produjeron activación celular. Sin embargo, observamos que dosis que reducían la migración en un 80% (HEL 10 nM), promovían sólo un 46% de activación. El mismo diseño experimental se realizó para CXCL12 (Fig. 16D) y obtuvimos resultados similares; en este caso además observamos que 1nM HEL disminuyó migración celular en un 60% sin inducir activación.

Los datos sugerían que existen diferencias entre la intensidad de señalización por BCR necesaria para afectar la migración y la necesaria para la activación de las células B, siendo más bajo el umbral de señal antigénica requerido para inhibir migración que para activar a la célula B.

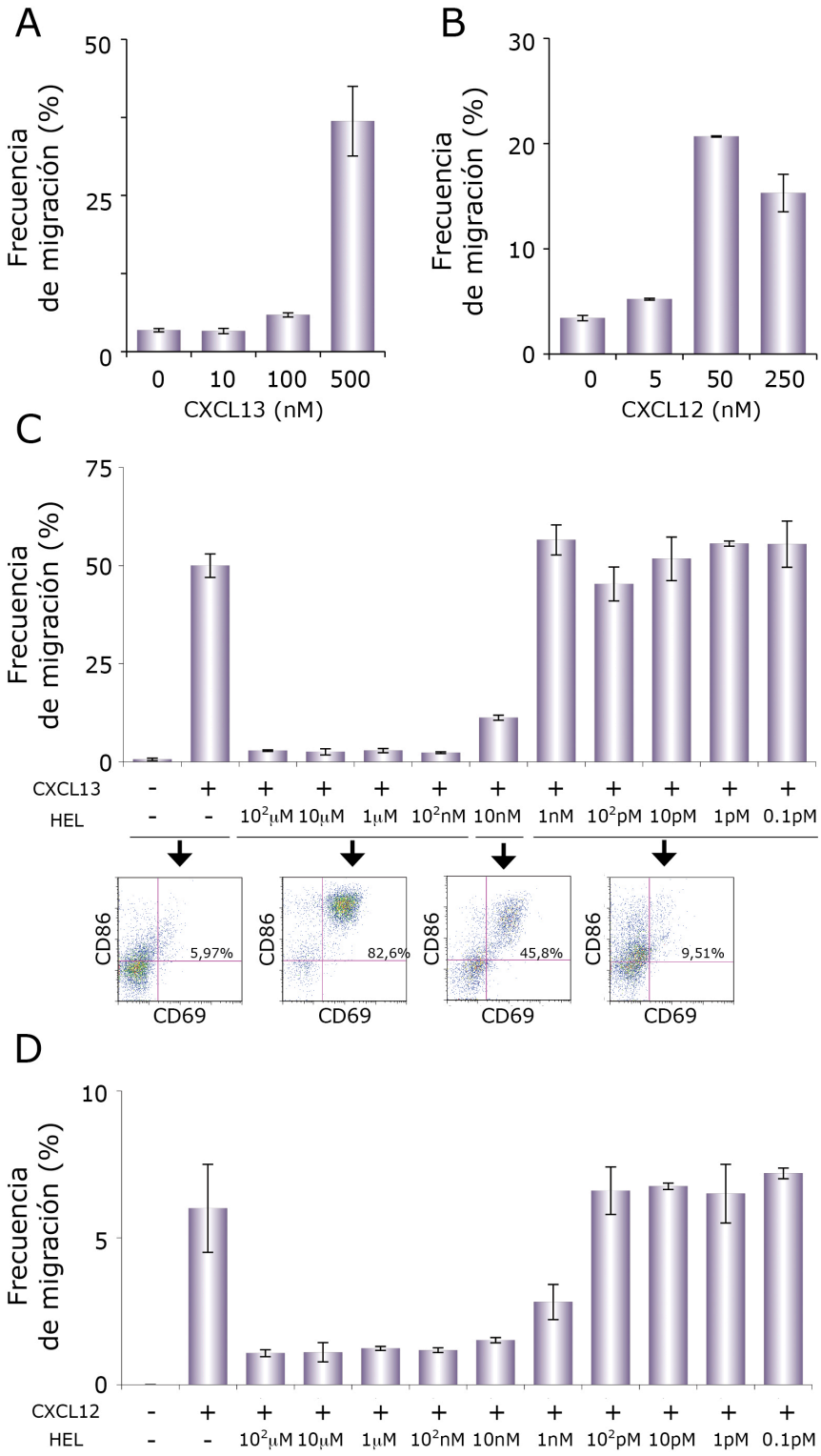

Figura 16. Efecto de la estimulación del BCR con distintas dosis de antígeno sobre la migración de células B en respuesta a CXCL13 y CXCL12. Frecuencia de migración de células B MD4 en respuesta a distintas dosis de CXCL13 (A) o CXCL12 (B). (C) Frecuencia de migración de células B MD4 en respuesta a CXCL13, en ausencia o presencia de HEL a las dosis indicadas (panel superior). Diagramas de expresión de CD69/CD86 en células B MD4 estimuladas con las mismas dosis de HEL durante 20h. (D) Igual que en (C), pero en respuesta a CXCL12. Los datos mostrados en (C) y (D) corresponden a 1 experimento representativo (n=3).

5.5. Puesta a punto de un modelo experimental de migración en 2-dimensiones

Las células B *in vivo* migran sobre la superficie de las células estromales presentes en los OLS, principalmente sobre FDC (Bajenoff et al, 2006). Estas células producen CXCL13 y CXCL12, y la exponen en su membrana unida posiblemente a través de glicosaminoglicanos como el heparan sulfato (Cyster, 2005; de Paz et al, 2007). Las células B encuentran el antígeno presentado en la superficie de estas células. Migración y reconocimiento de antígeno ocurren en un contexto molecular que incluye a las moléculas de adhesión ICAM-1 y VCAM-1 (Allen & Cyster, 2008). Teniendo en cuenta todo ello, el modelo de migración en *transwell* permitía sólo un estudio parcial y poco fisiológico de nuestros objetivos; sólo podíamos cuantificar porcentaje de migración, y antígeno y quimioquina eran presentados en forma soluble.

Con objeto de mimetizar las condiciones *in vivo*, pusimos a punto un modelo en 2-dimensiones (2D) para el estudio del comportamiento o dinámica de las células B, basado en el uso de bicapas lipídicas artificiales planas (Grakoui et al, 1999). Estas membranas artificiales son fluidas, simulan la superficie de una célula, y en ellas se puede controlar la composición y densidad de ligandos. Este sistema, previamente utilizado en estudios de células B (Carrasco et al, 2004), permite además visualizar morfología y comportamiento celular, interacciones moleculares en un plano focal, y realizar estudios cuantitativos y funcionales. Inicialmente, caracterizamos la respuesta de células B primarias en contacto con membranas que contenían ICAM-1 o VCAM-1 anclados por glicosil-fosfatidilinositol (GPI) a distintas densidades (600, 300, 150 o 75 moléculas(molec)/μm^2), y tapizadas con CXCL13 o CXCL12 (100nM); las quimioquinas quedaron retenidas mediante interacciones electrostáticas con los fosfolípidos que conformaban la membrana. Monitorizamos el comportamiento o dinámica de las células B mediante microscopía confocal en tiempo real.

5.5.1. Caracterización de la dinámica de células B en membranas con quimioquina

Observamos dos tipos de morfología en las células B en presencia de quimioquina, mediante microscopía DIC (*Differential Interference Contrast*): una forma redondeada y estable en el tiempo, y otra morfología más cambiante, en la que las células emitían extensiones de membrana en distintas direcciones y que denominamos como "polarizada" (Fig. 17A). Las células B polarizadas además eran capaces de migrar sobre las membranas, mostrando una morfología de tipo ameboide (Fig. 17B; video 1). El movimiento ameboide fue establecido por primera

vez en base al comportamiento celular de la ameba *Dictyostelium discoideum*; es una migración rápida, con una gran capacidad de adaptación al ambiente, e implica una baja adhesividad y una polarización celular con un cuerpo central elíptico, un extremo anterior ancho (lamelipodio) y un extremo posterior estrecho (urópodo). Las células B en migración presentaban un lamelipodio seguido del voluminoso núcleo en la parte posterior (Fig. 17B); el urópodo no fue detectable, al menos con la tecnología utilizada.

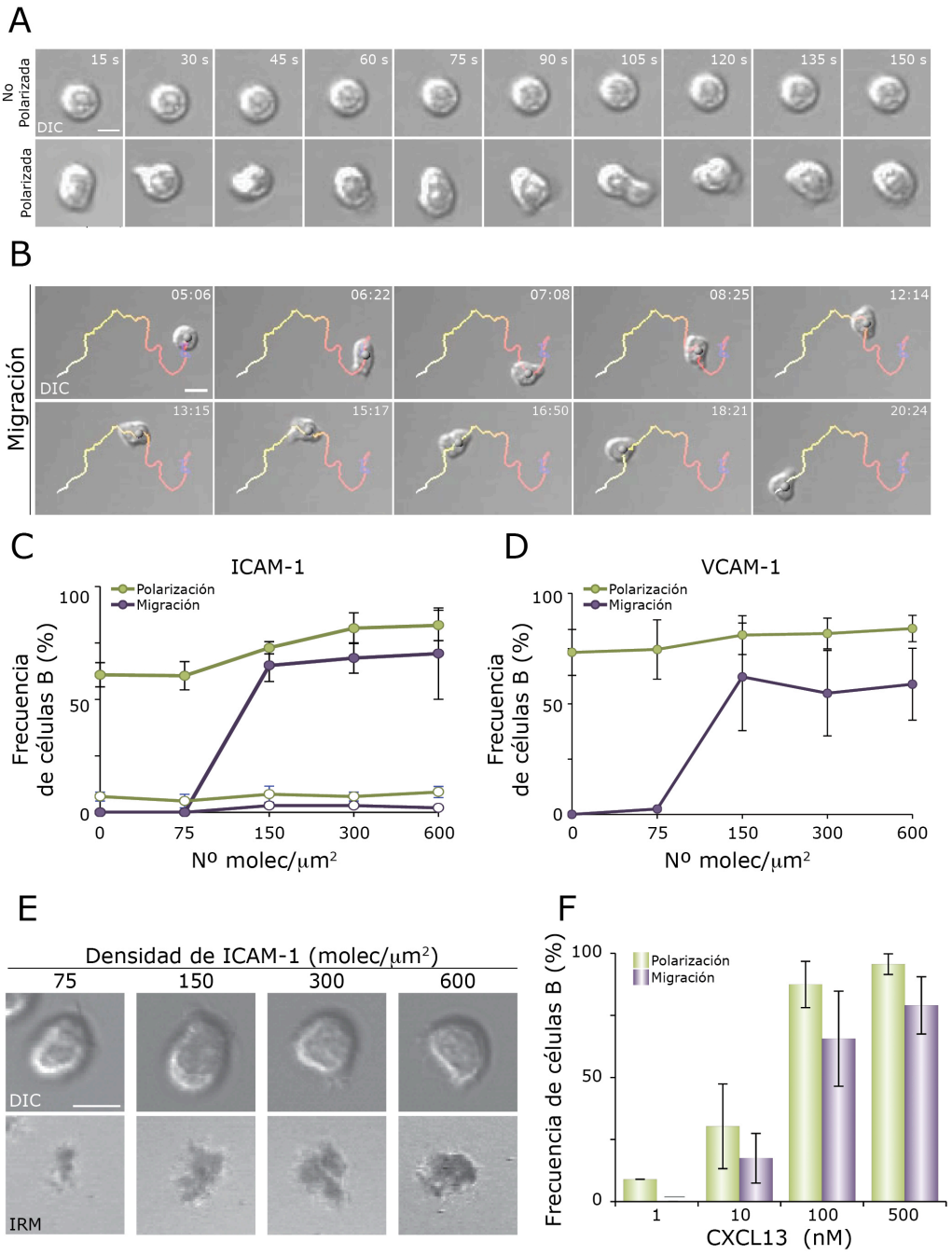

Figura 17. CXCL13 induce polarización celular y migración en células B en contacto con membranas artificiales. Células B primarias se pusieron en contacto con membranas artificiales tapizadas con CXCL13, y que contenían ICAM-1 o VCAM-1 a las

densidades indicadas. (A) Secuencia de imágenes de DIC de células B representativas en contacto con membranas que contienen ICAM-1 (150 molec/μm^2) y tapizadas con CXCL13 (100nM), mostrando morfologías no polarizada (fila superior) y polarizada (fila inferior). (B) Secuencia de imágenes de DIC de una célula B representativa migrando sobre membranas con ICAM-1 (150 molec/μm^2) y CXCL13 (100nM); línea en escala de color, trayectoria recorrida por la célula B; tiempo indicado en min:seg. Frecuencias de polarización y migración de células B WT (círculo coloreado) y de células B CXCR5$^{-/-}$ (círculos vacíos) en membranas tapizadas con CXCL13 (100nM) y que contienen ICAM-1 (C) o VCAM-1 (D) a las densidades indicadas. (E) Imágenes de DIC e IRM de células B representativas sobre membranas que contiene ICAM-1 a las densidades indicadas y tapizadas con CXCL13 (100nM). (F) Frecuencias de polarización y migración de células B en membranas con ICAM-1 (150 molec/μm^2) tapizadas con distintas concentraciones de CXCL13. Los datos mostrados en (C), (D) y (F) corresponden a la media ± SEM de 4 experimentos. Barra gris, no detectado; barra de escala, 5 μm.

El 75% de las células B se polarizó en presencia de CXCL13, con independencia de la presencia o densidad de ICAM-1 o VCAM-1 (Fig. 17C y D). Sin embargo, la frecuencia de migración resultó dependiente de la densidad de ligando de integrina; sólo densidades superiores a 75 molec/μm^2 permitieron el desplazamiento de las células B en respuesta a CXCL13. A densidades de ICAM-1 o VCAM-1 iguales o superiores a 150 molec/μm^2 observamos frecuencias de migración del 60% (Fig. 17C y D). Evaluamos el contacto de la célula B con la membrana artificial, y por tanto la interacción de la integrina LFA-1 con su ligando ICAM-1, mediante el uso de IRM (*Interference Reflection Microscopy*). Los contactos, se visualizaron como áreas oscuras y sólo fueron detectables en presencia de CXCL13; los contactos eran pequeños e intermitentes a densidades de ICAM-1 $\leq$ 75 molec/μm^2, mientras que las áreas eran mayores y más estables en el tiempo a densidades superiores de ICAM-1 (Fig. 17E). Células B deficientes en CXCR5 no se polarizaron, ni migraron (Fig. 17C), lo cual confirmaba que los efectos en comportamiento celular eran dependientes de la señalización de CXCL13 a través de su receptor CXCR5. Las frecuencias de polarización y migración de células B en presencia de CXCL12 tapizando las membranas, y con ICAM-1 o VCAM-1, fueron similares a las obtenidas con CXCL13 (datos no mostrados).

Finalmente, realizamos una titulación de la concentración de quimioquina usada para tapizar las membranas artificiales; dosis de 1-10nM no fueron suficientes para inducir polarización y migración celular de manera efectiva, mientras que a dosis de 100 nM y superiores, la respuesta de las células B fue alta (Fig. 17F). Datos similares se obtuvieron con CXCL12 (datos no mostrados). En base a estos datos, la concentración de quimioquina empleada para tapizar las membranas artificiales en los siguientes ensayos fue de 100 nM.

Los resultados obtenidos indicaban que la presencia de CXCL13 o CXCL12 es suficiente para estimular la polarización de las células B, pero es necesaria la presencia de una densidad mínima crítica de alguno de los ligandos de integrina estudiados para que las células B puedan migrar en nuestro modelo experimental.

5.5.2. Parámetros dinámicos de las células B en migración

A continuación, analizamos determinados parámetros dinámicos en las células B en migración en respuesta a CXCL13. La velocidad media fue dependiente de la densidad de ICAM-1; a 150 y 300 molec/μm^2 obtuvimos los valores más altos (valor promedio 5 μm/min) (Fig. 18A). Sin embargo, a 600 molec/μm^2, la velocidad media disminuyó de forma significativa (valor promedio 3 μm/min). Ello repercutía directamente en la longitud de la trayectoria recorrida por las células B en respuesta a CXCL13 (Fig. 18B). En el caso de membranas que contenían VCAM-1, los valores máximos de velocidad y longitud de la trayectoria se obtuvieron a densidades de 150 molec/μm^2 (valor promedio 4 μm/min), observándose una reducción significativa en ambos parámetros dinámicos a densidades superiores de VCAM-1. La trayectoria descrita por las células B en presencia de ICAM-1 o VCAM-1 a todas las densidades ensayadas fue aleatoria (Fig. 18C y datos no mostrados), carente de direccionalidad.

Los datos indicaban que el tipo de ligando de integrina y la densidad del mismo modulan el comportamiento de las células B en respuesta a CXCL13; la interacción LFA-1/ICAM-1 facilita una migración más rápida que VLA-4/VCAM-1. La cuantificación de los niveles de expresión en membrana para ICAM-1 y VCAM-1 en esplenocitos totales de ratones WT en condiciones homeostáticas o inflamatorias (estimulación con TNFα) reveló valores de densidad de 250 molec/μm^2 para ICAM-1 y 30 molec/μm^2 para VCAM-1 en homeostasis, y de 850 molec/μm^2 para ICAM-1 y 200 molec/μm^2 para VCAM-1 en inflamación (Fig. 18D). Estos datos sugieren que el rango de densidad de ligandos de integrinas empleados en nuestro sistema se encuentra dentro de los límites fisiológicos.

Establecimos por tanto un modelo de migración en 2D que permite el estudio de la migración de células B primarias en respuesta a CXCL12 y CXCL13. Los valores de velocidad media y el movimiento aleatorio (*random walking*) se asemejan a lo observado *in vivo* para células B en los folículos de OLS por microscopía multifotón (Miller et al, 2002; Okada et al, 2005). Para los siguientes estudios, decidimos centrarnos en CXCL13 (100nM), quimioquina principal que media migración de células B en los folículos primarios, y en ICAM-1 (150 molec/μm^2) por su mayor capacidad para promover migración de las células B a densidades fisiológicas y su conocido papel en el proceso de reconocimiento de antígeno.

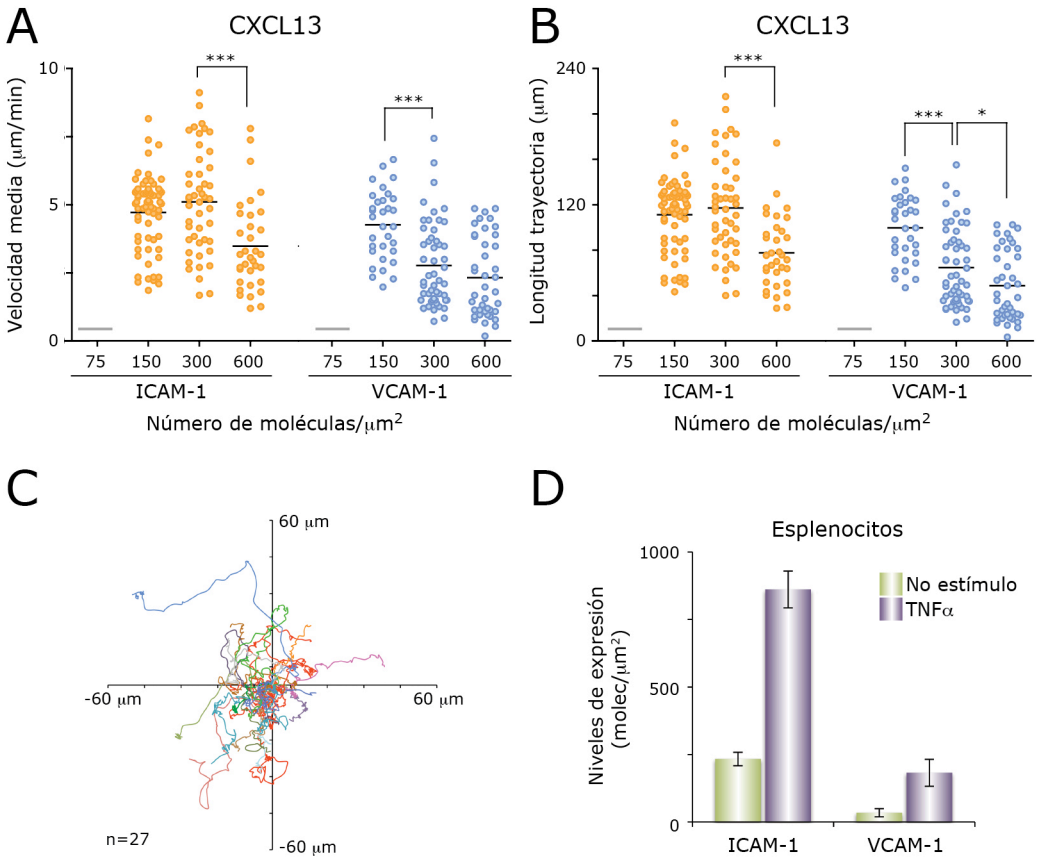

Figura 18. Parámetros dinámicos de células B migrando en presencia de CXCL13. Células B primarias en contacto con membranas artificiales tapizadas con CXCL13 (100nM) y que contenían ICAM-1 o VCAM-1 a las densidades indicadas. Valores de velocidad media (A) y longitud de la trayectoria recorrida (B); cada punto corresponde a una célula; barra negra, valor promedio de la población de células B analizada. (C) Trayectorias descritas por células B en migración sobre membranas con ICAM-1 (150 molec/μm^2) y CXCL13. (D) Cuantificación de los niveles de expresión de ICAM-1 y VCAM-1 por unidad de superficie en la membrana de esplenocitos sin estimular o estimulados con TNFα por 20h. Datos mostrados en (A), (B) y (C) corresponden a tres experimentos. (B) es un experimento representativo (n=2). Barra gris, no detectado.

5.6. La intensidad de la señal a través del BCR regula el comportamiento de las células B en presencia de CXCL13

Para estudiar cómo afecta el encuentro con el antígeno a la migración de las células B en nuestro sistema de 2D, utilizamos ratones BCR transgénicos 3-83, cuyas células B expresan un BCR específico para el antígeno p31 (Ka = 65x10^6 M^{-1}); utilizamos distintas densidades de p31 presentadas en las membranas artificiales. En ausencia de p31, las frecuencias de migración y valores de velocidad media fueron equivalentes a los de células B WT (Fig. 19A y B). El reconocimiento de p31 alteró la migración de manera heterogénea; densidades elevadas de

antígeno (100 molec/μm^2) inhibieron migración, muy pocas células se desplazaron, mostrando velocidades medias muy bajas y recorridos muy cortos, con independencia de la presencia de CXCL13 (Fig. 19A, B y C). A una densidad cinco veces menor (20 molec/μm^2), un 30% de las células B era capaz de migrar. La frecuencia de migración fue similar al control (no p31) a densidades de antígeno de 4 molec/μm^2, aunque los valores de velocidad media eran significativamente inferiores a la situación control y las trayectorias más confinadas (Fig. 19A, B y C). Experimentos similares se realizaron con células B aisladas de ratones BCR-transgénicos MD4, y su antígeno específico HEL; los resultados obtenidos fueron análogos a los de células B 3-83 (datos no mostrados).

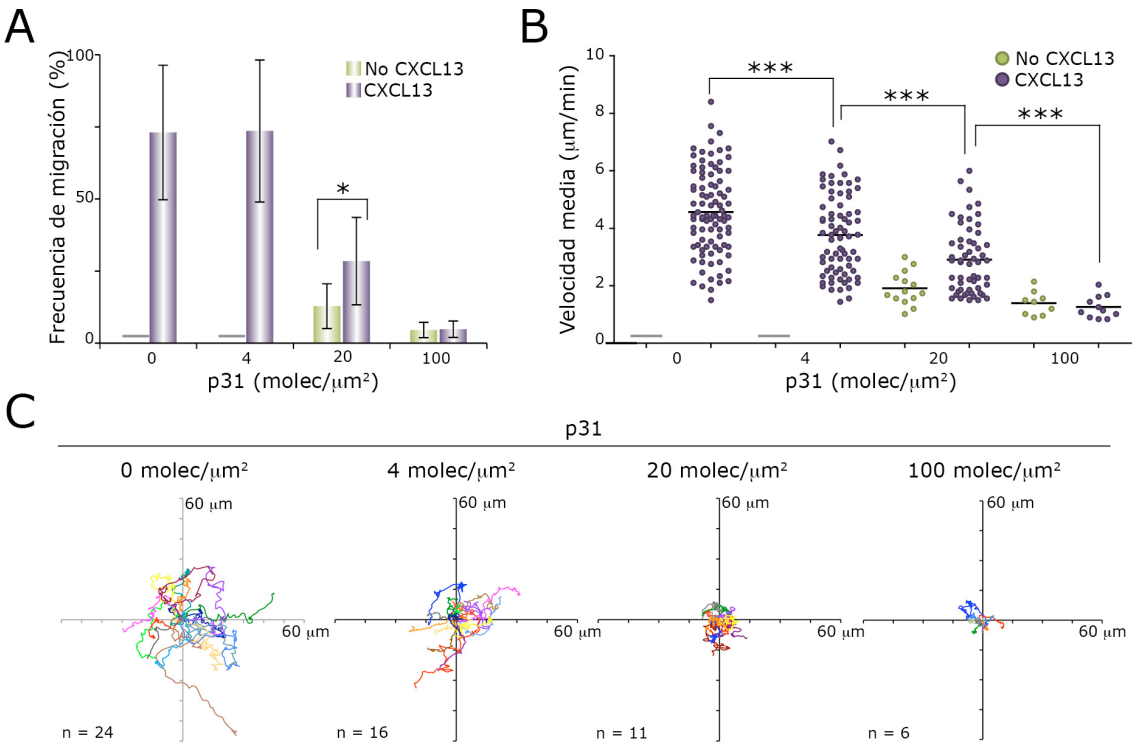

Figura 19. Migración de células B en respuesta a CXCL13 y en presencia de antígeno. Frecuencia de migración (A) y valores de velocidad media (B) de células B 3-83 sobre membranas que contiene p31 a las densidades indicadas, en ausencia o presencia de CXCL13. (C) Trayectorias de células B 3-83 en membranas con p31 a las densidades indicadas y en presenciad de CXCL13. Datos mostrados en (A) corresponden a la media ±SEM de 4 experimentos. Datos en (B) y (C) corresponden a tres experimentos. Barra gris, no detectado.

La intensidad de la señalización a través del BCR, que viene determinada por la densidad de antígeno y la afinidad del BCR por el mismo, modula por tanto la migración de las células B en respuesta a CXCL13, dando lugar a un rango de

comportamientos que van desde la parada total de la célula B hasta permitir migración a frecuencias similares a las observadas en ausencia de antígeno.

5.7.Efecto de CXCL13 sobre la formación de la SI en células B

Estudiamos cómo afecta CXCL13 a la formación de la SI de células B 3-83 tras el reconocimiento de p31 presentado en la membrana artificial. El establecimiento de la SI se evaluó mediante la detección del agregado central de antígeno (cSMAC) por microscopía confocal de fluorescencia, y del área de contacto de la célula B con la membrana por IRM, resultado de la formación de cSMAC (BCR/antígeno) y pSMAC (LFA-1/ICAM-1) (Fig. 20A; videos 2A-D).

La presencia de CXCL13 no alteró la frecuencia de SI observada a las distintas densidades de p31 (Fig. 20B); tampoco la cantidad de antígeno agregado en cada caso (Fig. 20C). Sin embargo, CXCL13 aumentó de manera significativa la frecuencia de células B que hacían contacto con la membrana (IRM^+) a densidades de 4 y 20 molec/μm^2 de p31, así como el tamaño del área de contacto en todo el rango de densidades de antígeno utilizadas (Fig. 20D y E). Los datos mostrados son similares a aquellos obtenidos con células B MD4 y el antígeno HEL (datos no mostrados).

Los resultados mostraban que, en presencia de antígeno, CXCL13 no afecta significativamente a la capacidad de las células B para establecer la SI, ni a la cantidad de antígeno que agregan en la misma. Sin embargo, CXCL13 fomenta la adhesión de la célula B con la membrana presentadora de antígeno; este aumento de adhesión podría favorecer la recepción de señales procedentes de la APC.

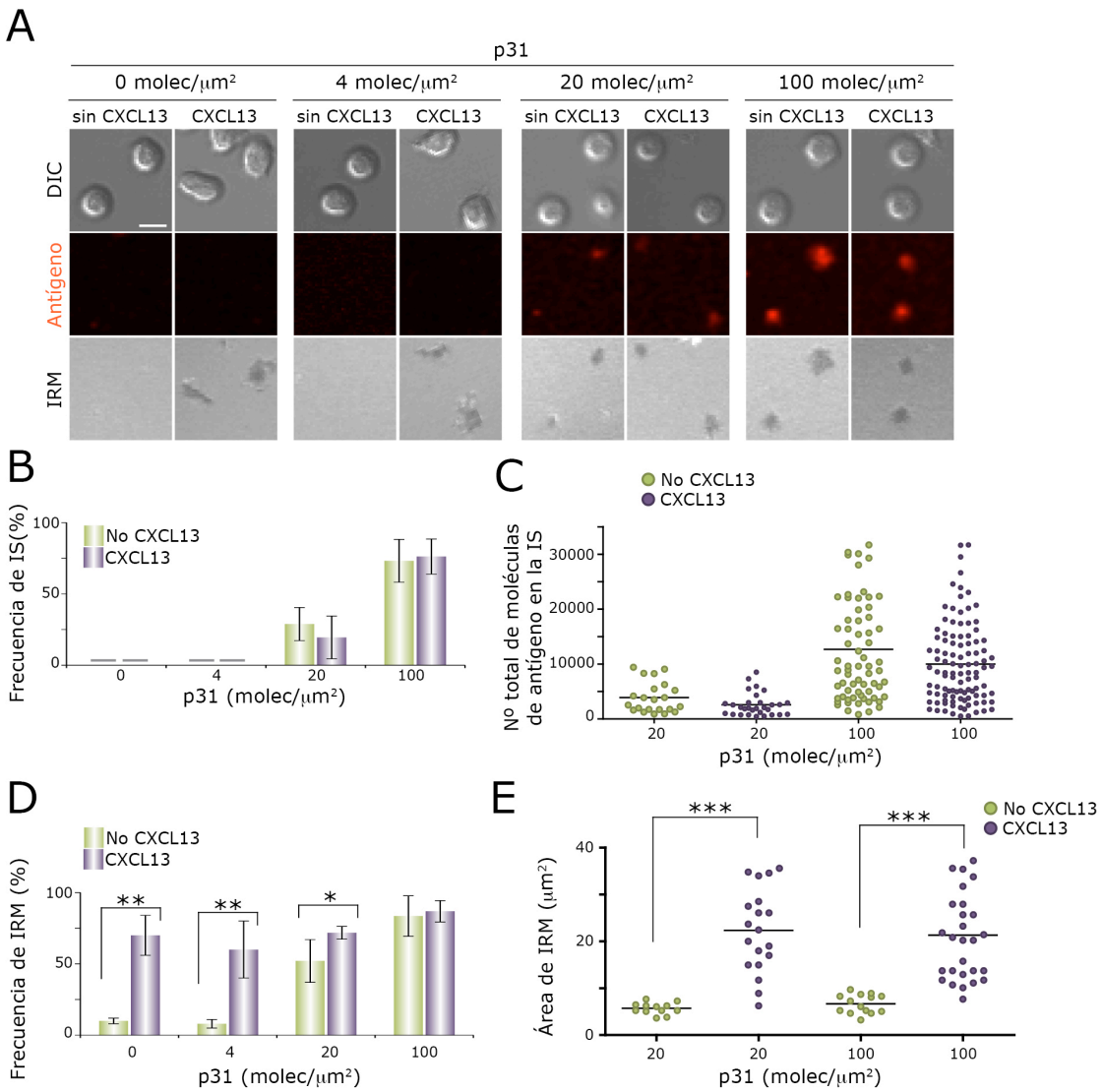

Figura 20. Formación de la SI en células B primarias en presencia de CXCL13. (A) Imágenes de DIC, antígeno e IRM de células B 3-83 representativas en contacto con membranas con ICAM-1 (150 molec/μm^2) y p31 a las densidades indicadas, en ausencia o presencia de CXCL13. (B) Frecuencia de formación de SI y (B) número total de moléculas de antígeno acumuladas en la SI establecida por células B 3-83. (D) Frecuencia de adhesión y (E) área de contacto (ambas estimadas por IRM) de células B 3-83. Los datos en (B) y (D) corresponden a la media ±SEM de 4 experimentos; en (C) corresponden a tres experimentos; en (E) se muestra un experimento representativo. Barra gris, no detectado. Barra de escala, 5μm.

5.8. Distribución de CXCR5 en células B en migración y en células B formando la SI

Quisimos analizar la distribución de CXCR5, receptor de CXCL13, en la superficie de células B en migración y formando la SI. Para ello, fusionamos CXCR5 con la proteína verde fluorescente (*Green Fluorescent Protein*, GFP), y transfectamos esta construcción (CXCR5-GFP) en la línea de células B A20. Transfectantes estables para CXCR5-GFP se pusieron en contacto con membranas artificiales que contenían ICAM-1, CXCL13, y en ausencia o presencia de antígeno (anticuerpo anti-κ, 20 molec/μm^2). Sólo un 20% de las células migraron en respuesta a CXCL13 (datos no mostrados). CXCR5-GFP presentaba una distribución bastante homogénea en el plano de contacto entre la célula y la membrana, aumentando su agregación (x2) en el borde del lamelipodio (Fig. 21A; video 3). En la SI, CXCR5 se situó en el pSMAC, siendo excluido del cSMAC (Fig. 21B y C; video 3); no obstante, CXCR5-GFP no era reclutado a la SI, como reflejó el análisis de la distribución de CXCR5 en todo el volumen celular (Fig. 21D).

Confirmamos estos datos en células B primarias en contacto con APC (células L que expresaban ICAM-1-GFP y la molécula de MHC-I H-$2K^K$, antígeno reconocido por el BCR de células B 3-83) por inmunofluorescencia (IF). CXCR5 se localizaba en el pSMAC, co-localizando con ICAM-1, y quedando excluido del cSMAC (Fig. 22A). Así mismo, no detectamos reclutamiento de CXCR5 a la zona de la SI (Fig. 22B).

Concluimos que CXCR5 no polariza a la zona de contacto de la célula B con el sustrato ni en migración ni en la SI. No obstante, CXCR5 está presente en el pSMAC de la SI.

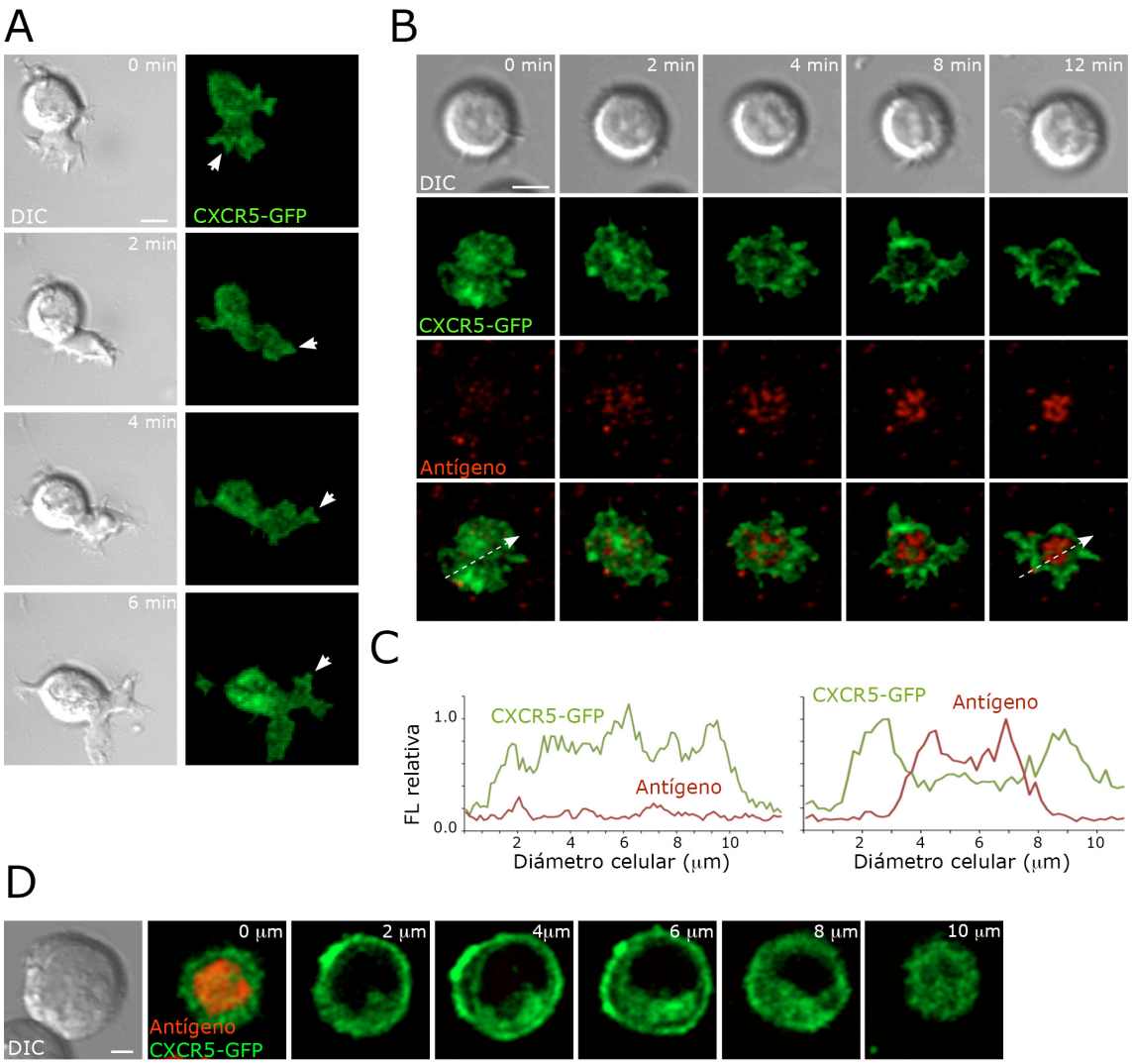

Figura 21. Distribución de CXCR5 en células B en migración y en la SI. Células B A20 expresando CXCR5-GFP en contacto con membranas artificiales que contienen ICAM-1, tapizadas con CXCL13, y en ausencia o presencia de antígeno (anti-κ; 20 molec/μm^2). (A) Imágenes de DIC y CXCR5-GFP en el plano de contacto de una célula B A20 representativa migrando en ausencia de antígeno. Flechas, indican agregados de CXCR5-GFP en los bordes del lamelipodio. (B) Imágenes de DIC, CXCR5-GFP y antígeno de una célula B A20 representativa formando la SI. (C) Perfiles de distribución de fluorescencia relativa de CXCR5-GFP (verde) y antígeno (rojo) en el plano de contacto de células B A20 a 0 minutos (izquierda; flecha en la parte inferior izquierda de la figura (B)) y 12 minutos (derecha; flecha en la parte inferior derecha de la figura (B)). (D) Imágenes seriadas en el plano (*x,y*) de CXCR5-GFP y antígeno, tomadas cada 2μm en el eje z de una célula B A20 representativa con una SI establecida. Barra de escala, 5 μm en (A) y (B), y 2 μm en (C).

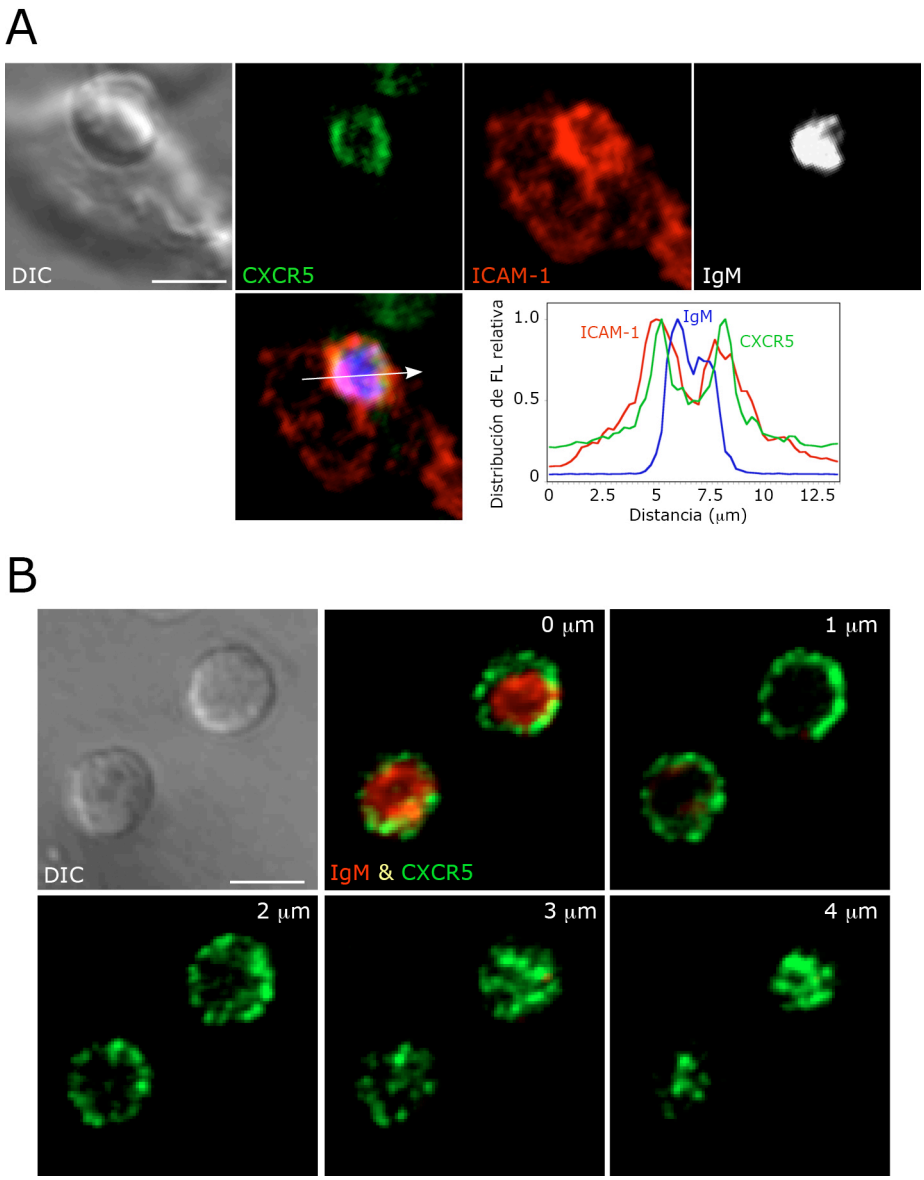

Figura 22. Distribución de CXCR5 en la SI de células B primarias. (A) Imágenes de DIC y de fluorescencia para CXCR5, ICAM-1-GFP e IgM en la SI entre una célula B 3-83 representativa y una APC (célula L transfectada con ICAM-1-GFP); las imágenes de fluorescencia mostradas corresponden a la proyección de tres secciones consecutivas del plano (x,y), de un grosor de 1 μm cada una en el eje z. Perfiles de distribución de la fluorescencia media relativa para ICAM-1-GFP (línea roja), CXCR5 (línea verde) e IgM (línea azul) en la SI (flecha en el panel inferior izquierdo). (B) Imágenes seriadas en el plano (*x,y*) de CXCR5 y antígeno, tomadas cada 1μm en el eje z de células B 3-83 representativas en contacto con APC. Barra de escala, 5 μm.

5.9. La estimulación por CXL13/CXCR5 aumenta la activación de las células B mediada por el BCR

LFA-1/ICAM-1 facilita la activación de las células B por antígeno al promover adhesión y formación de la SI (Carrasco et al, 2004). CXCL13/CXCR5 aumenta la adhesión mediada por LFA-1/ICAM-1 de células B a membranas que contienen

antígeno (Fig. 20). En base a estos datos, quisimos estudiar el efecto de CXCL13 en la activación de las células B mediada por antígeno. Para ello, cultivamos células B MD4 en contacto con membranas artificiales que contenían ICAM-1, antígeno HEL a distintas densidades, y en presencia o ausencia de CXCL13; 20h después, analizamos la expresión de CD69 y CD86 por citometría de flujo. La presencia de CXCL13 resultó en un aumento significativo del porcentaje de células B MD4 activadas ($CD86^{hi}$ $CD69^{+}$) a densidades medias y bajas de antígeno (4 y 1 molec/μm^2, respectivamente; Fig. 23). Datos similares se obtuvieron utilizando células B 3-83 y el antígeno p31 (datos no mostrados), o bien células B WT y anticuerpos anti-κ como antígeno (Fig. 24). Células B deficientes para CXCR5 no mostraron el aumento en activación (Fig. 24), lo cual indicaba que el efecto co-estimulatorio de CXCL13 era dependiente de la señalización a través de CXCR5.

CXCL13/CXCR5 aumenta por tanto la activación de las células B a través del BCR en condiciones limitantes de abundancia de antígeno.

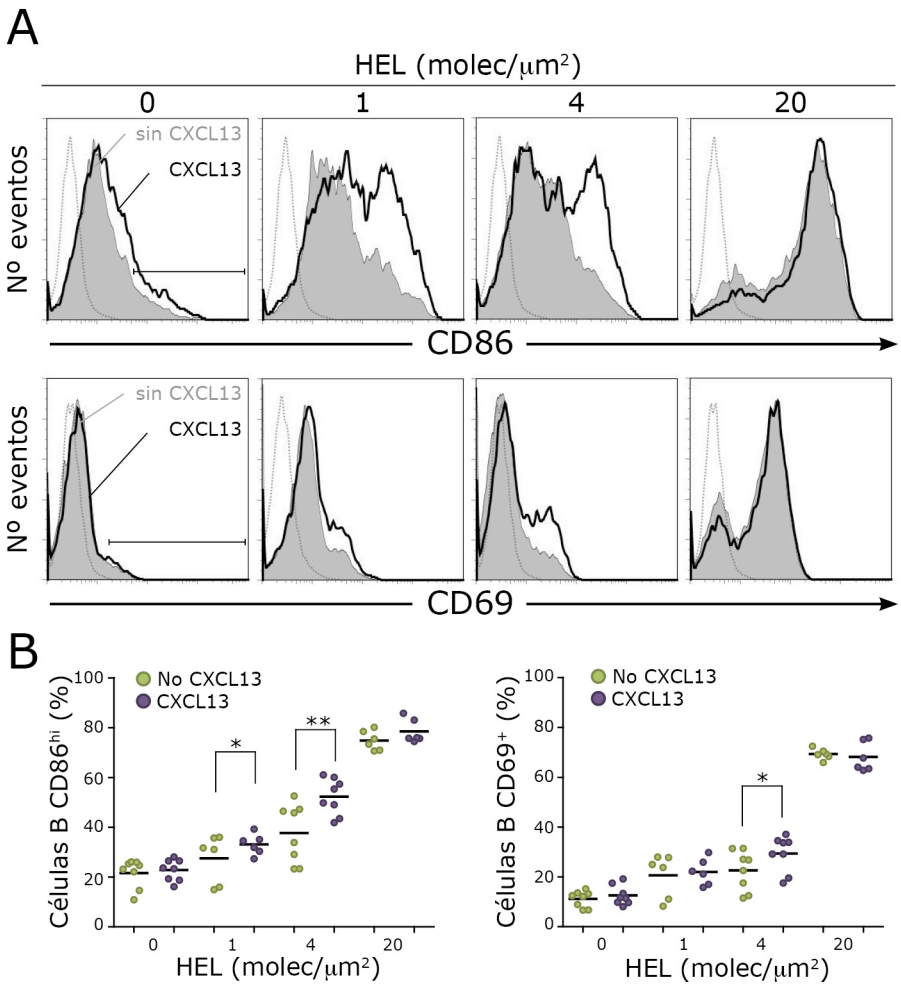

Figura 23. Efecto de la señalización de CXCL13 en la activación por antígeno de células B. (A) Niveles de expresión de CD86 (paneles superiores) y CD69 (paneles

inferiores) en células B MD4 incubadas sobre membranas artificiales con ICAM-1, HEL a las densidad especificadas, y en ausencia (histogramas en gris) o presencia de CXCL13 (línea negra); línea gris discontinua, control de isotipo; barra negra, células B CD86^{hi}CD69^{+}. Se muestra un experimento representativo. (B) Frecuencia de células B MD4 CD86^{hi} (panel de la izquierda) y CD69^{+} (panel de la derecha) en las mismas condiciones que en (A); cada punto representa un experimento.

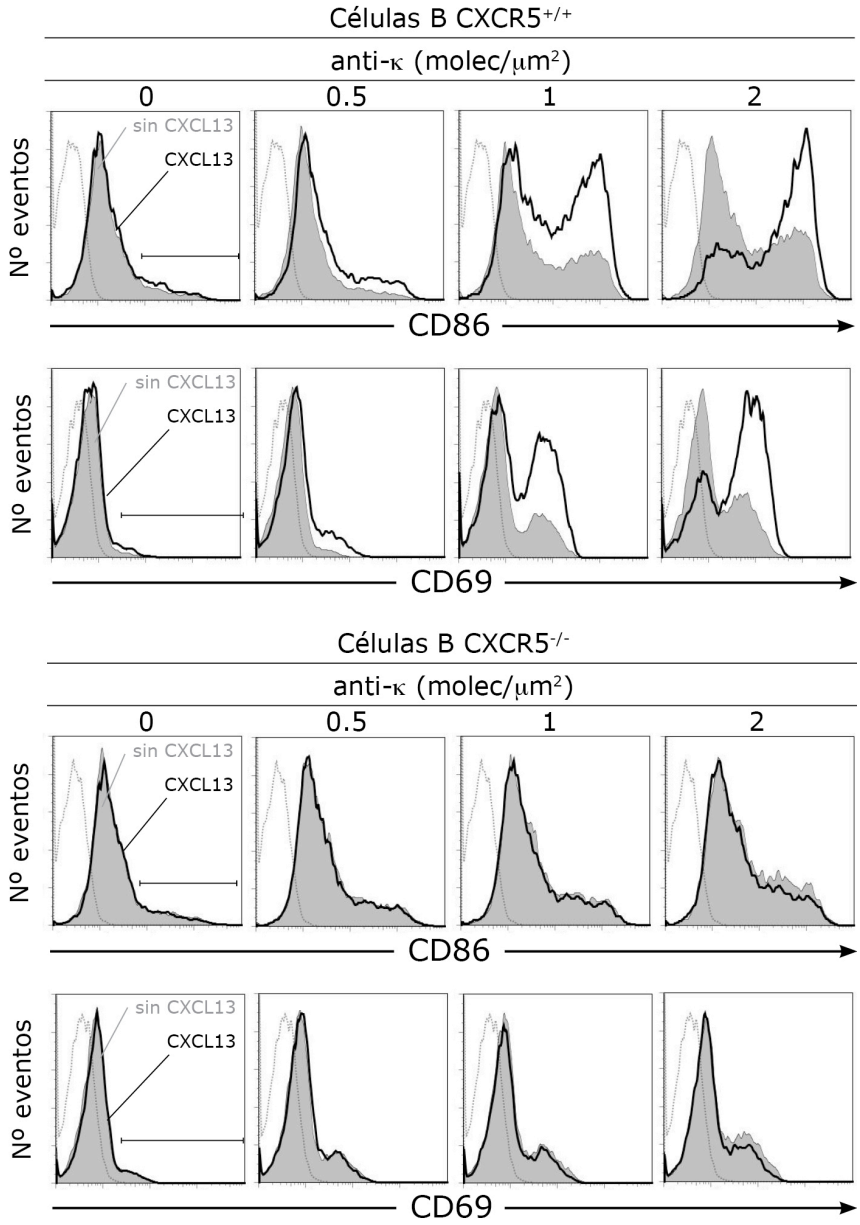

Figura 24. El efecto co-estimulador de CXCL13 es dependiente de su señalización a través de CXCR5. Niveles de expresión de CD86 y CD69 en células B CXCR5$^{+/+}$ (paneles superiores) y CXCR5$^{-/-}$ (paneles inferiores) incubadas sobre membranas artificiales con ICAM-1, antígeno (anti-κ) a las densidades especificadas y en ausencia (histogramas en gris) o presencia de CXCL13 (línea negra); línea gris discontinua, control de isotipo; barra negra, células B CD86^{hi}CD69^{+}. Los datos corresponden a un experimento representativo.

5.10. Mecanismos moleculares por los que CXCL13/CXCR5 aumenta la activación celular inducida por antígeno en células B

El efecto co-estimulatorio de CXCL13/CXCR5 lo observamos tanto en condiciones de densidad de antígeno que promovían la formación de la SI, como a densidades que permitían la migración en repuesta a CXCL13 (Fig. 19 y 20). Decidimos estudiar los mecanismos moleculares por los cuales CXCL13 aumentaba la activación por antígeno en ambos estadios dinámicos de las células B, migración y SI, de forma independiente.

5.10.1. Efecto de CXCL13/CXCR5 en células B formando la SI

CXCL13/CXCR5 aumentaba la adhesión mediada por LFA-1/ICAM-1 de las células B con la membrana presentadora de antígeno (Fig. 19). Monitorizamos el comportamiento de las células B MD4 con una SI establecida, en ausencia y en presencia de CXCL13. Observamos que la quimioquina promovía la formación continua de protusiones de membrana (*membrane ruffles*) en la célula B (observado por DIC) y el establecimiento de nuevas interacciones LFA-1/ICAM-1 (detectado por IRM) que permitían recolectar antígeno presente en las proximidades de la SI hacia el cSMAC (Fig. 25A; videos 4A y B). CXCL13 aumentó la frecuencia de células B en SI que emitían *membrane ruffles* en todas las densidades de HEL estudiadas (Fig.25B). En ausencia de ICAM-1 en la membrana artificial, las células B emitieron *membrane ruffles* pero éstos no entraron en contacto con la membrana (IRM^-) (Fig. 26A y B). La extensión de *membrane ruffles* fue totalmente dependiente de la señalización de CXCL13 a través de CXCR5 (Fig. 26C).

El citoesqueleto de actina es clave en la formación de protrusiones de membrana (lamelipodios y filopodios). El análisis de la actina filamentosa (F-actina) en la SI de las células B mediante tinción con Faloidina y microscopía confocal, reveló el anillo de F-actina característico del pSMAC, así como la presencia de F-actina en los *membrane ruffles* (Fig. 27A). El tratamiento de las células B en SI con Latrunculina A, droga que impide la polimerización de actina, inhibió la formación de *membrane ruffles* y la adhesión de la célula B a la membrana artificial (Fig. 27 B).

La proteína motora no muscular miosina-II (NM-II) media la contracción de los filamentos de actina y, con ello, de los *membrane ruffles* (Vicente-Manzanares et al, 2009). La actividad de NM-II depende de la fosforilación de sus cadenas ligeras (*Myosin Light Chains*, MLC). Mediante inmunofluorescencia, detectamos MLC fosforiladas (p-MLC) en la SI de las células B, tanto en los alrededores del cSMAC como en los *membrane ruffles* (Fig. 27A). El tratamiento con Blebbistatina, inhibidor químico de la actividad de NM-II, disminuyó la frecuencia de células B que

emitían *membrane ruffles*, sin alterar la adhesión de estas células a la membrana (Fig. 27B).

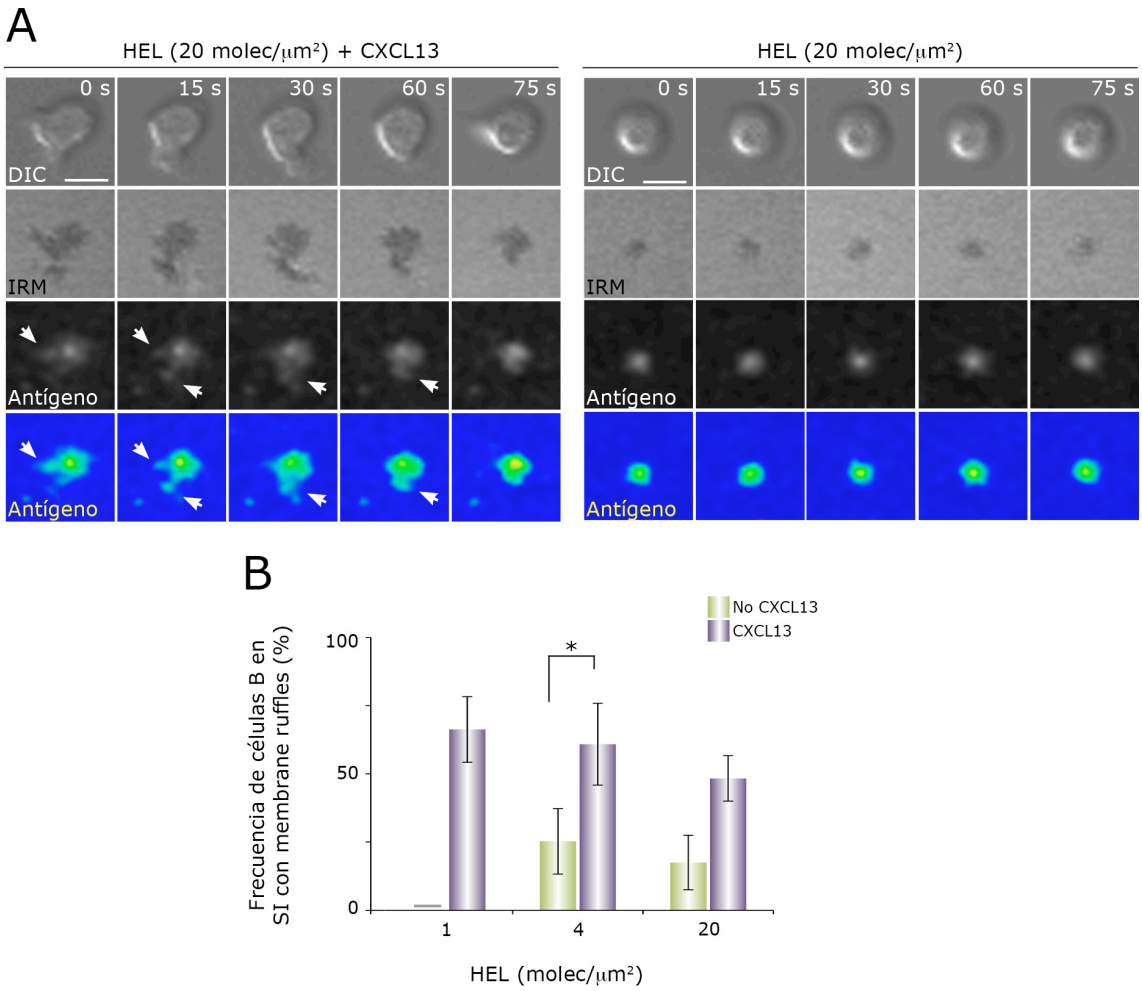

Figura 25. CXCL13/CXCR5 promueve la formación de *membrane ruffles* y nuevas interacciones LFA-1/ICAM-1 para aumentar la captación de antígeno a la SI de la célula B. (A) Imágenes de DIC, IRM y de fluorescencia para antígeno (en escala de grises y código de colores) en tiempo real de células B MD4 representativas sobre membranas con ICAM-1, HEL y en ausencia o presencia de CXCL13; las flechas blancas indican la captación de antígeno en la periferia de la SI. (B) Frecuencia de células B MD4 formando SI que muestran *membrane ruffles* sobre membranas en las mismas condiciones que en (A). Los datos corresponden a la media ±SEM de 4 experimentos; barra gris, no detectado; barra de escala, 5 μm.

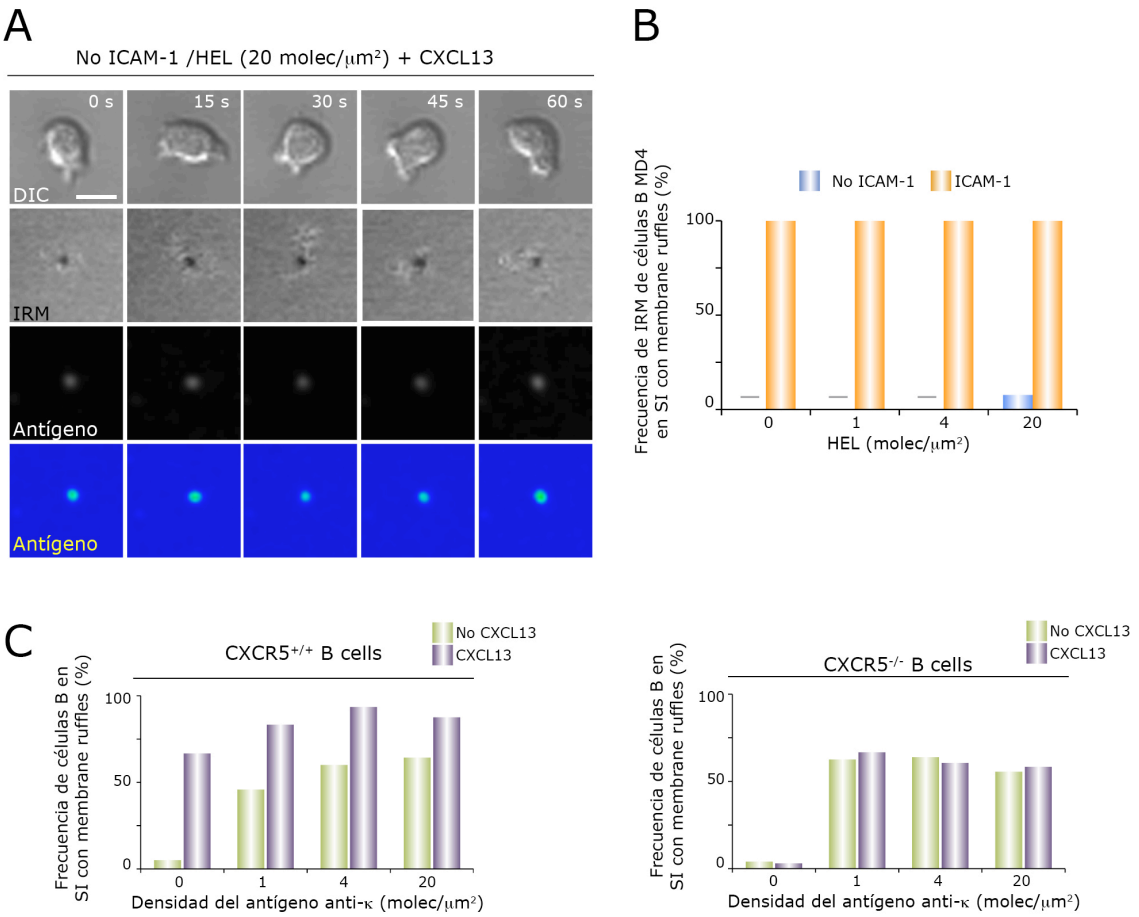

Figura 26. La captación de antígeno por *membrane ruffles* requiere de ICAM-1 y de la señalización por CXCR5. (A) Imágenes de DIC, IRM y de fluorescencia para antígeno (en escala de grises y código de colores) en tiempo real de una célula B MD4 representativa sobre membranas con HEL, CXCL13 y en ausencia de ICAM-1. (B) Frecuencia de contactos (estimados por IRM) realizados por los *membrane ruffles* de células B MD4 sobre membranas artificiales tapizadas con CXCL13, que contienen HEL a las densidades especificadas, y en ausencia o presencia de ICAM-1. (C) Frecuencia de células B CXCR5$^{+/+}$ (izquierda) y CXCR5$^{-/-}$ (derecha) en SI que muestran *membrane ruffles* sobre membranas con ICAM-1, antígeno (anti-κ) a las densidades especificadas, y en ausencia o presencia de CXCL13. Los datos mostrados en (B) y (C) corresponden a un experimento representativo en cada caso. Barra gris, no detectado; barra de escala, 5 μm.

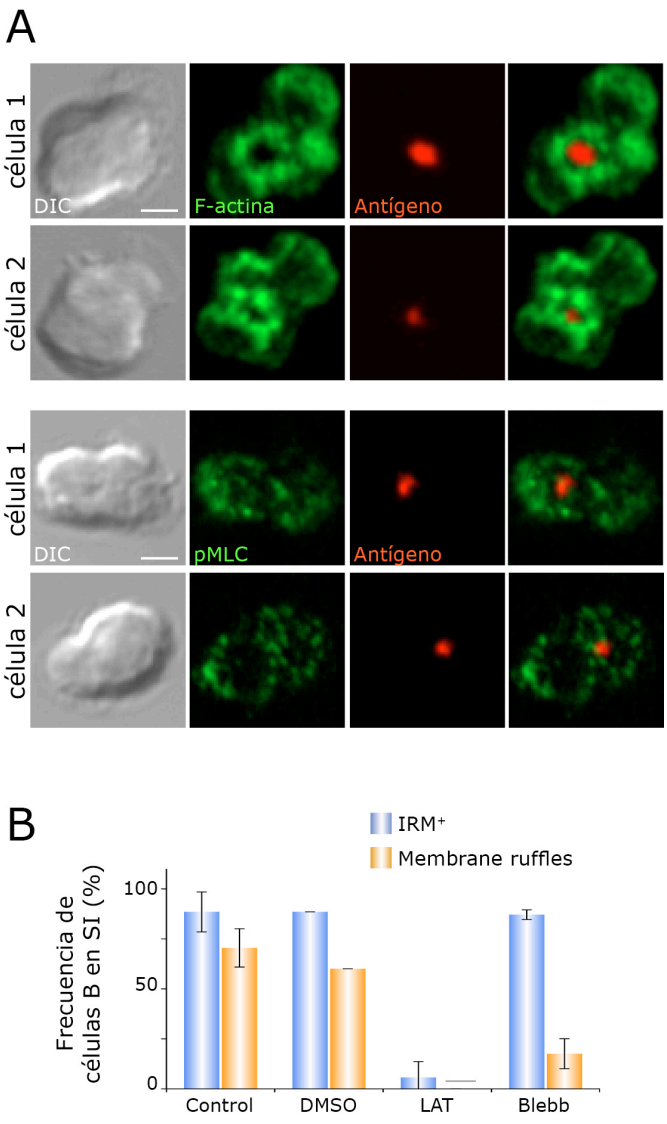

Figura 27. La formación de *membrane ruffles* mediada por CXCL13/CXCR5 en células B que forman SI depende del citoesqueleto de actina y de NM-II. (A) Imágenes de DIC y fluorescencia para F-actina, antígeno y p-MLC en el plano de la SI de células B MD4 representativas en contacto con membranas que contienen ICAM-1, CXCL13 y HEL (20 moléculas/μm^2); barra de escala, 2μm. (B) Frecuencia de células B MD4 en SI que muestran contacto con la membrana diana (estimado por IRM) y extienden *membrane ruffles* (estimado por DIC) sobre membranas que contienen ICAM-1, CXCL13 y HEL tras el tratamiento con DMSO, latrunculina A, blebistatina o no tratadas (control). Los datos corresponden a la media ±SEM de 4 experimentos; barra gris, no detectado; barra de escala, 2 μm.

Estos datos sugerían que CXCL13/CXCR5 aumenta la activación por antígeno de células B en SI al facilitar la captura de antígeno presente en los alrededores de la SI mediante la formación de *membrane ruffles*. Este proceso es dependiente del citoesqueleto de actina y de NM-II.

5.10.2. Efecto de CXCL13/CXCR5 en células B en migración

CXCL13/CXCR5 promovía la activación por antígeno en células B que no formaban una SI, sino que migraban en presencia de bajas dosis de antígeno (Fig. 19). Analizamos por inmunofluorescencia los niveles de la forma activa de Syk (forma fosforilada, p-Syk), quinasa implicada en la ruta de señalización a través del BCR y también de receptores de quimioquinas, en el plano de contacto de las células B con la membrana artificial. Los niveles de p-Syk fueron superiores en células B MD4 migrando en presencia de bajas dosis de antígeno (HEL, 1 molec/μm^2) en comparación a los niveles detectados sólo en presencia de CXCL13 (Fig. 28A); ello indicaba que las células B en migración estaban reconociendo antígeno a través del BCR. Monitorizamos la señalización por BCR durante la migración mediante la detección de flujos de calcio en tiempo real; para ello, marcamos las células B MD4 con la sonda Fluo4FF y medimos cambios en su fluorescencia por microscopía confocal. En presencia de CXCL13 y bajas densidades de HEL, las células B MD4 mostraron flujos detectables e intermitentes de calcio mientras migraban; sin la quimioquina, las células B flotaron sobre la membrana que contenía HEL y no se detectó señalización por calcio a través del BCR (Fig. 28B; video 5). La detección de señales de calcio intermitentes se observó en el 50% de las células B en migración, tanto en presencia como en ausencia de antígeno (Fig. 28C). Los receptores de quimioquinas señalizan también mediante flujos de calcio (Thelen & Stein, 2008). Sin embargo, la intensidad de los flujos de calcio intermitentes inducidos por CXCL13 sola fue inferior a la observada en presencia de bajas dosis de HEL y CXCL13 (Fig. 28D).

El citoesqueleto de actina y la NM-II son clave en la migración celular (Le Clainche & Carlier, 2008). Determinamos la presencia y distribución de F-actina y de la forma activa de las MLC (p-MLC) en el plano de contacto de las células B en migración sobre la membrana artificial. La F-actina se acumulaba principalmente en el lamelipodio, mientras que p-MLC estaba presente en toda la zona de contacto, mostrando una cierta acumulación hacia los bordes (Fig. 29A). El tratamiento con latrunculina A inhibió totalmente la migración de las células B en respuesta a CXCL13, así como la el contacto mediado por LFA-1/ICAM-1. La inhibición de NM-II mediante tratamiento con blebistatina también impidió migración, pero no la adhesión a la membrana (Fig. 29B).

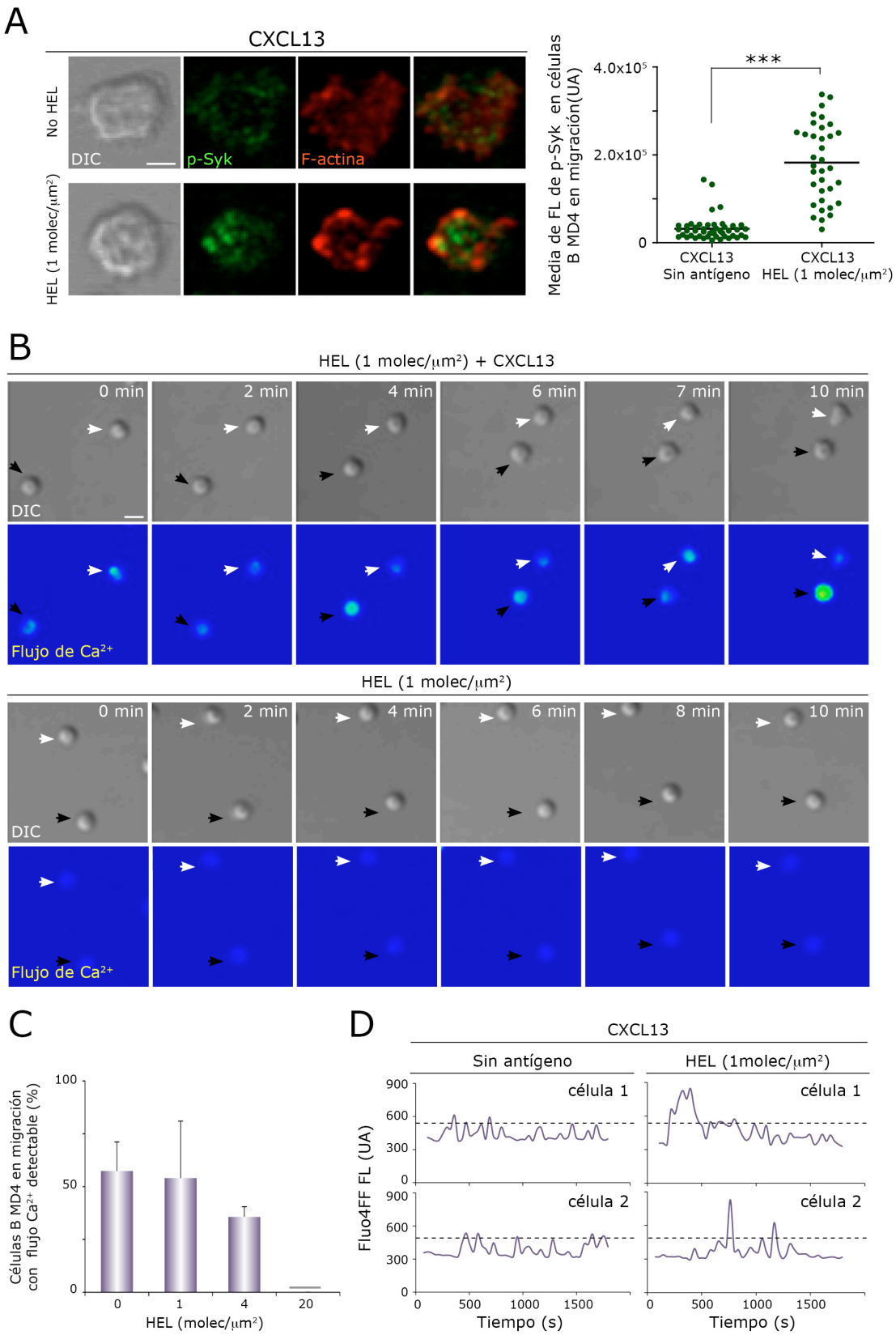

Figura 28. CXCL13/CXCR5 promueve el establecimiento de la kinapsis, estructura que facilita la integración de señales de antígeno a través del BCR en células B en movimiento. Células B MD4 en contacto con membranas que contienen ICAM-1, HEL a las densidades indicadas y tapizadas o no con CXCL13. (A) Imágenes de DIC y fluorescencia

para Syk fosforilado (p-Syk) y F-actina de células B MD4 representativas. Análisis cuantitativo de los niveles de p-Syk en la zona de contacto de células B MD4 con la membrana para cada condición (panel derecho); cada punto corresponde a una célula. (B) Imágenes en tiempo real de DIC y fluorescencia para Fluo4-FF (flujo de Ca^{2+}, en escala de código de color) de células B MD4 representativas en las condiciones indicadas; las flechas señalan células B monitorizadas en cada condición. (C) Frecuencia de células B MD4 en migración con flujo de Ca^{2+} detectable en las condiciones de HEL indicadas y en presencia de CXCL13. (D) Señal de flujo de Ca^{2+} de células B MD4 en migración representativas en cada condición; la línea negra discontinua indica el máximo de señal de Ca^{2+} detectado para CXCL13. Los datos en (C) representan la media ±SEM de 4 experimentos; barra gris, no detectado; barra de escala, 5 μm.

Por tanto, a densidades de antígeno incapaces de promover la formación de la SI, la migración celular inducida por CXCL13/CXCR5 permite el encuentro con el antígeno y la integración de señales a través del BCR. Para ello, CXCL13/CXCR5 media el establecimiento de una plataforma de migración mediada por la interacción LFA-1/ICAM-1, denominada *kinapsis*. El citoesqueleto de actina y NM-II son necesarios para su funcionalidad.

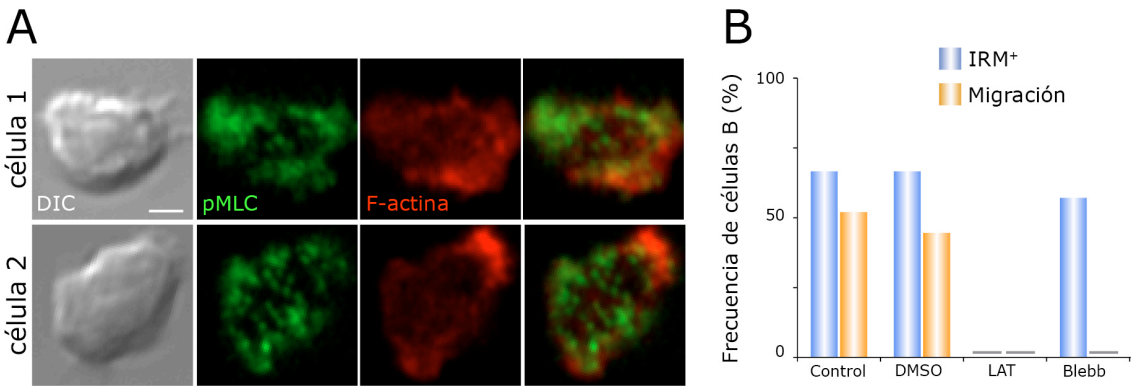

Figura 29. La formación de la kinapsis requiere del citoesqueleto de actina y de NM-II. (A) Imágenes de DIC y fluorescencia para F-actina y p-MLC de células B MD4 representativas sobre membranas que contienen ICAM-1 y CXCL13. (B) Frecuencias de contacto con la membrana (estimado por IRM) y migración (estimado por DIC) de células B primarias en contacto con membranas que contienen ICAM-1 y CXCL13 tras el tratamiento con DMSO, latrunculina A, blebistatina o no tratadas (control); se muestran datos de un experimento representativo; barra gris, no detectado; barra de escala, 2 μm.

5.11. La forma de presentación del antígeno determina la dinámica de las células B

Los datos mostrados en el apartado anterior indicaban que una célula B que migra sobre una membrana celular que contiene antígeno es capaz de integrar señales a través de su BCR. Pero, por encima de un umbral de densidad de antígeno y por tanto, de señalización a través del BCR, la célula B se detiene y establece una SI. Estudiamos los mecanismos moleculares responsables de dicha parada de la migración. La estimulación del BCR activa integrinas al promover el estado conformacional de alta-afinidad y su agregación o *clustering* en el pSMAC de la SI (Carrasco et al, 2004; Spaargaren et al, 2003). Con el objeto de analizar si la activación de LFA-1 a través del BCR era suficiente para detener la migración de la célula B, en ausencia del establecimiento de la SI, estimulamos células B MD4 con antígeno en forma soluble (sAg; anticuerpos anti-IgM, 1μg/ml) y en presencia de membranas artificiales que contenían ICAM-1 y CXCL13; monitorizamos su comportamiento por microscopía en tiempo real.

La capacidad de sAg para inducir adhesión mediada por LFA-1 (IRM^+) fue alta (>75%), independientemente de la presencia de CXCL13 (Fig. 30ª; video 6A y B); así mismo, observamos que la presencia de solo sAg inducía polarización en un 40% de las células B MD4 y apenas algo de migración (Fig. 30B). Sin embargo, y a diferencia de antígeno anclado a la membrana (*tethered-antigen*, tAg; HEL 20 molec/μm^2), sAg no alteró las frecuencias de polarización y migración de células B MD4 en respuesta a CXCL13 (Fig. 30B; video 6A y C), aunque sí redujo la velocidad de movimiento de forma significativa (Fig. 30C).

Comparamos la capacidad de sAg y tAg para activar a las células B por BCR. Para ello, analizamos los niveles de p-Syk en ambas condiciones por IF. La presencia de tAg supuso la formación de la SI, con la agregación central de antígeno (cSMAC) rodeada por el anillo de F-actina del pSMAC; p-Syk se localizó principalmente en el cSMAC (Fig. 25A). La activación de Syk se produjo principalmente en la zona de contacto entre la célula B y la membrana, como muestran los perfiles de fluorescencia de p-Syk en el plano de contacto y en el plano medio (Fig. 31A). Con sAg, la distribución de p-Syk fue bastante homogénea en la zona de contacto entre la célula B y la membrana; además, detectamos niveles similares de p-Syk en el plano de contacto y el plano medio (Fig. 31A). Cuantificamos los niveles de p-Syk en el plano de contacto y en todo el volumen celular, siendo en ambos casos significativamente superiores para tAg en comparación con sAg (Fig. 31B y C).

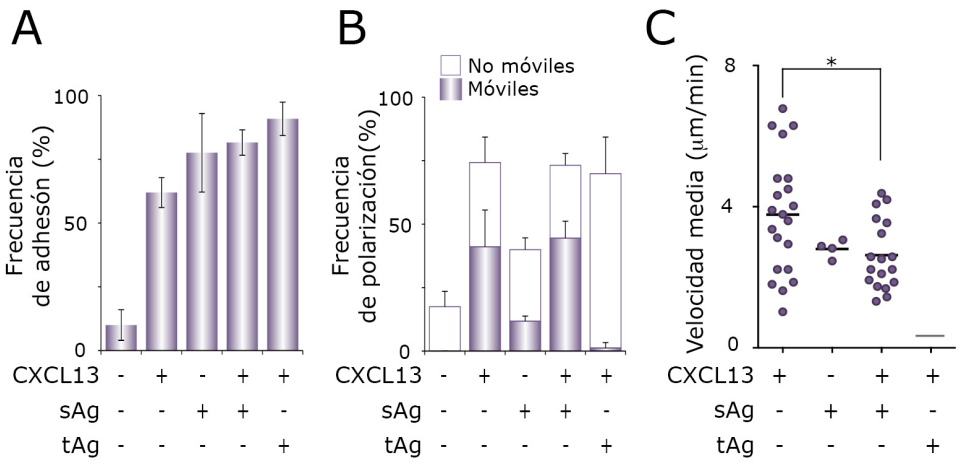

Figura 30. El establecimiento de la SI es necesario para detener la migración de las células B en respuesta a CXCL13. Células B primarias en contacto con membranas que contienen ICAM-1, CXCL13 y en ausencia o presencia de antígeno en forma soluble (sAg) o unido a la membrana (tethered Ag, tAg). (A) Frecuencias de adhesión (estimado por IRM), (B) polarización celular y migración (estimado por DIC) de células B en las condiciones de estimulación especificadas. (C) Valores de velocidad media de las células B que migran en (B); cada punto representa una única célula. Datos en (A) y (B) corresponden a 1 experimento representativo (n=3).

Los datos indicaban que es necesario el reconocimiento de antígeno presentado en la superficie de la APC y la formación de la SI para detener la migración de células B en respuesta a CXCL13; también sugerían que el *clustering* de LFA-1 en el pSMAC es importante para ello. Además, estos datos confirmaban trabajos de otros grupos al respecto de la mayor eficiencia del antígeno presentado sobre una membrana en comparación a su forma soluble para activar a la célula B a través del BCR.

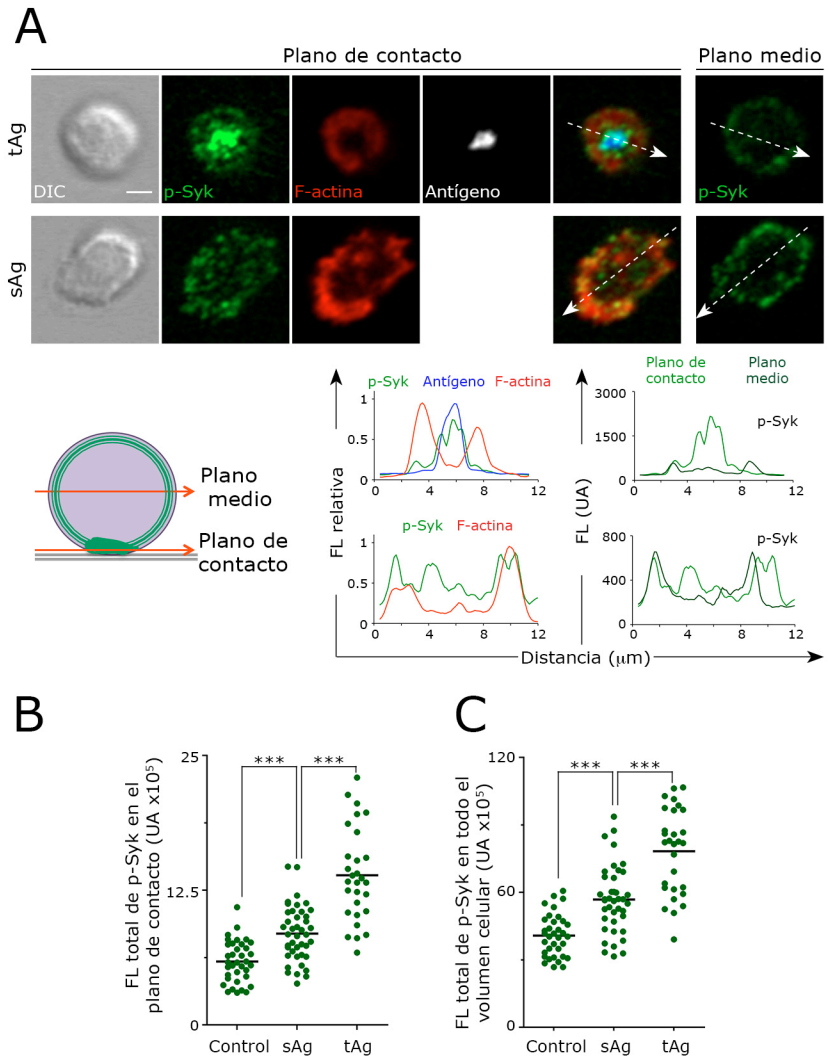

Figura 31. La señalización del tAg a través del BCR promueve la fosforilación de Syk localizada en la SI. Células B primarias en contacto con membranas que contienen ICAM-1, CXCL13 y en presencia de sAg o tAg. (A) Imágenes de DIC y fluorescencia para p-Syk, F-actina y antígeno en el plano de contacto y para p-Syk en el plano medio de células B representativas. Perfiles de distribución de la fluorescencia relativa de p-Syk, F-actina y antígeno en el plano de contacto (flecha en la imagen de *merge*) y perfiles de distribución de la fluorescencia de p-Syk en los planos de contacto y medio (flechas en las imágenes *merge* y del plano medio, respectivamente) en presencia de tAg y de sAg (paneles inferiores). (B) Valores de fluorescencia total de p-Syk en el plano de contacto y (C) en todo el volumen celular (en unidades arbitrarias, UA) de células B en ausencia de antígeno (control), con sAg o con tAg; cada punto representa una célula. Los datos de (B) y (C) corresponden a un experimento representativo (n=3). Barra de escala, 2 μm.

5.12. WASP regula la activación y/o localización de LFA-1 en la SI pero no la parada de las células B en migración

La proteína asociada al síndrome de Wiskott-Aldrich (WASP) está implicada en la polimerización de actina, y por tanto en procesos de polarización y migración celular en linfocitos. Está presente en la SI de células T y se la atribuye un papel en la parada de la migración y re-establecimiento de la SI (Sims et al, 2007). En células B, WASP es importante para los procesos de adhesión y migración (Meyer-Bahlburg et al, 2008; Westerberg et al, 2005). Quisimos estudiar el papel de WASP en el establecimiento de la SI en células B.

Analizamos la distribución de WASP en la SI de células B mediante IF. WASP se detectaba en todo el volumen celular, tanto en membrana como en citoplasma (datos no mostrados). WASP no se polarizó a la SI ni mostró una localización preferencial en alguno de sus dominios supramoleculares (Fig. 32A). Para interferir con la función de WASP, tratamos a las células B con wiskostatina (WKT), inhibidor químico de WASP. El tratamiento con WKT redujo el área de contacto de las células B con la membrana presentadora, sin alterar la frecuencia de células que hacían contacto (Fig. 32B y C); ello sugería una desorganización del pSMAC. El uso de WKT sin embargo inhibió totalmente la capacidad de las células B para migrar en respuesta a CXCL13, y para polarizarse en presencia de ambos estímulos, CXCL13 y tAg (Fig. 32C).

Algunos de los efectos producidos por WKT no son específicos de la ruta Cdc42-WASP-Arp2/3 (Bompard et al, 2008). Decidimos por tanto utilizar una aproximación genética al estudio del efecto de WASP en la dinámica de las células B en respuesta a CXCL13 y tAg, utilizando células B procedentes de ratones deficientes en la proteína WIP (*WASP interacting protein*). La mayoría de WASP está secuestrado por WIP; su asociación estabiliza a WASP, protegiéndola de la degradación por calpaína (de la Fuente et al, 2007). Así, los ratones deficientes en WIP tienen una reducción de hasta el 90% en WASP (Anton & Jones, 2006). Incubamos células B deficientes en WIP ($WIP^{-/-}$) y células B WT, teñidas con diferentes sondas fluorescentes, sobre membranas que contenían ICAM-1, CXCL13 y tAg. Ambos tipos de células B formaron la SI, observándose un área de contacto menor en las células B $WIP^{-/-}$ (Fig. 32D). La ausencia de WIP no alteró la frecuencia de células B que migraban en respuesta a CXCL13 y en ausencia de tAg, comparada con la de las células B WT; sin embargo, no se recuperó la capacidad de migración de las células B $WIP^{-/-}$ que establecieron SI (Fig. 32D).

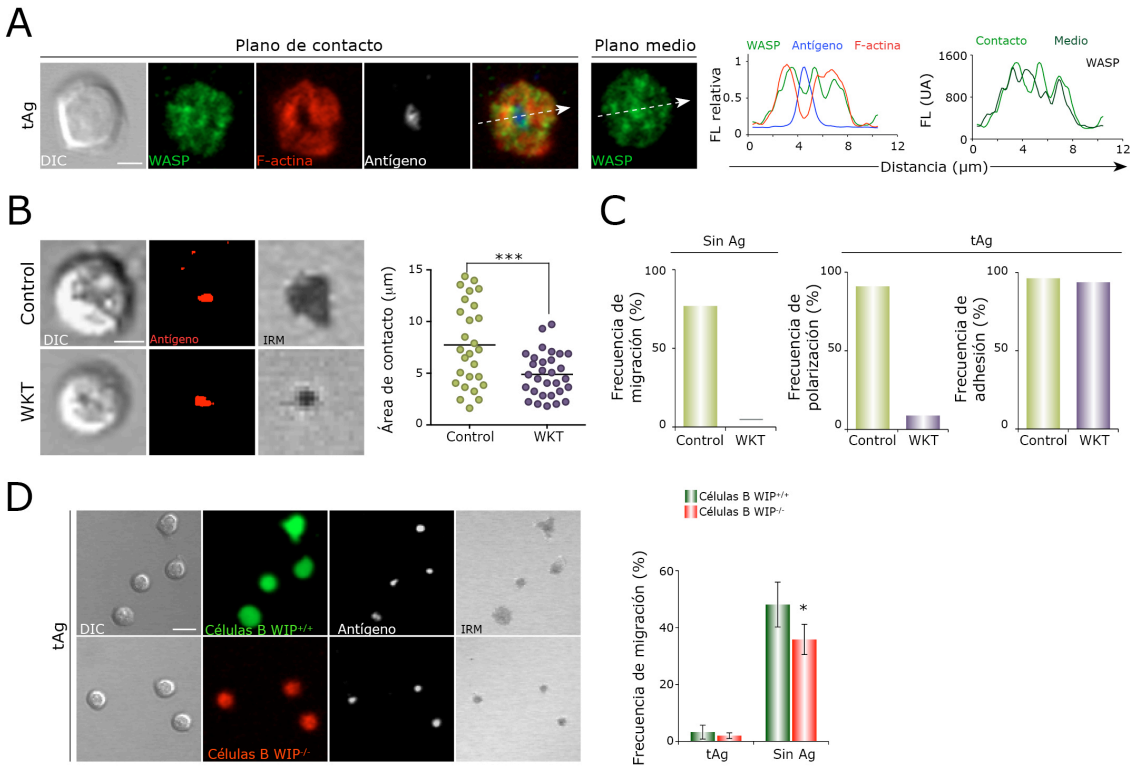

Figura 32. La alteración de la función de WASP afecta al pSMAC de la SI. (A) Imágenes de DIC y fluorescencia para WASP, F-actina y antígeno en el plano de contacto y para WASP en el plano medio de una célula B primaria representativa en membranas con ICAM-1, CXCL13 y tAg. Perfiles de distribución de la fluorescencia relativa de WASP, F-actina y antígeno en el plano de contacto (flecha en la imagen *merge*) y de WASP en los planos de contacto y medio (flechas en las imágenes merge y del plano medio, respectivamente) (paneles a la derecha). (B) Imágenes de DIC, IRM y de fluorescencia para antígeno de células B representativas no tratadas (Control) o tratadas con wiskostatina (WKT) sobre membranas que contienen tAg (paneles izquierdos). Cuantificación del área de contacto (determinada de IRM) entre la célula B y la membrana para cada condición indicada; cada punto corresponde a una célula (derecha). (C) Frecuencias de migración en ausencia de antígeno (Sin Ag) y de polarización y adhesión en presencia de tAg de células B no tratadas (Control) o tratadas con wiskostatina (WKT). (D) Imágenes de DIC, IRM y de fluorescencia para antígeno de células B $WIP^{+/+}$ (verdes) y $WIP^{-/-}$ (células rojas) sobre membranas con ICAM-1, CXCL13 y tAg (paneles izquierdos). Frecuencia de migración de células B $WIP^{+/+}$ y $WIP^{-/-}$ en ausencia o presencia de tAg. Los datos en (B), (C) y (D) corresponden a experimentos representativos (n=3). Barra gris, no detectado; barra de escala, 2 µm en (A) y (B), 5 µm en (D).

Los datos sugerían que WASP/WIP están implicados en la activación de las integrinas y/o en la formación del pSMAC en células B. Sin embargo, no parecen ser responsables de la parada de la migración de las células B promovida por tAg/BCR y la SI.

5.13. Vinculina se localiza en el pSMAC de la SI de las célula B

La SI es una plataforma de adhesión mediada por integrinas para el contacto estable de linfocitos con otras células. Las adhesiones focales (AF) son estructuras mediadas también por integrinas que permiten la unión de otros tipos celulares no-inmunes a la matriz extracelular. La proteína vinculina estabiliza las AF conectando las integrinas en su conformación activa con el citoesqueleto de actina mediante su unión con talina (Carisey & Ballestrem, 2010).

Con el fin de analizar el papel de vinculina en la regulación de la dinámica de las células B por BCR y CXCL13, determinamos la presencia y distribución de vinculina, junto con talina y F-actina en la SI de células B. Para la detección de vinculina, utilizamos un anticuerpo que reconoce específicamente la vinculina que se encuentra en zonas de contacto entre célula y célula o bien entre célula y sustrato, y que por tanto se encuentra en su conformación activa (Chen et al, 2005). Observamos reclutamiento de vinculina a la SI, al igual que para talina; vinculina se localizó en el pSMAC, coincidiendo con el anillo de F-actina (Fig. 33A). El patrón de vinculina fue muy diferente en células B estimuladas con sAg; vinculina no se localizó hacia la zona de contacto de la célula B con la membrana, presentando una distribución heterogénea (Fig. 33B). La cuantificación de vinculina y F-actina mostró una acumulación significativamente mayor para ambas en el plano de la SI en comparación al plano de contacto de la célula B con la membrana en presencia de sAg (Fig. 33C). Por tanto, el reconocimiento de tAg a través del BCR induce el reclutamiento de vinculina a la SI de células B y su localización en el pSMAC, junto con integrinas, F-actina y talina.

5.14. Reclutamiento de vinculina durante el establecimiento de la SI

Analizamos el reclutamiento de vinculina a la SI, junto con la polimerización de actina en tiempo real. Transfectamos células B A20 con vinculina-GFP y LifeAct fusionado con la proteína roja fluorescencte (RFP), y 24h después las pusimos en contacto con membranas que contenían ICAM-1, CXCL13 y tAg. Vinculina se fue acumulando gradualmente durante los primeros 3-4 min de formación de la SI, manteniendo luego unos niveles constantes mientras se localizaba en el pSMAC (Fig. 34A y B; video 7). Esta acumulación de vinculina se produjo una vez la célula B había entrado en contacto con la membrana, y por tanto activado integrinas. Observamos una polimerización de actina intensa durante los 2.5 min iniciales, que fue seguida de una reestructuración para formar el pSMAC, coincidiendo con la segregación de vinculina (Fig. 34A y B).

PIP_2 es producido localmente en las AF por PIPKIγ, y está implicado en la activación y el reclutamiento de vinculina a las AF. Estudiamos la dinámica molecular de PIPKIγ y PIP_2 en la SI de células B y su posible relación con el reclutamiento y/o activación de vinculina. Para ello, transfectamos células B de la línea A20 con la construcción PIPKIγ-GFP y con el dominio PH de la PLCδ unido a GFP, como sonda para detectar PIP_2. Después de 24h, analizamos el comportamiento de ambas moléculas durante la formación de la SI sobre membranas artificiales que contenían ICAM-1, CXCL13 y tAg. Para evitar el efecto debido a la sobre-expresión de PIPKIγ o al secuestro masivo de PIP_2, excluimos de nuestro análisis aquellos transfectantes con niveles altos de GFP.

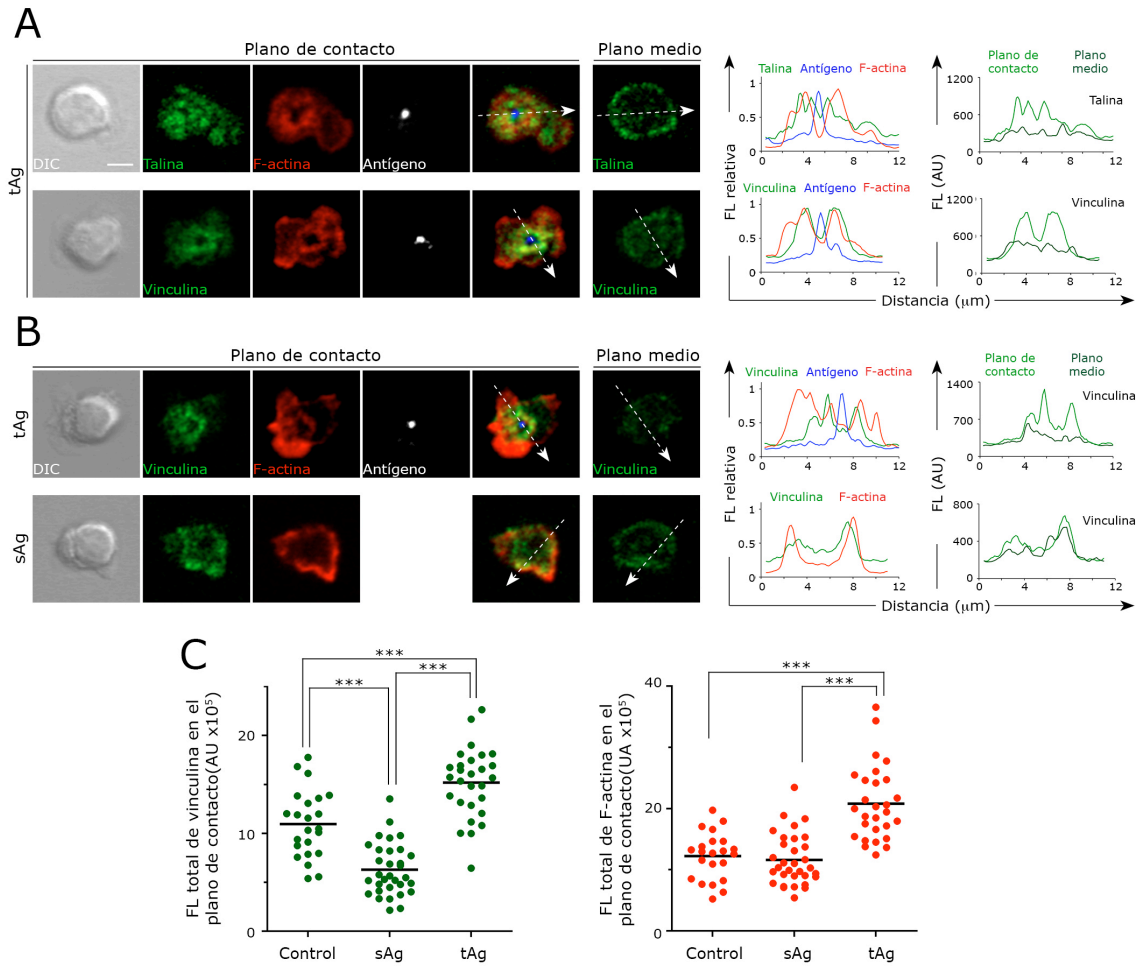

Figura 33. El reconocimiento de tAg a través del BCR promueve la localización de vinculina a la SI de la célula B. Células B MD4 en contacto con membranas que contienen ICAM-1, CXCL13 y en presencia de sAg o tAg. (A) Imágenes de DIC y fluorescencia para vinculina, talina, F-actina y antígeno en el plano de contacto, y para vinculina y talina en el plano medio de células B MD4 representativas en presencia de tAg. Perfiles de distribución de la fluorescencia relativa de vinculina, talina, F-actina y antígeno en el plano de contacto (flecha en la imagen de *merge*) y perfiles de distribución de fluorescencia (en unidades arbitrarias, UA) de vinculina y talina en los planos de contacto y medio (flechas en la imagen

de *merge* y en el plano medio, respectivamente). (B) Imágenes de DIC y fluorescencia para vinculina, F-actina y antígeno en el plano de contacto, y para vinculina en el plano medio de células B MD4 representativas en presencia de tAg o sAg. Perfiles de distribución de la fluorescencia relativa para vinculina, F-actina y antígeno en el plano de contacto (flecha en la imagen de *merge*) y perfiles de distribución de fluorescencia de vinculina en los planos de contacto y medio (flechas en la imagen de *merge* y en el plano medio, respectivamente). (C) Valores de fluorescencia total de vinculina y F-actina en el plano de contacto de la célula B MD4 con la membrana en ausencia (control) o presencia de sAg o tAg; cada punto representa una célula. Los datos corresponden a un experimento representativo (n=3). Barra de escala, 2 μm.

Durante los primeros dos minutos de formación de la SI, PIPKI γ incrementó sus niveles de forma transitoria, con un reclutamiento máximo a los 30 s, coincidiendo con el primer contacto de la células B A20 con la membrana (observado por IRM) y la formación de agregados de antígeno. (Fig. 35A; video 8). La dinámica de PIP_2 fue similar a la de PIPKIγ, con un pico de producción posterior al de reclutamiento de la quinasa (2.5 min) (Fig. 35B; video 9). PIPKIγ y PIP_2 recuperaron niveles basales similares a los detectados en el resto de la célula (datos no mostrados). La presencia de CXCL13 sola no supuso el reclutamiento de PIPKIγ ni el incremento de producción de PIP_2 en el plano de contacto de la célula B con la membrana (Fig. 35A y B). PIPKIγ y PIP_2 permanecieron en el pSMAC de la SI madura (Fig. 35C y D), co-localizando con vinculina, actina y LFA-1 activa.

Los datos en tiempo real sugerían que una célula B al entrar en contacto con una membrana que presenta antígeno, su reconocimiento a través del BCR promueve el rápido reclutamiento de PIPKIγ para la producción local y transitoria de PIP_2. Ello conduce al reclutamiento gradual de vinculina a la zona de contacto de la célula B con la APC, y su segregación al pSMAC. La permanencia de PIPKIγ y PIP_2 en el pSMAC de la SI madura pudiera estar implicada en mantener la conformación activa de vinculina.

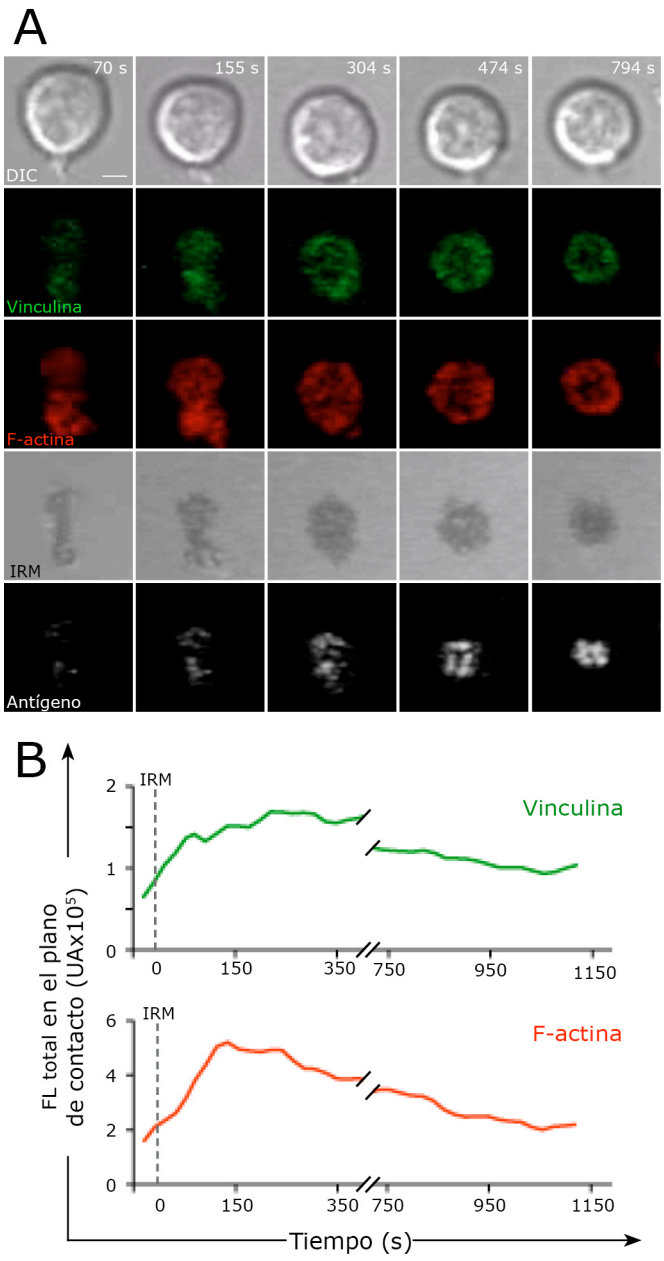

Figura 34 Reclutamiento de vinculina en las fases tempranas de formación de la SI. Células B A20 co-transfectadas con vinculina-GFP y la sonda para F-actina Lifeact-RFP en contacto con membranas que contienen ICAM-1, CXCL13 y tAg. (A) Imágenes en tiempo real de DIC, IRM y fluorescencia para vinculina y F-actina durante la formación de la SI de una célula B A20 representativa (paneles superiores). Valores de fluorescencia de vinculina y F-actina en el plano de interacción entre la célula B A20 y la membrana. La línea discontinua indica el inicio de la interacción de la célula B con la membrana (detectado por IRM; considerado tiempo cero). Barra de escala, 2 mm.

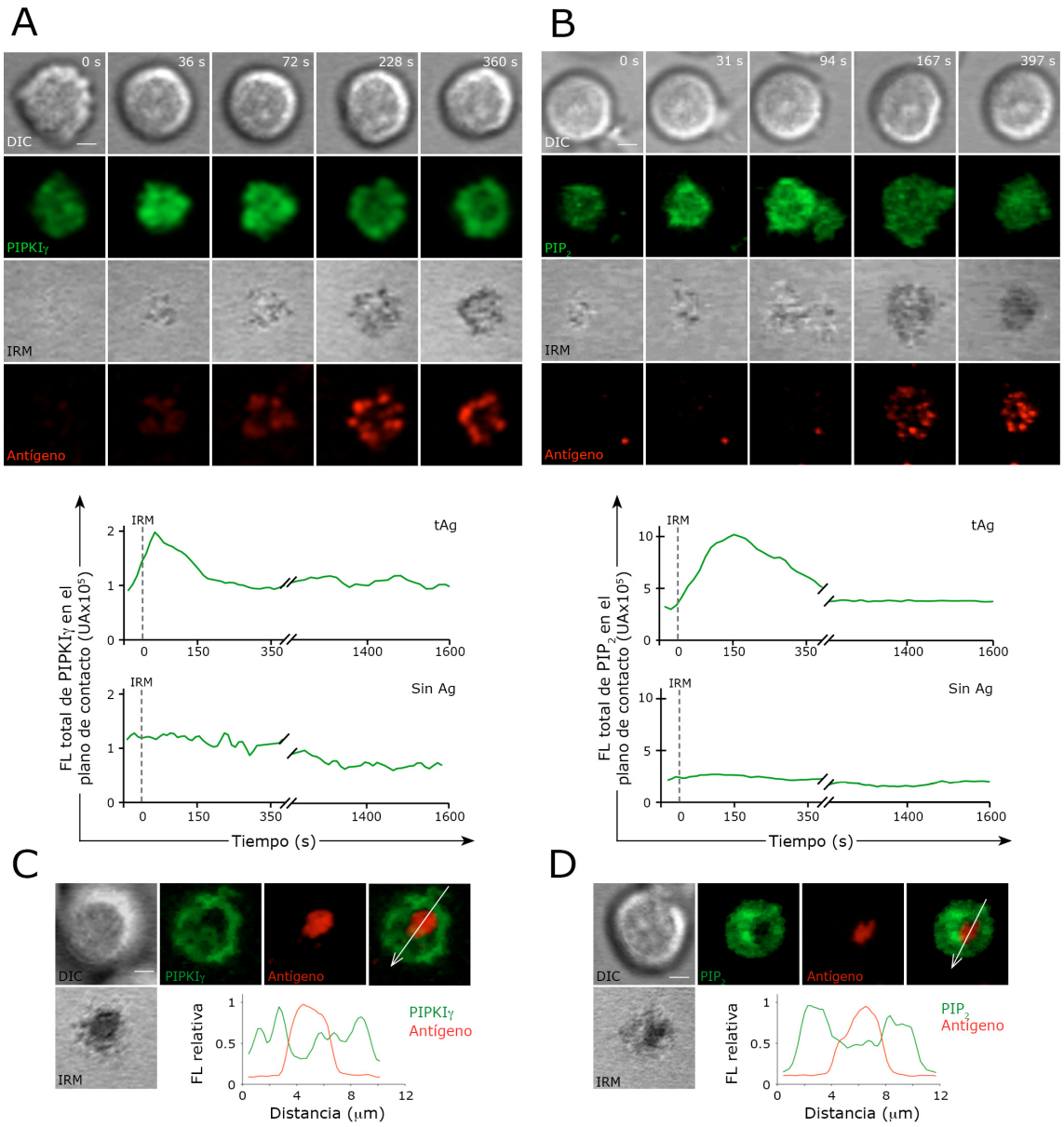

Figura 35. El reclutamiento de PIPKIγ y la producción de PIP_2 ocurren en estadios tempranos del establecimiento de la SI. Células B A20 transfectadas con PIPKIγ-GFP o la sonda para PIP_2 PLCδ-PH-GFP en contacto con membranas que contienen ICAM-1, CXCL13 y en ausencia o presencia de tAg. (A) Imágenes en tiempo real de DIC, IRM y fluorescencia para PIPKIγ y antígeno durante la formación de la SI de una célula B A20 representativa. Valores de fluorescencia de PIPKIγ en el plano de interacción entre la célula B A20 y la membrana, en ausencia (gráfico inferior) o presencia de tAg (gráfico superior). La línea discontinua indica el inicio de la interacción de la célula B con la membrana (detectado por IRM; considerado tiempo cero). (B) Imágenes en tiempo real de DIC, IRM y fluorescencia para PIP_2 y antígeno de una célula B A20 representativa. Valores de fluorescencia de PIP_2, como se indica en (A). (C) Imágenes de DIC, IRM y fluorescencia para PIPKIγ y antígeno de una célula B A20 representativa en SI. Perfil de distribución de la fluorescencia relativa para PIPKIγ y antígeno en el plano de contacto (flecha en la imagen de *merge*). (D) Imágenes de DIC, IRM y fluorescencia para PIP_2 y antígeno de una célula B A20 representativa formando SI. Perfil de distribución de fluorescencia relativa para PIP_2 y antígeno en el plano de contacto (flecha en la imagen de *merge*). Barra de escala, 2 μm.

5.15. Un reclutamiento deficiente de vinculina permite a las células B migrar en presencia de tAg

Decidimos estudiar de forma directa el papel de vinculina en la parada por tAg de las células B en migración mediante una aproximación genética, utilizando ARN de interferencia para reducir los niveles de expresión de vinculina. Las células B primarias son muy sensibles a los diferentes procedimientos de transfección celular, por lo que intentamos infectarlas con partículas lentivirales portadoras de ADN codificante para un shARN (*short hairpin* ARN) específico para vinculina de ratón. Usamos dos tipos de vectores lentivirales de expresión (pGIPZ y pLKO.1) y distintos shRNA específicos para vinculina (ver métodos). Infectamos células B WT con partículas lentivirales en ausencia o presencia de diferentes estímulos (IL-4, CpG, LPS), y 48h después analizamos los niveles de expresión de vinculina por *western-blot* (WB). Los estímulos CpG y LPS favorecieron la infección de las células B WT, determinada por los niveles de expresión de GFP; no se observó sin embargo reducción en la expresión de vinculina con ninguno de los shARN probados (Fig. 36A y datos no mostrados). Tampoco disminuyó la expresión de vinculina en las células B WT infectadas con particulas virales portadoras de pLKO.1 en presencia de LPS; se probaron tres shARN diferentes (Fig. 36B y datos no mostrados). Los resultados fueron similares con la línea de células B A20 (Fig. 36C).

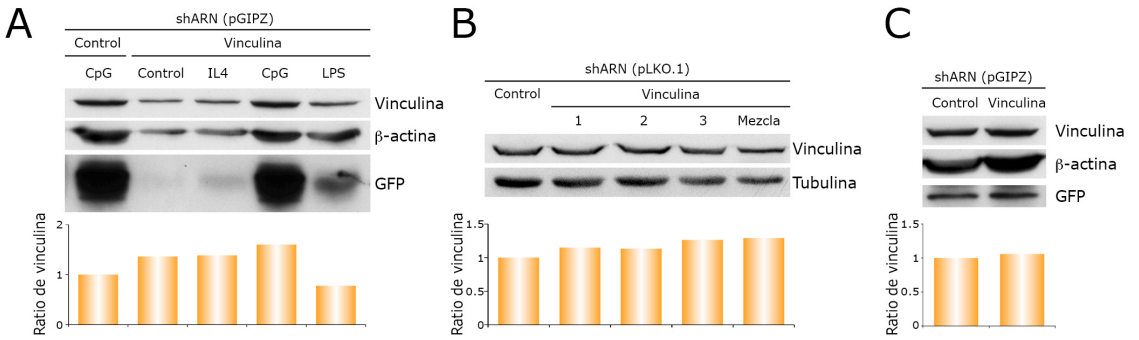

Figura 36. Infección de células B con partículas lentivirales para reducir la expresión de vinculina. (A) Niveles de vinculina endógena y de GFP en células B primarias en presencia de los estímulos indicados, detectadas por western blot 48h después de la infección con partículas lentivirales que codifican para un shARN que no silencia (Control) o que silencia vinculina (clon V2LMM_56452) en el vector pGIPZ; β-actin, control de carga. Cuantificación de los niveles de vinculina para cada condición comparados con el control (panel inferior). (B) Niveles de vinculina en células B primarias 48h tras su infección en presencia de CpG, usando partículas lentivirales que no silencian (Control) o que silencian vinculina (1, clon NM_009502.3-3466s1c1; 2, clon NM_009502.3-1331s1c1; 3, clon NM_009502.3-3154s1c1; Mezcla, los tres clones); vector codificante pLKO.1. Tubulina, control de carga. Cuantificación de los niveles de vinculina para cada condición comparados con el control (panel inferior). (C) Niveles de vinculina en células B A20 48h después de ser electroporadas con vectores pGIPZ que codifican shARN no silenciante (Control) o que silencia vinculina (clon V2LMM_56452). Cuantificación de los niveles de vinculina para cada

condición comparados con el control (inferior). Los datos corresponden a un experimento representativo de cinco en (A) y (B), y de dos en (C).

Diseñamos otra aproximación para interferir con la función de vinculina en la SI. El reclutamiento de vinculina a la SI se asociaba con una fuerte estimulación local de Syk (p-Syk) por la señalización de tAg/BCR (Fig. 31 y 33). Utilizamos el inhibidor químico BAY 61-3603 (BAY) para alterar la función de Syk. Inicialmente tratamos células B WT con distintas dosis de BAY (de 1 a 0.1 μM), las estimulamos por BCR y analizamos el grado de inhibición de la actividad de Syk mediante la detección de ERK fosforilado (p-Erk), efector en la ruta de señalización de Syk, por WB. Además, y dado que las quimioquinas señalizan a través de Syk, también evaluamos la migración en respuesta a CXCL13 de células B WT tratadas con BAY en membranas que contenían ICAM-1. Concentraciones de 1-0.6 μM inhibieron totalmente la actividad de Syk por BCR y alteraron frecuencia de migración y velocidad (Fig. 37A y B). La dosis de 0.3 μM redujo la actividad de Syk por BCR en un 85%, pero disminuyó migración sólo en un 50% y no afectó los valores de velocidad de las células B WT; dosis inferiores de BAY afectaron solo parcialmente a la señal a través del BCR (Fig. 37A y B).

El tratamiento de las células B WT con BAY 0.3 μM alteró la localización y disminuyó significativamente el reclutamiento de vinculina en la SI (Fig. 38A y B); la polimerización de actina también resultó afectada de manera significativa (Fig. 38A y B). La cuantificación de vinculina y F-actina en el plano de la SI mostró una reducción casi del 50% para ambas en las células B tratadas con BAY 0.3 μM en comparación a las no tratadas (Fig. 38C). No se afectó la formación del cSMAC (Fig. 38A) ni el reclutamiento y distribución de talina en la SI (Fig. 38D). Dosis más bajas de BAY no alteraron el reclutamiento ni la distribución de vinculina y F-actina en la SI (Fig. 38C y E).

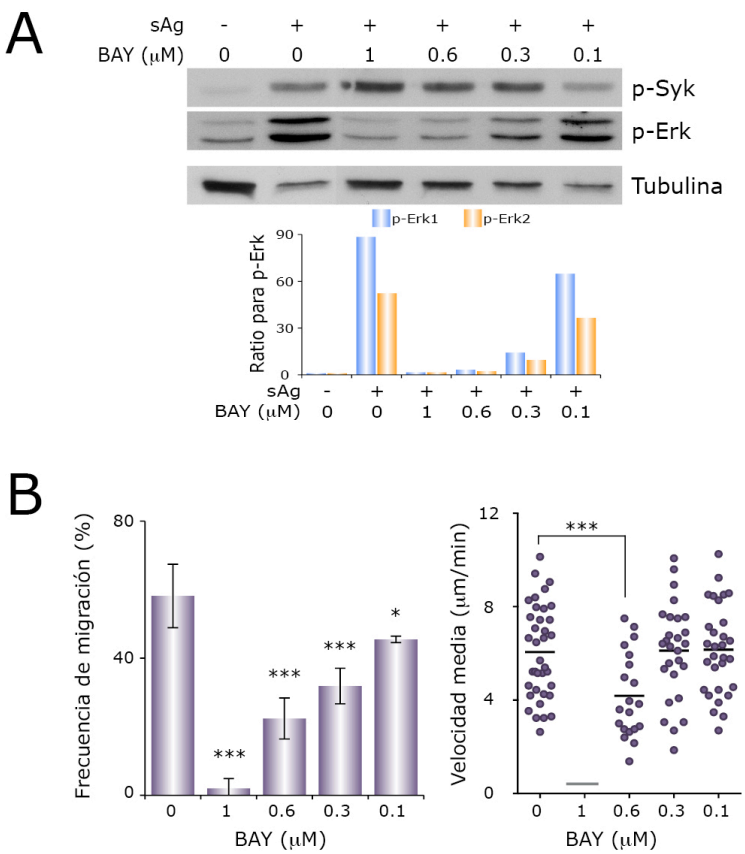

Figura 37. Efecto del tratamiento con BAY en la señalización por BCR y por CXCR5. (A) Niveles de p-Syk y p-Erk1/2 en células B primarias, tratadas o no con las dosis indicadas de BAY y estimuladas a través del BCR con sAg, determinados por *western blot*; tubulina, control de carga. Cuantificación de p-ERK1/2 (gráfico inferior) para cada condición comparado con la condición basal (no sAg, no BAY). (B) Frecuencia de migración (izquierda) y valores de velocidad media (derecha) de células B primarias sin tratar o tratadas con BAY a las dosis indicadas en contacto con membranas que contienen ICAM-1 y CXCL13; cada punto representa una célula. Datos en (A) corresponden a un experimento representativo; datos en (B) corresponden a dos experimentos. Barra gris, no detectado.

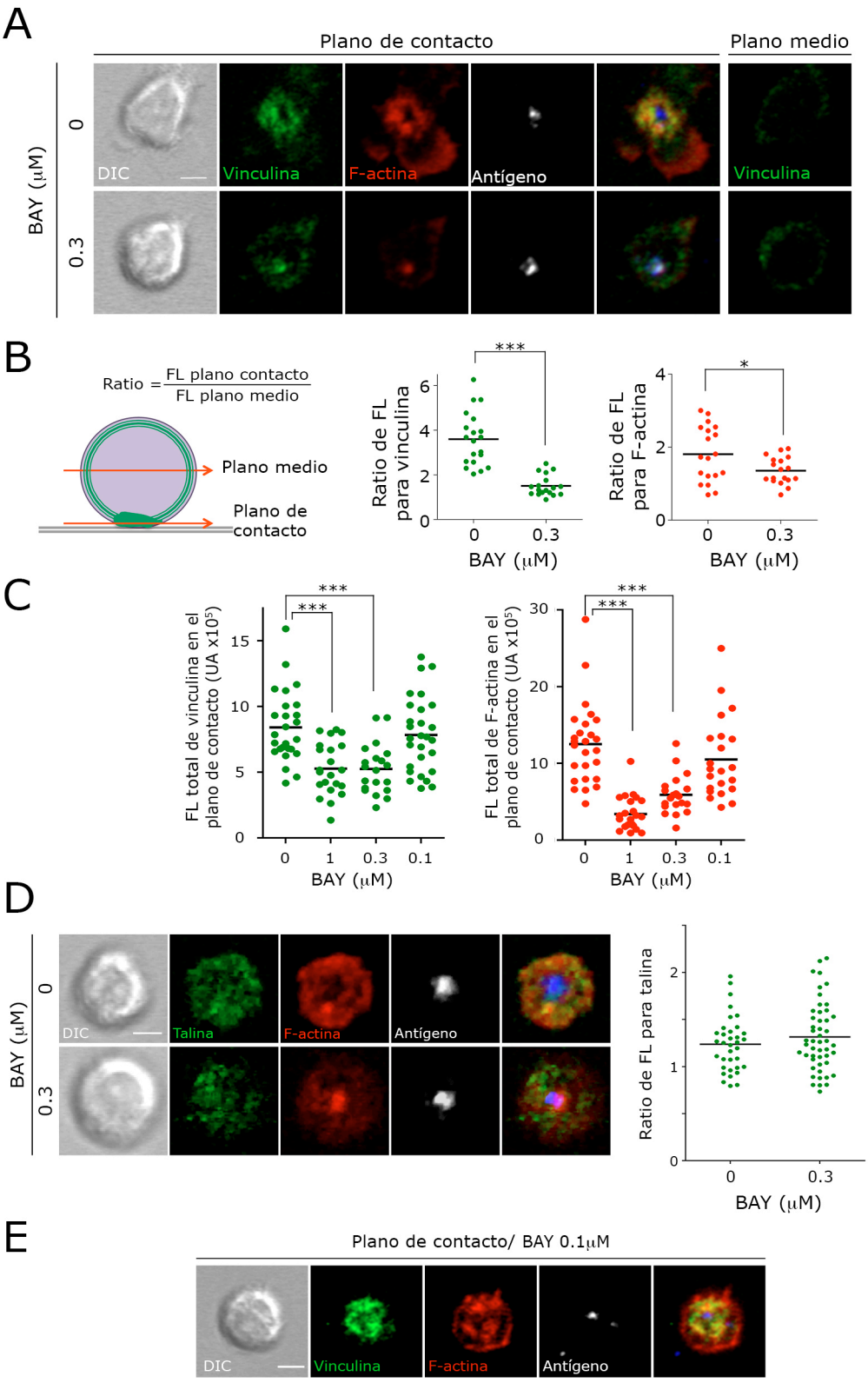

Figura 38. Efecto de la inhibición de Syk en la localización de vinculina en la SI. (A) Imágenes de DIC y fluorescencia para vinculina, F-actina y antígeno en el plano de la SI y de vinculina en el plano medio de células B MD4 representativas no tratadas o tratadas con BAY, en contacto con membranas que contiene ICAM-1, CXCL13 y tAg. (B) Ratio de fluorescencia de vinculina y F-actina de células B MD4 tratadas o no con BAY, calculado como se muestra en el esquema de la izquierda; cada punto representa una célula. (C) Valores de

fluorescencia total de vinculina y F-actina (en unidades arbitrarias, UA) en el plano de contacto de células B no tratadas o tratadas con BAY a las dosis especificadas, con membranas que contienen ICAM-1, CXCL13 y tAg; cada punto representa una célula. (D) Imágenes de DIC y fluorescencia para talina, F-actina y antígeno en el plano de la SI de células B MD4 representativas no tratadas o tratadas con BAY, y puestas sobre membranas que contienen ICAM-1, CXCL13 y tAg. Ratio de fluorescencia de talina en células B MD4 tratadas o no con BAY, calculado como se indica en (B) (gráfico derecho); cada punto representa una célula. (E) Imágenes de DIC y fluorescencia para vinculina, F-actina y antígeno de una célula B MD4 representativa tratada con BAY (0.1 μM) y formando SI en membranas con ICAM-1, CXCL13 y tAg. Los datos mostrados en (B) y (D) corresponden a experimentos representativos (n=3, y n=4, respectivamente); los datos en (C) corresponden a dos experimentos. Barra gris, no detectado; barra de escala, 2 μm.

A continuación estudiamos el comportamiento en tiempo real de células B WT no tratadas (control) o tratadas con BAY 0.3 μM , sobre membranas que contenían ICAM-1, CXCL13 y tAg. En la situación control, las células B establecieron la SI, estaban paradas, y emitían *membrane ruffles* en respuesta a la presencia de CXCL13 (Fig. 39A y B; videos 10A y B). Sin embargo, el 40% de las células B tratadas con BAY migraron en respuesta a la quimioquina, alcanzando velocidades medias de 3 μm/min (Fig. 39B y C). Esta células presentaban un lamelipodio en el extremo anterior, y migraban transportando el agregado de antígeno (cSMAC) en la parte posterior de la célula o urópodo. Cabe mencionar que células B WT tratadas con dosis inferiores de BAY (0.1 μM) no migraron sobre membranas que contenían tAg (datos no mostrados), lo cual correlacionaba con la ausencia de alteraciones en el reclutamiento y la distribución de vinculina a la SI (Fig. 38C y E).

Los resultados indicaban que vinculina es necesaria en la SI para su estabilización y por tanto, para la parada de las células B migrando en respuesta a CXCL13. Además, la activación local de Syk determina el reclutamiento de vinculina a la SI.

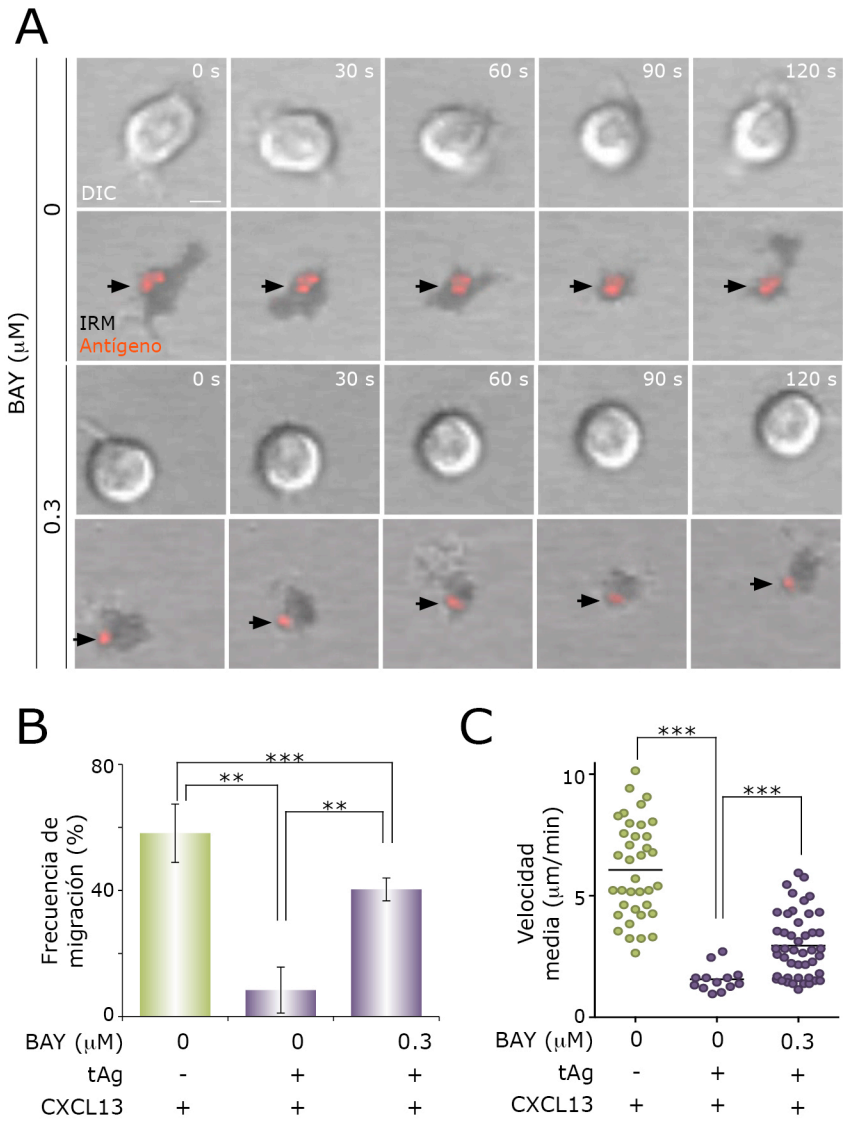

Figura 39. La ausencia de vinculina en la SI permite la migración de las células B en presencia de CXCL13. (A) Imágenes en tiempo real de DIC y superposición de IRM con fluorescencia de antígeno células B MD4 representativas no tratadas (paneles superiores) o tratadas (paneles inferiores) con BAY y en contacto con membranas que contienen ICAM-1, CXCL13 y tAg; las flechas indican la posición del agregado de antígeno. (B) Frecuencia de migración de células B MD4 no tratadas o tratadas con BAY sobre membranas con ICAM-1 en las condiciones indicadas. (C) Valores de velocidad media de las células B MD4 en migración en (B); cada punto corresponde a una célula. Los datos mostrados en (B) y (C) corresponden a dos experimentos. Barra de escala, 2 μm.

5.16. Papel de NM-II en el mantenimiento de vinculina en la SI

La proteína motora NM-II regula el reclutamiento de vinculina a las AF (Pasapera et al, 2010). NM-II está presente en la SI de las células B (Fig. 27A). Estudiamos el papel de NM-II en la función de vinculina en la SI. Para ello, dejamos que células B WT establecieran la SI con membranas que contenían ICAM-1, CXCL13 y tAg, y a

continuación las tratamos con blebistatina, inhibidor de la actividad de NM-II. Tras 20 min, analizamos el reclutamiento y la distribución de vinculina en la SI. La inhibición de NM-II resultó en la desorganización del anillo de vinculina (Fig. 40A) y la pérdida de su reclutamiento a la SI (Fig. 40B). El anillo de F-actina permaneció tras el tratamiento, pero observamos una reducción significativa de la polimerización de actina en la SI (Fig. 40A y B). La reducción del área de contacto de las células B tratadas, cuantificado por IRM y previo a su fijación con PFA, indicaba alteraciones en el mantenimiento del pSMAC (Fig. 40C). Las células B tratadas con blebistatina no migraron, puesto que NM-II es necesaria para la migración de células B mediada por CXCL13 (Fig. 29).

A continuación estudiamos el efecto de la inhibición de NM-II por blebistatina en la dinámica molecular de vinculina y F-actina en la SI de células B en tiempo real. Para ello transfectamos células B A20 con las construcciones vinculina-GFP y LifeAct-RFP; tras 20h, pusimos los transfectantes en contacto con membranas que contenían ICAM-1, CXCL13 y tAg. Una vez establecida la SI, añadimos blebistatina y monitorizamos vinculina y F-actin por microscopía confocal. El patrón en forma de anillo de vinculina se desorganizó con el tiempo, junto con una bajada en los niveles de fluorescencia; también observamos la pérdida de F-actina en la SI (Fig. 40D; video 11).

Los datos sugerían que NM-II está implicada en el mantenimiento y/o estabilidad de vinculina en la SI. La pérdida del anillo de vinculina se acompaña de una bajada en los niveles de F-actina en la SI.

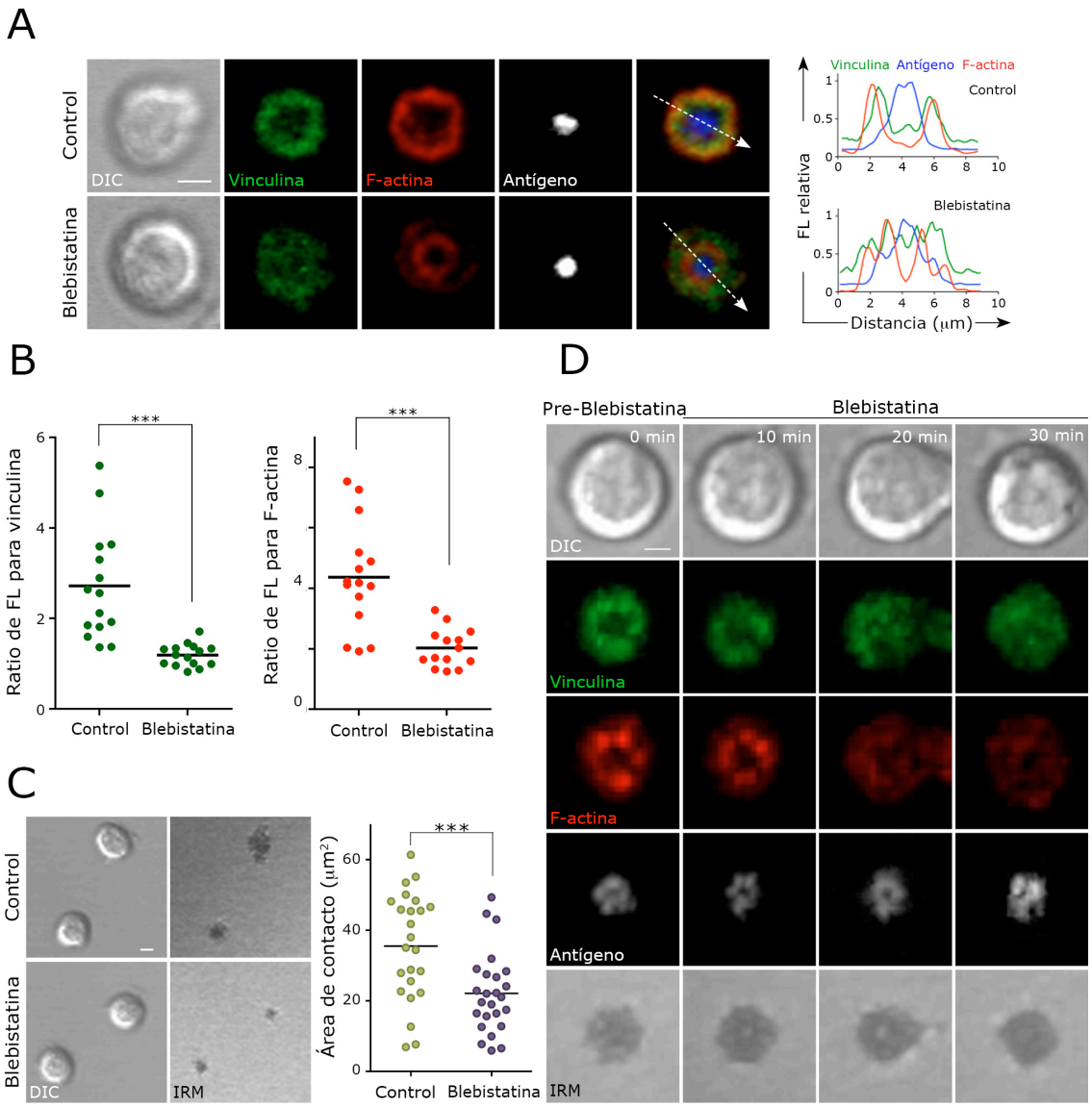

Figura 40. La actividad de NM-II regula la localización de vinculina en la SI. (A) Imágenes de DIC y fluorescencia para vinculina, F-actina y antígeno en el plano de la SI de células B MD4 no tratadas (control) o tratadas con blebistatina sobre membranas que contiene ICAM-1, CXCL13 y tAg. Perfiles de distribución de la fluorescencia relativa de vinculina, F-actina y antígeno en el plano de la IS (flechas en la imagen de *merge*). (B) Ratio de la fluorescencia de vinculina y F-actina en el plano de contacto respecto del plano medio de células B MD4 no tratadas (control) o tratadas con blebistatina; cada punto representa una célula. (C) Imágenes de DIC e IRM de células B primarias representativas no tratadas (control) o tratadas con blebistatina en membranas con ICAM-1, CXCL13 y tAg. Cuantificación del área de contacto (determinada de IRM) entre la célula B y la membrana para cada condición indicada; cada punto corresponde a una célula (gráfico izquierdo). (D) Imágenes en tiempo real de DIC, IRM y fluorescencia para vinculina, F-actina y antígeno de células B A20 co-transfectadas con vinculina-GFP y Lifeact-RFP, con SI establecida, antes (Pre-Blebistatina) y después de la adición de blebistatina. Datos en (B) corresponden a un experimento representativo (n=3); los datos mostrados en (C) corresponden a dos experimentos. Barra de escala, 2 μm.

6. DISCUSIÓN

6.1.Modelo experimental en 2D para estudiar la dinámica de células B

Al comienzo de este trabajo de investigación el conocimiento sobre la regulación de la dinámica de células B era escaso. Los estudios realizados *in vivo* mediante microscopía multifotón mostraron los primeros datos sobre la migración intersticial de células B en los folículos y, posteriormente, en los centros germinales de los OLS (Carrasco & Batista, 2007; Miller et al, 2002; Okada & Cyster, 2006; Okada et al, 2005). Quisimos profundizar en el estudio del movimiento de las células B en respuesta a quimioquinas y su regulación por otros estímulos tales como antígeno.

Las células B respondieron a dos de las quimioquinas homeostáticas presentes en los OLS, CXCL13 y CXCL12. CXCL13, localizada fundamentalmente en las FDC, media un escaneo muy activo y eficiente del folículo. CXCL12, que se encuentra en la médula del ganglio linfático, y en menor nivel en las zonas T y B y en la zona oscura de los CG (Allen et al, 2004; Hargreaves et al, 2001), tiene un papel importante en el movimiento de las células B activadas en los CG. CXCL13 promovió mayores frecuencias de migración de células B que CXCL12 en ensayos de *transwell*. Estos datos contrastaban con los obtenidos en el modelo de bicapas lipídicas, donde ambas quimioquinas indujeron una respuesta similar en las células B. Además, la concentración de CXCL13 que promovió migración en las membranas fue cinco veces menor que la necesaria para inducir una migración detectable en los ensayos de *transwell*. El encuentro de la quimioquina presentada sobre una superficie parece ser más eficiente para estimular la migración de las células B que en forma soluble; trabajos previos han mostrado conclusiones similares (Feigelson et al, 2003).

La presencia de CXCL13 o CXCL12 tapizando las membranas artificiales fue estímulo suficiente para inducir polarización en las células B, provocando cambios en su morfología necesarios para que la célula pueda migrar. Esta observación confirma datos previos que mostraban polarización de células B humanas de sangre periférica en presencia de CXCL12 (Vicente-Manzanares et al, 2007), y que CXCL13 es necesaria para la polarización de células B sobre cristales tapizados con ICAM-1 (Stachowiak et al, 2006). Por otro lado, la quimioquina por sí sola fue incapaz de inducir la migración de las células B, siendo necesaria una densidad mínima de ligandos de integrinas (>75 molec/μm^2) para ello. Datos similares en otro tipo de ensayos llevaron a proponer un efecto sinérgico de CXCL13 y ICAM-1 en la migración de células B (Stachowiak et al, 2006). No observamos diferencias apreciables en la frecuencia de migración entre ICAM-1 y VCAM-1 a distintas

densidades; por tanto, ambos ligandos y sus respectivos receptores, las integrinas LFA-1 y VLA-4, son capaces de promover movimiento de las células B.

El análisis de diferentes parámetros dinámicos de las células B en el sistema de bicapas lipídicas pone de manifiesto un comportamiento y características del movimiento muy próximas a lo observado *in vivo* (Miller et al, 2002). A igual densidad o niveles de expresión, ICAM-1 es más eficiente en promover motilidad de células B que VCAM-1. Diversos trabajos relacionan la migración de leucocitos (Laudanna & Alon, 2006), células T (Brown et al, 2001; Dustin et al, 1997; Jacobelli et al, 2009) e incluso células B (Stachowiak et al, 2006) con ICAM-1. VCAM-1 se ha relacionado con el reclutamiento de células B a la médula ósea y con diferentes procesos inflamatorios e infecciosos (Cook-Mills et al, 2011). Sin embargo se sabe muy poco de la implicación de VCAM-1 en la migración intersticial de las células B. VCAM-1 se expresa constitutivamente en las FDC de los folículos, es posible que la menor velocidad de migración de las células B en presencia de VCAM-1, facilite el escaneo más exhaustivo de la superficie de las FDC en busca de antígeno. Nuevos estudios serán necesarios para determinar la función de VCAM-1 en este proceso.

La velocidad de movimiento dependió de la densidad de ICAM-1 o VCAM-1; altas densidades o niveles de expresión ralentizan la migración de las células B. En condiciones basales, los niveles de expresión en esplenocitos para ICAM-1 (100-200 molec/μm^2) se corresponden a los que en nuestro modelo *in vitro* dieron lugar a parámetros de migración similares a los observados *in vivo.* Estímulos inflamatorios aumentaron cuatro veces la expresión de ICAM-1 en los esplenocitos. En base a nuestras observaciones proponemos que ante una situación de inflamación, el aumento de ICAM-1 reduciría la velocidad de las células B, promoviendo una búsqueda más minuciosa de antígeno. Los niveles de VCAM-1 detectados *ex vivo* fueron inferiores a los de ICAM-1; sólo en respuesta a inflamación se alcanzarían los niveles de expresión de VCAM-1 necesarios para promover migración. Estos datos sugieren un papel secundario de VCAM-1 en migración de células B en condiciones homeostáticas; sólo en situaciones de inflamación su participación sería más importante.

Aunque la migración de los leucocitos puede ocurrir en ausencia de integrinas (Lammermann et al, 2008), recientemente el mismo grupo ha descrito que los leucocitos prefieren migrar sobre superficies que contienen ICAM-1 y están tapizadas con quimioquina (*haptokinesis*), incluso en presencia de señales quimiotácticas (Schumann et al, 2010). Nuestro modelo de migración sobre bicapas lipídicas que contienen ligandos de integrinas y quimioquina unida proporciona las condiciones necesarias para este tipo de migración haptocinética, siendo el comportamiento dinámico de las células B similar al observado en los folículos.

6.2. Modulación de la dinámica de las células B por quimioquinas y antígeno

Los ensayos de migración en *transwell* mostraron que la activación a través del BCR inhibe la quimiotaxis hacia CXCL13 y CXCL12 dependiendo de la cantidad de antígeno presente. Tras un *priming* de 2h sin embargo las células B migraron a CXCL13 y CXCL12 a frecuencias similares al control sin antígeno. Esto puede ser debido a una necesidad de señalización constante a través del BCR para afectar la migración, o a que el efecto del antígeno es transitorio. Nuestros datos contrastan con los datos obtenidos en células T humanas, en los que una estimulación de 2h a través del TCR aumenta su migración en respuesta a CCL19 y CCL21 (Schaeuble et al, 2011). Esta diferencia puede ser consecuencia del tipo celular empleado en el estudio, pero también del receptor de quimioquina. Así, en este mismo trabajo muestran que la estimulación por TCR durante 2h no afecta a la migración de las células T en respuesta a CXCL12. El conjunto de los datos ponen de manifiesto la importancia de las diferentes quimioquinas y sus receptores en la motilidad de los linfocitos en los órganos linfoides. Cada compartimento de estos órganos se caracteriza por distintas células estromales, con perfiles de producción y presentación de quimioquinas propios, que darán lugar a diferentes respuestas dinámicas en los linfocitos.

El sistema de bicapas lipídicas ha sido previamente empleado para describir la SI de células B, y demostrar la importancia de LFA-1/ICAM-1 y VLA-4/VCAM-1 en la discriminación por afinidad de antígeno y en el umbral de antígeno necesario para la activación de células B (Carrasco & Batista, 2006; Carrasco et al, 2004; Fleire et al, 2006). La combinación de los estímulos CXCL13 y antígeno en estas membranas desencadenó un conjunto de comportamientos heterogéneos en las células B que dependió de la fuerza de la señal de antígeno. Una señal antigénica fuerte (elevada cantidad y/o afinidad) implicó la parada total de las células B, mientras que una señal débil no impidió la migración. CXCL13/CXCR5 no afectó a la formación de SI, pero sí aumentó la activación de las células B a través del BCR. Hemos descrito dos mecanismos que explican el efecto co-estimulador de CXCL13/CXCR5; mientras que en células B en SI, CXCL13 aumenta la formación de *membrane ruffles* y de interacciones LFA-1/ICAM-1 favoreciendo la captación de antígeno de las zonas adyacentes a la SI, en condiciones de baja presencia de antígeno, CXCL13 favorece el establecimiento de una plataforma migratoria basada en la interacción LFA-1/ICAM-1 entre la célula B y la membrana diana que permite la integración de señales a través del BCR durante la migración de la célula B. Esta plataforma, denominada *kinapsis*, fue descrita inicialmente en células T (Dustin, 2008). Nuestros datos concuerdan con trabajos en células T donde se observó migración

sobre sustratos que contienen antígeno y la integración de señales a través del TCR (Gunzer et al, 2000; Mempel et al, 2004; Underhill et al, 1999). Diversos estudios proponen que el contacto de una célula T con una APC que presenta quimioquina en su membrana tiene un efecto de *priming* en la activación de las células T por antígeno. La activación de LFA-1 mediada por quimioquinas promueve la localización de los orgánulos de las células T a la zona de contacto con la APC y prepara a la célula para el encuentro con el antígeno (Contento et al, 2010). El contacto de la célula T con una APC que lleva CCL21, promueve la activación de contactos LFA-1/ICAM-1, y ello potencia la respuesta de la célula T a los siguientes contactos con otras APC, produciéndose un efecto co-estimulatorio en *trans* (Friedman et al, 2006). CCL21/CCR7 incrementa la proliferación inducida por TCR en células T $CD4^+$ (Gollmer et al, 2009). En células B, nosotros proponemos un mecanismo basado en la modulación de la dinámica de las células B subyacente a la co-estimulación en *cis* por CXCL13/CXCR5. No podemos descartar sin embargo que otras rutas de señalización activadas por la quimioquina contribuyan a ello; futuros estudios serán necesarios para determinarlo.

En células B en migración, CXCR5 presentó una distribución homogénea en la zona de contacto con el sustrato, observándose algunos agregados en los bordes de los lamelipodios. Estos datos contrastan con lo descrito por otros grupos, con una localización preferencial de los receptores de quimioquinas en el lamelipodio de células T y B. CCR2 y CCR5 localizan en el lamelipodio de células T activadas que migran en un gradiente de quimioquina (Nieto et al, 1997); CXCR4 se recluta al lamelipodio de células B humanas estimuladas con CXCL12 (Vicente-Manzanares et al, 1998). Proponemos que el patrón observado en células B para CXCR5, presente tanto en la zona de contacto con la membrana como en el resto de la superficie celular, puede ser responsable de los cambios rápidos y aleatorios en la dirección de migración de la célula B. Por otro lado, CXCR5 estaba en el pSMAC de la SI de células B, excluido del cSMAC, pero sin mostrar un localización preferencial en el plano de la sinapsis. La presencia de CXCR5 disponible en toda la superficie celular puede así facilitar la interacción con APC adyacentes y la modulación de la dinámica en la célula B para captar más antígeno; este dato se relaciona con el hecho de que las células B establecen varias SI *in vivo* (Carrasco & Batista, 2007). La localización observada para CXCR5 en la SI de células B contrasta con la distribución de otros receptores de quimioquinas en la SI de células T. CXCR4 y CCR5 son reclutados a la SI de células T Jurkat, teniendo un papel co-estimulador en la activación de estas células (Molon et al, 2005). La diferencia en esta distribución puede atribuirse a la distinta función de cada receptor de quimioquina; mientras que CXCR4 promueve

migración en condiciones homeostáticas, CCR5 está relacionado con procesos inflamatorios (Thomas & Baumgart, 2012; Zimmermann & Tacke, 2011).

Durante la formación de la SI de las células B se produce una fase de expansión de la membrana celular (*spreading*), durante la cual se forman micro-agregados de BCR/antígeno (*microclusters*), denominados *microsignalosomas*, que inician la señalización a través del BCR (Depoil et al, 2008; Fleire et al, 2006). En una segunda fase, la contracción de la célula B recluta los *microclusters* hacia el centro de la célula para formar el cSMAC y la SI (Fleire et al, 2006). Se postula que la señalización a través del BCR es mediada por los *microclusters* y que el cSMAC es un lugar de internalización de antígeno y de atenuación de la señal (Harwood & Batista, 2011). En células T se propone que el cSMAC está implicado en la atenuación de la señal por el TCR, y que la formación de nuevos *microclusters* de TCR en la periferia de la zona de contacto mantendría una señalización constante y sostenida (Dustin et al, 2010). Teniendo en cuenta estos datos, los *membrane ruffles* y nuevos contactos LFA-1/ICAM-1 mediados por CXCL13/CXCR5 en células B en SI favorecen la unión BCR/antígeno y la formación de nuevos *microclusters* de señalización, promoviendo la activación de la célula B.

6.3.Mecanismos moleculares implicados en la parada de las células B

En este trabajo hemos estudiado los mecanismos moleculares que subyacen a la señalización por CXCR5 y BCR, y que definen la adhesión estable y la motilidad de las células B. La señalización a través del BCR induce la activación de las integrinas (Carrasco et al, 2004; Spaargaren et al, 2003); se pensaba que el estado de alta afinidad de las integrinas era suficiente para impedir la motilidad. Nosotros demostramos que la activación de integrinas a través del BCR, utilizando antígeno en forma soluble, no es suficiente para detener la migración en respuesta a CXCL13. Es necesario el reconocimiento de antígeno presentado en una membrana y por tanto, una activación local o polarizada del BCR y el correcto ensamblaje del pSMAC de la SI para detener a la célula B.

Un dominio rico en F-actina y de forma anular co-localiza con el anillo de integrinas del pSMAC (Carrasco et al, 2004). La inhibición de la actividad de WASP, proteína implicada en la polimerización de actina, resultó en alteraciones en la formación del pSMAC; observamos efectos similares en células B con deficiente expresión de WASP, debido a la falta de WIP. La activación de integrinas y migración por CXCL13 está disminuida en células B deficientes en WIP. Se ha descrito que la deficiencia de WASP en células B afecta a la activación de integrinas mediada por BCR (Meyer-Bahlburg et al, 2008) así como la migración en respuesta

a gradientes de quimioquinas (Gallego et al, 2006; Meyer-Bahlburg et al, 2008; Westerberg et al, 2005). WASP está implicado en la alternancia de SI y migración en células T; la ausencia de WASP impide la parada y formación de la SI (Sims et al, 2007). Según nuestros datos, WASP no parece tener el mismo papel en células B; es importante para la integridad del pSMAC, pero una actividad deficiente de WASP no permite que las células B recuperen motilidad.

La proteínas de citoesqueleto talina y vinculina son fundamentales para la activación de integrinas y la formación de adhesiones estables (Ziegler et al, 2006). La señalización a través del TCR desencadena la formación de un complejo que incluye a WAVE-2, Arp2/3, vinculina y talina en la sinapsis de células T, imprescindible para la polimerización de actina y la activación de integrinas (Nolz et al, 2007). Nuestros datos muestran que aunque ambas, talina y vinculina, se reclutan a la SI en células B, la presencia de vinculina en el pSMAC es determinante para regular el comportamiento de la célula B, para mediar la parada de la migración. Vinculina presenta dos conformaciones en la célula: una conformación auto-inhibida en el citoplasma y una conformación activa que localiza en los sitios de adhesión tales como las AF (Chen et al, 2005). Estudios in vitro indican que la unión simultanea de talina y F-actina activa vinculina (Chen et al, 2005). La forma activa de vinculina forma un complejo estable con talina e integrinas que mantiene los receptores de adhesión en un estado de alta afinidad, promoviendo el crecimiento de las AF (Humphries et al, 2007).

Existen datos controvertidos sobre el papel de PIP_2 en la activación de vinculina: PIP_2 está implicado en el reclutamiento de vinculina a las AF (Bakolitsa et al, 2004; Legate et al, 2011) pero por otro lado parece que facilita su liberación de las AF, favoreciendo el reciclaje de estas estructuras (Chandrasekar et al, 2005). Nosotros observamos que el reconocimiento de antígeno presentado en la membrana a través del BCR da lugar al reclutamiento temprano (1 min) de PIPKIγ a la zona de contacto entre la célula B y la membrana; esta quinasa produjo PIP_2 a nivel local, observándose un pico de producción a los 2.5 min. A esos tiempos empezamos también a detectar una fuerte polimerización de actina y el reclutamiento gradual de vinculina a la zona de contacto; posteriormente, vinculina y F-actina se distribuyeron en el dominio anular característico del pSMAC. Estos datos apoyan un modelo en el cual PIPKIγ y su producto PIP_2 estarían implicados en la localización de vinculina en la SI de las células B. Tras la activación del BCR, parece ser Btk quien transporta a PIPKIγ a la membrana plasmática para producir PIP_2 (Saito et al, 2003).

Nuestros datos indican que la integridad del citoesqueleto de actina y la acción de NM-II son clave en la regulación de la dinámica de las células B. La inhibición de la polimerización de actina impidió la polarización celular, la migración y la adhesión al sustrato. Estos procesos también dependen del citoesqueleto de actina en células T (Lammermann & Sixt, 2009). Por otro lado, la inhibición de NM-II afectó a la migración y formación de *membranes ruffles*. NM-II es necesaria para el movimiento ameboide tanto en 2D como en 3D, regulando la interacción entre integrinas y sus ligandos (Jacobelli et al, 2009; Jacobelli et al, 2004; Jacobelli et al, 2010). La NM-II participa en la formación y estabilidad de la SI y de la kinapsis en células B y T (Ilani et al, 2009; Jacobelli et al, 2004; Jacobelli et al, 2010) y datos mostrados a lo largo de este trabajo). Nuestros datos muestran que la actividad de NM-II es importante para la localización de vinculina en la SI de la célula B; en células no-inmunes, la contractilidad mediada por NM-II controla la localización de vinculina y otras proteínas adaptadoras a las AF (Pasapera et al, 2010).

Datos derivados de este estudio junto con aportaciones de otros grupos ponen de manifiesto que la actividad de Syk es fundamental para la migración y la adhesión a través de integrinas de células B (Matsusaka et al, 2005; Pearce et al, 2011). Syk regula la actividad de LFA-1 inducida tanto por CXCR5/CXCL13 como por BCR/antígeno, además de regular el reclutamiento de vinculina a la sinapsis para promover la parada de la célula B en respuesta a antígeno. Según nuestro modelo, cuando una célula B en migración reconoce antígeno específico expuesto sobre la superficie de FDC u otro APC a través del BCR, se produce una activación local de Syk (Fig. 41A y B). Esta señal promueve el reclutamiento de PIPKIγ a la zona de contacto entre la célula B y la APC y la consecuente producción local de PIP_2 (Fig. 41C); se incorpora talina y vinculina a esta zona, promoviendo la activación de las integrinas y su conexión con F-actina (Fig. 41D). Se forma el pSMAC, que es estabilizado por vinculina al fijar y mantener la unión de integrinas activas al citoesqueleto de actina (Fig. 41E). La acción de NM-II mantiene la localización de vinculina en esta estructura (Fig. 41F). Vinculina estabiliza la SI impidiendo que la célula B pueda migrar, a pesar de recibir señales a través de CXCR5 (Fig. 41G). La alteración de la localización de vinculina en la SI conlleva una desorganización del pSMAC y, en último término, permite a la célula B migrar estimulada por CXCL13 (Fig. 41H).

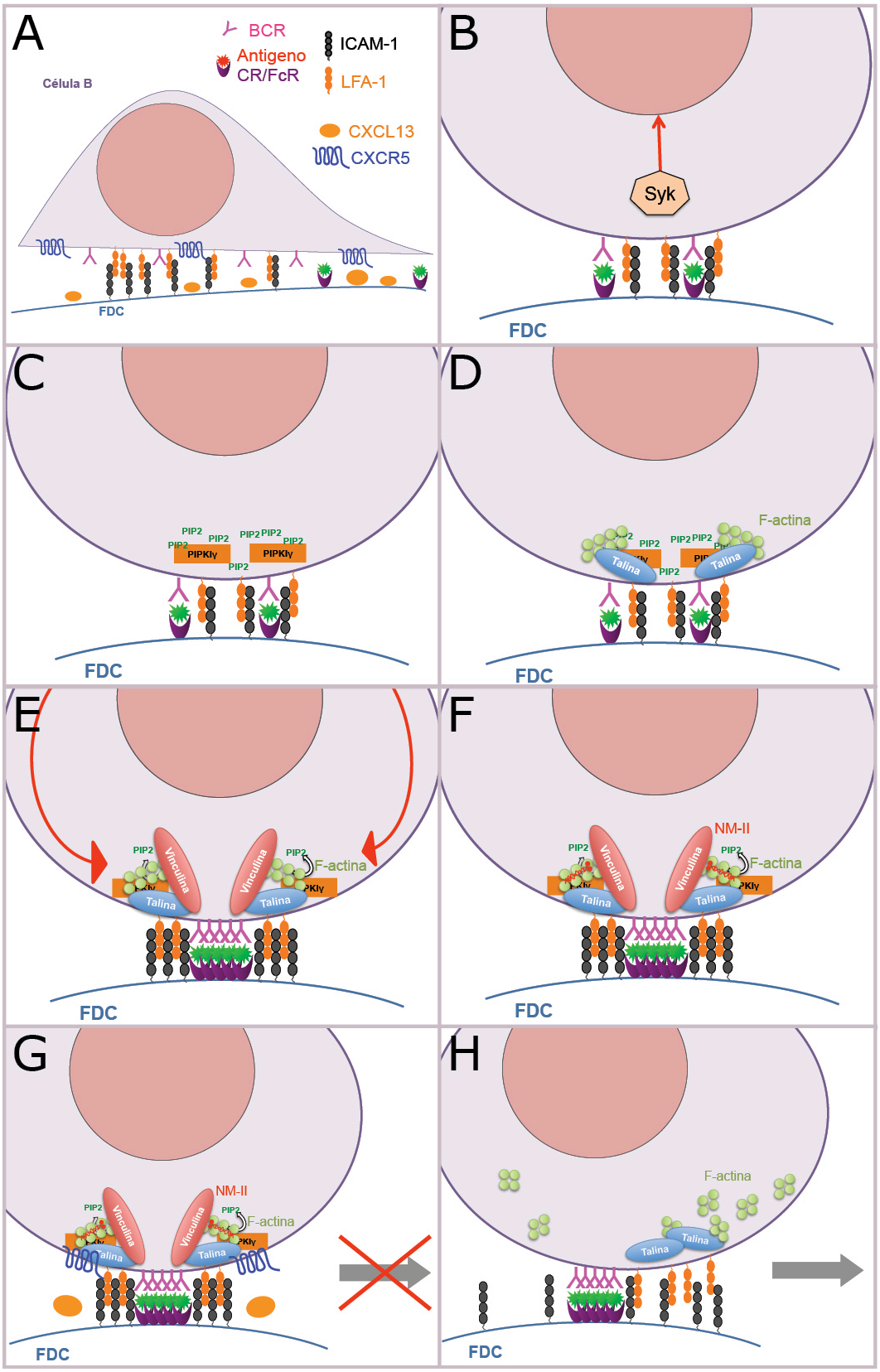

Figura 41. Secuencia de eventos moleculares que conducen a la parada de la célula B en migración.

7. CONCLUSIONES

1. La estimulación a través del BCR modula la migración de células B primarias en respuesta a un gradiente quimiotáctico de CXCL13 o CXCL12 en función de la dosis de antígeno presente. El umbral de señal antigénico necesario para interferir con migración es inferior al requerido para activación celular.

2. Hemos establecido un sistema experimental *in vitro* en dos-dimensiones (2D) que recrea la dinámica de las células B primarias descrita en condiciones de homeostasis en los folículos de OLS por microscopía multifotón. Esta tecnología se basa en el uso de bicapas lipídicas artificiales planas que mimetizan la membrana plasmática de una potencial APC.

3. El tipo de ligando de integrina presente, ICAM-1 o VCAM-1, así como sus niveles de expresión en la membrana regulan la migración de las células B en respuesta a CXCL13 o CXCL12.

4. La intensidad de señal a través del BCR modula la migración de las células B en respuesta a CXCL13, dando como resultado un rango heterogéneo de comportamientos en las células B.

5. La señalización de CXCL13/CXCR5 aumenta la activación de células B a través del BCR en condiciones limitantes de antígeno. Esto ocurre al menos mediante dos mecanismos: 1) en células B en sinapsis, CXCL13/CXCR5 promueve la formación de *membrane ruffles* y nuevos contactos con la membrana presentadora de antígeno mediante la interacción LFA-1/ICAM-1 para facilitar la captura de antígeno en los alrededores de la sinapsis; 2) en células B en migración, CXCL13/CXCR5 facilitan el establecimiento de una plataforma de migración mediada por LFA-1/ICAM-1 (*kinapsis*) que permite el reconocimiento de antígeno y la integración de señales a través del BCR.

6. El establecimiento de la estructura de la sinapsis inmunológica promovido por el reconocimiento de antígeno presentado sobre una membrana a través del BCR es necesario para impedir la migración de las células B en respuesta a CXCL13.

7. Vinculina es reclutada al dominio rico en integrinas de la sinapsis inmunológica (pSMAC) en células B, donde co-localiza con F-actina, talina, PIPKIγ y el lípido PIP_2. Su reclutamiento ocurre paralelamente a un pico de

producción local de PIP_2, y posterior a la localización de PIPKIγ en la sinapsis.

8. La ausencia de vinculina en la SI resulta en alteraciones en la formación y estabilización del pSMAC, que permiten la migración de la célula B en respuesta a CXCL13, transportando el agregado de antígeno en el urópodo. Vinculina es por tanto regulador clave en la adhesión estable de la célula B a la APC mediada por la sinapsis.

9. La localización de vinculina en la sinapsis inmunológica depende de un umbral de activación local de Syk mediado por el reconocimiento de antígeno de membrana a través del BCR. Además, la proteína motora NM-II está implicada en el mantenimiento y/o estabilidad de vinculina en la SI.

8. BIBLIOGRAFÍA

Allen CD, Ansel KM, Low C, Lesley R, Tamamura H, Fujii N, Cyster JG (2004) Germinal center dark and light zone organization is mediated by CXCR4 and CXCR5. *Nat Immunol* **5**(9)**:** 943-952

Allen CD, Cyster JG (2008) Follicular dendritic cell networks of primary follicles and germinal centers: phenotype and function. *Semin Immunol* **20**(1)**:** 14-25

Allen CD, Okada T, Tang HL, Cyster JG (2007) Imaging of germinal center selection events during affinity maturation. *Science* **315**(5811)**:** 528-531

Allman D, Pillai S (2008) Peripheral B cell subsets. *Curr Opin Immunol* **20**(2)**:** 149-157

Anton IM, de la Fuente MA, Sims TN, Freeman S, Ramesh N, Hartwig JH, Dustin ML, Geha RS (2002) WIP deficiency reveals a differential role for WIP and the actin cytoskeleton in T and B cell activation. *Immunity* **16**(2)**:** 193-204

Anton IM, Jones GE (2006) WIP: a multifunctional protein involved in actin cytoskeleton regulation. *Eur J Cell Biol* **85**(3-4)**:** 295-304

Arana E, Vehlow A, Harwood NE, Vigorito E, Henderson R, Turner M, Tybulewicz VL, Batista FD (2008) Activation of the small GTPase Rac2 via the B cell receptor regulates B cell adhesion and immunological-synapse formation. *Immunity* **28**(1)**:** 88-99

Arthur WT, Quilliam LA, Cooper JA (2004) Rap1 promotes cell spreading by localizing Rac guanine nucleotide exchange factors. *J Cell Biol* **167**(1)**:** 111-122

Bajenoff M, Egen JG, Koo LY, Laugier JP, Brau F, Glaichenhaus N, Germain RN (2006) Stromal cell networks regulate lymphocyte entry, migration, and territoriality in lymph nodes. *Immunity* **25**(6)**:** 989-1001

Bajenoff M, Germain RN (2009) B-cell follicle development remodels the conduit system and allows soluble antigen delivery to follicular dendritic cells. *Blood* **114**(24)**:** 4989-4997

Bakolitsa C, Cohen DM, Bankston LA, Bobkov AA, Cadwell GW, Jennings L, Critchley DR, Craig SW, Liddington RC (2004) Structural basis for vinculin activation at sites of cell adhesion. *Nature* **430**(6999)**:** 583-586

Balazs M, Martin F, Zhou T, Kearney J (2002) Blood dendritic cells interact with splenic marginal zone B cells to initiate T-independent immune responses. *Immunity* **17**(3)**:** 341-352

Batista FD, Iber D, Neuberger MS (2001) B cells acquire antigen from target cells after synapse formation. *Nature* **411**(6836)**:** 489-494

Berney C, Herren S, Power CA, Gordon S, Martinez-Pomares L, Kosco-Vilbois MH (1999) A member of the dendritic cell family that enters B cell follicles and stimulates

primary antibody responses identified by a mannose receptor fusion protein. *J Exp Med* **190**(6)**:** 851-860

Bompard G, Rabeharivelo G, Morin N (2008) Inhibition of cytokinesis by wiskostatin does not rely on N-WASP/Arp2/3 complex pathway. *BMC Cell Biol* **9:** 42

Brown MJ, Hallam JA, Liu Y, Yamada KM, Shaw S (2001) Cutting edge: integration of human T lymphocyte cytoskeleton by the cytolinker plectin. *J Immunol* **167**(2)**:** 641-645

Buettner M, Pabst R, Bode U (2010) Stromal cell heterogeneity in lymphoid organs. *Trends Immunol* **31**(2)**:** 80-86

Cariappa A, Chase C, Liu H, Russell P, Pillai S (2007) Naive recirculating B cells mature simultaneously in the spleen and bone marrow. *Blood* **109**(6)**:** 2339-2345

Carisey A, Ballestrem C (2010) Vinculin, an adapter protein in control of cell adhesion signalling. *Eur J Cell Biol* **90**(2-3)**:** 157-163

Carrasco YR (2010) Molecular and cellular dynamics at the early stages of antigen encounter: the B-cell immunological synapse. *Curr Top Microbiol Immunol* **340:** 51-62

Carrasco YR, Batista FD (2006) B-cell activation by membrane-bound antigens is facilitated by the interaction of VLA-4 with VCAM-1. *Embo J* **25**(4)**:** 889-899

Carrasco YR, Batista FD (2007) B cells acquire particulate antigen in a macrophage-rich area at the boundary between the follicle and the subcapsular sinus of the lymph node. *Immunity* **27**(1)**:** 160-171

Carrasco YR, Fleire SJ, Cameron T, Dustin ML, Batista FD (2004) LFA-1/ICAM-1 interaction lowers the threshold of B cell activation by facilitating B cell adhesion and synapse formation. *Immunity* **20**(5)**:** 589-599

Chandrasekar I, Stradal TE, Holt MR, Entschladen F, Jockusch BM, Ziegler WH (2005) Vinculin acts as a sensor in lipid regulation of adhesion-site turnover. *J Cell Sci* **118**(Pt 7)**:** 1461-1472

Chen H, Cohen DM, Choudhury DM, Kioka N, Craig SW (2005) Spatial distribution and functional significance of activated vinculin in living cells. *J Cell Biol* **169**(3)**:** 459-470

Cinamon G, Zachariah MA, Lam OM, Foss FW, Jr., Cyster JG (2008) Follicular shuttling of marginal zone B cells facilitates antigen transport. *Nat Immunol* **9**(1)**:** 54-62

Coffey F, Alabyev B, Manser T (2009) Initial clonal expansion of germinal center B cells takes place at the perimeter of follicles. *Immunity* **30**(4)**:** 599-609

Colino J, Shen Y, Snapper CM (2002) Dendritic cells pulsed with intact Streptococcus pneumoniae elicit both protein- and polysaccharide-specific immunoglobulin isotype responses in vivo through distinct mechanisms. *J Exp Med* **195**(1)**:** 1-13

Contento RL, Campello S, Trovato AE, Magrini E, Anselmi F, Viola A (2010) Adhesion shapes T cells for prompt and sustained T-cell receptor signalling. *EMBO J* **29**(23)**:** 4035-4047

Cook-Mills JM, Marchese ME, Abdala-Valencia H (2011) Vascular cell adhesion molecule-1 expression and signaling during disease: regulation by reactive oxygen species and antioxidants. *Antioxid Redox Signal* **15**(6)**:** 1607-1638

Critchley DR (2009) Biochemical and structural properties of the integrin-associated cytoskeletal protein talin. *Annu Rev Biophys* **38:** 235-254

Critchley DR, Gingras AR (2008) Talin at a glance. *J Cell Sci* **121**(Pt 9)**:** 1345-1347

Cyster JG (2005) Chemokines, sphingosine-1-phosphate, and cell migration in secondary lymphoid organs. *Annu Rev Immunol* **23:** 127-159

Cyster JG (2010) B cell follicles and antigen encounters of the third kind. *Nat Immunol* **11**(11)**:** 989-996

Cyster JG, Ansel KM, Reif K, Ekland EH, Hyman PL, Tang HL, Luther SA, Ngo VN (2000) Follicular stromal cells and lymphocyte homing to follicles. *Immunol Rev* **176:** 181-193

Davis DM, Chiu I, Fassett M, Cohen GB, Mandelboim O, Strominger JL (1999) The human natural killer cell immune synapse. *Proc Natl Acad Sci U S A* **96**(26)**:** 15062-15067

de la Fuente MA, Sasahara Y, Calamito M, Anton IM, Elkhal A, Gallego MD, Suresh K, Siminovitch K, Ochs HD, Anderson KC, Rosen FS, Geha RS, Ramesh N (2007) WIP is a chaperone for Wiskott-Aldrich syndrome protein (WASP). *Proc Natl Acad Sci U S A* **104**(3)**:** 926-931

de Paz JL, Moseman EA, Noti C, Polito L, von Andrian UH, Seeberger PH (2007) Profiling heparin-chemokine interactions using synthetic tools. *ACS Chem Biol* **2**(11)**:** 735-744

Depoil D, Fleire S, Treanor BL, Weber M, Harwood NE, Marchbank KL, Tybulewicz VL, Batista FD (2008) CD19 is essential for B cell activation by promoting B cell receptor-antigen microcluster formation in response to membrane-bound ligand. *Nat Immunol* **9**(1)**:** 63-72

Desjarlais JR, Lazar GA (2011) Modulation of antibody effector function. *Exp Cell Res* **317**(9)**:** 1278-1285

Devreotes PN, Zigmond SH (1988) Chemotaxis in eukaryotic cells: a focus on leukocytes and Dictyostelium. *Annu Rev Cell Biol* **4:** 649-686

Drake R WVA, Mitchell AWM (2009) *Gray's Anatomy for Students*: Churchill Livingstone Elsevier.

Durand CA, Westendorf J, Tse KW, Gold MR (2006) The Rap GTPases mediate CXCL13- and sphingosine1-phosphate-induced chemotaxis, adhesion, and Pyk2 tyrosine phosphorylation in B lymphocytes. *Eur J Immunol* **36**(8)**:** 2235-2249

Dustin ML (2007) Cell adhesion molecules and actin cytoskeleton at immune synapses and kinapses. *Curr Opin Cell Biol* **19**(5)**:** 529-533

Dustin ML (2008) Hunter to gatherer and back: immunological synapses and kinapses as variations on the theme of amoeboid locomotion. *Annu Rev Cell Dev Biol* **24:** 577-596

Dustin ML, Bromley SK, Kan Z, Peterson DA, Unanue ER (1997) Antigen receptor engagement delivers a stop signal to migrating T lymphocytes. *Proc Natl Acad Sci U S A* **94**(8)**:** 3909-3913

Dustin ML, Chakraborty AK, Shaw AS (2010) Understanding the structure and function of the immunological synapse. *Cold Spring Harb Perspect Biol* **2**(10)**:** a002311

Falasca M, Logan SK, Lehto VP, Baccante G, Lemmon MA, Schlessinger J (1998) Activation of phospholipase C gamma by PI 3-kinase-induced PH domain-mediated membrane targeting. *EMBO J* **17**(2)**:** 414-422

Feigelson SW, Grabovsky V, Shamri R, Levy S, Alon R (2003) The CD81 tetraspanin facilitates instantaneous leukocyte VLA-4 adhesion strengthening to vascular cell adhesion molecule 1 (VCAM-1) under shear flow. *J Biol Chem* **278**(51)**:** 51203-51212

Fleire SJ, Goldman JP, Carrasco YR, Weber M, Bray D, Batista FD (2006) B cell ligand discrimination through a spreading and contraction response. *Science* **312**(5774)**:** 738-741

Forster R, Mattis AE, Kremmer E, Wolf E, Brem G, Lipp M (1996) A putative chemokine receptor, BLR1, directs B cell migration to defined lymphoid organs and specific anatomic compartments of the spleen. *Cell* **87**(6)**:** 1037-1047

Friedl P, Borgmann S, Brocker EB (2001) Amoeboid leukocyte crawling through extracellular matrix: lessons from the Dictyostelium paradigm of cell movement. *J Leukoc Biol* **70**(4)**:** 491-509

Friedl P, Weigelin B (2008) Interstitial leukocyte migration and immune function. *Nat Immunol* **9**(9)**:** 960-969

Friedman RS, Jacobelli J, Krummel MF (2006) Surface-bound chemokines capture and prime T cells for synapse formation. *Nat Immunol* **7**(10)**:** 1101-1108

Fukui Y (2002) [A critical role of the CDM family molecule DOCK2 in lymphocyte migration]. *Tanpakushitsu Kakusan Koso* **47**(16 Suppl)**:** 2194-2199

Gallego MD, de la Fuente MA, Anton IM, Snapper S, Fuhlbrigge R, Geha RS (2006) WIP and WASP play complementary roles in T cell homing and chemotaxis to SDF-1alpha. *Int Immunol* **18**(2)**:** 221-232

Garside P, Ingulli E, Merica RR, Johnson JG, Noelle RJ, Jenkins MK (1998) Visualization of specific B and T lymphocyte interactions in the lymph node. *Science* **281**(5373)**:** 96-99

Gerard A, Mertens AE, van der Kammen RA, Collard JG (2007) The Par polarity complex regulates Rap1- and chemokine-induced T cell polarization. *J Cell Biol* **176**(6)**:** 863-875

Gollmer K, Asperti-Boursin F, Tanaka Y, Okkenhaug K, Vanhaesebroeck B, Peterson JR, Fukui Y, Donnadieu E, Stein JV (2009) CCL21 mediates CD4+ T-cell costimulation via a DOCK2/Rac-dependent pathway. *Blood* **114**(3)**:** 580-588

Goodnow CC, Crosbie J, Adelstein S, Lavoie TB, Smith-Gill SJ, Brink RA, Pritchard-Briscoe H, Wotherspoon JS, Loblay RH, Raphael K, et al. (1988) Altered immunoglobulin expression and functional silencing of self-reactive B lymphocytes in transgenic mice. *Nature* **334**(6184)**:** 676-682

Grakoui A, Bromley SK, Sumen C, Davis MM, Shaw AS, Allen PM, Dustin ML (1999) The immunological synapse: a molecular machine controlling T cell activation. *Science* **285**(5425)**:** 221-227

Gretz JE, Norbury CC, Anderson AO, Proudfoot AE, Shaw S (2000) Lymph-borne chemokines and other low molecular weight molecules reach high endothelial venules via specialized conduits while a functional barrier limits access to the lymphocyte microenvironments in lymph node cortex. *J Exp Med* **192**(10)**:** 1425-1440

Gunzer M, Schafer A, Borgmann S, Grabbe S, Zanker KS, Brocker EB, Kampgen E, Friedl P (2000) Antigen presentation in extracellular matrix: interactions of T cells with dendritic cells are dynamic, short lived, and sequential. *Immunity* **13**(3)**:** 323-332

Guo F, Velu CS, Grimes HL, Zheng Y (2009) Rho GTPase Cdc42 is essential for B-lymphocyte development and activation. *Blood* **114**(14)**:** 2909-2916

Haberman AM, Shlomchik MJ (2003) Reassessing the function of immune-complex retention by follicular dendritic cells. *Nat Rev Immunol* **3**(9)**:** 757-764

Hargreaves DC, Hyman PL, Lu TT, Ngo VN, Bidgol A, Suzuki G, Zou YR, Littman DR, Cyster JG (2001) A coordinated change in chemokine responsiveness guides plasma cell movements. *J Exp Med* **194**(1)**:** 45-56

Harwood NE, Batista FD (2008) New insights into the early molecular events underlying B cell activation. *Immunity* **28**(5)**:** 609-619

Harwood NE, Batista FD (2011) The cytoskeleton coordinates the early events of B-cell activation. *Cold Spring Harb Perspect Biol* **3**(2)

Hess KL, Donahue AC, Ng KL, Moore TI, Oak J, Fruman DA (2004) Frontline: The p85alpha isoform of phosphoinositide 3-kinase is essential for a subset of B cell receptor-initiated signaling responses. *Eur J Immunol* **34**(11)**:** 2968-2976

Hogg N, Henderson R, Leitinger B, McDowall A, Porter J, Stanley P (2002) Mechanisms contributing to the activity of integrins on leukocytes. *Immunol Rev* **186:** 164-171

Humphries JD, Wang P, Streuli C, Geiger B, Humphries MJ, Ballestrem C (2007) Vinculin controls focal adhesion formation by direct interactions with talin and actin. *J Cell Biol* **179**(5)**:** 1043-1057

Ilani T, Vasiliver-Shamis G, Vardhana S, Bretscher A, Dustin ML (2009) T cell antigen receptor signaling and immunological synapse stability require myosin IIA. *Nat Immunol* **10**(5)**:** 531-539

Jacobelli J, Bennett FC, Pandurangi P, Tooley AJ, Krummel MF (2009) Myosin-IIA and ICAM-1 regulate the interchange between two distinct modes of T cell migration. *J Immunol* **182**(4)**:** 2041-2050

Jacobelli J, Chmura SA, Buxton DB, Davis MM, Krummel MF (2004) A single class II myosin modulates T cell motility and stopping, but not synapse formation. *Nat Immunol* **5**(5)**:** 531-538

Jacobelli J, Friedman RS, Conti MA, Lennon-Dumenil AM, Piel M, Sorensen CM, Adelstein RS, Krummel MF (2010) Confinement-optimized three-dimensional T cell amoeboid motility is modulated via myosin IIA-regulated adhesions. *Nat Immunol* **11**(10)**:** 953-961

Junt T, Moseman EA, Iannacone M, Massberg S, Lang PA, Boes M, Fink K, Henrickson SE, Shayakhmetov DM, Di Paolo NC, van Rooijen N, Mempel TR, Whelan SP, von Andrian UH (2007) Subcapsular sinus macrophages in lymph nodes clear lymph-borne viruses and present them to antiviral B cells. *Nature* **450**(7166)**:** 110-114

Katakai T, Hara T, Lee JH, Gonda H, Sugai M, Shimizu A (2004) A novel reticular stromal structure in lymph node cortex: an immuno-platform for interactions among dendritic cells, T cells and B cells. *Int Immunol* **16**(8)**:** 1133-1142

Kehrl JH (1998) Heterotrimeric G protein signaling: roles in immune function and fine-tuning by RGS proteins. *Immunity* **8**(1)**:** 1-10

Kinashi T (2005) Intracellular signalling controlling integrin activation in lymphocytes. *Nat Rev Immunol* **5**(7)**:** 546-559

Kosco-Vilbois MH (2003) Are follicular dendritic cells really good for nothing? *Nat Rev Immunol* **3**(9)**:** 764-769

Kurosaki T (2002) Regulation of B-cell signal transduction by adaptor proteins. *Nat Rev Immunol* **2**(5)**:** 354-363

Kurosaki T (2011) Regulation of BCR signaling. *Mol Immunol* **48**(11)**:** 1287-1291

Kurosaki T, Hikida M (2009) Tyrosine kinases and their substrates in B lymphocytes. *Immunol Rev* **228**(1)**:** 132-148

Lacalle RA, Peregil RM, Albar JP, Merino E, Martinez AC, Merida I, Manes S (2007) Type I phosphatidylinositol 4-phosphate 5-kinase controls neutrophil polarity and directional movement. *J Cell Biol* **179**(7)**:** 1539-1553

Lammermann T, Bader BL, Monkley SJ, Worbs T, Wedlich-Soldner R, Hirsch K, Keller M, Forster R, Critchley DR, Fassler R, Sixt M (2008) Rapid leukocyte migration by integrin-independent flowing and squeezing. *Nature* **453**(7191)**:** 51-55

Lammermann T, Sixt M (2009) Mechanical modes of 'amoeboid' cell migration. *Curr Opin Cell Biol* **21**(5)**:** 636-644

Laudanna C, Alon R (2006) Right on the spot. Chemokine triggering of integrin-mediated arrest of rolling leukocytes. *Thromb Haemost* **95**(1)**:** 5-11

Le Clainche C, Carlier MF (2008) Regulation of actin assembly associated with protrusion and adhesion in cell migration. *Physiol Rev* **88**(2)**:** 489-513

Legate KR, Takahashi S, Bonakdar N, Fabry B, Boettiger D, Zent R, Fassler R (2011) Integrin adhesion and force coupling are independently regulated by localized PtdIns(4,5)2 synthesis. *EMBO J* **30**(22)**:** 4539-4553

Li R, Mitra N, Gratkowski H, Vilaire G, Litvinov R, Nagasami C, Weisel JW, Lear JD, DeGrado WF, Bennett JS (2003) Activation of integrin alphaIIbbeta3 by modulation of transmembrane helix associations. *Science* **300**(5620)**:** 795-798

Lin KB, Freeman SA, Zabetian S, Brugger H, Weber M, Lei V, Dang-Lawson M, Tse KW, Santamaria R, Batista FD, Gold MR (2008) The rap GTPases regulate B cell morphology, immune-synapse formation, and signaling by particulate B cell receptor ligands. *Immunity* **28**(1)**:** 75-87

Luo BH, Carman CV, Springer TA (2007) Structural basis of integrin regulation and signaling. *Annu Rev Immunol* **25:** 619-647

Manz RA, Arce S, Cassese G, Hauser AE, Hiepe F, Radbruch A (2002) Humoral immunity and long-lived plasma cells. *Curr Opin Immunol* **14**(4)**:** 517-521

Matsusaka S, Tohyama Y, He J, Shi Y, Hazama R, Kadono T, Kurihara R, Tohyama K, Yamamura H (2005) Protein-tyrosine kinase, Syk, is required for CXCL12-induced polarization of B cells. *Biochem Biophys Res Commun* **328**(4)**:** 1163-1169

McHeyzer-Williams MG (2003) B cells as effectors. *Curr Opin Immunol* **15**(3)**:** 354-361

McLeod SJ, Shum AJ, Lee RL, Takei F, Gold MR (2004) The Rap GTPases regulate integrin-mediated adhesion, cell spreading, actin polymerization, and Pyk2 tyrosine phosphorylation in B lymphocytes. *J Biol Chem* **279**(13)**:** 12009-12019

Mempel TR, Henrickson SE, Von Andrian UH (2004) T-cell priming by dendritic cells in lymph nodes occurs in three distinct phases. *Nature* **427**(6970)**:** 154-159

Meyer-Bahlburg A, Becker-Herman S, Humblet-Baron S, Khim S, Weber M, Bouma G, Thrasher AJ, Batista FD, Rawlings DJ (2008) Wiskott-Aldrich syndrome protein deficiency in B cells results in impaired peripheral homeostasis. *Blood* **112**(10)**:** 4158-4169

Miller MJ, Wei SH, Parker I, Cahalan MD (2002) Two-photon imaging of lymphocyte motility and antigen response in intact lymph node. *Science* **296**(5574)**:** 1869-1873

Molon B, Gri G, Bettella M, Gomez-Mouton C, Lanzavecchia A, Martinez AC, Manes S, Viola A (2005) T cell costimulation by chemokine receptors. *Nat Immunol* **6**(5)**:** 465-471

Monks CR, Freiberg BA, Kupfer H, Sciaky N, Kupfer A (1998) Three-dimensional segregation of supramolecular activation clusters in T cells. *Nature* **395**(6697)**:** 82-86

Monypenny J, Chou HC, Banon-Rodriguez I, Thrasher AJ, Anton IM, Jones GE, Calle Y (2010) Role of WASP in cell polarity and podosome dynamics of myeloid cells. *Eur J Cell Biol* **90**(2-3)**:** 198-204

Mor A, Dustin ML, Philips MR (2007) Small GTPases and LFA-1 reciprocally modulate adhesion and signaling. *Immunol Rev* **218:** 114-125

Murphy K TP, Walport M (2008) *Janeway's Immunobiology*, Seventh Edition edn.: Garland Science.

Neitzel KL, Hepler JR (2006) Cellular mechanisms that determine selective RGS protein regulation of G protein-coupled receptor signaling. *Semin Cell Dev Biol* **17**(3)**:** 383-389

Ni N, Kevil CG, Bullard DC, Kucik DF (2003) Avidity modulation activates adhesion under flow and requires cooperativity among adhesion receptors. *Biophys J* **85**(6)**:** 4122-4133

Nieto M, Frade JM, Sancho D, Mellado M, Martinez AC, Sanchez-Madrid F (1997) Polarization of chemokine receptors to the leading edge during lymphocyte chemotaxis. *J Exp Med* **186**(1)**:** 153-158

Nolte MA, Belien JA, Schadee-Eestermans I, Jansen W, Unger WW, van Rooijen N, Kraal G, Mebius RE (2003) A conduit system distributes chemokines and small blood-borne molecules through the splenic white pulp. *J Exp Med* **198**(3)**:** 505-512

Nolz JC, Medeiros RB, Mitchell JS, Zhu P, Freedman BD, Shimizu Y, Billadeau DD (2007) WAVE2 regulates high-affinity integrin binding by recruiting vinculin and talin to the immunological synapse. *Mol Cell Biol* **27**(17)**:** 5986-6000

Okada T, Cyster JG (2006) B cell migration and interactions in the early phase of antibody responses. *Curr Opin Immunol* **18**(3)**:** 278-285

Okada T, Miller MJ, Parker I, Krummel MF, Neighbors M, Hartley SB, O'Garra A, Cahalan MD, Cyster JG (2005) Antigen-engaged B cells undergo chemotaxis toward the T zone and form motile conjugates with helper T cells. *PLoS Biol* **3**(6)**:** e150

Oldham WM, Hamm HE (2008) Heterotrimeric G protein activation by G-protein-coupled receptors. *Nat Rev Mol Cell Biol* **9**(1)**:** 60-71

Pasapera AM, Schneider IC, Rericha E, Schlaepfer DD, Waterman CM (2010) Myosin II activity regulates vinculin recruitment to focal adhesions through FAK-mediated paxillin phosphorylation. *J Cell Biol* **188**(6)**:** 877-890

Pearce G, Audzevich T, Jessberger R (2011) SYK regulates B-cell migration by phosphorylation of the F-actin interacting protein SWAP-70. *Blood* **117**(5)**:** 1574-1584

Phan TG, Grigorova I, Okada T, Cyster JG (2007) Subcapsular encounter and complement-dependent transport of immune complexes by lymph node B cells. *Nat Immunol* **8**(9)**:** 992-1000

Qi H, Egen JG, Huang AY, Germain RN (2006) Extrafollicular activation of lymph node B cells by antigen-bearing dendritic cells. *Science* **312**(5780)**:** 1672-1676

Randall KL, Lambe T, Johnson A, Treanor B, Kucharska E, Domaschenz H, Whittle B, Tze LE, Enders A, Crockford TL, Bouriez-Jones T, Alston D, Cyster JG, Lenardo MJ, Mackay F, Deenick EK, Tangye SG, Chan TD, Camidge T, Brink R, Vinuesa CG, Batista FD, Cornall RJ, Goodnow CC (2009) Dock8 mutations cripple B cell immunological synapses, germinal centers and long-lived antibody production. *Nat Immunol* **10**(12)**:** 1283-1291

Reth M, Wienands J (1997) Initiation and processing of signals from the B cell antigen receptor. *Annu Rev Immunol* **15:** 453-479

Riedl J, Crevenna AH, Kessenbrock K, Yu JH, Neukirchen D, Bista M, Bradke F, Jenne D, Holak TA, Werb Z, Sixt M, Wedlich-Soldner R (2008) Lifeact: a versatile marker to visualize F-actin. *Nat Methods* **5**(7)**:** 605-607

Rodriguez-Frade JM, Mellado M, Martinez AC (2001) Chemokine receptor dimerization: two are better than one. *Trends Immunol* **22**(11)**:** 612-617

Roozendaal R, Mempel TR, Pitcher LA, Gonzalez SF, Verschoor A, Mebius RE, von Andrian UH, Carroll MC (2009) Conduits mediate transport of low-molecular-weight antigen to lymph node follicles. *Immunity* **30**(2)**:** 264-276

Russell DM, Dembic Z, Morahan G, Miller JF, Burki K, Nemazee D (1991) Peripheral deletion of self-reactive B cells. *Nature* **354**(6351)**:** 308-311

Saito K, Tolias KF, Saci A, Koon HB, Humphries LA, Scharenberg A, Rawlings DJ, Kinet JP, Carpenter CL (2003) BTK regulates PtdIns-4,5-P2 synthesis: importance for calcium signaling and PI3K activity. *Immunity* **19**(5)**:** 669-678

Schaeuble K, Hauser MA, Singer E, Groettrup M, Legler DF (2011) Cross-talk between TCR and CCR7 signaling sets a temporal threshold for enhanced T lymphocyte migration. *J Immunol* **187**(11)**:** 5645-5652

Schumann K, Lammermann T, Bruckner M, Legler DF, Polleux J, Spatz JP, Schuler G, Forster R, Lutz MB, Sorokin L, Sixt M (2010) Immobilized chemokine fields and soluble chemokine gradients cooperatively shape migration patterns of dendritic cells. *Immunity* **32**(5)**:** 703-713

Serrador JM, Nieto M, Sanchez-Madrid F (1999) Cytoskeletal rearrangement during migration and activation of T lymphocytes. *Trends Cell Biol* **9**(6)**:** 228-233

Shen K, Tolbert CE, Guilluy C, Swaminathan VS, Berginski ME, Burridge K, Superfine R, Campbell SL (2011) The vinculin C-terminal hairpin mediates F-actin bundle formation, focal adhesion, and cell mechanical properties. *J Biol Chem* **286**(52)**:** 45103-45115

Shlomchik MJ, Weisel F (2012) Germinal center selection and the development of memory B and plasma cells. *Immunol Rev* **247**(1)**:** 52-63

Simon MI, Strathmann MP, Gautam N (1991) Diversity of G proteins in signal transduction. *Science* **252**(5007)**:** 802-808

Simonson WT, Franco SJ, Huttenlocher A (2006) Talin1 regulates TCR-mediated LFA-1 function. *J Immunol* **177**(11)**:** 7707-7714

Sims TN, Soos TJ, Xenias HS, Dubin-Thaler B, Hofman JM, Waite JC, Cameron TO, Thomas VK, Varma R, Wiggins CH, Sheetz MP, Littman DR, Dustin ML (2007) Opposing effects of PKCtheta and WASp on symmetry breaking and relocation of the immunological synapse. *Cell* **129**(4)**:** 773-785

Sixt M, Kanazawa N, Selg M, Samson T, Roos G, Reinhardt DP, Pabst R, Lutz MB, Sorokin L (2005) The conduit system transports soluble antigens from the afferent lymph to resident dendritic cells in the T cell area of the lymph node. *Immunity* **22**(1)**:** 19-29

Smith A, Bracke M, Leitinger B, Porter JC, Hogg N (2003) LFA-1-induced T cell migration on ICAM-1 involves regulation of MLCK-mediated attachment and ROCK-dependent detachment. *J Cell Sci* **116**(Pt 15)**:** 3123-3133

Spaargaren M, Beuling EA, Rurup ML, Meijer HP, Klok MD, Middendorp S, Hendriks RW, Pals ST (2003) The B cell antigen receptor controls integrin activity through Btk and PLCgamma2. *J Exp Med* **198**(10)**:** 1539-1550

Stachowiak AN, Wang Y, Huang YC, Irvine DJ (2006) Homeostatic lymphoid chemokines synergize with adhesion ligands to trigger T and B lymphocyte chemokinesis. *J Immunol* **177**(4)**:** 2340-2348

Tadokoro S, Shattil SJ, Eto K, Tai V, Liddington RC, de Pereda JM, Ginsberg MH, Calderwood DA (2003) Talin binding to integrin beta tails: a final common step in integrin activation. *Science* **302**(5642)**:** 103-106

Tedder TF (2009) CD19: a promising B cell target for rheumatoid arthritis. *Nat Rev Rheumatol* **5**(10)**:** 572-577

Thelen M (2001) Dancing to the tune of chemokines. *Nat Immunol* **2**(2)**:** 129-134

Thelen M, Stein JV (2008) How chemokines invite leukocytes to dance. *Nat Immunol* **9**(9)**:** 953-959

Thomas S, Baumgart DC (2012) Targeting leukocyte migration and adhesion in Crohn's disease and ulcerative colitis. *Inflammopharmacology* **20**(1)**:** 1-18

Underhill DM, Bassetti M, Rudensky A, Aderem A (1999) Dynamic interactions of macrophages with T cells during antigen presentation. *J Exp Med* **190**(12)**:** 1909-1914

Vascotto F, Lankar D, Faure-Andre G, Vargas P, Diaz J, Le Roux D, Yuseff MI, Sibarita JB, Boes M, Raposo G, Mougneau E, Glaichenhaus N, Bonnerot C, Manoury B, Lennon-Dumenil AM (2007) The actin-based motor protein myosin II regulates MHC class II trafficking and BCR-driven antigen presentation. *J Cell Biol* **176**(7)**:** 1007-1019

Vicente-Manzanares M, Ma X, Adelstein RS, Horwitz AR (2009) Non-muscle myosin II takes centre stage in cell adhesion and migration. *Nat Rev Mol Cell Biol* **10**(11)**:** 778-790

Vicente-Manzanares M, Montoya MC, Mellado M, Frade JM, del Pozo MA, Nieto M, de Landazuri MO, Martinez AC, Sanchez-Madrid F (1998) The chemokine SDF-1alpha triggers a chemotactic response and induces cell polarization in human B lymphocytes. *Eur J Immunol* **28**(7)**:** 2197-2207

Vicente-Manzanares M, Zareno J, Whitmore L, Choi CK, Horwitz AF (2007) Regulation of protrusion, adhesion dynamics, and polarity by myosins IIA and IIB in migrating cells. *J Cell Biol* **176**(5)**:** 573-580

Vinogradova O, Velyvis A, Velyviene A, Hu B, Haas T, Plow E, Qin J (2002) A structural mechanism of integrin alpha(IIb)beta(3) "inside-out" activation as regulated by its cytoplasmic face. *Cell* **110**(5)**:** 587-597

Watanabe N, Bodin L, Pandey M, Krause M, Coughlin S, Boussiotis VA, Ginsberg MH, Shattil SJ (2008) Mechanisms and consequences of agonist-induced talin recruitment to platelet integrin alphaIIbbeta3. *J Cell Biol* **181**(7)**:** 1211-1222

Weber M, Treanor B, Depoil D, Shinohara H, Harwood NE, Hikida M, Kurosaki T, Batista FD (2008) Phospholipase C-gamma2 and Vav cooperate within signaling microclusters to propagate B cell spreading in response to membrane-bound antigen. *J Exp Med* **205**(4)**:** 853-868

Westerberg L, Greicius G, Snapper SB, Aspenstrom P, Severinson E (2001) Cdc42, Rac1, and the Wiskott-Aldrich syndrome protein are involved in the cytoskeletal regulation of B lymphocytes. *Blood* **98**(4)**:** 1086-1094

Westerberg L, Larsson M, Hardy SJ, Fernandez C, Thrasher AJ, Severinson E (2005) Wiskott-Aldrich syndrome protein deficiency leads to reduced B-cell adhesion, migration, and homing, and a delayed humoral immune response. *Blood* **105**(3)**:** 1144-1152

Wykes M, Pombo A, Jenkins C, MacPherson GG (1998) Dendritic cells interact directly with naive B lymphocytes to transfer antigen and initiate class switching in a primary T-dependent response. *J Immunol* **161**(3)**:** 1313-1319

Yu T, Wu X, Gupta KB, Kucik DF (2010) Affinity, lateral mobility, and clustering contribute independently to beta 2-integrin-mediated adhesion. *Am J Physiol Cell Physiol* **299**(2)**:** C399-410

Ziegler WH, Liddington RC, Critchley DR (2006) The structure and regulation of vinculin. *Trends Cell Biol* **16**(9)**:** 453-460

Zimmermann HW, Tacke F (2011) Modification of chemokine pathways and immune cell infiltration as a novel therapeutic approach in liver inflammation and fibrosis. *Inflamm Allergy Drug Targets* **10**(6)**:** 509-536

Zufferey R, Nagy D, Mandel RJ, Naldini L, Trono D (1997) Multiply attenuated lentiviral vector achieves efficient gene delivery in vivo. *Nat Biotechnol* **15**(9)**:** 871-875

9. ANEXOS

ANEXO 1. VIDEOS

Video 1. Migración de células B en respuesta a CXCL13 sobre membranas que contienen ICAM-1. Dinámica de células B primarias en contacto con membranas que contienen GPI-ICAM-1 (150 molec/μm^2) y que han sido previamente tapizadas con CXCL13 (100nM). Se muestran imágenes de DIC, fluorescencia de CFSE (verde) e IRM a lo largo del tiempo (25 min; 8 *frames per second*, fps).

Video 2. Modulación de la dinámica de las células B en presencia de antígeno específico. (A-D) Dinámica de células B 3-83 representativas en contacto con membranas que contienen ICAM-1, p31 a las densidades indicadas (A, 0 molec/μm^2; B, 4 molec/μm^2; C, 20 molec/μm^2; D, 100 molec/μm^2) y tapizadas con CXCL13. Se muestran imágenes de DIC (panel superior), fluorescencia de p31 (panel medio) e IRM (panel inferior) en el plano de contacto a lo largo del tiempo (20 min; 8 fps).

Video 3. Dinámica molecular de CXCR5-GFP en el plano de contacto de células B A20 en migración y durante el establecimiento de la SI. (A) Dinámica de una célula B A20 representativa, transfectada con CXCR5-GFP, en membranas que contienen ICAM-1 y CXCL13. Se muestran imágenes de DIC, fluorescencia de CXCR5 (verde, y en escala de código de color) e IRM en el plano de contacto a lo largo del tiempo (15 min; 5 fps). Flechas blancas, agregados de CXCR5-GFP. (B) Imágenes de DIC y fluorescencia de CXCR5 (verde) y antígeno (rojo) a lo largo del tiempo (15 min; 5 fps), en el plano de la SI de células B A20 representativas, transfectadas con CXCR5-GFP, en contacto con membranas tapizadas con CXCL13 y que contienen ICAM-1 y antígeno (anti-κ mAb).

Video 4. Aumento de la captura de antígeno en la SI de células B mediante la formación de *membrane ruffles* y contactos LFA-1/ICAM-1. Dinámica de células B MD4 representativas que forman SI en membranas con ICAM-1 y HEL (20 molec/ μm^2) en ausencia (video 4A) o en presencia de CXCL13 (video 4B). Imágenes de DIC, IRM y fluorescencia de antígeno (en escala de grises) a largo del tiempo (10 min; 8fps). Las flechas blancas monitorizan los *membrane ruffles* emitidos, que hacen un nuevo contacto con la membrana y capturan antígeno.

Video 5. Señal de calcio en células B en presencia de una densidad sub-óptima de antígeno, y en ausencia o presencia de CXCL13. Imágenes de DIC

y fluorescencia de Fluo4FF (flujo de Ca^{2+}, en escala de código de color) a lo largo del tiempo (30 min; 8 fps) de células B MD4 representativas en contacto con membranas que contienen ICAM-1 y HEL (1 molec/ μm^2), solo o con CXCL13.

Video 6. Comportamiento de células B en presencia de CXCL13 y en ausencia o presencia de antígeno presentado de distinta forma. Dinámica de células B en contacto con membranas que contienen ICAM-1, CXCL13 y en ausencia (A) o presencia de antígeno en forma soluble (sAg; B) o de antígeno presentado sobre la membrana (tAg; C). Imágenes de DIC e IRM a lo largo del tiempo (15 min; 7 fps); las flechas en (B) indican células B en migración.

Video 7. Reclutamiento de Vinculina y F-actina durante la formación de la sinapsis de la célula B. Monitorización de la formación de la SI de células B A20 co-transfectadas con las construcciones vinculina-GFP y LifeAct-RFP en contacto con membranas que contienen ICAM-1, CXCL13 y tAg. Imágenes de DIC, IRM y fluorescencia de vinculina (verde), F-actina (rojo) y antígeno (en escala de grises) de una célula B A20 representativa a lo largo del tiempo (18 min; 5 fps).

Video 8. Reclutamiento temprano y distribución de PIPKIγ en la sinapsis de la célula B. Monitorización de la formación de la SI de células B A20 transfectadas con la construcción PIPKIγ-GFP en contacto con membranas que contienen ICAM-1, CXCL13 y tAg. Imágenes de DIC, IRM y fluorescencia de PIPKIγ (en escala de código de color) y de antígeno (rojo) de una célula B A20 representativa a lo largo del tiempo (8 min; 5 fps).

Video 9. Producción local y distribución de PIP_2 en la sinapsis de la célula B. Monitorización de la formación de la SI de células B A20 transfectadas con la sonda fluorescente para PIP_2 PLCδ-PH-GFP en contacto con membranas que contienen ICAM-1, CXCL13 y tAg. Imágenes de DIC, IRM y fluorescencia de PIP_2 (en escala de código de color) y antígeno (rojo) de una célula B A20 representativa a lo largo del tiempo (9 min; 5 fps).

Video 10. Dinámica de células B tratadas con BAY sobre membranas con tAg. Comportamiento de células B primarias no tratadas (A) o tratadas con BAY (B) en contacto con membranas que contiene ICAM-1, CXCL13 y tAg. Imágenes de DIC y de IRM superpuesto con fluorescencia de antígeno (rojo) a lo largo del tiempo (10 min, 7 fps); las flechas en (A) indican la dinámica de una célula B representativa (A) que ha formado SI (agregado de antígeno fluorescente en rojo, cSMAC) y emite

membrane ruffles (detectados por IRM y DIC), y en (B) células B migrando con el agregado de antígeno (rojo) en el urópodo.

Video 11. La inhibición de NM-II provoca la pérdida de vinculina de la sinapsis. Monitorización de la SI de células B A20 co-transfectadas con las construcciones vinculina-GFP y LifeAct-RFP en contacto con membranas que contienen ICAM-1, CXCL13 y tAg, durante el tratamiento con blebistatina. Imágenes de DIC, IRM y fluorescencia de vinculina (verde), F-actina (rojo) y antígeno (escala de grises) de una célula B A20 representativa a lo largo del tiempo (20 min; 5 fps); se indica el tiempo en el que se añade blebistatina y un intervalo de 10 min no monitorizado.

ANEXO 2. PUBLICACIONES I

Publicaciones originadas a partir de este trabajo de investigación

blood

2011 118: 1560-1569
Prepublished online June 9, 2011;
doi:10.1182/blood-2011-01-332106

CXCL13/CXCR5 signaling enhances BCR-triggered B-cell activation by shaping cell dynamics

Julia Sáez de Guinoa, Laura Barrio, Mario Mellado and Yolanda R. Carrasco

Blood (print ISSN 0006-4971, online ISSN 1528-0020), is published weekly by the American Society of Hematology, 2021 L St, NW, Suite 900, Washington DC 20036.

CXCL13/CXCR5 signaling enhances BCR-triggered B-cell activation by shaping cell dynamics

Julia Sáez de Guinoa,[1] Laura Barrio,[1] Mario Mellado,[2] and Yolanda R. Carrasco[1]

[1]B Cell Dynamics Group, Department of Immunology and Oncology, Centro Nacional de Biotecnología/Consejo Superior de Investigaciones Científicas, Madrid, Spain; and [2]Chemokine Signaling Group, Department of Immunology and Oncology, Centro Nacional de Biotecnología/Consejo Superior de Investigaciones Científicas, Madrid, Spain

Continuous migration of B cells at the follicle contrasts with their stable arrest after encounter with antigen. Two main ligand/receptor pairs are involved in these cell behaviors: the chemokine CXCL13/chemokine receptor CXCR5 and antigen/BCR. Little is known regarding the interplay between CXCR5 and BCR signaling in the modulation of B-cell dynamics and its effect on B-cell activation. We used a 2-dimensional model to study B-cell migration and antigen recognition in real time, and found that BCR signaling strength alters CXCL13-mediated migration, leading to a heterogeneous B-cell behavior pattern. In addition, we demonstrate that CXCL13/CXCR5 signaling does not impair BCR-triggered immune synapse formation and that CXCR5 is excluded from the central antigen cluster. CXCL13/CXCR5 signaling enhances BCR-mediated B-cell activation in at least 2 ways: (1) it assists antigen gathering at the synapse by promoting membrane ruffling and lymphocyte function–associated antigen 1 (LFA-1)–supported adhesion, and (2) it allows BCR signaling integration in motile B cells through establishment of LFA-1–supported migratory junctions. Both processes require functional actin cytoskeleton and nonmuscle myosin II motor protein. Therefore, the CXCL13/CXCR5 signaling effect on shaping B-cell dynamics is an effective mechanism that enhances antigen encounter and BCR-triggered B-cell activation. (*Blood.* 2011;118(6):1560-1569)

Introduction

The incessant migration of B cells in vivo in the secondary lymphoid organs (ie, the lymph nodes and spleen) is a search for specific antigens.[1,2] Once B cells enter lymph nodes through the high endothelial venules, they move toward the follicles, guided by the chemokine CXCL13 and a network of stromal cells.[3] B cells concentrate in the proximity of the follicular dendritic cell (FDC) network to form the follicles, which are confined by a ceiling of subcapsular sinus macrophages, a floor of fibroblastic reticular cells and dendritic cells, and interfollicular walls composed mainly of macrophages and fibroblastic reticular cells. In steady-state conditions, B cells explore the entire follicular volume, moving randomly at an average speed of 6 μm/min.[1,2] CXCL13, which is produced mainly by FDCs, underlies this B-cell behavior by signaling through its receptor, CXCR5.[4]

Specific antigen recognition through BCR alters steady-state B-cell dynamics at the follicle. B cells stop to gather antigen into a central cluster at the site of contact with the antigen-presenting cell, establishing an immune synapse (IS).[5] IS formation is critical for B-cell activation, antigen internalization, and affinity discrimination, as shown by in vitro[6,7] and in vivo approaches.[8] Although the B cell IS persists for at least 20-30 minutes, it is a transient stage. In vivo, B cells accumulate particulate antigen with time[5] up to a threshold that triggers their capacity to respond to CCL21 through CCR7, after which they exit the follicle in search of T-cell help.[2] These data suggest a series of "stop plus IS" events, followed by "go or motile" events on the B cell to achieve antigen accumulation. Modulation of B-cell dynamics thus becomes critical for shaping the process of antigen encounter and subsequent B-cell activation. The nature of the interplay between BCR and CXCR5 in regulating B-cell behavior is nonetheless almost entirely unknown.

We established a 2-dimensional model that allows the study of CXCL13-mediated B-cell migration and antigen encounter in real time. To mimic the cell surface, we used planar lipid bilayers containing the lymphocyte function–associated antigen 1 (LFA-1) integrin ligand ICAM-1 as the GPI-linked protein, as well as tethered antigen and a CXCL13 coating. This model allowed us to reproduce steady-state B-cell dynamic parameters similar to those observed in vivo with multiphoton microscopy techniques. Using distinct BCR transgenic models, we show herein that BCR signaling strength alters CXCL13-mediated B-cell migration. CXCL13/CXCR5 signaling does not significantly affect BCR-triggered IS formation, and CXCR5 segregates outside of the central antigen/BCR cluster of the synapse; however, it enhances BCR-mediated cell activation. CXCL13/CXCR5 facilitated antigen encounter and BCR signaling by promoting membrane ruffling and LFA-1–supported adhesion in stopped/IS-forming B cells, and through the establishment of an LFA-1–supported migratory junction ("kinapse") in motile B cells. Both mechanisms require a functional actin cytoskeleton and the activity of the motor protein non-muscle myosin II (NM-II).

Submitted January 21, 2011; accepted May 30, 2011. Prepublished online as *Blood* First Edition paper, June 9, 2011; DOI 10.1182/blood-2011-01-332106.

The online version of this article contains a data supplement.

The publication costs of this article were defrayed in part by page charge payment. Therefore, and solely to indicate this fact, this article is hereby marked "advertisement" in accordance with 18 USC section 1734.

Methods

Mice and cells

Wild-type (C57BL/6, BALB/c) and genetically modified naive B cells (BCR-transgenic and CXCR5-deficient) were freshly isolated from spleens of wild-type, MD4,[9] 3-83,[10] and CXCR5-deficient mice[11] by negative selection (> 95% purity), as described previously.[6] Purified B cells were labeled with 0.1μM CFSE long-term dye (Molecular Probes) for 10 minutes at 37°C before use. Animal experimentation was approved by the Centro Nacional de Biotecnología/Consejo Superior de Investigaciones Científicas Bioethics Committee and conforms to institutional and national regulations. The murine A20 B-cell line was stably transfected with the CXCR5-green fluorescent protein (GFP) construct (see supplemental Methods, available on the *Blood* Web site; see the Supplemental Materials link at the top of the online article).

Time-lapse microscopy on planar lipid bilayers

Planar lipid bilayers were prepared as described previously.[6] Briefly, unlabeled GPI-linked ICAM-1 liposomes and/or liposomes containing biotinylated lipids were mixed with 1,2-dioleoyl-PC at various ratios to obtain specified molecular densities. Membranes were assembled in FCS2 chambers (Bioptechs) and then blocked with PBS with 2% FCS for 1 hour at room temperature. Antigen was tethered by incubating membranes with Alexa Fluor 647–streptavidin (Molecular Probes), followed by monobiotinylated peptide p31 for 3-83 B cells,[12] monobiotinylated F10 anti–hen egg lysozyme (anti-HEL) mAb plus HEL (Sigma-Aldrich) for MD4 B cells,[6] or monobiotinylated anti-κ light chain mAb (BD Biosciences) for non-BCR transgenic B cells and the A20 B-cell line. The final step was coating with recombinant murine CXCL13 (Peprotech) at the indicated concentration for 30 minutes at room temperature immediately before imaging. CFSE-labeled B cells were injected into the warmed (37°C) chamber at time zero; confocal fluorescence, differential interference contrast (DIC), and interference reflection microscopy (IRM) images were acquired every 10 seconds for 25 minutes. All assays were performed in PBS with 0.5% FCS, 0.5 g/L of D-glucose, 2mM $MgCl_2$, and 0.5mM $CaCl_2$, followed by injection with latrunculin A (0.5μM; Calbiochem) or blebbistatin (50μM; Calbiochem) to the FCS2, waiting for 5-10 minutes, and then imaging again for 20 minutes. Images were acquired on a Zeiss Axiovert LSM 510-META inverted microscope with a 40× oil-immersion objective and analyzed by LSM 510 software (Zeiss) and Imaris 6.0 software (Bitplane). Graphs and statistical analyses were generated with Prism 4.0 software (GraphPad); the unpaired Student *t* test was applied. For quantitative studies at the target membrane and the cell surface, see supplemental Methods.

For intracellular Ca^{2+} flux measurement, purified B cells were labeled with 1μM Fluo-4FF (Molecular Probes) for 30 minutes at room temperature, immediately injected into the warmed FCS2 chamber, and imaged every 10 seconds for 15 or 30 minutes at low quality to speed up acquisition. Ca^{2+} flux was monitored by fluorescence and DIC images, and analyzed by LSM 510 software (Zeiss).

Immunofluorescence and B-cell activation assays

For details of the immunofluorescence and B-cell activation assays, please see supplemental Methods.

Results

Two-dimensional model to study B-cell dynamics in response to CXCR5 and BCR signaling

To dissect the control of naive B-cell dynamics by CXCR5 and BCR signaling, we established a model that allowed simultaneous study of CXCL13-mediated B-cell migration, B-cell antigen recognition, and IS formation. The planar lipid bilayer system mimics the fluid surface of a cell[13] and has been used to study B-cell antigen encounter[6]; we optimized conditions for migration of primary naive B cells in response to CXCL13 on this substrate. Data for CXCL13 immunostaining in lymphoid tissue,[14] as well as its ability to bind certain glycosaminoglycans present on cell surfaces,[15] suggest that, in vivo, B cells encounter CXCL13 on the FDC surface; the FDC network has a central role in orchestrating B-cell motility at the follicle.[3] To mimic this in vivo situation, we coated the artificial membranes with CXCL13 and, given the positive charge of chemokines, CXCL13 easily associated with the negatively charged phospholipids through electrostatic interaction. Homogeneous CXCL13 binding to the lipid bilayer might provide a chemokinetic stimulus and thus lead to random B-cell migration, as described in vivo[1,2]; to date, no CXCL13 gradient has been reported within the follicle. As a GPI-linked membrane protein, we included the adhesion molecule ICAM-1, the principal ligand of the integrin LFA-1. LFA-1/ICAM-1 have a critical role in B-cell IS formation,[6] and are implicated in B-cell contact with FDCs[16] and in lymphocyte movement.[17-19] In addition, leukocytes show a preference for migrating on adhesive substrates coated with immobilized chemokine.[20] The setup of our model might therefore promote this type of "haptokinetic" response in B cells.

We isolated wild-type naive B cells from mouse spleen and assayed their migratory capacity on CXCL13-coated, ICAM-1–containing membranes in real time using confocal microscopy approaches (supplemental Video 1). DIC examination of naive B cells on ICAM-1–containing membranes with CXCL13 coating showed 2 distinct morphologies: nonpolarized B cells (round shape) and cells with a flattened leading-edge extension at the front (lamellipodium), followed by the bulky nucleus at the back (polarized B cells; Figure 1A). The presence of CXCL13 on the membrane was sufficient to promote polarization of the naive B-cell population (Figure 1B). Nonetheless, naive B cells migrated only when CXCL13 was combined with ICAM-1. Both CXCL13-mediated cell polarization and migration were dependent on the expression of CXCR5 at the B-cell surface, as the results with CXCR5-deficient B cells indicated (Figure 1B).

Above a minimum ICAM-1 density of 75 molecules/μm^2, most of the B-cell population migrated in response to CXCL13 (Figure 1B). Both cell polarization and migration were dependent on the chemokine concentration used to coat the membranes, and therefore on the amount of CXCL13 on the bilayer (Figure 1C); 100nM CXCL13 yielded optimal B-cell polarization and migratory responses. Analysis of the cell dynamic parameters showed an average speed of > 5 μm/min at ICAM-1 densities of 150 and 300 molecules/μm^2 (Figure 1D), which is very close to the in vivo B-cell interstitial velocity within the follicle (6 μm/min).[1] The tracks stress the characteristic random B-cell motility, with average total lengths of 120 μm for the time recorded (Figure 1D-E). Migration of naive B cells slowed when they were exposed to higher ICAM-1 densities (600 molecules/μm^2; Figure 1D), highlighting the effect of the integrin ligand on B-cell dynamics. We used IRM to analyze the nature of the contacts established by B cells with the lipid bilayer at different ICAM-1 densities (Figure 1F). Migration failure at ICAM-1 densities of < 75 molecules/μm^2 correlated with small, intermittent B-cell contacts. B cell: membrane interactions were similar in area and were stable over time at higher densities.

We established a 2-dimensional model that supports naive B-cell migration in response to CXCL13. The use of 100nM CXCL13 to coat the membrane plus an ICAM-1 density of 150 molecules/μm^2 yielded optimal conditions for B-cell motility,

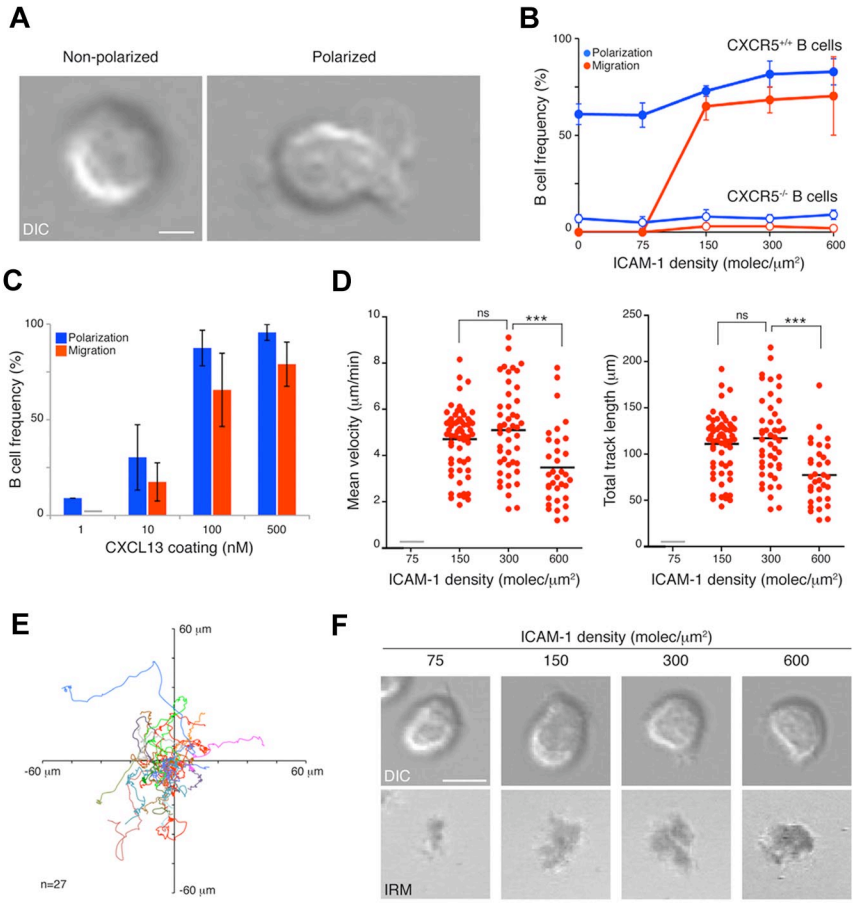

Figure 1. Naive B-cell dynamics on 2-dimensional membranes. (A) DIC images of representative nonpolarized and polarized naive B cells on ICAM-1–containing membranes, coated with 100nM CXCL13. Scale bar indicates 2 μm. (B) Frequency of naive B-cell polarization and migration on membranes containing ICAM-1 at different densities and coated with 100nM CXCL13. Filled symbols indicate wild-type B cells; open symbols, CXCR5-deficient B cells. (C) Frequency of naive B-cell polarization and migration on ICAM-1 (150 molecules/μm²)–containing membranes coated with different concentrations of CXCL13. Values for mean velocity and total track length (D) and tracks of migratory B cells (E) on ICAM-1–containing membranes coated with 100nM CXCL13. (F) Representative DIC and IRM images of naive B cells on ICAM-1–containing membranes at specified densities and CXCL13 coating (100nM). Scale bar indicates 5 μm. Data in panels B and C represent the mean ± SEM of 4 experiments; data in panels D and E correspond to the merge of 3 experiments. Gray bar indicates not detected; ns, not significant. ***$P < .0001$.

and resembled in vivo steady-state dynamics in the follicle. We used these conditions for the remainder of the study.

BCR signaling strength alters CXCL13-mediated B-cell migration

To study the effect of antigen encounter on CXCL13-induced B-cell migration, we used BCR-transgenic 3-83 B cells, which recognize the p31 antigenic peptide with low affinity (K_A 65 × 10^6 M^{-1}). We anchored p31 to the membrane, as described previously[6] (see "Methods"). The dynamic parameters of 3-83 naive B-cell movement across the ICAM-1–containing membranes were equivalent to those of wild-type B cells in response to CXCL13 (Figure 2A-C). Depending on its density, tethered p31 altered cell migration in several ways (Figure 2A-C and supplemental Videos 2-5). B-cell motility was completely abolished at high p31 densities (100 molecules/μm²); only a few cells moved and did so at low speed, describing very short tracks independently of the presence of CXCL13. Five times less p31 (20 molecules/μm²) allowed 30% of the B cells to migrate, but at approximately half the average speed and with tiny tracks. This motility was due mainly to CXCL13 signals, because p31 alone promoted some migration in only 10% of B cells. B-cell migration was recovered at low p31 densities (4 molecules/μm²), although with significant differences in average speed and cell tracks relative to controls (no p31).

To confirm our results in a different BCR-transgenic model and with another antigen, we used MD4 BCR-transgenic B cells that recognize HEL with very high affinity (K_A 5 × 10^{10} M^{-1}; see "Methods"). MD4 B cells migrated on ICAM-1–containing membranes in response to CXCL13, although in lower numbers and at a lower average speed than wild-type B cells (supplemental Figure 1A-C). Results were nonetheless similar to those obtained above. Because of the higher affinity and consequent stronger BCR signaling, MD4 B-cell migration stopped at 20 molecules/μm² antigen density. As HEL decreased (4 and 1 molecule/μm²), the CXCL13 signal overcame the BCR signaling effect and promoted migration of a percentage of the B-cell population (33% and 66%, respectively, of migration in the absence of antigen). These cells nonetheless moved more slowly and had short tracks (supplemental Figure 1A-C). To verify that the moving cells detected the low HEL density, we analyzed the levels of phosphorylated Syk (p-Syk), an early marker of BCR signaling,[21] at the B-cell contact zone with the membrane (see "Methods"). We costained with phalloidin, which identifies migratory cells by the lack of the F-actin ring characteristic of stopped cells that form an immune synapse.[22] Quantitative analyses of p-Syk fluorescence showed higher p-Syk levels in migratory MD4 B cells on CXCL13-coated membranes containing low doses of HEL than on membranes with chemokine alone (supplemental Figure 1D). Results were similar for 3-83 B cells in the presence of low p31 doses (not shown).

Our data indicate that BCR signaling strength, which is a direct function of abundance of and BCR affinity for antigen, models CXCL13-mediated B-cell migration with a wide range of consequences. Whereas strong BCR signals drive the B cell to halt its movement (STOP signal), weak BCR signals allow B cells to migrate in response to CXCL13 (GO signal) at frequencies near those of no antigen. A heterogeneous pattern of B-cell behaviors (lower migration frequency, diminished velocity, and shorter tracks) lies between the STOP and GO states.

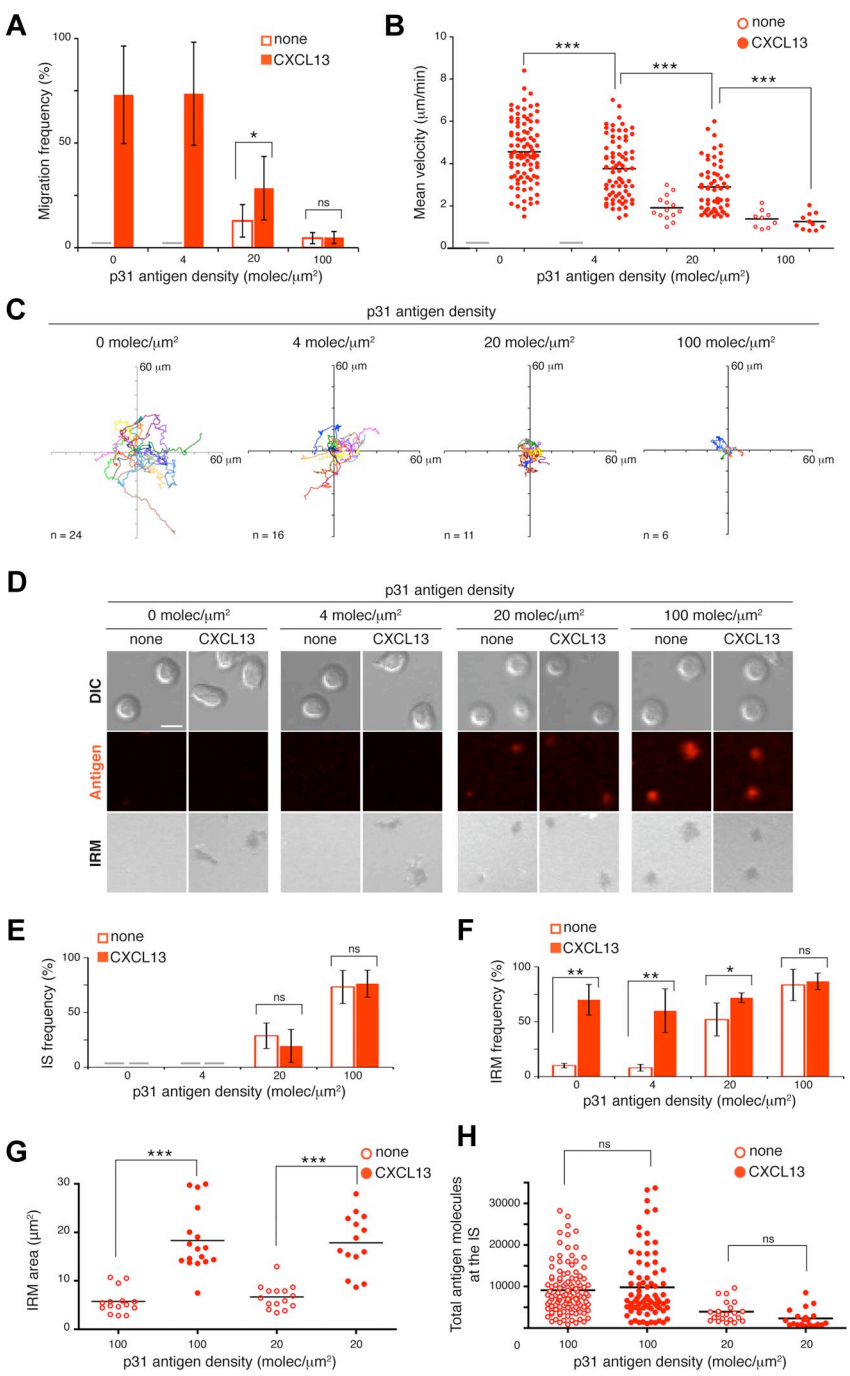

Figure 2. B-cell migration and IS formation in response to CXCL13 and antigen stimuli. Frequency of migration (A) and mean velocity (B) of 3-83 B cells on membranes with tethered p31 at different densities alone or with CXCL13. (C) Tracks of migratory 3-83 B cells in the presence of tethered p31 at the specified densities with CXCL13. (D) Representative DIC, fluorescent antigen, and IRM images at 30 minutes of naive 3-83 B cells settled on membranes bearing p31 at the indicated densities alone or with CXCL13. Scale bar indicates 5 μm. Frequency of IS formation estimated by fluorescence (E) and frequency (F) and area of B cell: membrane contacts estimated by IRM (G) 30 minutes after 3-83 B cells settling on membranes. (H) Total antigen molecules accumulated at the 3-83 IS established after 30 minutes on membranes with tethered p31 at the indicated densities alone or with CXCL13. All experiments were performed in the presence of ICAM-1 (150 molecules/μm²). Data in panels A, E, and F represent the means ± SEM of 4 experiments; data in panels B, C, and H correspond to the merge of 3 experiments; data of a representative experiment are shown in panel G. Gray bar indicates not detected; ns, not significant. $^*P < .05$; $^{**}P < .001$; $^{***}P < .0001$.

CXCL13/CXCR5 signaling does not interfere with BCR-triggered IS formation

To analyze BCR-promoted B-cell IS formation in the presence of CXCL13, we used confocal microscopy to follow the fluorescent signal of tethered antigen (Figure 2D and supplemental Videos 2-5). B-cell synapse formation was inversely correlated with CXCL13-induced B-cell migration. At a p31 density of 100 molecules/μm², nearly all 3-83 B cells formed a detectable IS as measured by antigen accumulation and formation of a central cluster (Figure 2D-E). This observation was correlated with a high frequency of B cell:membrane contacts (detected by IRM), which were CXCL13 independent (Figure 2F). At a 5-fold lower antigen density, only 20%-30% of 3-83 B cells showed measurable aggregation of p31; however, 75% of the cells were IRM positive in the presence of CXCL13 and 50% were in its absence (Figure 2E-F). The IRM areas were larger in the presence of CXCL13 than in its absence at both p31 densities (Figure 2G). We detected no IS at a p31 density of 4 molecules/μm², although LFA-1 was active on the 3-83 B-cell surface in the presence of CXCL13 (~ 70% of B cells were IRM positive; Figure 2E-F). There were no significant differences in the total number of p31 molecule at the IS using antigen alone or with CXCL13 (Figure 2G). Results were similar for MD4 B cells and the high-affinity HEL antigen (supplemental Figure 1E-H).

Our data indicate that CXCL13/CXCR5 signaling does not significantly affect the frequency of BCR-triggered B cells that

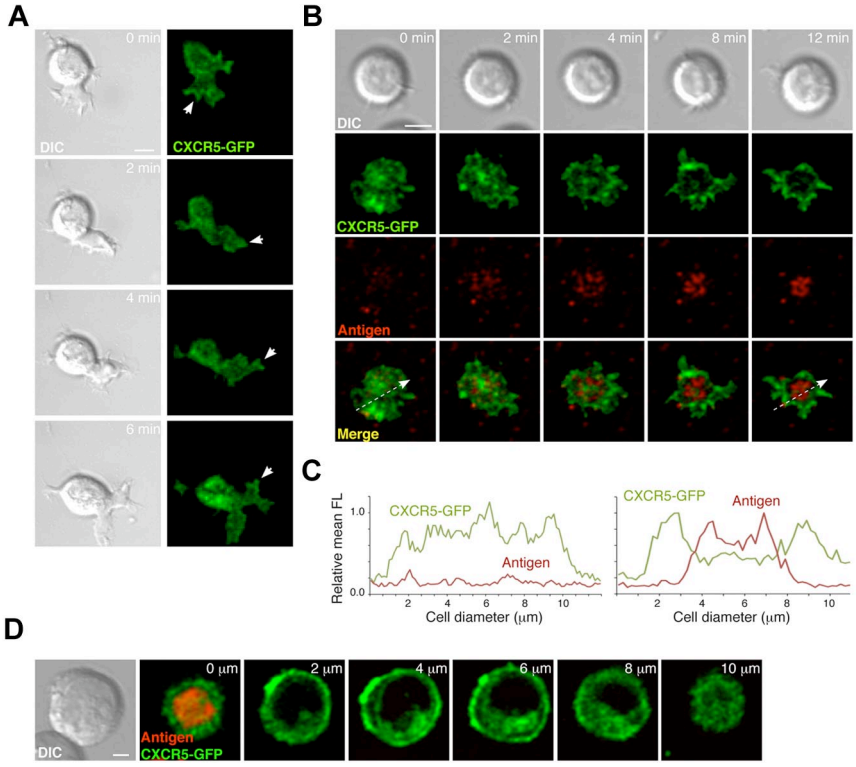

Figure 3. CXCR5 distribution at the contact site of migratory B cells and at the B-cell IS. (A) Representative DIC and fluorescence images at the contact site of a typical migratory A20 B cell in the absence of tethered antigen at the indicated times. White arrows indicate aggregates of CXCR5-GFP at the tips of the leading edge. Scale bar indicates 5 μm. (B) DIC and fluorescent images of a representative A20 B cell forming the IS after surrogate antigen (anti-κ mAb) recognition on the membrane. Scale bar indicates 5 μm. (C) Profiles of relative mean fluorescence distribution of CXCR5-GFP (green line) and antigen (red line) at the contact site of the A20 B cell with the membrane at 0 minutes (left; white arrow at bottom left panel in B) and 12 minutes (right; white arrow at bottom right panel in B). (D) Serial *z*-stack sections taken every 2 μm of a representative A20 B cell with an established IS on membranes with tethered surrogate antigen. Scale bar indicates 2 μm. All experiments were performed in the presence of ICAM-1 (150 molecules/μm^2).

establish an IS or the quantity of antigen accumulated at the IS. By promoting the LFA-1/ICAM-1 interaction, CXCL13/CXCR5 signaling nonetheless enhances the frequency and/or area of contact with the membrane.

CXCR5 is excluded from the cSMAC but does not polarize to the B-cell IS

To study the molecular dynamics of CXCR5 at the B cell:target membrane interface in the migratory stage compared with IS formation, we generated the CXCR5-GFP construct and transfected it into the A20 B-cell line; we then used confocal microscopy to follow CXCR5-GFP distribution at the B cell:membrane interface through time. Contact with CXCL13-coated ICAM-1–containing membranes promoted movement in 15%-20% of A20 B cells (data not shown), in which CXCR5-GFP was distributed homogenously at the contact zone, with some aggregates at the tips of the leading cell edge (Figure 3A and supplemental Video 6). In contact with membranes that included tethered surrogate antigen (anti-κ mAb; see "Methods"), CXCR5-GFP segregated to the periphery of the contact zone, whereas antigen accumulated at the center to form the so-called central supramolecular activation cluster (cSMAC; Figure 3B-C and supplemental Video 6). Analysis of the GFP signal in the remainder of the cell body nevertheless indicated that CXCR5-GFP did not polarize to the IS (Figure 3D). To confirm these data in primary naive B cells, we immunostained fixed cells and used confocal microscopy to analyze endogenous CXCR5 distribution in conjugates of 3-83 B cells with antigen-presenting cells (ICAM-1-GFP transfectants of L cells expressing H-2K^K, an antigen recognized by the 3-83 BCR; see "Methods"). Three-dimensional reconstruction of confocal images at the IS site showed CXCR5 exclusion from the cSMAC, whereas it colocalized with the distinctive ICAM-1 ring of the peripheral SMAC (pSMAC; supplemental Figure 2); again, we observed no CXCR5 polarization to the B-cell IS; the chemokine receptor remained evenly distributed over the remainder of the B-cell surface.

Our results show that whereas the B cell migrates, CXCR5 distribution is relatively homogenous on the area of contact with the target cell. Antigen recognition through the BCR triggers IS formation; CXCR5 subsequently segregates toward the periphery of the contact zone and is excluded from the cSMAC but not from the pSMAC. Nevertheless, CXCR5 does not polarize to the target cell contact site in the B-cell synaptic phase.

CXCL13/CXCR5 signaling enhances BCR-mediated B-cell activation

To determine the effect of CXCL13 in the process of B-cell activation by antigen, we cultured naive MD4 B cells (18-20 hours) on membranes bearing different densities of tethered HEL alone or with chemokine. Cells were collected and CD86 and CD69 activation marker expression analyzed at the B-cell surface by flow cytometry (Figure 4). We found a significant increase in the frequency of B-cell activation ($CD86^{hi}CD69^{+}$) in the presence of CXCL13 at HEL densities of 4 and 1 molecule/μm^2 (conditions in which no IS was detected and a fraction of B cells migrated; supplemental Figure 1). No significant chemokine effect was detected at 20 molecules/μm^2. Results were similar for naive 3-83 B cells and p31 (supplemental Figure 3A).

To confirm that enhanced B-cell activation was due to CXCL13 signaling through CXCR5, we carried out activation assays using naive B cells isolated from wild-type and CXCR5-deficient mice. Membrane-bound anti-κ mAb was used as a surrogate antigen because these cells were not BCR transgenic; we focused on low antigen densities at the membrane to improve detection of the chemokine effect. Whereas CXCL13 increased wild-type B-cell activation in response to the surrogate antigen, no effect was

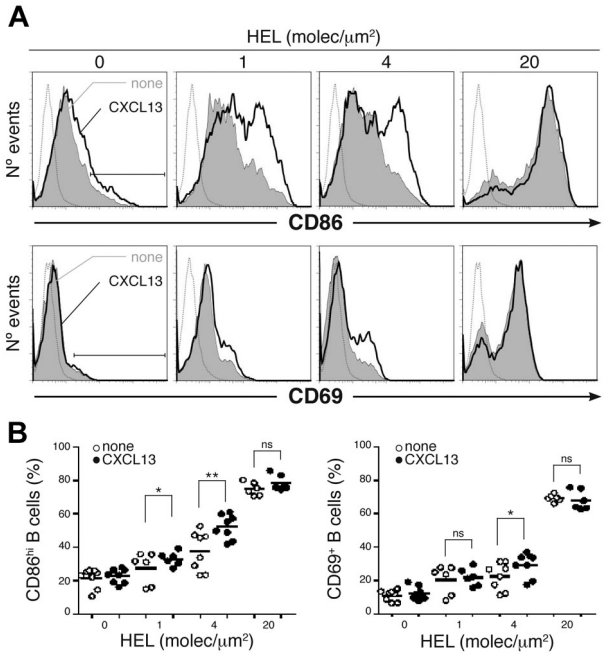

Figure 4. CXCL13/CXCR5 signaling effect on B-cell activation by antigen. (A) CD86 (top panels) and CD69 (bottom panels) profiles of a representative experiment of MD4 B cells settled on membranes with tethered HEL at the specified densities alone (gray filled histogram) or with CXCL13 (black line). Dashed gray line is the isotype control; black bar, $CD86^{hi}$ and $CD69^{+}$ B cells. (B) Frequency of $CD86^{hi}$ (left panel) and $CD69^{+}$ (right panel) MD4 B cells in the same conditions as in panel A; dots represent single experiments; black horizontal bars, averaged values. All experiments were performed in the presence of ICAM-1 (150 molecules/μm^2). ns indicates not significant. $^{*}P < .05$; $^{**}P < .001$.

observed on CXCR5-deficient B cell activation at any antigen density tested (supplemental Figure 3B).

We conclude that CXCL13/CXCR5 signaling boosts BCR-mediated B-cell activation. This effect is more robust in limiting conditions of BCR stimulation (low antigen abundance).

CXCL13/CXCR5 signaling assists antigen gathering at the B-cell IS by promoting membrane ruffling and LFA-1–supported contact

We studied the molecular mechanism underlying the CXCL13/CXCR5–mediated increase in antigen activation of B cells. We observed enhanced frequency and area of B cell:target membrane contacts when CXCL13 was present (Figure 2F-G and supplemental Figure 1G-H); therefore, CXCR5 signaling promoted LFA-1/ICAM-1 interactions. This pair of adhesion molecules facilitates antigen-mediated B-cell activation by mediating adhesion and IS formation.[6] We focused on the membrane contacts established by halted B cells (IS stage); the presence of CXCL13 supported dynamic contact over time, with constant changes in shape and area as determined by IRM (Figure 5A, supplemental Videos 7 and 8, and supplemental Figure 4A). Establishment of new contacts coincided with the detection of membrane ruffles extension by DIC, and was usually accompanied by detectable antigen gathering from the area near the IS toward the cSMAC (measured by fluorescence; Figure 5A and supplemental Figure 4A). CXCL13-mediated enhancement of membrane ruffling on halted B cells was detected at all antigen densities tested (Figure 5B and supplemental Figure 4B), and was also observed in the absence of antigen on the

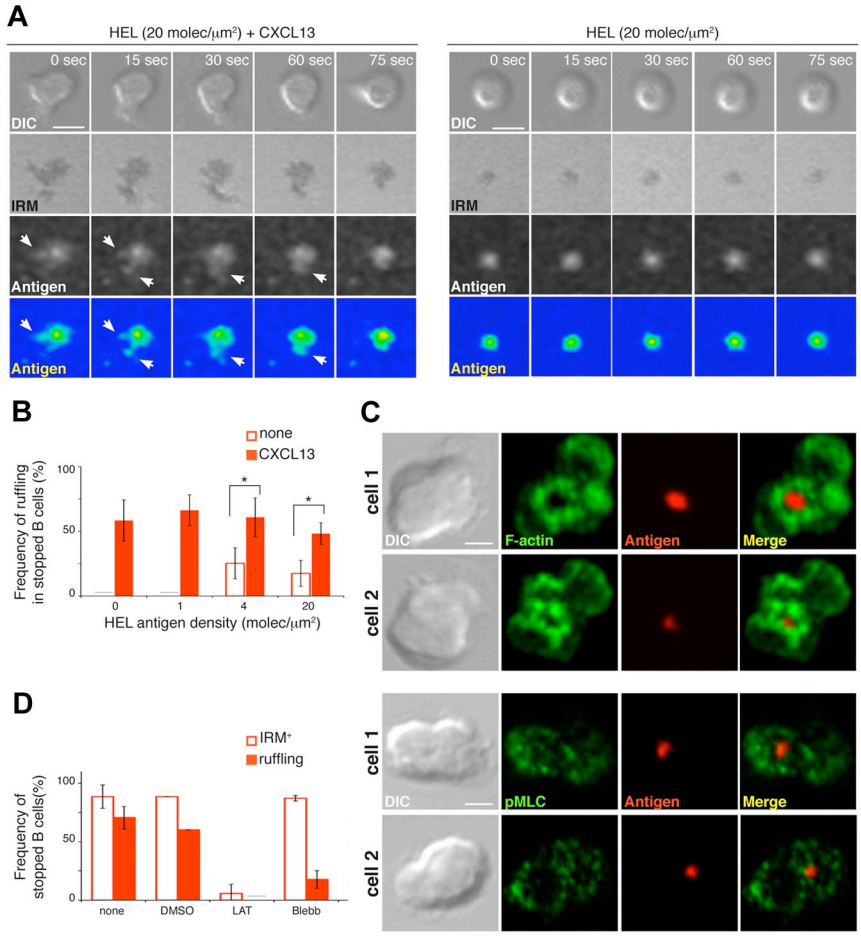

Figure 5. CXCL13/CXCR5 signaling promotes membrane ruffling and LFA-1–supported contacts to enhance antigen gathering at the B-cell IS. (A) Time-lapse DIC, IRM, and fluorescence antigen images (in gray scale and color-coded scale) of representative MD4 B cells on membranes with tethered HEL (20 molecules/μm^2) alone or with CXCL13. White arrows indicate monitored antigen gathering. Scale bar indicates 5 μm. (B) Proportion of halted MD4 B cells showing membrane ruffles on membranes bearing HEL at the specified density alone and with CXCL13. (C) DIC and fluorescent images for antigen, F-actin, and pMLCs of 2 representative fixed MD4 B cells in each case on CXCL13-coated membranes tethered with HEL (20 molecules/μm^2). Scale bar indicates 2 μm. (D) Frequency of stopped MD4 B cells that show target membrane contact (IRM^{+}) and extend ruffles (estimated by DIC) on CXCL13-coated membranes with tethered HEL after treatment with 0.1% DMSO (carrier), 0.5μM latrunculin A (LAT), 50μM blebbistatin (Blebb), or no treatment (none). All experiments were performed in the presence of ICAM-1 (150 molecules/μm^2). Data in panels B and D represent the mean ± SEM of 4 experiments. Gray bar indicates not detected. $^{*}P < .05$.

few halted B cells found. The absence of ICAM-1 prevented contact of the CXCL13-triggered ruffle with the target membrane and therefore antigen gathering from the synapse vicinity (supplemental Figure 4C-D). Similar studies of wild-type compared with CXCR5-deficient B cells confirmed that this effect requires CXCR5 signaling (supplemental Figure 5).

F-actin analysis by phalloidin staining on fixed B cells showed actin cytoskeleton reorganization at the CXCL13-mediated membrane ruffles, in addition to the classic F-actin ring that surrounds the antigen cluster at the IS (Figure 5C). Once IS were established, the addition of latrunculin A (a drug that inhibits actin polymerization) to planar lipid bilayers completely abolished membrane ruffling on halted B cells, also leading to their detachment from the target membrane within minutes (Figure 5D). Membrane ruffle extension was followed by its contraction to the cell body, which led us to target NM-II, a motor protein that exerts contraction of actin filaments.[23] NM-II function requires phosphorylation of the regulatory myosin light chains (MLCs). Using immunofluorescence techniques, we detected phosphorylated MLCs (pMLCs) at the B-cell contact area with the target membrane (Figure 5C). pMLCs showed patched distribution in the vicinity of the B-cell IS antigen cluster, but associated mainly with the outer edges of the cell. Therefore, these data suggested the presence of active NM-II at the membrane ruffles. Treatment of halted B cells with the specific NM-II inhibitor blebbistatin blocked CXCL13-mediated membrane ruffling within minutes; halted B cells nonetheless remained adhered to the target membrane (Figure 5D).

Our data show that CXCL13/CXCR5 signaling enhances BCR-mediated B-cell activation by assisting antigen gathering from the IS surroundings through membrane ruffling and LFA-1–supported contacts with the target membrane. Both events depend on a functional actin cytoskeleton and NM-II motor protein activity.

CXCL13-mediated migration allows BCR signal integration through establishment of an LFA-1–supported migratory junction or kinapse

CXCL13-mediated enhancement of membrane contacts detected at low antigen densities (p31 density of 4 molecules/μm^2; HEL density of 1 molecule/μm^2) was correlated with high cell migration frequency (Figure 2A, F and supplemental Figure 1A, G). Several studies indicated that T cells integrate antigen/TCR-mediated signals while migrating over the surface of the antigen-presenting cell,[24-26] and this migratory junction is called a kinapse.[27] We studied this possibility on migratory B cells as an additional mechanism for the CXCL13/CXCR5–mediated increase in BCR-mediated B-cell activation. To track BCR signaling, we monitored Ca^{2+} flux in MD4 B cells in contact with membranes bearing HEL at a density of 1 molecule/μm^2 alone or with CXCL13. B cells were preloaded with Fluo4FF and Ca^{2+} changes were followed by real-time confocal microscopy; we detected intermittent Ca^{2+} signals in half of the migratory B cells on CXCL13-coated target membranes (Figure 6A-B and supplemental Video 9). There were no measurable changes in Ca^{2+} levels on B cells settled on target membranes in the absence of chemokine (Figure 6A) or in the absence of ICAM-1 (not shown); in both conditions, cells floated above the membrane due to lack of contact (supplemental Figures 1G and 6D). In the presence of CXCL13, we also detected Ca^{2+} signals on migratory B cells at 4 molecules/μm^2 HEL or even with no antigen (Figure 6B). Chemokine receptors trigger Ca^{2+} influx after ligand binding[28]; however, single-cell Ca^{2+} profiles showed higher intensity peaks when antigen was available than with chemokine alone at the target membrane (Figure 6C). Results were similar for 3-83 B cells (supplemental Figure 6A-C).

We used immunofluorescence techniques to analyze the actomyosin network on migratory B cells at the contact zone with the target membrane. Phalloidin staining indicated actin cytoskeleton rearrangement at the leading edge; pMLCs showed a patched pattern across the entire contact area, with brightest signals near the border (Figure 6D). Latrunculin A inhibition of actin polymerization on migratory B cells eliminated cell motility within minutes, as well as adhesion to the ICAM-1–containing target membrane (Figure 6E). Blebbistatin treatment of migratory B cells to inhibit NM-II eradicated cell motility, but not LFA-1–supported membrane contact (Figure 6E).

Our data indicated that at antigen densities unable to promote B-cell stop and IS formation, CXCL13-mediated migration allows antigen encounter and integration of BCR signals by establishing an LFA-1–supported kinapse, and this process requires operative actin cytoskeleton and NM-II motor protein. Through this mechanism, CXCR5 signaling could also enhance BCR-mediated B-cell activation.

Discussion

In the present study, we sought to understand the interplay between 2 ligand/receptor pairs involved in B-cell dynamics at the follicle, CXCL13/CXCR5 and antigen/BCR, and to determine how B-cell fate could be affected by instructing cell behavior. We established a 2-dimensional model based on ICAM-1–containing planar membranes, in which naive B cells move in response to a CXCL13 coating. The migration pattern resembles the in vivo dynamics of B cells on the FDC network in lymph nodes (random tracks, average speed ~ 6 μm/min). The combination of CXCL13 and antigen stimulation at the membrane results in a wide range of B-cell behaviors based on BCR signaling strength. We observed that CXCL13/CXCR5 signaling did not impair BCR-triggered B-cell IS formation; however, it significantly enhanced BCR-mediated B-cell activation. The presence of CXCL13 led to markedly increased membrane ruffling and LFA-1–supported adhesion in halted/IS-forming B cells; both events assisted antigen gathering from the synapse vicinity and thus BCR signaling. At limiting conditions of antigen abundance, CXCL13-mediated migration promoted the formation of an LFA-1–supported kinapse that allowed antigen encounter and BCR signaling events (Ca^{2+} influx) on motile B cells. Through these 2 means, dependent on a functional actomyosin network, CXCR5 signaling boosts BCR-mediated B-cell activation.

Our data showed modulation of CXCL13-mediated B-cell migration by integrin ligand density at the target membrane. We found ICAM-1 densities of 100-200 molecules/μm^2 on the surface of splenocytes in steady state (not shown; see supplemental Methods). After inflammatory stimulation, adhesion molecule expression increased at the surface of different cell types (after 20 hours of in vitro TNF stimulation, splenocytes expressed ICAM-1 densities of > 600 molecules/μm^2; data not shown). These changes in the environment could retard B-cell movement in vivo, promoting a more meticulous search for antigen. Although leukocyte movement can occur in the absence of integrins,[29] the same investigators recently described a cell preference for movement over a surface with an ICAM-1 and a chemokine coating (haptokinesis), even when chemotactic signals were present.[20] Adhesion molecule levels and possibly their distribution pattern,[30]

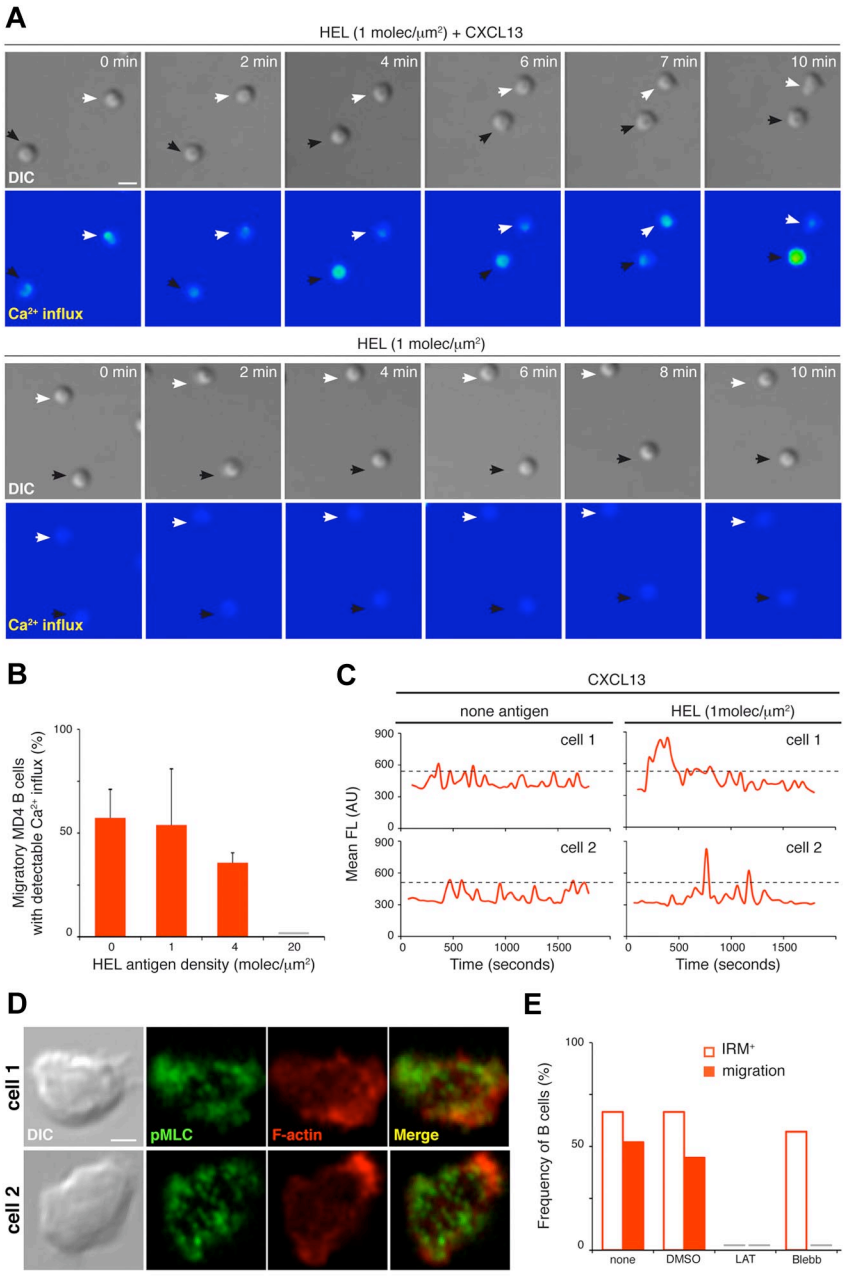

Figure 6. CXCL13/CXCR5 signaling establishes an LFA-1–supported kinapse to facilitate BCR signal integration on motile B cells. (A) Time-lapse DIC and fluorescence images (Ca^{2+} influx, color-coded scale) of representative MD4 B cells on membranes with tethered HEL (1 molecule/μm^2) alone or with CXCL13. White and black arrows identify B cells monitored in each condition. Scale bar indicates 5 μm. (B) Proportion of migratory MD4 B cells showing Ca^{2+} influx on membranes bearing HEL at the specified density and with CXCL13; data represent the means ± SEM of 4 experiments. (C) Ca^{2+} influx profiles of single migratory MD4 B cells on CXCL13-coated membranes with no antigen or tethered HEL (1 molecule/μm^2). Profiles of 2 representative cells are shown in each case; dashed black line indicates maximum Ca^{2+} signal for only chemokine stimuli. (D) DIC and fluorescent images for F-actin (red) and pMLC (green) of 2 representative fixed MD4 B cells on CXCL13-coated membranes in the absence of antigen. Scale bar indicates 2 μm. (E) Frequency of B cells that show target membrane contact (IRM^+) and migration (estimated by DIC) on CXCL13-coated membranes in the absence of antigen after treatment with 0.1% DMSO (carrier), 0.5μM latrunculin A (LAT), 50μM blebbistatin (Blebb), or no treatment (none); data of one representative experiment are shown. Gray bar indicates not detected. All experiments were performed in the presence of ICAM-1 (150 molecules/μm^2).

as well as chemokine-regulated integrin adhesiveness,[19] thus appear to be pivotal factors in the modulation of interstitial leukocyte dynamics, which remains to be explored in depth.

Few studies have addressed the molecular dynamics of chemokine receptors at the IS. In T cells, CXCR4 and CCR5 are recruited to the IS[31]; specifically, CXCR4 appears to localize at the pSMAC.[32] Our study establishes CXCR5 distribution at the B-cell synapse. CXCR5 localization at the pSMAC could help to promote membrane ruffling at the synaptic stage; in addition, its nonpolarization to the IS might maintain B cells' ability to respond to CXCL13 in the vicinity of the target cell. During B-cell migration, CXCR5 is distributed nearly homogeneously at the target membrane contact site. Although we detected some receptor aggregates or clusters at the leading edge tips, CXCR5 did not polarize, as suggested for other chemokine receptors.[33,34] Relatively uniform CXCR5 distribution at the contact site could help to explain the rapid, random changes in direction during B-cell migration.

Our results identify a costimulatory function for CXCL13/CXCR5 signaling in BCR-triggered B-cell activation; this effect was more pronounced in suboptimal BCR stimulation conditions. We found that the CXCR5-mediated effect on cell dynamics assists BCR-triggered B-cell activation. At limiting conditions of antigen density, naive B cells established an LFA-1–supported kinapse with the target membrane in response to CXCL13; through this migratory junction, they encountered antigen and integrated BCR signals. When antigen density was sufficient to trigger a stop signal through the BCR, naive B cells established a synapse with the target membrane; CXCR5 signaling then promoted membrane ruffling and LFA-1/ICAM-1 contacts that increased antigen gathering near the IS and thus BCR signaling. Other studies have highlighted the importance of cell behavior modulation for lymphocyte fate. APC-bound CCL21 appears to prime T cells for IS formation.[35] CXCR4 and CCR5 promote more stable T cell:APC

conjugates by increasing adhesion.[31] Chemokine-guided recruitment of CD8 T cells to CD4 T cell/dendritic cell interaction sites fosters generation of memory CD8 T cells.[36] Regulation of thymocyte dynamics also appears to be critical for positive selection events in the thymus.[37] In any case, we cannot discard a role for CXCR5-mediated activation of other signaling pathways in costimulation, and further studies are clearly needed.

The actomyosin network has a critical role in cell polarization, migration, and adhesion. In T cells, NM-II is necessary for fast ameboid motility; this motor protein regulates surface contact area to allow high speed of movement.[38-40] NM-II is also important for the formation and persistence of T-cell synapses and for TCR signaling.[41] In B cells, this motor protein is needed for BCR-driven antigen processing and presentation.[42] Our immunofluorescence and drug-treatment data also suggest participation by and the necessity for an operative actomyosin network for CXCL13-mediated, LFA-1–supported B-cell motility and membrane ruffling. At longer treatment times, NM-II inhibition also provoked disassembly of the antigen cluster at the B-cell synapse (not shown).

The detection of antigen/BCR early signaling (Ca^{2+} flux) during B-cell migration led us to question the need to establish an immune synapse for B-cell activation. Several studies in T cells have indicated TCR signal integration during migration in response to chemokines[24,25]; the moving cell-cell junction that permits signal integration was defined as the kinapse.[27] Recent in vivo studies showed antigen-triggered TCR internalization in the absence of T-cell arrest; the investigators proposed a flexible relationship between motility and the immune synapse, and that successful signaling does not necessarily require cSMAC formation.[43] Based on our data, we propose that B cells also exploit both types of interfaces, kinapses and synapses, to integrate BCR signals, with the use of one or the other being determined mainly by antigen quality and abundance. In T cells, PKCθ and WASp proteins regulate kinapse/synapse interconversion.[44] We have not observed this interconversion in our assays; nonetheless, further studies will lead to a better comprehension of this phenomenon in B-cell dynamics.

Acknowledgments

The authors thank F. Batista, E. Fernández, S. Minguet, I. Moreno de Alborán, and L. Planelles for critical reading of the manuscript and C. Mark for editorial assistance.

This work was supported by grants from the European Union (FP7-integrated project Masterswitch 223404 FP7) and from the Spanish Ministry of Science (BFU2008-01194). J.S. is supported by a contract from the Comunidad Autónoma de Madrid. Y.R.C. is supported by a Ramón y Cajal contract from the Spanish Ministry of Science.

Authorship

Contribution: J.S.d.G. designed parts of the study, performed the experiments, analyzed the data, and assisted in manuscript preparation; L.B. performed some of the experiments, analyzed the data, and assisted in manuscript preparation; M.M. provided input into the project; and Y.R.C. designed and supervised all aspects of the work and wrote the manuscript.

Conflict-of-interest disclosure: The authors declare no competing financial interests.

Correspondence: Yolanda R. Carrasco, B Cell Dynamics Group, Department of Immunology and Oncology, Centro Nacional de Biotecnología/CSIC, Darwin 3, UAM Campus Cantoblanco, Madrid E-28049 Spain; e-mail: ycarrasco@cnb.csic.es.

References

1. Miller MJ, Wei SH, Parker I, Cahalan MD. Two-photon imaging of lymphocyte motility and antigen response in intact lymph node. *Science.* 2002;296(5574):1869-1873.
2. Okada T, Miller MJ, Parker I, et al. Antigen-engaged B cells undergo chemotaxis toward the T zone and form motile conjugates with helper T cells. *PLoS Biol.* 2005;3(6):e150.
3. Bajénoff M, Egen JG, Koo LY, et al. Stromal cell networks regulate lymphocyte entry, migration, and territoriality in lymph nodes. *Immunity.* 2006; 25(6):989-1001.
4. Allen CD, Cyster JG. Follicular dendritic cell networks of primary follicles and germinal centers: phenotype and function. *Semin Immunol.* 2008; 20(1):14-25.
5. Carrasco YR, Batista FD. B cells acquire particulate antigen in a macrophage-rich area at the boundary between the follicle and the subcapsular sinus of the lymph node. *Immunity.* 2007; 27(1):160-171.
6. Carrasco YR, Fleire SJ, Cameron T, Dustin ML, Batista FD. LFA-1/ICAM-1 interaction lowers the threshold of B cell activation by facilitating B cell adhesion and synapse formation. *Immunity.* 2004;20(5):589-599.
7. Fleire SJ, Goldman JP, Carrasco YR, Weber M, Bray D, Batista FD. B cell ligand discrimination through a spreading and contraction response. *Science.* 2006;312(5774):738-741.
8. Randall KL, Lambe T, Johnson A, et al. Dock8 mutations cripple B cell immunological synapses, germinal centers and long-lived antibody production. *Nat Immunol.* 2009;10(12):1283-1291.
9. Goodnow CC, Crosbie J, Adelstein S, et al. Altered immunoglobulin expression and functional silencing of self-reactive B lymphocytes in transgenic mice. *Nature.* 1988;334(6184):676-682.
10. Russell DM, Dembic Z, Morahan G, Miller JF, Burki K, Nemazee D. Peripheral deletion of self-reactive B cells. *Nature.* 1991;354(6351):308-311.
11. Förster R, Mattis AE, Kremmer E, Wolf E, Brem G, Lipp M. A putative chemokine receptor, BLR1, directs B cell migration to defined lymphoid organs and specific anatomic compartments of the spleen. *Cell.* 1996;87(6):1037-1047.
12. Kouskoff V, Famiglietti S, Lacaud G, et al. Antigens varying in affinity for the B cell receptor induce differential B lymphocyte responses. *J Exp Med.* 1998;188(8):1453-1464.
13. Grakoui A, Bromley SK, Sumen C, et al. The immunological synapse: a molecular machine controlling T cell activation. *Science.* 1999; 285(5425):221-227.
14. Cyster JG, Ansel KM, Reif K, et al. Follicular stromal cells and lymphocyte homing to follicles. *Immunol Rev.* 2000;176:181-193.
15. de Paz JL, Moseman EA, Noti C, Polito L, von Andrian UH, Seeberger PH. Profiling heparin-chemokine interactions using synthetic tools. *ACS Chem Biol.* 2007;2(11):735-744.
16. Koopman G, Parmentier HK, Schuurman HJ, Newman W, Meijer CJ, Pals ST. Adhesion of human B cells to follicular dendritic cells involves both the lymphocyte function-associated antigen 1/intercellular adhesion molecule 1 and very late antigen 4/vascular cell adhesion molecule 1 pathways. *J Exp Med.* 1991;173(6):1297-1304.
17. Dustin ML. Cell adhesion molecules and actin cytoskeleton at immune synapses and kinapses. *Curr Opin Cell Biol.* 2007;19(5):529-533.
18. Smith A, Stanley P, Jones K, Svensson L, McDowall A, Hogg N. The role of the integrin LFA-1 in T-lymphocyte migration. *Immunol Rev.* 2007;218:135-146.
19. Woolf E, Grigorova I, Sagiv A, et al. Lymph node chemokines promote sustained T lymphocyte motility without triggering stable integrin adhesiveness in the absence of shear forces. *Nat Immunol.* 2007;8(10):1076-1085.
20. Schumann K, Lammermann T, Bruckner M, et al. Immobilized chemokine fields and soluble chemokine gradients cooperatively shape migration patterns of dendritic cells. *Immunity.* 2010; 32(5):703-713.
21. Johnson SA, Pleiman CM, Pao L, Schneringer J, Hippen K, Cambier JC. Phosphorylated immunoreceptor signaling motifs (ITAMs) exhibit unique abilities to bind and activate Lyn and Syk tyrosine kinases. *J Immunol.* 1995;155(10):4596-4603.
22. Arana E, Vehlow A, Harwood NE, et al. Activation of the small GTPase Rac2 via the B cell receptor regulates B cell adhesion and immunological-synapse formation. *Immunity.* 2008;28(1):88-99.
23. Vicente-Manzanares M, Ma X, Adelstein RS, Horwitz AR. Non-muscle myosin II takes centre stage in cell adhesion and migration. *Nat Rev Mol Cell Biol.* 2009;10(11):778-790.
24. Underhill DM, Bassetti M, Rudensky A,

Aderem A. Dynamic interactions of macrophages with T cells during antigen presentation. *J Exp Med.* 1999;190(12):1909-1914.

25. Gunzer M, Schafer A, Borgmann S, et al. Antigen presentation in extracellular matrix: interactions of T cells with dendritic cells are dynamic, short lived, and sequential. *Immunity.* 2000;13(3):323-332.
26. Mempel TR, Henrickson SE, Von Andrian UH. T-cell priming by dendritic cells in lymph nodes occurs in three distinct phases. *Nature.* 2004; 427(6970):154-159.
27. Dustin ML. Hunter to gatherer and back: immunological synapses and kinapses as variations on the theme of amoeboid locomotion. *Annu Rev Cell Dev Biol.* 2008;24:577-596.
28. Thelen M, Stein JV. How chemokines invite leukocytes to dance. *Nat Immunol.* 2008;9(9):953-959.
29. Lämmermann T, Bader BL, Monkley SJ, et al. Rapid leukocyte migration by integrin-independent flowing and squeezing. *Nature.* 2008; 453(7191):51-55.
30. Barreiro O, Zamai M, Yanez-Mo M, et al. Endothelial adhesion receptors are recruited to adherent leukocytes by inclusion in preformed tetraspanin nanoplatforms. *J Cell Biol.* 2008;183(3):527-542.
31. Molon B, Gri G, Bettella M, et al. T cell costimulation by chemokine receptors. *Nat Immunol.* 2005; 6(5):465-471.
32. Pérez-Martínez M, Gordon-Alonso M, Cabrero JR, et al. F-actin-binding protein drebrin regulates CXCR4 recruitment to the immune synapse. *J Cell Sci.* 2010;123(pt 7):1160-1170.
33. Nieto M, Frade JM, Sancho D, Mellado M, Martinez AC, Sanchez-Madrid F. Polarization of chemokine receptors to the leading edge during lymphocyte chemotaxis. *J Exp Med.* 1997;186(1): 153-158.
34. Vicente-Manzanares M, Montoya MC, Mellado M, et al. The chemokine SDF-1alpha triggers a chemotactic response and induces cell polarization in human B lymphocytes. *Eur J Immunol.* 1998; 28(7):2197-2207.
35. Friedman RS, Jacobelli J, Krummel MF. Surface-bound chemokines capture and prime T cells for synapse formation. *Nat Immunol.* 2006;7(10): 1101-1108.
36. Castellino F, Huang AY, Altan-Bonnet G, Stoll S, Scheinecker C, Germain RN. Chemokines enhance immunity by guiding naive CD8+ T cells to sites of CD4+ T cell-dendritic cell interaction. *Nature.* 2006;440(7086):890-895.
37. Phee H, Dzhagalov I, Mollenauer M, et al. Regulation of thymocyte positive selection and motility by GIT2. *Nat Immunol.* 2010;11(6):503-511.
38. Jacobelli J, Chmura SA, Buxton DB, Davis MM, Krummel MF. A single class II myosin modulates T cell motility and stopping, but not synapse formation. *Nat Immunol.* 2004;5(5):531-538.
39. Jacobelli J, Bennett FC, Pandurangi P, Tooley AJ, Krummel MF. Myosin-IIA and ICAM-1 regulate the interchange between two distinct modes of T cell migration. *J Immunol.* 2009;182(4):2041-2050.
40. Jacobelli J, Friedman RS, Conti MA, et al. Confinement-optimized three-dimensional T cell amoeboid motility is modulated via myosin IIA-regulated adhesions. *Nat Immunol.* 2010;11(10): 953-961.
41. Ilani T, Vasiliver-Shamis G, Vardhana S, Bretscher A, Dustin ML. T cell antigen receptor signaling and immunological synapse stability require myosin IIA. *Nat Immunol.* 2009;10(5):531-539.
42. Vascotto F, Lankar D, Faure-Andre G, et al. The actin-based motor protein myosin II regulates MHC class II trafficking and BCR-driven antigen presentation. *J Cell Biol.* 2007;176(7):1007-1019.
43. Friedman RS, Beemiller P, Sorensen CM, Jacobelli J, Krummel MF. Real-time analysis of T cell receptors in naive cells in vitro and in vivo reveals flexibility in synapse and signaling dynamics. *J Exp Med.* 2010;207(12):2733-2749.
44. Sims TN, Soos TJ, Xenias HS, et al. Opposing effects of PKCtheta and WASp on symmetry breaking and relocation of the immunological synapse. *Cell.* 2007;129(4):773-785.

Vinculin arrests motile B cells by stabilizing integrin clustering at the immune synapse

Julia Saez de Guinoa[1], Laura Barrio[1] and Yolanda R. Carrasco[1]

[1]B cell Dynamics Laboratory, Department of Immunology and Oncology, Centro Nacional de Biotecnología (CNB)-CSIC. Darwin 3, UAM-Campus Cantoblanco, Madrid E-28049, Spain

Corresponding author: Yolanda R. Carrasco

Tel: +34 915 854 852

Fax: +34 913 720 493

e-mail: ycarrasco@cnb.csic.es

Running title: Vinculin regulates B cell adhesion dynamics

Total characters (including spaces): 43551

Abstract word count: 150

Figure count: 6

Reference count: 50

Abstract

Lymphocytes use integrin-based platforms to move and to adhere firmly to the surface of other cells. The molecular mechanisms governing lymphocyte adhesion dynamics are however poorly understood. Here we show that in B lymphocytes, the actin binding protein Vinculin localizes to the ring-shaped integrin-rich domain of the immune synapse (IS); the assembly of this platform, triggered by cognate immune interactions, is needed for chemokine-mediated B cell motility arrest, and leads to firm, long-lasting B cell adhesion to the antigen-presenting cell. Vinculin is recruited early in IS formation, in parallel to a local phosphatidylinositol (4, 5)-bisphosphate (PIP_2) wave, and requires spleen tyrosine kinase (Syk) activity. Lack of vinculin at the IS impairs firm adhesion, promoting in turn cell migration with antigen clustered at the uropod. Vinculin localization to the B cell contact area depends on actomyosin. These results identify vinculin as a major controller of integrin-mediated adhesion dynamics in B cells.

Key words: Vinculin / B cells / immune synapse / motility / integrins

Introduction

The regulated interplay between cell adhesion and cell motility is critical for B lymphocyte function. B cells must explore entire follicles in secondary lymphoid organs, where antigens are collected and presented by various antigen-presenting cells (APC) (Cyster, 2010). To do this, B cells migrate continuously by random walking in response to the chemokine CXCL13 (Bajenoff et al, 2006; Miller et al, 2002; Okada et al, 2005). This chemokine is produced mainly at the network of follicular dendritic cells (FDC); they expose it on their surface in the context of integrin ligands, which might assist in B cell motility (Allen & Cyster, 2008; Bajenoff et al, 2006). Specific B cell receptor (BCR) recognition of antigen above a signalling threshold leads B cells to adhere firmly to the APC; a large ring-shaped lymphocyte function-associated antigen-1 (LFA-1) integrin cluster is assembled and the IS is formed (Carrasco et al, 2004; Saez de Guinoa et al, 2011). The synapse platform has an important role in several aspects of the B cell activation process (Carrasco et al, 2004; Fleire et al, 2006; Randall et al, 2009). Observations *in vivo* indicate that before they are fully activated, B cells establish more than one IS with distinct APC in the follicle (Carrasco & Batista, 2007). The B cell must then break the synapse, detach from the APC and move in search of additional specific antigen presented by another APC. The control of integrin activation, clustering and localization thus underlies the precise modulation of B cell behaviour.

Chemokine receptor and BCR signalling activate LFA-1 by modulating integrin affinity (conformational change) and avidity (spatial distribution, clustering) for its ligand intercellular adhesion molecule-1 (ICAM-1) (Batista et al, 2007; Kinashi, 2007). Chemokines promote transient integrin activation, however, whereas antigen recognition leads to stable adhesion (Kinashi, 2007). IS formation also drives LFA-1/ICAM-1 segregation into a peripheral ring (peripheral supramolecular activation cluster, pSMAC) that

surrounds the central BCR/antigen cluster (central SMAC, cSMAC) at the site of B cell:APC contact (Carrasco et al, 2004). The assembly of the synapse platform involves actin cytoskeleton remodelling and the formation of an F-actin-rich ring at the pSMAC, where LFA-1 anchors through the scaffold protein Talin (Dustin, 2007; Harwood & Batista, 2011). BCR signalling strength, which is a direct function of abundance and BCR affinity for antigen, alters CXCL13-mediated B cell migration; while weak BCR signals allow B cell motility through establishment of LFA-1-supported migratory platforms (kinapse), strong BCR signals drive motile B cells to halt and form the IS (Saez de Guinoa et al, 2011). The molecular mechanisms used by the CXCL13 receptor CXCR5 and the BCR to coordinate LFA-1 function and thus, B cell adhesion (synapse, STOP signal) and motility (kinapse, GO signal), remains almost unexplored.

The scaffold protein Vinculin is being recognised as a key regulatory element of adhesion dynamics in non-immune cells. It controls assembly, strength and transmission of mechanical forces at focal adhesions (FA); these specialized structures support integrin-mediated cell contact with the extracellular matrix (Carisey & Ballestrem, 2010; Carisey et al, 2013; Grashoff et al, 2010; Humphries et al, 2007). Vinculin links the actin cytoskeleton with integrins at the plasma membrane through its association with talin and F-actin (Humphries et al, 2007). Vinculin activation and translocation from cytosol to adhesion sites require its interaction with the membrane phospholipid PIP_2 (Bakolitsa et al, 2004). Local and temporal PIP_2 production at the plasma membrane controls adhesion site assembly and actin dynamics (Ling et al, 2006). PIP_2 is generated mainly through PIP (4)-phosphate phosphorylation at the 5-position by type I PIP kinases (PIPKI); of the PIPKI isoforms and splice variants, PIPKIγ targets to FA (Di Paolo et al, 2002; Ling et al, 2002). Vinculin is essential for embryonic development (Xu et al, 1998a); cancer cells that lack vinculin are highly motile and metastatic

(Coll et al, 1995; Lifschitz-Mercer et al, 1997; Xu et al, 1998b), and vinculin overexpression reduces cell motility and enhances cell adhesion (Rodriguez Fernandez et al, 1992).

Here we identified a major role for vinculin in governing LFA-1-mediated B cell adhesion and motility and thus, in the STOP versus GO signals. We showed that BCR recognition of membrane-tethered antigen led to vinculin recruitment to the immune synapse. Vinculin localized to the pSMAC to strength B cell adhesion; loss of vinculin impeded appropriate pSMAC assembly and in turn, B cells moved in response to CXCL13, bearing the antigen cluster at the uropod. We demonstrated that spleen tyrosine kinase (Syk) and actomyosin controls vinculin recruitment and stability at the B cell synapse.

Results

B cell motility arrest requires IS assembly triggered by membrane-tethered antigen recognition

We tested whether, in the absence of IS establishment, BCR-induced LFA-1 activation was sufficient to halt CXCL13-mediated B cell migration. BCR recognition of membrane tethered antigen (tAg) leads to B cell synapse formation; to trigger LFA-1 activation in the absence of IS assembly, we used antigen in soluble form (soluble antigen, sAg). To study B cell dynamics in response to CXCL13 and antigen, we utilized a two-dimensional model combined with time-lapse confocal microscopy; this experimental system is based on the assembly of planar lipid bilayers containing glycosyl phosphatidylinositol (GPI)-linked ICAM-1, a chemokine coating, and membrane-tethered antigen. The model mimics the surface of an APC and reproduces B cell dynamics to those observed in vivo by multiphoton microscopy (Saez de Guinoa et al, 2011).

Freshly isolated naïve B cells from wild type mouse spleen were labelled with the fluorescent probe CFSE and allowed to settle on artificial planar lipid bilayers containing GPI-linked ICAM-1 and a CXCL13 coating (ICAM-1/CXCL13 membranes), alone or with sAg (1 μg/ml $F(ab')_2$ anti-IgM antibody) or tAg (anti-κ light chain at 20 molec/μm^2). We monitored B cell dynamics by time-lapse microscopy. B cells migrated by random walking across CXCL13 coated ICAM-1-containing artificial membranes (Supplementary Movie S1). CXCL13 alone promoted LFA-1/ICAM-1 interactions (65%; detected by interference reflection microscopy, IRM; Figure 1A) and a high frequency of cell polarization (70%), estimated by differential interference contrast (DIC) as the fraction of cells with membrane protrusion activity (membrane ruffles) (Figure 1B), as reported (Saez de Guinoa et al, 2011). Half of the polarized cells migrated across the substrate at a mean velocity of 4 μm/min (Figures 1B and C; Supplementary Movie S2). Although the presence of sAg increased the

fraction of B cells with active LFA-1 (85% IRM^+), it did not alter CXCL13-mediated cell polarization and migration. Motile B cells nonetheless showed a significant reduction in mean velocity, suggesting that sAg/BCR signalling impairs chemokine-mediated B cell motility (Figures 1A and C). Recognition of tAg induced the highest frequencies of LFA-1-active B cells (95% IRM^+); however, it completely abolished CXCL13-mediated B cell migration (Figures 1A and C; Supplementary Movie S3), as expected. We obtained similar results using MD4 BCR-transgenic B cells, their specific antigen hen egg lysozyme (HEL) in membrane-tethered form and $F(ab')_2$ anti-IgM antibody as sAg (Supplementary Figure S1A and B). These data thus indicated that tAg/BCR-mediated IS assembly is needed for B cell arrest, as LFA-1 activation triggered by soluble antigen allowed motility.

Syk is important for integrin activation by the BCR (Spaargaren et al, 2003) and by chemokine receptor stimulation (Pearce et al, 2011). We compared the intensity of signals transmitted through the BCR after tAg and sAg stimulation by measuring phosphorylated Syk (p-Syk) levels in B cells. B cells settled on ICAM-1/CXCL13 membranes, alone or with tAg or sAg (20 min), were fixed, permeabilized, and stained for p-Syk and F-actin. Each stimulation condition led to distinct p-Syk patterns at the B cell:target membrane contact plane; with tAg, p-Syk concentrated at the IS cSMAC, while distribution was homogeneous in the case of sAg (Figure 1D). Comparison of p-Syk fluorescence intensity at the B cell contact plane and the mid-plane showed polarization at the contact plane only in tAg conditions (Figure 1D). p-Syk values at the B cell contact plane were significantly higher in presence of tAg than with sAg; results were similar for p-Syk quantified in the entire B cell volume (Figures 1E and F). Syk protein levels were comparable in all conditions analyzed (Supplementary Figure S1C). Greater Syk activation and localization at the B cell contact plane promoted by tAg/BCR signalling might be important for LFA-1 activation, synapse assembly and B cell arrest.

Vinculin is recruited to the integrin-rich domain of the B cell IS

To determine the role of vinculin in stabilizing the B cell IS and arresting B cell motility, we analyzed vinculin at the B cell synapse. B cells in contact with ICAM-1/CXCL13 membranes with tAg (20 min) were fixed and stained for talin, vinculin and F-actin. We detected vinculin at the B cell IS; it accumulated markedly in the ring-shaped pSMAC structure that matched the F-actin-rich domain (Figure 2A). Its binding partner talin was also found at the IS, which co-localized mainly with the F-actin-rich pSMAC, but also in other parts of the contact area such as membrane ruffles (Figure 2A). Comparison of fluorescent signals at the B cell contact plane with those at the mid-plane indicated that both vinculin and talin adaptor proteins were recruited to the IS (Figure 2A). As we found that sAg/BCR signalling did not halt B cell motility, we tested the implication of vinculin in this observation by analyzing its localization to the contact site in sAg stimulation conditions. At difference from the recruitment and precise localization observed with tAg, after sAg exposure, vinculin did not localized nor was it distributed in a specific pattern at the plane of B cell contact with the target membrane; it accumulated mainly near the F-actin-rich cell edges (Figure 2B). Quantification of vinculin at the contact area showed significantly lower values after BCR stimulation with sAg than with tAg (Figure 2C); results were comparable when we analysed total F-actin at the contact area (Figure 2C).

Thus, membrane-tethered antigen/BCR stimulation leads to vinculin recruitment to the synapse. Vinculin localization at the pSMAC suggested a role for this scaffold protein in adhesion strength and stability of the B cell IS.

Vinculin recruitment coincides with a PIPKIγ-produced local PIP_2 wave at the synapse

To study the molecular dynamics of vinculin localization and F-actin polymerization at the IS, we performed time-lapse confocal microscopy experiments with A20 B cells expressing a vinculin-GFP construct and the F-actin probe Lifeact-RFP. Vinculin recruitment followed the

formation of nascent antigen clusters and LFA-1/ICAM-1 interactions (Supplementary Figure S2; Supplementary Movie S4). Vinculin accumulated gradually and segregated to the pSMAC in the first 5 min of synapse formation, after which its levels remained almost constant over time (1 h). The Lifeact-RFP profile showed an acute F-actin polymerization phase at the IS in the first 2.5 min, followed by formation of the ring structure in which it merged with vinculin (Supplementary Figure S2; Supplementary Movie S4).

Vinculin activation and translocation from cytosol to adhesion sites require its interaction with the membrane phospholipid PIP_2 produced by PIPKI in other non-immune cells. We studied PIPKIγ and PIP_2 dynamics at the B cell:target membrane contact plane by time-lapse confocal microscopy. We used a PIPKIγ-GFP construct and the PIP_2 probe PLCδ-PH-GFP construct to transfect the A20 mouse B cell line; transfectants were tracked for synapse formation in contact with ICAM-1/CXCL13 membranes and tAg (anti-κ; 20 molec/μm^2). We discarded those transfected cells showing high GFP levels for analysis. We detected short-lived PIPKIγ recruitment at early stages of synapse formation, coinciding with nascent LFA-1/ICAM-1 interactions (detected by IRM) and antigen clusters; with time, PIPKIγ persisted at the contact plane at lower levels, comparable to those in the rest of the B cell (Figures 3A and B; Supplementary Movie S5). PIP_2 production followed a similar pattern, with a maximum immediately after the PIPKIγ peak early in synapse formation (Figures 3C and D; Supplementary Movie S6). Both PIPKIγ and PIP_2 dynamics were triggered by tAg recognition; neither PIPKIγ recruitment nor marked changes in PIP_2 levels were detected at the B cell:target membrane contact area in the presence of the CXCL13 coating only (Figures 3B and D). We also observed that PIPKIγ and PIP_2 localized mainly at the pSMAC of the mature B cell synapse, where vinculin accumulated (Figures 3E and F).

Then, after PIPKIγ produced the local PIP_2 increase, vinculin localized gradually to the synapse; the local PIP_2 wave might be needed for vinculin recruitment to the site of B

cell:target membrane contact. In addition, PIPKIγ and PIP_2 remained at the pSMAC of the mature B cell synapse, where co-localized with vinculin.

Impaired vinculin recruitment to the synapse allows B cell motility

To determine the relevance of vinculin in arresting motile B cells after tAg encounter, we attempted to knock down its expression in primary B cells. Lentiviral vectors coding for distinct mouse vinculin-specific shRNA under different promoters (pGIPZ and pLKO.1 vectors) were used to generate lentiviral particles and to infect B cells in several conditions (no stimulus, IL-4, CpG or LPS; see Methods). At 48 h post-infection, we used western blot to analyze vinculin levels in infected B cells. GFP reporter expression confirmed primary B cell infection by the lentiviral particles, with distinct efficiency depending on the stimulation (Supplementary Figure S3A). We nonetheless found no clear reduction in vinculin levels with any of the shRNA used (Supplementary Figures S3A and B). We did not analyze longer time points since infected primary B cells died or differentiated into plasma cells.

As vinculin recruitment was associated with strong local Syk activation through tAg/BCR signalling (Figures 1D and 2B), we tested another approach to impair vinculin function. We used the specific chemical inhibitor BAY 61-3606 (BAY) to interfere with Syk activity. B cells were treated with several BAY doses (1 to 0.1 μM); after BCR stimulation, we evaluated Syk activity by detection of phosphorylated ERK (p-ERK), a downstream effector. We also assessed the ability of BAY-treated B cells to migrate on ICAM-1/CXCL13 membranes to determine Syk inhibition downstream of CXCR5. High BAY doses (1 and 0.6 μM) abolished BCR-mediated Syk activation, and reduced chemokine-triggered B cell motility (Supplementary Figures S4A and B). Treatment with 0.3 μM BAY impaired BCR-triggered Syk activity, but allowed a higher frequency of migrating B cells, with no significant alteration in mean velocity compared to controls (Supplementary Figures S4A and B). We evaluated the effect of this BAY dose on vinculin recruitment to the IS. BAY-treated B cells

showed lower vinculin levels at the contact plane and a distribution pattern distinct from that of untreated B cells (Figure 4A; Supplementary Figure S4C). Absence of the F-actin-rich ring indicated profound alterations in pSMAC assembly in BAY-treated B cells (Figure 4A). The ratio of vinculin at the contact plane with those at the mid-plane indicated almost no vinculin recruitment to the IS in BAY-treated B cells; F-actin polymerization was also impaired (Figure 4B; Supplementary Figure S4C). BAY treatment did not alter cSMAC formation or talin polarization to the contact plane (Figure 4C). B cells treated with a lower BAY dose (0.1 μM) did not show any change in vinculin recruitment and localization at the IS (Supplementary Figures S4C and D).

We used time-lapse microscopy to monitor the behaviour of CFSE-labelled B cells, untreated or treated with 0.3 μM BAY in contact with ICAM-1/CXCL13 membranes with tAg. Untreated B cells showed the predicted IS establishment and CXCL13-driven membrane ruffles; cells hardly moved from their position (Figure 5A; Supplementary Movie S7). A large percentage of BAY-treated B cells (40%) assembled an antigen cluster and migrated across the membrane (Figures 5A and B; Supplementary Movie S8). Motile BAY-treated B cells extended a clear lamellipodium at the cell front and carried the antigen cluster at the back uropod (Figure 5A; Supplementary Movie S8); they reached mean velocity values near 3 μm/min (Figure 5C).

These data indicated that vinculin recruitment is important for adhesion strength at the IS and to arrest chemokine-mediated B cell motility. In addition, the level of tAg/BCR-triggered Syk activation determines vinculin localization to the IS.

Non-muscle myosin-II activity is necessary for vinculin function at the B cell synapse

In non-immune cells, vinculin recruitment to and function at focal adhesions requires non-muscle motor protein myosin-II (NM-II) activity (Pasapera et al, 2010). Active NM-II is present at the B cell synapse (Saez de Guinoa et al, 2011). We studied the role of NM-II in

vinculin function at the B cell IS using the specific chemical inhibitor blebbistatin to interfere with NM-II activity. B cells were allowed to settle and establish an IS in contact with ICAM-1/CXCL13 membranes and tAg. After blebbistatin treatment (20 min), we fixed cells and stained for vinculin and F-actin. NM-II inhibition resulted in vinculin ring disorganization and loss of vinculin localization to the synapse (Figures 6A and B). At the time analyzed, F-actin distribution was maintained surrounding the cSMAC, its levels at the IS contact plane were lost (Figures 6A and B). Before fixation, blebbistatin-treated B cells remained adhered to the membrane (detected by IRM), although the contact area was significantly reduced (Figure 6C), suggesting internal disorganization of the pSMAC structure. Blebbistatin-treated B cells showed no sign of motility on the membranes, as full NM-II activity is needed for CXCL13-mediated B cell migration.

We used A20 B cells expressing a vinculin-GFP construct and Lifeact-RFP to monitor the effect of NM-II inhibition in time-lapse experiments. A20 B cells formed a mature IS in contact with ICAM-1/CXCL13 membranes and tAg; vinculin and F-actin distributed in a ring surrounding the cSMAC (Figure 6D). After adding blebbistatin, we tracked the molecular dynamics of vinculin and F-actin at the IS by confocal microcopy. By 20 min post-treatment, the vinculin pattern was completely disorganized and its fluorescent signal declined; F-actin polymerization was reduced, and no longer confined to the vicinity of the cSMAC (Figure 6D; Supplementary Movie S9).

The stability of the vinculin-rich domain at the B cell IS thus depends on appropriate NM-II activity. The data also indicated that loss of vinculin is accompanied by diminished F-actin polymerization and F-actin-ring disassembly at the contact plane.

Discussion

Our study focussed on the molecular mechanisms that underlie CXCR5 and BCR signalling and instruct B cell firm adhesion and motility. Here we showed that the scaffold protein vinculin is recruited to the B cell IS, and distributes in the LFA-1-rich pSMAC domain together with F-actin, talin, PIPKIγ and the lipid PIP_2. tAg/BCR-triggered Syk activity is needed for vinculin localization to the B cell:APC contact site; absence of vinculin recruitment allows B cells to continue moving in response to CXCL13 while assembling and carrying the synapse-characteristic antigen cluster at the uropod. The loss of vinculin also reduced F-actin polymerization, but not talin recruitment to the synapse. The motor protein NM-II is also implicated in maintaining vinculin at the IS. These data identify vinculin as a key regulatory element of the assembly and stability of the LFA-1-mediated platforms that support B cell dynamics, i.e. synapse and kinapse.

Vinculin is found in the synapse of other lymphocyte types. In Jurkat cells, T cell receptor (TCR) signalling promotes formation of a complex containing WAVE-2, Arp2/3, vinculin and talin; vinculin is necessary for talin recruitment, but not for F-actin polymerization or integrin accumulation at the T cell IS (Nolz et al, 2007). Primary talin-deficient T cells do not adhere firmly to APC or arrest migration; they are able to assemble some LFA-1 clustering, but not to recruit vinculin or F-actin to the short-lived synapse; the authors highlighted the importance of talin for T cell IS stability (Wernimont et al, 2011). In NK cells, LFA-1/ICAM-1 interaction leads to vinculin accumulation at the synapse, together with talin, actin, Arp2/3 and WASP; talin is needed for vinculin and F-actin localization to the contact site (Mace et al, 2010). Here we report that vinculin is recruited to the B cell synapse, specifically to the ring-shaped LFA-1-rich pSMAC domain, where it co-localizes with talin and F-actin. Talin might be also important for vinculin recruitment to the B cell synapse, a subject for further study. We nonetheless found that, without affecting talin localization, vinculin at the

B cell synapse was essential for F-actin accumulation, pSMAC assembly and synapse stability.

PIP_2 represents 1-2% of phospholipids at the plasma membrane, where is quite evenly distributed (Hilgemann, 2007). PIPKI localization and activity regulates the targeted, limited production of PIP_2, which in turn governs the temporal and spatial requirements of FA assembly and actin dynamics. In neutrophils, correct distribution of distinct PIPKI family members regulates cell polarity and migration (Lacalle et al, 2007; Xu et al, 2010). PIP_2 is involved in vinculin translocation from cytosol to FA; structural studies indicate that PIP_2 association promotes a conformational change in vinculin that enables binding of a second partner, thus stabilizing the active vinculin conformation (Bakolitsa et al, 2004). PIPKIγ deficiency specifically at FA impairs talin and vinculin recruitment to nascent adhesion sites, which reduces integrin-mediated cell adhesion and force coupling (Legate et al, 2011). Another report does not implicate PIP_2 in vinculin recruitment to adhesion sites, but rather in vinculin release and FA disassembly (Chandrasekar et al, 2005), which is reinforced by the finding that PIPKIγ-deficient T cells show increased integrin-mediated adhesion (Wernimont et al, 2010). Our findings coincide with the first model; tAg/BCR stimulation promoted PIPKIγ localization and thus, local PIP_2 production at the nascent synapse that could support vinculin recruitment. Both PIPKIγ and PIP_2 reach a transient peak and return to basal levels; however, they remain detectable at the pSMAC of the mature synapse, possibly assisting the active vinculin conformation. PIPKIγ is also found at the T cell synapse; the spatiotemporal regulation of PIP_2 synthesis appears to control T cell rigidity and signalling organization (Sun et al, 2011).

FA are mechanosensitive structures that transmit cell forces to the extracellular matrix. Cell forces are generated as a consequence of NM-II action on the actin cytoskeleton (Cai et al, 2006). NM-II-mediated contractility controls the localization to FA of vinculin and other

adaptor proteins (Pasapera et al, 2010). The ability of vinculin to bear force determines the assembly or disassembly of adhesion sites under tension (Carisey et al, 2013; Grashoff et al, 2010). In the podosome, another type of actomyosin-based integrin-rich platform, NM-II activity is not necessary for adaptor protein composition, which is controlled by the actin network (van den Dries et al, 2013). NM-II participates in the formation and stability of synapse platforms and migratory junctions in lymphocytes (Ilani et al, 2009; Jacobelli et al, 2004; Jacobelli et al, 2010; Saez de Guinoa et al, 2011). Our data show that NM-II activity is important for vinculin localization at the B cell synapse, as described for FA. In addition, lack of vinculin due to NM-II inhibition led to reduced, mislocalized F-actin polymerization and pSMAC disassembly. We propose that vinculin is the mechanical sensor also at the lymphocyte synapse; it regulates assembly and disassembly of the adhesion structure based on cell force input.

Syk kinase has a role in integrin activation downstream of the BCR and of chemokine receptors (Pearce et al, 2011; Spaargaren et al, 2003). Our data indicate that the Syk activity level and localization determine vinculin recruitment and function at the B cell synapse. tAg stimulation of the BCR resulted in higher Syk activation than stimulation with sAg, although both antigen treatments promoted similar levels of B cell activation at 24 h, as determined by measuring cell surface CD86 and CD69 expression (unpublished observations). In addition, BCR recognition of tAg led to concentration of Syk activity at the synapse plane. Syk promotes Btk recruitment to the plasma membrane by PH domain binding to the lipid PIP_3, produced by PI3K (Saito et al, 2003). Btk associates with and transports PIPKI to the cell membrane to produce PIP_2, the substrate of the Btk upstream activator PI3K. Here we show that vinculin recruitment parallels the PIP_2 wave generated by PIPKIγ early in synapse formation. Btk-mediated PIP_2 production might thus support PI3K activity, but also assists vinculin localization to the synapse. In our model, above a certain threshold of tAg/BCR-

promoted Syk activity, there is a local increase in Btk and PIPKIγ-dependent PIP_2 at the B cell:APC contact site; the PIP_2 wave leads to vinculin recruitment and thus, to pSMAC assembly and adhesion strength. This model explains our previous observations that below a tAg/BCR signalling threshold, B cells remain motile in response to chemokines and integrate BCR signals through the LFA-1-mediated migratory junction, the kinapse (Saez de Guinoa et al, 2011).

Methods

Mice and cells

Primary B cells were freshly isolated from spleens of wild type and MD4 BCR transgenic mice on the C57BL/6 genetic background by negative selection (>95% purity), as described (Saez de Guinoa et al, 2011). For time-lapse experiments, purified B cells were labelled before use with 0.1 μM CFSE long-term dye (Molecular Probes; 10 min, 37ºC). Animal experimentation was approved by the CNB-CSIC Bioethics Committee and conforms to institutional, national and EU regulations. The A20 murine B cell line was transiently transfected by electroporation with PIPKIγ-GFP (a kind gift from Rosana Lacalle; (Lacalle et al, 2007)), the PIP_2 probe PLCδ-PH-GFP (a kind gift from Isabel Mérida; (Falasca et al, 1998)), vinculin-GFP (a kind gift from Miguel Vicente-Manzanares; (Shen et al, 2011)) and the F-actin probe Lifeact-RFP constructs (a kind gift from Mario Mellado; (Riedl et al, 2008)) and used 20 h later for time-lapse experiments.

Time-lapse microscopy on planar lipid bilayers

We prepared artificial planar lipid bilayers containing GPI-linked mouse ICAM-1 (density 150 molec/μm^2) and when indicated, biotin-modified phospholipids at specific molecular densities (Saez de Guinoa et al, 2011). Membranes were assembled on FCS2 closed chambers (Bioptechs) and blocked with PBS/2% FCS (1 h, room temperature (RT)). Antigen (density 20 molec/μm^2) was tethered to the membranes by incubating with Alexa Fluor 647 or Alexa Fluor 555-streptavidin (Molecular Probes), followed by monobiotinylated HEL (hen egg lysozyme, Sigma) for MD4 B cells or monobiotinylated anti-κ light chain mAb (BD Biosciences) for wild type B cells and the A20 B cell line. Before imaging, membranes were coated with 100 nM recombinant murine CXCL13 (Peprotech). Unlabelled or CFSE-labelled primary B cells (2×10^6) and transfected A20 B cells (1×10^6) were injected into the warmed chamber (37ºC) and imaging was started. Confocal fluorescence, differential interference

contrast (DIC) and interference reflection microscopy (IRM) images were acquired every 30 seconds for 20 minutes; when indicated, consecutive movies were acquired. Assays were performed in PBS with 0.5% FCS, 0.5 g/L D-glucose, 2 mM $MgCl_2$ and 0.5 mM $CaCl_2$. For soluble antigen stimulation, $F(ab')_2$ anti-IgM antibody (Jackson ImmunoResearch) was added at 1 μg/ml final concentration to the B cell suspension immediately before injection into the FCS2 chamber. When indicated, primary B cells were treated with specified doses of the chemical inhibitor BAY 61-3606 (Calbiochem; 20 min, 30ºC) before injection. B cells were treated with Blebbistatin (50 μM; Calbiochem) *in situ* by injection into the FCS2 chamber, incubated 5-10 min, and imaged. Images were acquired on an Axiovert LSM 510-META inverted microscope with a 40x oil immersion objective (Zeiss) and analyzed with Imaris 7.0 software (Bitplane).

Immunofluorescence

Primary B cells were in contact with planar lipid bilayers containing GPI-linked ICAM-1 and CXCL13 coating, alone or with tethered antigen or with soluble antigen (30 min), fixed with 4% paraformaldehyde (PFA; 10 min, 37ºC), permeabilized with PBS/0.1% Triton-X100 (5 min, RT), blocked with PBS with 2% FCS and 2%BSA (overnight, 4ºC), and stained with Alexa Fluor 647-phalloidin (Molecular Probes), rabbit anti-phospho-Syk (Tyr352) (Cell Signaling) plus Alexa Fluor 488-goat anti-rabbit IgG (Southern Biotechnology), and mouse anti-talin or -vinculin (clones 8d4 and hVIN-1, respectively; Sigma) plus FITC goat-anti-mouse IgG1 (BD Biosciences) (30 min, RT). FCS2 chambers were imaged by confocal fluorescent microscopy on a Zeiss Axiovert inverted microscope as above. We used Imaris 7.0 software for qualitative and quantitative analysis of fluorescence signals at distinct cell planes and in the whole cell volume, as well as IRM area measurements. Ratios were obtained dividing the total fluorescence of the indicated protein at the synapse/contact plane between

the total fluorescence at the mid-plane. Total fluorescence at the entire cell volume was obtained from z-stack images (optical slice thickness 1μm) using Imaris 7.0 software.

Infection using lentiviral vectors

Recombinant lentiviral particle stocks were obtained from HEK 293T cells by co-transfecting the shRNA-coding vector (pLKO.1, pGIPZ), the pMD.2G envelope vector, and the pCMVR8.91 packaging vector (Zufferey et al, 1997). We used two types of shRNA coding vectors: Mouse GIPZ lentiviral shRNAmir vectors (clones V2LMM_45006, V2LMM_56452, V3LMM_437636, coding for mouse vinculin-specific shRNA, and a non-silencing-GIPZ lentiviral shRNAmir control; Thermo Scientific) and Mouse vinculin shRNA in pLKO.1 vector backbones (clones NM_009502.3-3466s1c1, NM_009502.3-1331s1c1, NM_009502.3-3154s1c1; Mission shRNA, Sigma). Briefly, 2 x 10^6 cells were plated on p150 dishes (48 h), and then transfected with 2 μg envelope vector, 5 μg packaging vector and 7 μg shRNA-coding vector by precomplexing with JetPEI (0.1 mM final concentration; Polyplus Transfection; 30 min, RT) in OptiMEM (Gibco). After 4 h at 37ºC, we replaced medium with fresh DMEM/2% FCS; virus particles were harvested 48 or 72 h post-transfection. The virus suspension was filtered (0.45 μM pore size) and concentrated by ultracentrifugation (23,000 rpm, 2 h, 4ºC). The pellet was resuspended in RPMI and stored at -80ºC. Freshly isolated primary B cells (2 x 10^6) were infected with lentiviral particles (MOI 1-10) in 500 μl RPMI/10% FCS, alone or with recombinant murine IL-4 (50 ng/ml; Peprotech), CpG (1 μg/ml; Invivogen) or LPS (2.5 μg/ml; Sigma) for 6 h at 37ºC. Medium was replaced with fresh RPMI/10% FCS, alone or with the specified stimuli, and infected B cells cultured (48 h) to allow shRNA and gene reporter expression. Vinculin protein levels and GFP reporter expression were analyzed in western blot.

Western blot analysis

Freshly isolated primary B cells (5 x 10^6) were cultured in depletion medium (RPMI/0.5% FCS; 1 h, 37ºC) and then stimulated with F(ab')$_2$ anti-IgM antibody (1 μg/ml; with shaking) or with ICAM-1/CXCL13-membranes in absence or presence of tethered antigen for 30 minutes at 37ºC. Ice-cold PBS was added and B cells centrifuged (2,000 rpm, 5 min, 4ºC) and lysed in RIPA lysis buffer with protease and phosphatase inhibitors (Roche; 30 min, 4ºC). Lysates were centrifuged (14,000 rpm, 30 min, 4ºC), supernatants collected and stored at -80ºC. Lentiviral particle-infected B cell lysates were obtained similarly. Total protein was quantified with the Micro BCA Protein assay kit (Thermo Scientific), separated by SDS-PAGE and transferred to PVDF membranes (BioRad). Blots were blocked with 2% BSA in TBS-T (10mM Tris-HCL pH 8, 150mM NaCl, 0.1% Tween-20) (1 h, RT), and incubated with rabbit anti-Syk, rabbit anti-phospho-Syk (Tyr352), rabbit anti-phospho-ERK1/2 (Cell Signaling), mouse anti-vinculin (clone hVIN-1; Sigma), mouse anti-β-actin (Sigma) or mouse anti-α-tubulin (clone DM1A; Sigma) (overnight, 4ºC), followed by horseradish peroxidase-conjugated secondary antibodies (1 h, RT); the signal was detected with the enhanced chemiluminiscence detection system (ECL; GE Healthcare). Signal intensity values in arbitrary units for each protein (p-Erk, vinculin) were quantified using ImajeJ software (NIH), normalized to tubulin or β-actin signal, relative to individual controls.

Statistical analysis

Graphs and statistical analysis were done using Prism 4.0 software (GraphPad). Two-tailed unpaired Student *t*-test was applied.*, $p<0.05$; **, $p<0.001$; ***, $p<0.0001$.

Acknowledgements

We thank I. Antón and M. Vicente-Manzanares for critical reading of the manuscript and C Mark for editorial assistance.

JSdG is supported by a contract from the Comunidad Autónoma de Madrid. LB is supported by a contract associated to project grant BFU2008-01194 from the Spanish Ministry of Economy and Competitiveness (MINECO). This work was supported by grants from the European Union (FP7-integrated project Masterswitch 223404 FP7) and from the Spanish MINECO (BFU2011-30097) to YRC.

Author Contributions

Contribution: JSdG designed parts of the study, performed the experiments, analyzed the data and assisted in manuscript preparation. LB assisted in performing experiments, data analysis and manuscript preparation. YRC designed and supervised all aspects of the project and wrote the manuscript.

Conflict-of-interest disclosure: The authors declare no competing financial interests.

References

Allen CD, Cyster JG (2008) Follicular dendritic cell networks of primary follicles and germinal centers: phenotype and function. *Semin Immunol* 20(1): 14-25

Bajenoff M, Egen JG, Koo LY, Laugier JP, Brau F, Glaichenhaus N, Germain RN (2006) Stromal cell networks regulate lymphocyte entry, migration, and territoriality in lymph nodes. *Immunity* 25(6): 989-1001

Bakolitsa C, Cohen DM, Bankston LA, Bobkov AA, Cadwell GW, Jennings L, Critchley DR, Craig SW, Liddington RC (2004) Structural basis for vinculin activation at sites of cell adhesion. *Nature* 430(6999): 583-586

Batista FD, Arana E, Barral P, Carrasco YR, Depoil D, Eckl-Dorna J, Fleire S, Howe K, Vehlow A, Weber M, Treanor B (2007) The role of integrins and coreceptors in refining thresholds for B-cell responses. *Immunol Rev* 218: 197-213

Cai Y, Biais N, Giannone G, Tanase M, Jiang G, Hofman JM, Wiggins CH, Silberzan P, Buguin A, Ladoux B, Sheetz MP (2006) Nonmuscle myosin IIA-dependent force inhibits cell spreading and drives F-actin flow. *Biophys J* 91(10): 3907-3920

Carisey A, Ballestrem C (2010) Vinculin, an adapter protein in control of cell adhesion signalling. *Eur J Cell Biol* 90(2-3): 157-163

Carisey A, Tsang R, Greiner AM, Nijenhuis N, Heath N, Nazgiewicz A, Kemkemer R, Derby B, Spatz J, Ballestrem C (2013) Vinculin Regulates the Recruitment and Release of Core Focal Adhesion Proteins in a Force-Dependent Manner. *Curr Biol* 23: 271-281

Carrasco YR, Batista FD (2007) B cells acquire particulate antigen in a macrophage-rich area at the boundary between the follicle and the subcapsular sinus of the lymph node. *Immunity* 27(1): 160-171

Carrasco YR, Fleire SJ, Cameron T, Dustin ML, Batista FD (2004) LFA-1/ICAM-1 interaction lowers the threshold of B cell activation by facilitating B cell adhesion and synapse formation. *Immunity* 20(5): 589-599

Chandrasekar I, Stradal TE, Holt MR, Entschladen F, Jockusch BM, Ziegler WH (2005) Vinculin acts as a sensor in lipid regulation of adhesion-site turnover. *J Cell Sci* 118(Pt 7): 1461-1472

Coll JL, Ben-Ze'ev A, Ezzell RM, Rodriguez Fernandez JL, Baribault H, Oshima RG, Adamson ED (1995) Targeted disruption of vinculin genes in F9 and embryonic stem cells changes cell morphology, adhesion, and locomotion. *Proc Natl Acad Sci U S A* 92(20): 9161-9165

Cyster JG (2010) B cell follicles and antigen encounters of the third kind. *Nat Immunol* 11(11): 989-996

Di Paolo G, Pellegrini L, Letinic K, Cestra G, Zoncu R, Voronov S, Chang S, Guo J, Wenk MR, De Camilli P (2002) Recruitment and regulation of phosphatidylinositol phosphate kinase type 1 gamma by the FERM domain of talin. *Nature* 420(6911): 85-89

Dustin ML (2007) Cell adhesion molecules and actin cytoskeleton at immune synapses and kinapses. *Curr Opin Cell Biol* 19(5): 529-533

Falasca M, Logan SK, Lehto VP, Baccante G, Lemmon MA, Schlessinger J (1998) Activation of phospholipase C gamma by PI 3-kinase-induced PH domain-mediated membrane targeting. *EMBO J* 17(2): 414-422

Fleire SJ, Goldman JP, Carrasco YR, Weber M, Bray D, Batista FD (2006) B cell ligand discrimination through a spreading and contraction response. *Science* 312(5774): 738-741

Grashoff C, Hoffman BD, Brenner MD, Zhou R, Parsons M, Yang MT, McLean MA, Sligar SG, Chen CS, Ha T, Schwartz MA (2010) Measuring mechanical tension across vinculin reveals regulation of focal adhesion dynamics. *Nature* 466(7303): 263-266

Harwood NE, Batista FD (2011) The cytoskeleton coordinates the early events of B-cell activation. *Cold Spring Harb Perspect Biol* 3(2)

Hilgemann DW (2007) Local PIP(2) signals: when, where, and how? *Pflugers Arch* 455(1): 55-67

Humphries JD, Wang P, Streuli C, Geiger B, Humphries MJ, Ballestrem C (2007) Vinculin controls focal adhesion formation by direct interactions with talin and actin. *J Cell Biol* 179(5): 1043-1057

Ilani T, Vasiliver-Shamis G, Vardhana S, Bretscher A, Dustin ML (2009) T cell antigen receptor signaling and immunological synapse stability require myosin IIA. *Nat Immunol* 10(5): 531-539

Jacobelli J, Chmura SA, Buxton DB, Davis MM, Krummel MF (2004) A single class II myosin modulates T cell motility and stopping, but not synapse formation. *Nat Immunol* 5(5): 531-538

Jacobelli J, Friedman RS, Conti MA, Lennon-Dumenil AM, Piel M, Sorensen CM, Adelstein RS, Krummel MF (2010) Confinement-optimized three-dimensional T cell amoeboid motility is modulated via myosin IIA-regulated adhesions. *Nat Immunol* 11(10): 953-961

Kinashi T (2007) Integrin regulation of lymphocyte trafficking: lessons from structural and signaling studies. *Adv Immunol* 93: 185-227

Lacalle RA, Peregil RM, Albar JP, Merino E, Martinez AC, Merida I, Manes S (2007) Type I phosphatidylinositol 4-phosphate 5-kinase controls neutrophil polarity and directional movement. *J Cell Biol* 179(7): 1539-1553

Legate KR, Takahashi S, Bonakdar N, Fabry B, Boettiger D, Zent R, Fassler R (2011) Integrin adhesion and force coupling are independently regulated by localized PtdIns(4,5)2 synthesis. *EMBO J* 30(22): 4539-4553

Lifschitz-Mercer B, Czernobilsky B, Feldberg E, Geiger B (1997) Expression of the adherens junction protein vinculin in human basal and squamous cell tumors: relationship to invasiveness and metastatic potential. *Hum Pathol* 28(11): 1230-1236

Ling K, Doughman RL, Firestone AJ, Bunce MW, Anderson RA (2002) Type I gamma phosphatidylinositol phosphate kinase targets and regulates focal adhesions. *Nature* 420(6911): 89-93

Ling K, Schill NJ, Wagoner MP, Sun Y, Anderson RA (2006) Movin' on up: the role of PtdIns(4,5)P(2) in cell migration. *Trends Cell Biol* 16(6): 276-284

Mace EM, Zhang J, Siminovitch KA, Takei F (2010) Elucidation of the integrin LFA-1-mediated signaling pathway of actin polarization in natural killer cells. *Blood* 116(8): 1272-1279

Miller MJ, Wei SH, Parker I, Cahalan MD (2002) Two-photon imaging of lymphocyte motility and antigen response in intact lymph node. *Science* 296(5574): 1869-1873

Nolz JC, Medeiros RB, Mitchell JS, Zhu P, Freedman BD, Shimizu Y, Billadeau DD (2007) WAVE2 regulates high-affinity integrin binding by recruiting vinculin and talin to the immunological synapse. *Mol Cell Biol* 27(17): 5986-6000

Okada T, Miller MJ, Parker I, Krummel MF, Neighbors M, Hartley SB, O'Garra A, Cahalan MD, Cyster JG (2005) Antigen-engaged B cells undergo chemotaxis toward the T zone and form motile conjugates with helper T cells. *PLoS Biol* 3(6): e150

Pasapera AM, Schneider IC, Rericha E, Schlaepfer DD, Waterman CM (2010) Myosin II activity regulates vinculin recruitment to focal adhesions through FAK-mediated paxillin phosphorylation. *J Cell Biol* 188(6): 877-890

Pearce G, Audzevich T, Jessberger R (2011) SYK regulates B-cell migration by phosphorylation of the F-actin interacting protein SWAP-70. *Blood* 117(5): 1574-1584

Randall KL, Lambe T, Johnson A, Treanor B, Kucharska E, Domaschenz H, Whittle B, Tze LE, Enders A, Crockford TL, Bouriez-Jones T, Alston D, Cyster JG, Lenardo MJ, Mackay F, Deenick EK, Tangye SG, Chan TD, Camidge T, Brink R, Vinuesa CG, Batista FD, Cornall RJ, Goodnow CC (2009) Dock8 mutations cripple B cell immunological synapses, germinal centers and long-lived antibody production. *Nat Immunol* 10(12): 1283-1291

Riedl J, Crevenna AH, Kessenbrock K, Yu JH, Neukirchen D, Bista M, Bradke F, Jenne D, Holak TA, Werb Z, Sixt M, Wedlich-Soldner R (2008) Lifeact: a versatile marker to visualize F-actin. *Nat Methods* 5(7): 605-607

Rodriguez Fernandez JL, Geiger B, Salomon D, Sabanay I, Zoller M, Ben-Ze'ev A (1992) Suppression of tumorigenicity in transformed cells after transfection with vinculin cDNA. *J Cell Biol* 119(2): 427-438

Saez de Guinoa J, Barrio L, Mellado M, Carrasco YR (2011) CXCL13/CXCR5 signaling enhances B-cell receptor-triggered B-cell activation by shaping cell dynamics. *Blood*

Saito K, Tolias KF, Saci A, Koon HB, Humphries LA, Scharenberg A, Rawlings DJ, Kinet JP, Carpenter CL (2003) BTK regulates PtdIns-4,5-P2 synthesis: importance for calcium signaling and PI3K activity. *Immunity* 19(5): 669-678

Shen K, Tolbert CE, Guilluy C, Swaminathan VS, Berginski ME, Burridge K, Superfine R, Campbell SL (2011) The vinculin C-terminal hairpin mediates F-actin bundle formation, focal adhesion, and cell mechanical properties. *J Biol Chem* 286(52): 45103-45115

Spaargaren M, Beuling EA, Rurup ML, Meijer HP, Klok MD, Middendorp S, Hendriks RW, Pals ST (2003) The B cell antigen receptor controls integrin activity through Btk and PLCgamma2. *J Exp Med* 198(10): 1539-1550

Sun Y, Dandekar RD, Mao YS, Yin HL, Wulfing C (2011) Phosphatidylinositol (4,5) bisphosphate controls T cell activation by regulating T cell rigidity and organization. *PLoS One* 6(11): e27227

van den Dries K, Meddens MB, de Keijzer S, Shekhar S, Subramaniam V, Figdor CG, Cambi A (2013) Interplay between myosin IIA-mediated contractility and actin network integrity orchestrates podosome composition and oscillations. *Nat Commun* 4: 1412

Wernimont SA, Legate KR, Simonson WT, Fassler R, Huttenlocher A (2010) PIPKI gamma 90 negatively regulates LFA-1-mediated adhesion and activation in antigen-induced CD4+ T cells. *J Immunol* 185(8): 4714-4723

Wernimont SA, Wiemer AJ, Bennin DA, Monkley SJ, Ludwig T, Critchley DR, Huttenlocher A (2011) Contact-dependent T cell activation and T cell stopping require talin1. *J Immunol* 187(12): 6256-6267

Xu W, Baribault H, Adamson ED (1998a) Vinculin knockout results in heart and brain defects during embryonic development. *Development* 125(2): 327-337

Xu W, Coll JL, Adamson ED (1998b) Rescue of the mutant phenotype by reexpression of full-length vinculin in null F9 cells; effects on cell locomotion by domain deleted vinculin. *J Cell Sci* 111 (Pt 11): 1535-1544

Xu W, Wang P, Petri B, Zhang Y, Tang W, Sun L, Kress H, Mann T, Shi Y, Kubes P, Wu D (2010) Integrin-induced PIP5K1C kinase polarization regulates neutrophil polarization, directionality, and in vivo infiltration. *Immunity* 33(3): 340-350

Zufferey R, Nagy D, Mandel RJ, Naldini L, Trono D (1997) Multiply attenuated lentiviral vector achieves efficient gene delivery in vivo. *Nat Biotechnol* 15(9): 871-875

Figure Legends

Figure 1. tAg/BCR-triggered synapse assembly is necessary to arrest B cell motility. Primary wild type B cells were allowed to settle on membranes containing GPI-ICAM-1 and coated with CXCL13, alone or with membrane-tethered (t)Ag or soluble (s)Ag. (A) Frequency of cell adhesion (estimated by IRM) and (B) cell polarization and motility (estimated by DIC microscopy) in the specified stimulation conditions. Data from a representative experiment are shown (n = 3). (C) Mean velocity values of motile B cells in (B); each dot represents a single cell. (D) DIC and fluorescence images for p-Syk, F-actin and antigen at the contact plane, and for p-Syk at the mid-plane of representative B cells in contact with ICAM-1/CXCL13 membranes with tAg or sAg. Profiles of relative mean fluorescence distribution of p-Syk, F-actin and antigen at the contact plane (arrow in the merge image), and profiles of p-Syk fluorescence distribution at contact and mid-planes (arrows in merge and mid-plane images, respectively) in the presence of tAg or sAg (right). (E) Total p-Syk fluorescence values at the contact plane and (F) in the entire cell volume (in arbitrary units, AU) of B cells settled on ICAM-1/CXCL13 membranes, alone (none) and with tAg or sAg; each dot represents a single cell. Data in (E) and (F) correspond to a representative experiment (n = 3). Scale bar, 2 μm.

Figure 2. tAg/BCR signalling promotes vinculin polarization to the B cell synapse. Primary MD4 B cells in contact with ICAM-1/CXCL13 membranes with tAg or sAg were fixed and stained for the indicated markers. (A) DIC and fluorescence images are shown for vinculin, talin, F-actin and antigen at the contact plane, and for vinculin and talin at the mid-plane of representative B cells in the presence of tAg. Relative mean fluorescence distribution profiles of vinculin, talin, F-actin and antigen at the contact plane (arrow, merge image), and fluorescence distribution profiles of vinculin and talin at contact and mid-planes (arrows in merge and mid-plane images, respectively) (right). (B) DIC and fluorescence

images are shown for vinculin, F-actin and antigen at the contact plane, and for vinculin at the mid-plane of representative B cells in the presence of tAg or sAg. Relative mean fluorescence distribution profiles of vinculin, F-actin and antigen at the contact plane (arrow, merge image), and fluorescence distribution profiles for vinculin at contact and mid-cell planes (arrows in merge and middle plane images, respectively) (right). (C) Total vinculin (left) and F-actin (right) fluorescence values in the B cell contact plane with the membrane alone (none) or with tAg or sAg; each dot represents a single cell. Data from a representative experiment are shown (n = 3). Scale bar, 2 μm.

Figure 3. A wave of PIPKIγ and PIP_2 lipid is detected early in synapse formation. A20 B cells transfected with PIPKIγ-GFP or PLCδ-PH-GFP (PIP_2 probe) constructs, in contact with ICAM-1/CXCL13 membranes and tAg, were monitored for synapse formation by time-lapse confocal microscopy. (A) Time-lapse DIC, IRM, and fluorescence PIPKIγ and antigen images of a representative B cell are shown. (B) Profiles of total PIPKIγ fluorescence values at the B cell:membrane interface plane over time, alone (none; bottom) and with tAg (top) of representative B cells; dashed line indicates initiation of B cell interaction with the membrane (detected by IRM; considered time zero). (C) Time-lapse DIC, IRM, and fluorescence PIP_2 and antigen images of a representative B cell. (D) As in (B), for the PIP_2 probe. (E) DIC, IRM and fluorescence PIPKIγ and antigen images of a representative B cell. Relative mean fluorescence distribution profile of PIPKIγ and antigen at the contact plane (arrow, merge image) (bottom). (F) DIC, IRM and fluorescence PIP_2 and antigen images of a representative B cell. Relative mean fluorescence distribution profile of PIP_2 and antigen at the contact plane (arrow, merge image) (bottom). Scale bar, 2 μm.

Figure 4. Syk activity inhibition impedes vinculin localization to the IS. Untreated or BAY-treated primary MD4 B cells in contact with ICAM-1/CXCL13 membranes and tAg. (A) DIC and fluorescence images of vinculin, F-actin and antigen at the synapse plane and of

vinculin at the mid-plane of a representative B cell. (B) Ratio of total vinculin (middle) and total F-actin (right) fluorescence at the synapse plane to that at the mid-plane for untreated and BAY-treated B cells; each dot represents a single cell. Data from a representative experiment are shown (n = 3). (C) DIC and fluorescence images are shown of talin, F-actin and antigen at the synapse plane of representative B cells. Ratio of total talin fluorescence at the synapse plane to that of the mid-plane for untreated and BAY-treated B cells (right); each dot represents a single cell. Data from a representative experiment (n = 4).

Figure 5. Lack of vinculin at the synapse allows B cell motility. Untreated or BAY-treated primary B cells in contact with ICAM-1/CXCL13 membranes and tAg. (A) Time-lapse DIC and overlaid IRM/fluorescence antigen images of representative untreated (top) and BAY-treated (bottom) B cells. Arrows indicate antigen cluster position. (B) Migration frequency of untreated or BAY-treated B cells on ICAM-1/CXCL13 membranes, alone (empty bar) or with tAg (filled bars). (C) Mean velocity values of the motile B cells in (B); each dot represents a single cell. Data in (B) and (C) are the merge of three experiments. Scale bar, 2 μm.

Figure 6. NM-II activity regulates vinculin function at the synapse. Primary MD4 B cells in contact with ICAM-1/CXCL13 membranes and tAg were untreated or treated with blebbistatin (20 min), fixed and stained for the indicated markers. (A) DIC and fluorescence images for vinculin, F-actin and antigen of representative untreated (control) and blebbistatin-treated B cells. Relative mean fluorescence distribution profiles of vinculin, F-actin and antigen at the contact plane (arrow, merge image) (right). (B) Ratio of total vinculin (left) and total F-actin (right) fluorescence at the synapse plane to that at the mid-plane for untreated (control) and blebbistatin-treated B cells; each dot represents a single cell. Data from a representative experiment (n = 3). (C) DIC and IRM images of representative B cells, untreated or treated with blebbistatin before fixing (left). B cell:membrane contact area values in the indicated conditions (right); each dot represents a single cell. Data correspond to

the merge of two experiments. (D) A20 B cells co-transfected with vinculin-GFP and Lifeact-RFP constructs were allowed to form a synapse with ICAM-1/CXCL13 membranes and tAg, and blebbistatin was added. Time-lapse DIC, IRM and fluorescence vinculin, F-actin and antigen images of a representive A20 B cell before (pre-blebbistatin) and after blebbistatin addition. Scale bar, 2 μm.

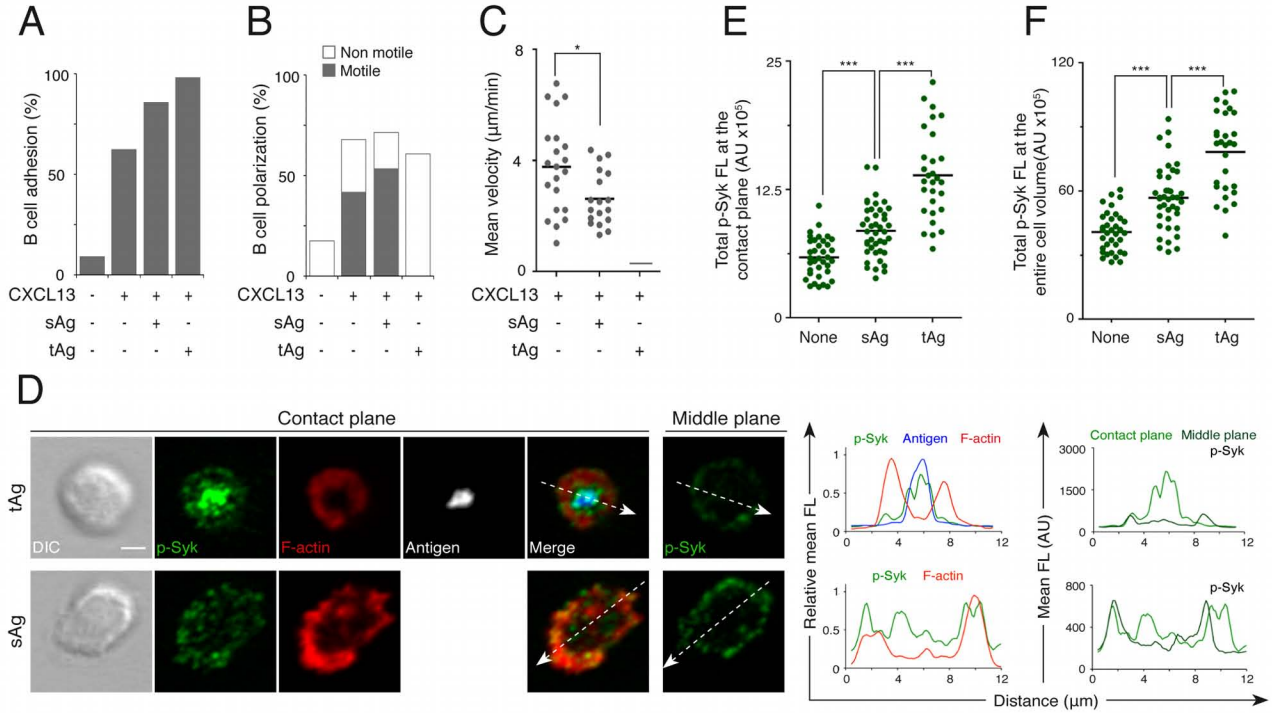

Figure 1. Saez de Guinoa *et al*.

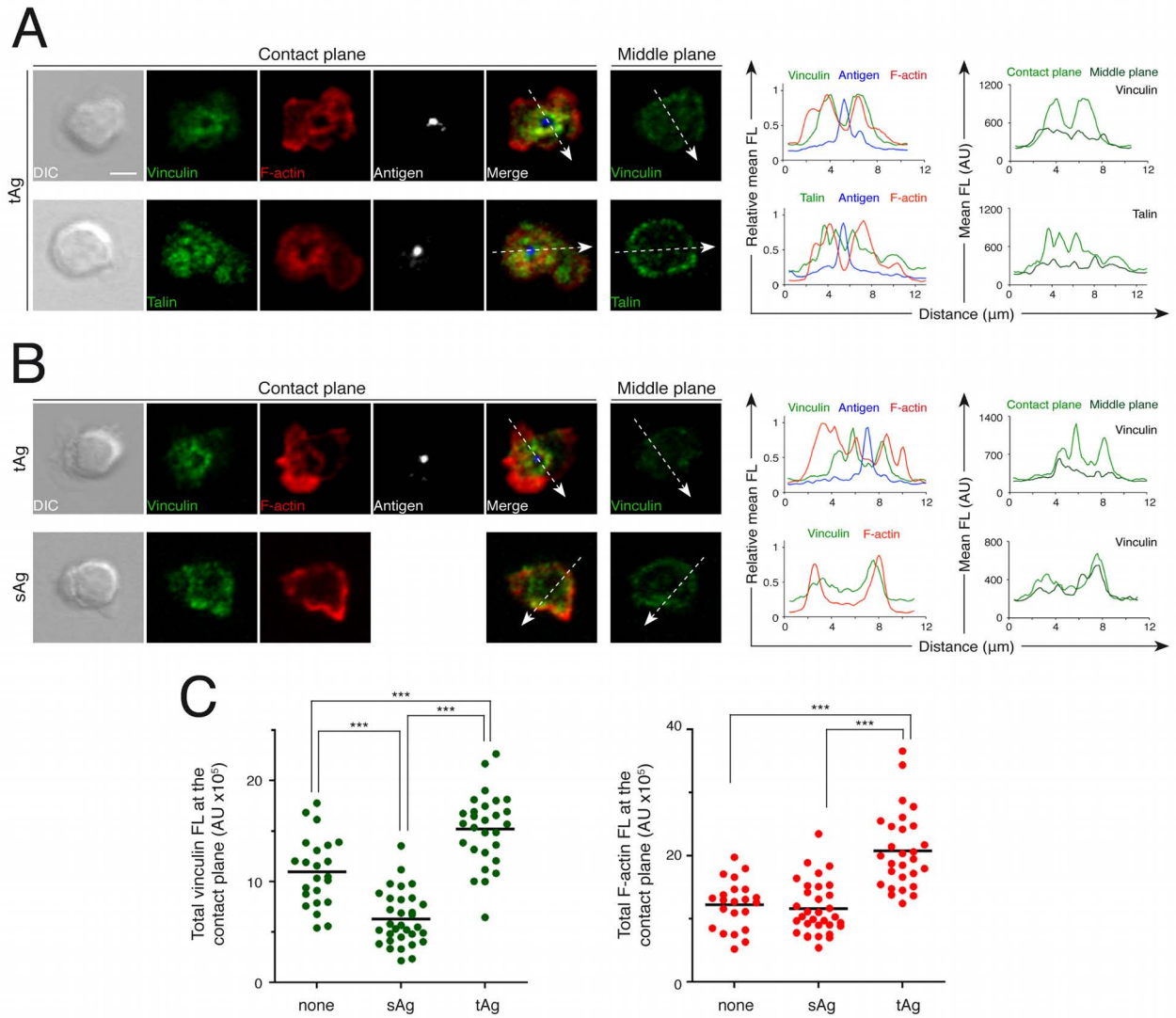

Figure 2. Saez de Guinoa *et al*.

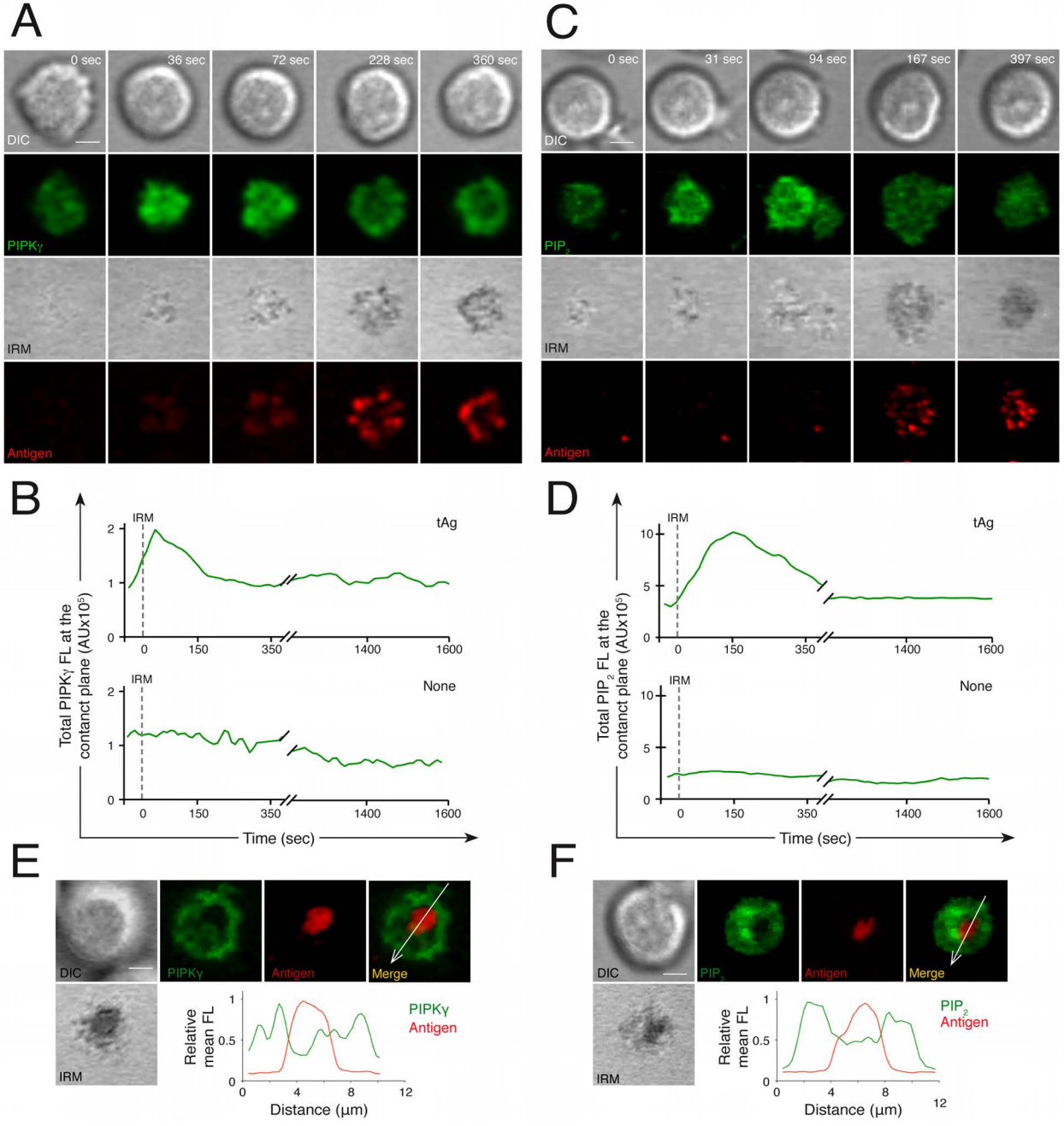

Figure 3. Saez de Guinoa *et al.*

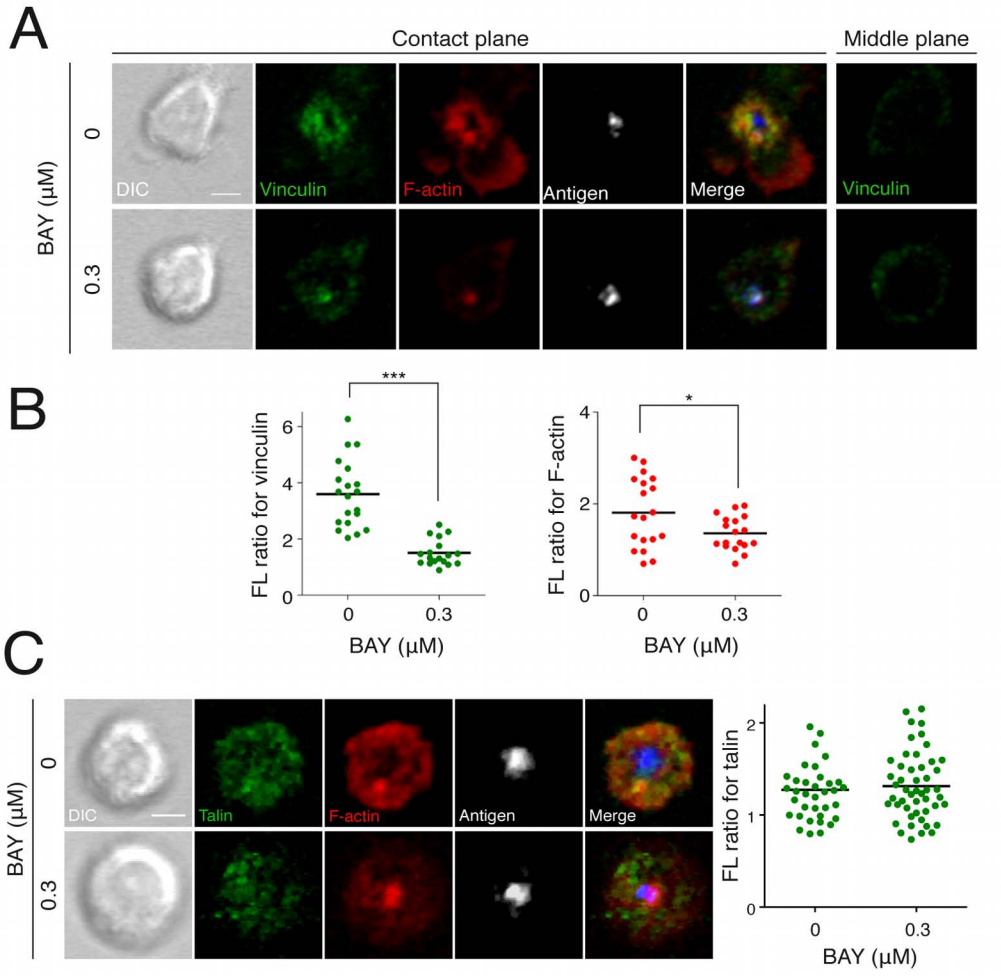

Figure 4. Saez de Guinoa *et al.*

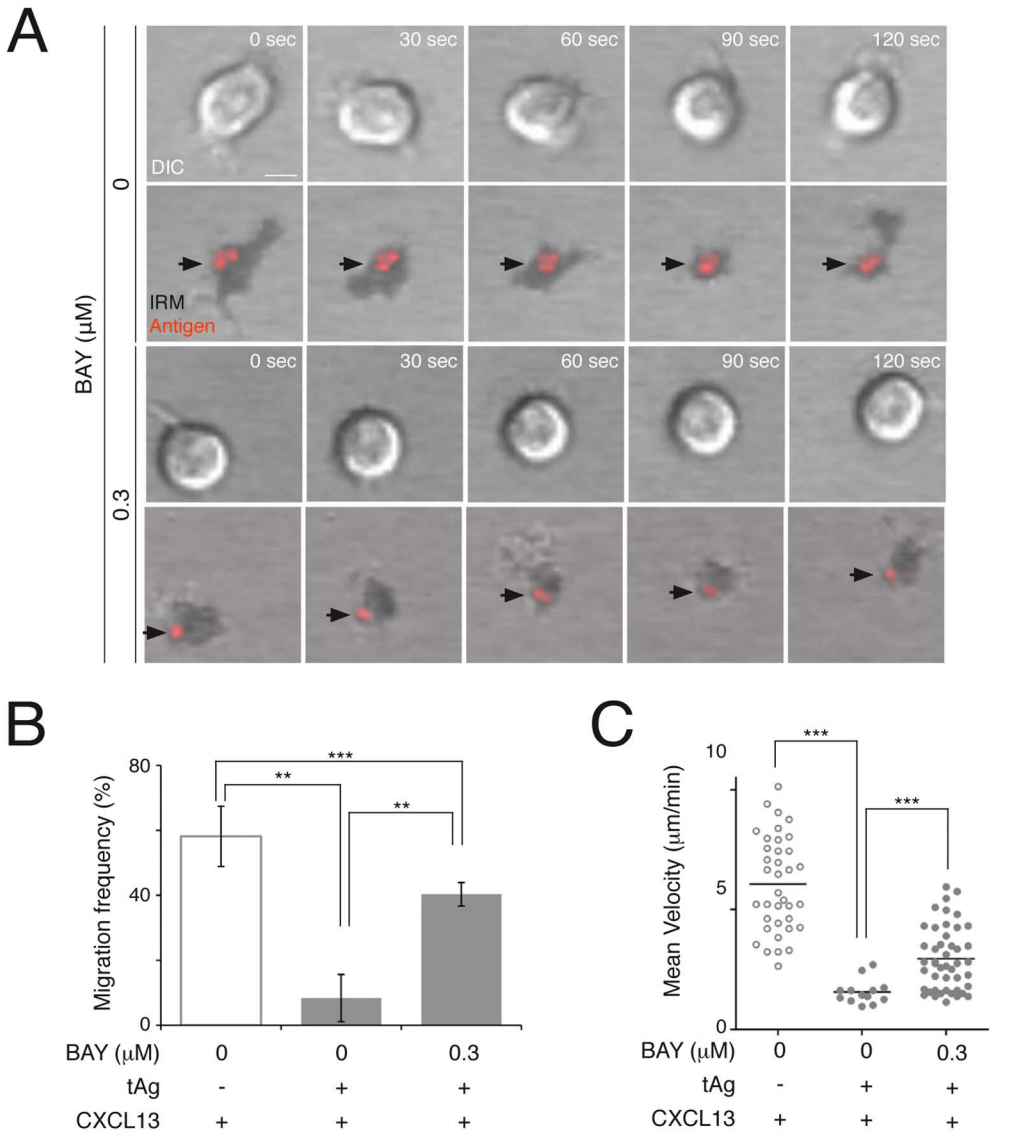

Figure 5. Saez de Guinoa *et al.*

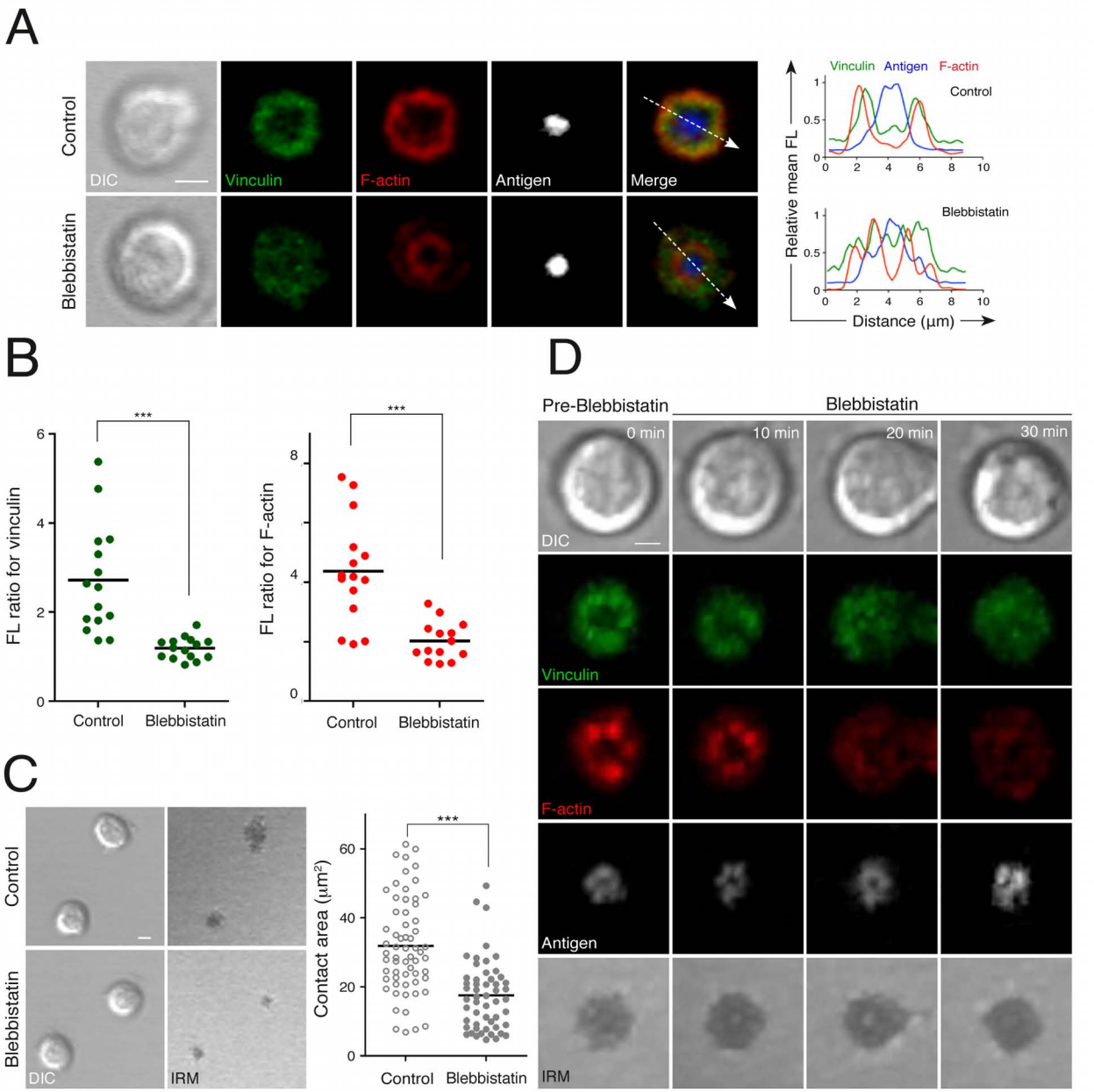

Figure 6. Saez de Guinoa *et al.*

Supplementary Figure Legends

Supplementary Figure S1. IS assembly is necessary to arrest MD4 B cell motility. Primary MD4 B cells were allowed to settle on membranes containing GPI-ICAM-1 and coated with CXCL13, alone or with membrane-tethered (t)Ag or soluble (s)Ag. (A) Frequency of cell adhesion (estimated by IRM) and (B) cell polarization and motility (estimated by DIC microscopy) in the specified stimulation conditions. Data correspond to the merge of two experiments. (C) Syk levels in primary B cells, untreated and treated with indicated stimuli, detected by western blot; see Methods for details. Tubulin was used as loading control. Data from a representative experiment (*n* = 3).

Supplementary Figure S2. Early recruitment of vinculin and F-actin to the B cell synapse. A20 B cells co-transfected with vinculin-GFP and Lifeact-RFP constructs in contact with ICAM-1/CXCL13 membranes and tAg were monitored for synapse formation by time-lapse confocal microscopy. (A) Time-lapse DIC, IRM, and fluorescence vinculin, F-actin and antigen images of a representative B cell are shown. (B) Representative profiles of total vinculin (top) and F-actin (bottom) fluorescence values at the B cell:membrane interface plane over time; dashed line indicates initiation of B cell interaction with the membrane (detected by IRM; considered time zero).

Supplementary Figure S3. Lentiviral infection of primary B cells for vinculin protein knockdown. (A) Endogenous vinculin and GFP reporter expression in B cells with indicated stimuli, detected by western blot 48 h after infection with lentiviral particles encoding non-silencing (scramble) and vinculin-silencing (clone V2LMM_56452) shRNA in the pGIPZ backbone; β-actin was used as loading control. Quantification of vinculin levels for each condition compared to non-silencing

(scramble)(bottom); see Methods for details. (B) B cells as in (A), with CpG stimuli, using lentiviral particles encoding non-silencing (scramble) and vinculin-silencing (1, clone NM_009502.3-3466s1c1; 2, clone NM_009502.3-1331s1c1; 3, clone NM_009502.3-3154s1c1; Mix, all three clones) shRNA in the pLKO.1 backbone; tubulin was used as loading control. Quantification of vinculin levels in each condition compared to non-silencing (scramble)(bottom). Data in (A) and (B) correspond to a representative experiment (n = 5).

Supplementary Figure S4. Analysis of BAY treatment in primary B cells. (A) p-ERK1/2 levels in primary B cells, untreated and treated with indicated BAY doses and stimulated with sAg. Quantification of p-ERK1/2 (bottom) for each condition compared to basal control (no BAY treatment, no sAg stimulation); see Methods for details. Tubulin was used as loading control. Data from a representative experiment. (B) Migration frequency of untreated and BAY-treated primary B cells in contact with ICAM-1/CXCL13 membranes (left). Mean velocity of the motile B cells at the left; each dot represents a single cell (right). Data correspond to the merge of two experiments. (C) Total vinculin (left) and F-actin (right) fluorescence values at the contact plane (in arbitrary units, AU) of untreated and BAY-treated (doses specified) B cells settled on ICAM-1/CXCL13 membranes with tAg; each dot represents a single cell. Data correspond to the merge of two experiments. (D) DIC and fluorescence vinculin, F-actin and antigen images of a representative BAY-treated (0.1 μM) B cell forming a synapse on ICAM-1/CXCL13 membranes with tAg.

Supplementary Movie Legends

Supplementary Movie S1. CXCL13-mediated B cell migration on ICAM-1/CXCL13 membranes. Primary B cells migrating on ICAM-1/CXCL13 membranes. DIC and IRM images over time (15 min; 7 frames/sec).

Supplementary Movie S2. sAg/BCR stimulation does not arrest CXCL13-mediated B cell motility. Behavior of primary B cells settled on ICAM-1/CXCL13 membranes with sAg. DIC and IRM images over time (15 min; 7 frames/sec); arrows indicate B cell motility.

Supplementary Movie S3. tAg/BCR stimulation abolishes B cell motility. Behavior of primary B cells settled on ICAM-1/CXCL13 membranes with tAg, showing an established synapse. DIC and IRM images over time (15 min; 7 frames/sec).

Supplementary Movie S4. Vinculin and F-actin recruitment during B cell synapse formation. A20 B cells co-transfected with vinculin-GFP and Lifeact-RFP constructs, settled on ICAM-1/CXCL13 membranes with fluorescent tAg, were tracked for synapse formation. DIC, IRM and fluorescence images of a representative A20 B cell for vinculin (green), F-actin (red) and antigen (white) over time (18 min; 5 frames/sec).

Supplementary Movie S5. Early PIPKIγ recruitment wave and distribution at the B cell synapse. A20 B cells transfected with PIPKIγ-GFP construct, settled on ICAM-1/CXCL13 membranes with fluorescent tAg were tracked for synapse formation. DIC, IRM and fluorescence images of a representative A20 B cell for PIPKIγ (color-coded) and antigen (red) over time (8 min; 5 frames/sec).

Supplementary Movie S6. PIP_2 production wave and distribution at the B cell synapse. A20 B cells transfected with the PIP_2 probe PLCδ-PH-GFP construct,

settled on ICAM-1/CXCL13 membranes with fluorescent tAg, were tracked for synapse formation. DIC, IRM and fluorescence images of a representative A20 B cell for PIP_2 (color-coded) and antigen (red) over time (9 min; 5 frames/sec).

Supplementary Movie S7. Dynamics of BAY-untreated B cells with synapse established. Behavior of primary B cells settled on ICAM-1/CXCL13 membranes with fluorescent tAg. DIC and overlaid IRM/fluorescent tAg images over time (10 min; 7 frames/sec); arrowhead indicates dynamics of a representative B cell with synapse formed (red antigen cluster, cSMAC) and CXCL13-induced membrane ruffles (detected by IRM and DIC).

Supplementary Movie S8. Dynamics of BAY-treated B cells with tAg. Behavior of BAY-treated primary B cells settled on ICAM-1/CXCL13 membranes with fluorescent tAg. DIC and overlaid IRM/fluorescent tAg images over time (10 min; 7 frames/sec); arrowheads show dynamics of representative B cells migrating in response to CXCL13 and bearing the antigen cluster (red) at the uropod.

Supplementary Movie S9. NM-II inhibition promotes vinculin loss from the synapse. A20 B cells co-transfected with vinculin-GFP and Lifeact-RFP constructs, settled on ICAM-1/CXCL13 membranes with fluorescent tAg, were allowed to form the synapse, treated with blebbistatin and tracked for vinculin and F-actin molecular dynamics. DIC, IRM and fluorescence images of a representative blebbistatin-treated A20 B cell for vinculin (green), F-actin (red) and antigen (white) over time (20 min; 5 frames/sec); time frames for blebbistatin addition and the 10-min time point are shown.

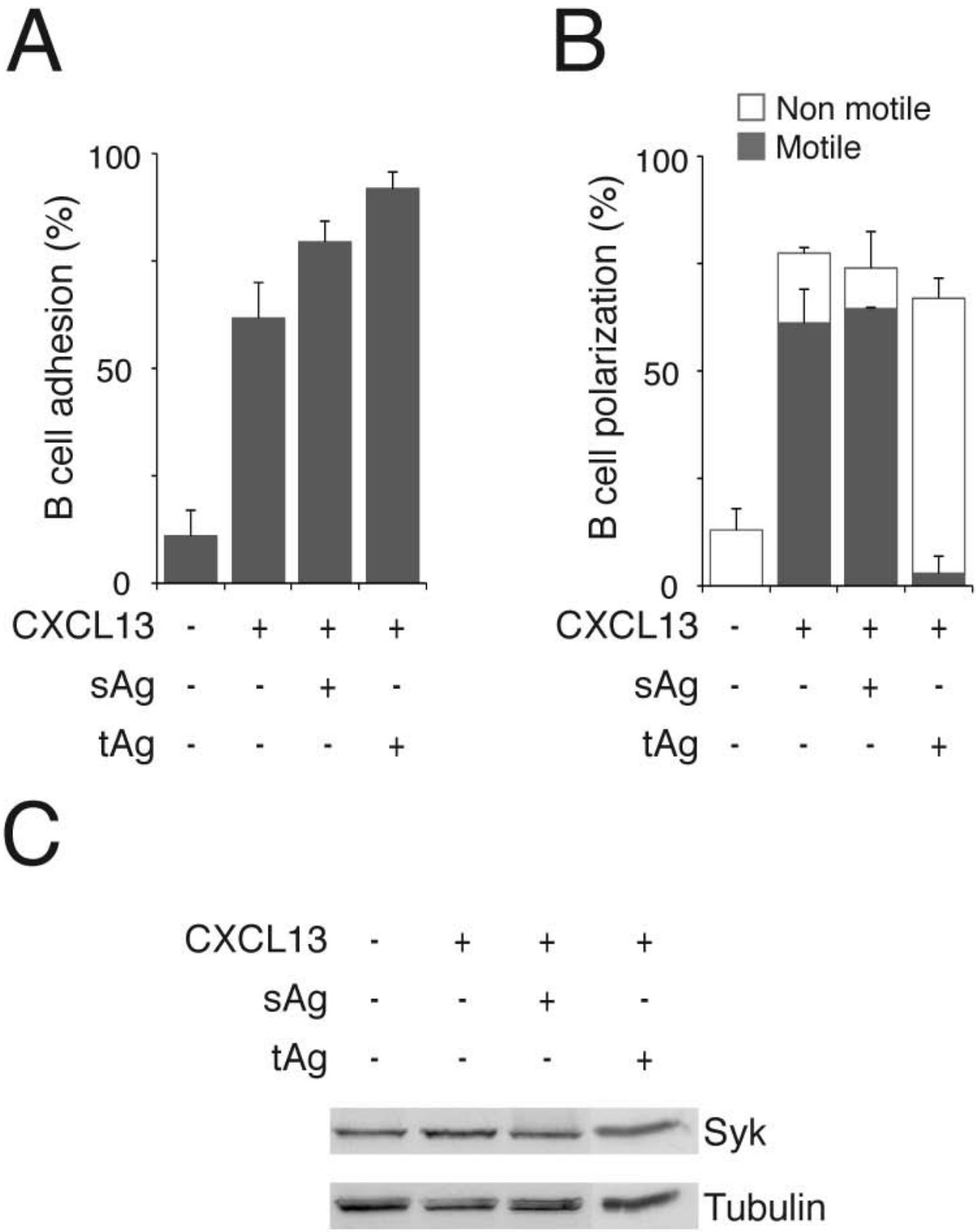

Supplementary Figure S1. Saez de Guinoa *et al.*

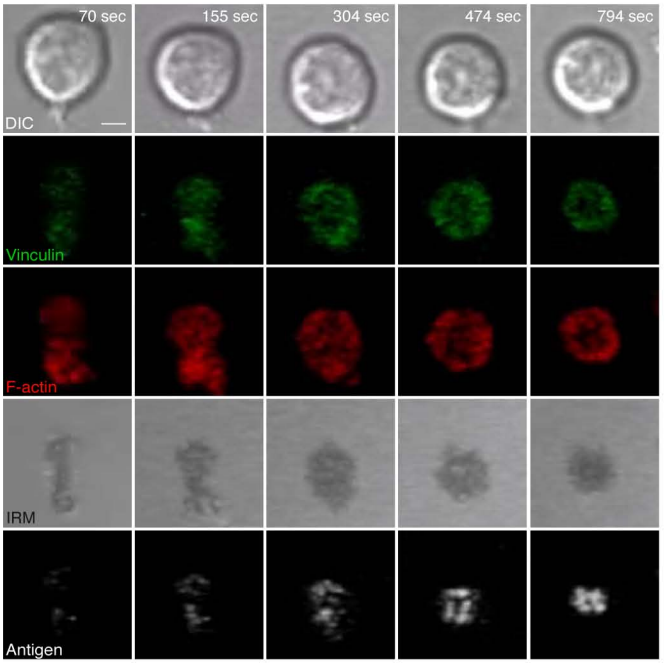

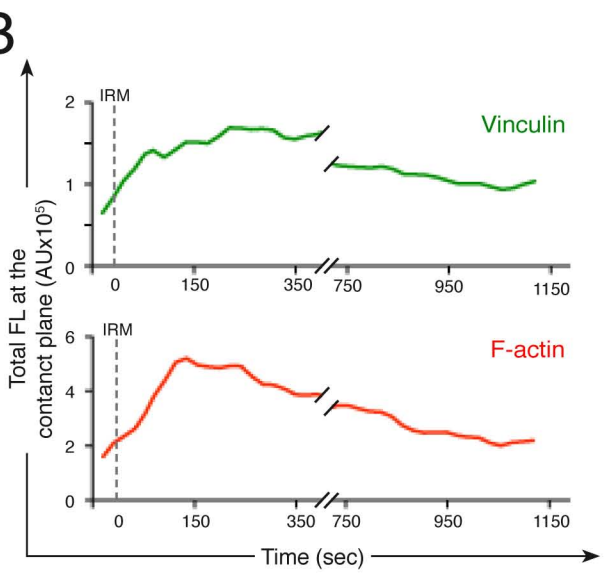

Supplementary Figure S2. Saez de Guinoa *et al.*

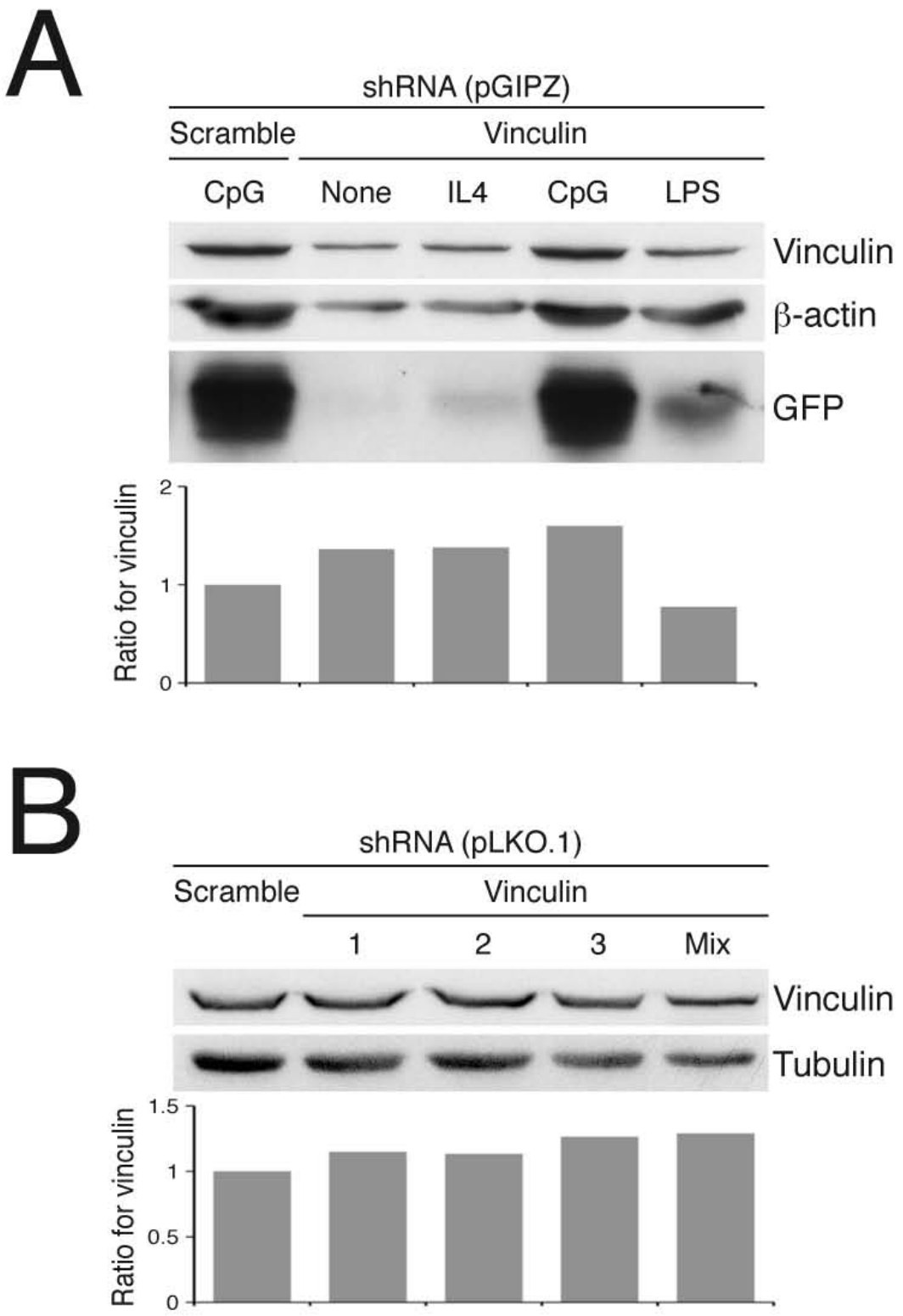

Supplementary Figure S3. Saez de Guinoa *et al.*

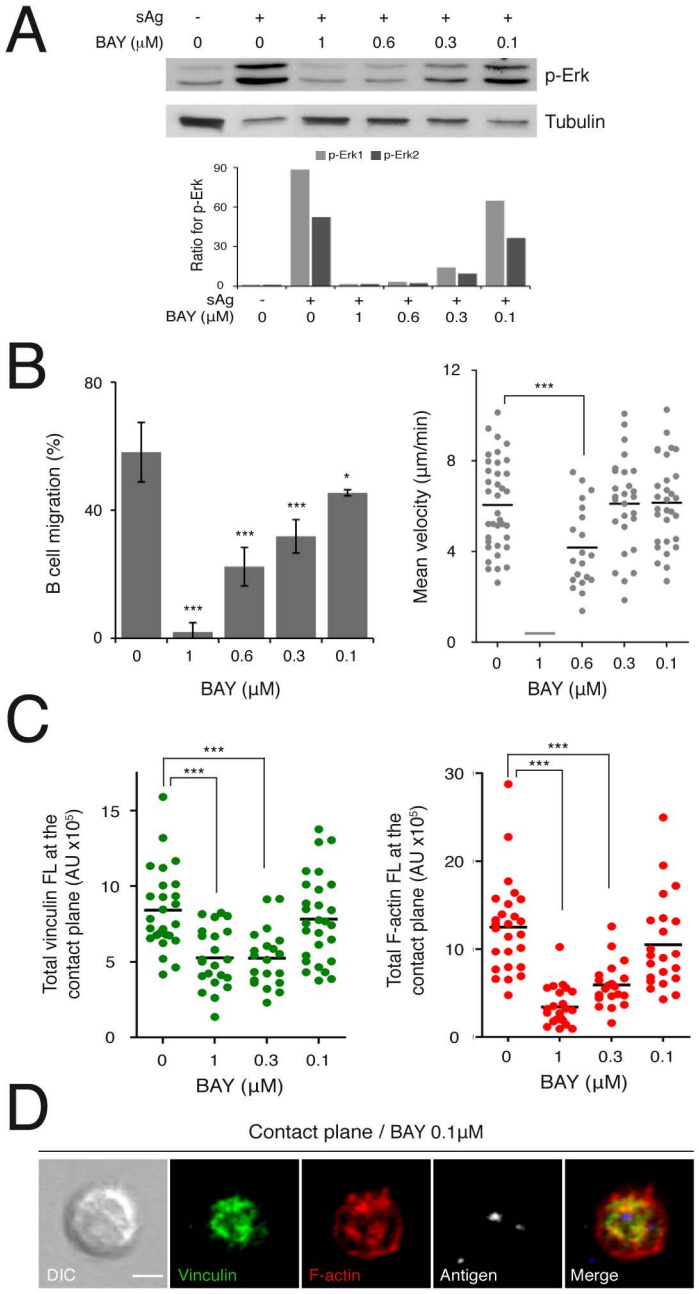

Supplementary Figure S4. Saez de Guinoa *et al.*

ANEXO 2. PUBLICACIONES II

Publicaciones originadas a partir de colaboraciones con otros grupos de investigación

Translocation dynamics of sorting nexin 27 in activated T cells

Esther Rincón[1], Julia Sáez de Guinoa[2], Severine I. Gharbi[1], Carlos O. S. Sorzano[3], Yolanda R. Carrasco[2] and Isabel Mérida[1,*]

[1]Lipid signalling Laboratory, Centro Nacional de Biotecnología (CNB)/CSIC, E-28049 Madrid, Spain
[2]B cell Dynamics Laboratory, Department of Immunology and Oncology, Centro Nacional de Biotecnología (CNB)/CSIC, E-28049 Madrid, Spain
[3]Biocomputing Unit, Centro Nacional de Biotecnología (CNB)/CSIC, E-28049 Madrid, Spain
*Author for correspondence (imerida@cnb.csic.es)

Accepted 22 October 2010
Journal of Cell Science 124, 776-788

doi:10.1242/jcs.072447

Summary

Sorting nexin 27 (SNX27) belongs to the sorting nexin family of proteins, which participate in vesicular and protein trafficking. Similarly to all sorting nexin proteins, SNX27 has a functional PX domain that is important for endosome binding, but it is the only sorting nexin with a PDZ domain. We identified SNX27 as a partner of diacylglycerol kinase ζ (DGKζ), a negative regulator of T cell function that metabolises diacylglycerol to yield phosphatidic acid. SNX27 interacts with the DGKζ PDZ-binding motif in early/recycling endosomes in resting T cells; however, the dynamics and mechanisms underlying SNX27 subcellular localisation during T cell activation are unknown. We demonstrate that in T cells that encounter pulsed antigen-presenting cells, SNX27 in transit on early/recycling endosomes polarise to the immunological synapse. A fraction of SNX27 accumulates at the mature immunological synapse in a process that is dependent on vesicular trafficking, binding of the PX domain to phosphatidylinositol 3-phosphate and the presence of the PDZ region. Downmodulation of expression of either SNX27 or DGKζ results in enhanced basal and antigen-triggered ERK phosphorylation. These results identify SNX27 as a PDZ-containing component of the T cell immunological synapse, and demonstrate a role for this protein in the regulation of the Ras–ERK pathway, suggesting a functional relationship between SNX27 and DGKζ.

Key words: Sorting nexins, PDZ, Membrane trafficking, T cells, Immunological synapse, Diacylglycerol kinase

Introduction

Generation of the immune response requires the formation of a specialised contact area between T cells and antigen-presenting cells (APCs) at the immunological synapse (Friedl et al., 2005). After establishing contact with APCs, T cells acquire a polarised phenotype, characterised by the orientation of the endocytic and secretory machineries, together with the microtubule-organising centre (MTOC), toward the cell–cell contact zone (Billadeau et al., 2007; Cemerski and Shaw, 2006). One function of this repositioning to the immunological synapse is to direct T-cell-secreted cytokines, including interleukin-2 and interferon-γ, to the bound APC (Huse et al., 2006; Huse et al., 2008); in cytotoxic T cells, secretory granules are also delivered by this means (Blott and Griffiths, 2002). Another effect is to guarantee correct formation of the immunological synapse through endocytosis and exocytosis from the recycling pathway (Cemerski and Shaw, 2006), which regulates appropriate expression of specific proteins that accumulate in this zone, such as the T cell antigen receptor (TCR), co-receptors and signalling molecules (Das et al., 2004; Ehrlich et al., 2002; Lee et al., 2003).

The sorting nexins are a large protein family that participate in vesicular and protein trafficking. Over 33 mammalian sorting nexins have been identified and are thought to regulate distinct steps in vesicular trafficking, generally through spatial association with lipid or protein partners (Carlton et al., 2005; Cullen, 2008; Worby and Dixon, 2002). We recently identified SNX27 in early and recycling endosomes in T cells (Rincon et al., 2007). This protein has a specific phox homology (PX) region that is the signature of all sorting nexin family members (Worby and Dixon, 2002). SNX27 is the only member of this group that has a PDZ [post-synaptic density protein (PSD), disc-large and zonula occludens-1] domain, as well as a Ras association (RA) and a FERM (4.1 protein, ezrin, radixin, moesin) domain, which overlap considerably (Cullen, 2008). SNX27 is thought to target its partners to the early endosomal fraction through PDZ-mediated interaction, as reported for SNX27 binding partners such as the 5-hydroxytriptamine type-4 (a) (5-$HT_{4(a)}$) receptor (Joubert et al., 2004), the cytohesin-associated scaffolding protein (CASP) (MacNeil et al., 2007) and G-protein-gated potassium (Kir.3) channels (Lunn et al., 2007).

Our previous experiments identified SNX27 as a protein that interacts with diacylglycerol kinase ζ (DGKζ); this interaction is dependent on the SNX27 PDZ domain (Rincon et al., 2007). DGKζ is a member of the extensive DGK family of enzymes that metabolise diacylglycerol (DAG) into phosphatidic acid. In T cells, DGKζ functions as a negative regulator of Ras activation by limiting the DAG-dependent activation of Ras guanyl nucleotide-releasing protein 1 (RasGRP1), a Ras exchange factor that is selectively expressed in T cells (Olenchock et al., 2006; Zhong et al., 2003; Zhong et al., 2002). DGKζ is transported rapidly to the plasma membrane following stimulation of an ectopically expressed, G-protein-coupled, muscarinic type I receptor (M1R) that is known to mimic TCR responses in T cells (Santos et al., 2002). This translocation is dependent on phosphorylation of the protein-kinase-C-driven MARCKS (myristoylated alanine-rich C kinase substrate) domain and intact zinc fingers. In addition, the presence of a PDZ-binding motif at the DGKζ C-terminus suggests that PDZ interactions participate in targeting of DGKζ to membrane compartments.

Accordingly, DGKζ interacts with several PDZ-containing proteins, including syntrophin (Hogan et al., 2001), TIP15 (Fabre et al., 2000) and PSD-95 (Kim et al., 2009). We showed colocalisation of DGKζ and SXN27 at microsomal compartments, which suggests a role for PDZ interaction at this site (Rincon et al., 2007). The characterisation of a SNX27–DGKζ complex provided a putative role for DGKζ as a negative regulator of recycling endosomal compartments, as DGKζ knockdown cells showed enhanced transferrin receptor recycling (Rincon et al., 2007).

We previously characterised SNX27 in resting T cells (Rincon et al., 2007), but the dynamics and mechanisms underlying SNX27 subcellular localisation during T cell activation have not been described. We analysed SNX27 regulation following T cell activation, and show using superantigen (SEE)-pulsed APCs that SNX27 polarised in endocytic/recycling endosomes to the contact zone of T cells that encountered an APC. A fraction of this protein accumulated at the mature immunological synapse through a mechanism that is dependent on the synergistic function of the PX and PDZ domains. Because SNX27 and DGKζ interact in a PDZ-dependent manner, we studied regulation of these proteins after antigen presentation. Our results reveal that when overexpressed, DGKζ appeared to recruit SNX27 to the plasma membrane, consequently reducing the specific pool of SNX27 at the immunological synapse. However, downmodulation of either SNX27 or DGKζ resulted in enhanced phosphorylation of ERK (extracellular signal regulated kinase), suggesting a functional relationship between these two proteins. In summary, our results identify SNX27 as a component of the T cell immunological synapse, which could regulate protein trafficking through PDZ-mediated interactions, and reveal a role for this protein in the control of Ras activation.

Results

SNX27 polarises to the T cell synapse in response to TCR triggering

To determine whether SNX27 was regulated by triggering of TCRs, we examined the localisation of GFP–SNX27 in an in vitro model of TCR activation using transiently transfected Jurkat T cells plated on anti-CD3 or anti-CD28 antibodies (van der Merwe, 2002), and GFP–RasGRP1 as a control. We observed that, whereas GFP–RasGRP1 translocates to the plasma membrane in these conditions (Sanjuan et al., 2003), GFP–SNX27 was unable to do so, and instead remained in vesicular structures (Fig. 1A, left). Integrins are an important family of molecules with costimulatory properties (Wang et al., 2010); however, we observed no relocalisation of GFP–SNX27 when cells were plated on integrin fibronectin (Fig. 1A, right).

As an alternative form of stimulation, we incubated Jurkat cells with antibody-coated beads. We labelled Jurkat cells with transferrin tetramethylrhodamine (Tf-Rhod) to track the early/recycling endosomal compartment (Maxfield and McGraw, 2004), and compared GFP–SNX27 translocation with that of GFP–RasGRP1. As predicted, RasGRP1 accumulated at the bead-contact area (Carrasco and Merida, 2004), and the Tf-Rhod-positive compartment polarised to the activation site (Das et al., 2004) (Fig. 1B, top). Under these conditions, GFP–SNX27-positive vesicles colocalised with Tf-Rhod and polarised to the T cell synapse as part of this endosomal compartment (Fig. 1B, bottom), but did not colocalise with markers of the immunological synapse, such as RasGRP1.

SNX27 is recruited to the immunological synapse

We next tested a more physiological system of T cell activation with a model of antigen presentation (Friedl and Storim, 2004), using Raji B cells alone or pulsed with the *Staphylococcal* enterotoxin E (SEE) superantigen (Fraser et al., 2000). The formation of cell–cell conjugates was analysed both by immunofluorescence and videomicroscopy. As a control for synapse accumulation, we examined cells transfected with GFP–PKCθ, which relocates to the T cell synapse (Monks et al., 1997) (Fig. 2A, left column). When Jurkat T cells were incubated with SEE-pulsed APCs, SNX27-rich compartments polarised rapidly to the cell contact zone, with a SNX27 fraction

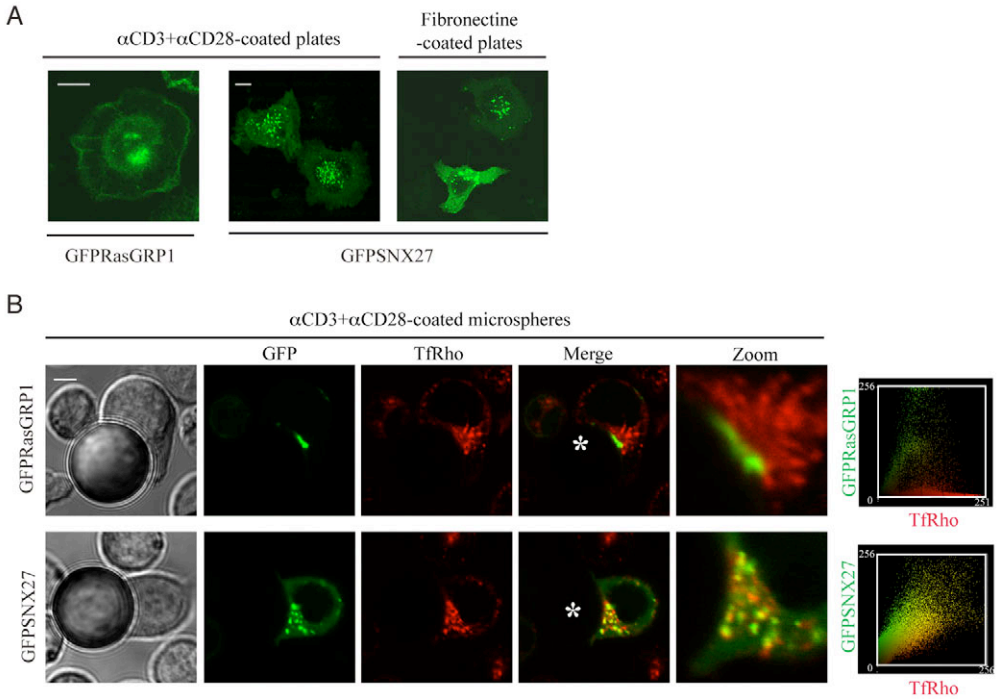

Fig. 1. Stimulation with antibodies against CD3 and CD28 induces SNX27 polarisation under conditions of synapse formation. Transiently transfected Jurkat T were transferred to anti-CD3 and anti-CD28 antibody or fibronectin-coated chambered coverslips (**A**), or treated with Tf-Rhod, suspended in HBSS, and mixed with microspheres coated with anti-CD3 and anti-CD28 antibodies a 1:1 cell:bead ratio and plated on poly-L-lysine-coated chambers (**B**). Slides were mounted on a 37°C plate and images were directly acquired by confocal microscopy. The asterisk marks the bead position. The plots on the right show Pearson's correlation coefficient between SNX27 and Tf-Rhod (=0.831) and RasGRP and Tf-Rhod (=0.185). Scale bars: 3 µm.

accumulating at the immunological synapse, similarly to PKCθ (Fig. 2A, right column). To analyse in more detail the apparent existence of two SNX27 pools at two distinct sites, we determined the percentage of cells showing GFP–SNX27 accumulation at the T-cell–APC contact zone. GFP–SNX27 localised at the immunological synapse in 86% of cells (Fig. 2A; Fig. 2B, top panel) amongst which only 60% also showed polarisation of vesicular compartments (Fig. 2Ae; Fig. 2B, top panel). Quantification of the amount of GFP–SNX27 clustered at the synapse (determined as fluorescence intensity at the immunological synapse/total fluorescence) showed that GFP–SNX27 accumulation at the synapse was higher in cells with polarised vesicular compartment (Fig. 2B, bottom panel). Endogenous SNX27 showed a similar vesicle localisation in the presence of unpulsed or pulsed APCs (Fig. 2C). This could suggest that relocalisation of SNX27-rich vesicular compartments occurs in a dynamic way and that they migrate towards the site of cell–cell contact at the the immunological synapse.

To corroborate this hypothesis, we next used videomicroscopy to examine the dynamic relocalisation of GFP–SNX27 during synapse formation. We observed rapid, clear polarisation of SNX27-positive vesicles to the T-cell–APC contact area, followed shortly thereafter by accumulation of GFP–SNX27 at the contact zone (Fig. 2D and supplementary material Movie 1). This happened from the second minute of SEE-pulsed APC contact, which coincides with the formation of a mature immunological synapse (Friedl and Gunzer, 2001).

These experiments suggest that SNX27 is associated with vesicle compartments; after antigen presentation, the endocytic compartment is polarised and an SNX27-rich pool is further recruited to the plasma membrane at the contact zone.

Recruitment of SNX27 to the immunological synapse is dependent on early or recycling endosome machinery

Protein in vesicle structures can reach the plasma membrane in a highly regulated manner through specific cellular

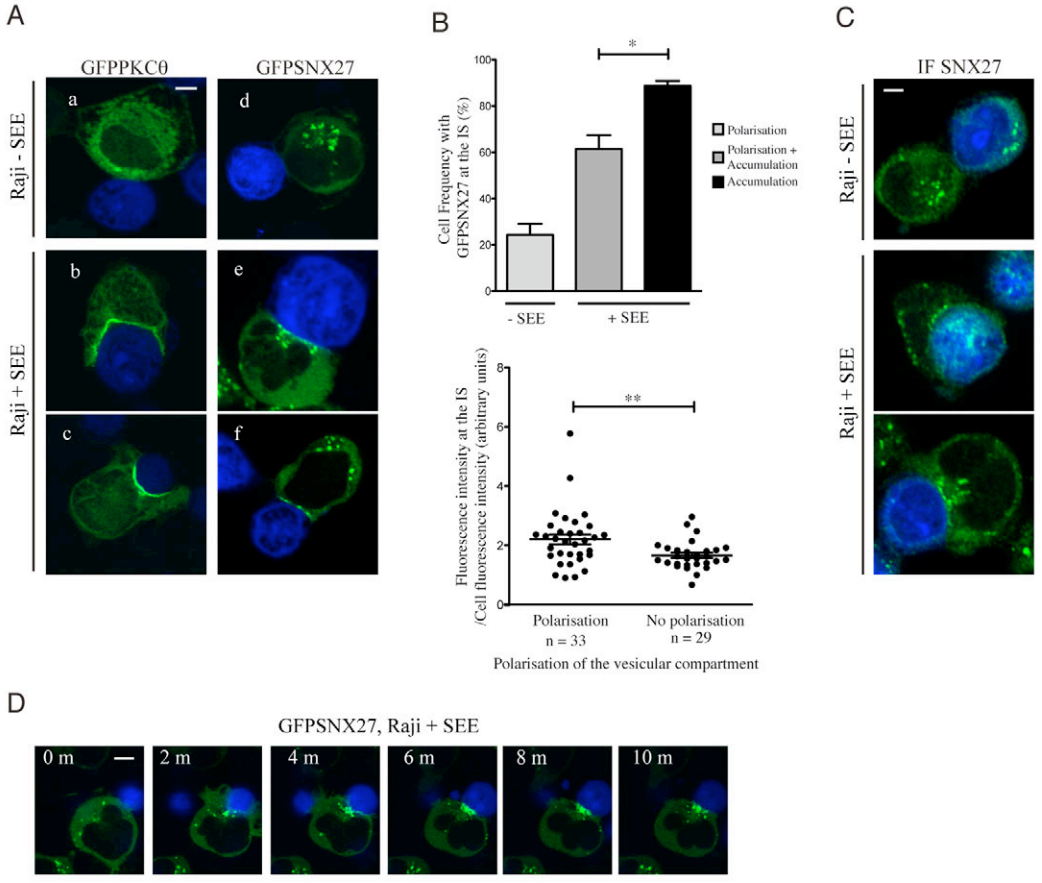

Fig. 2. SNX27 is recruited to the immunological synapse in Jurkat T cells stimulated with SEE-pulsed APCs. (**A**) GFP–PKCθ- or GFP–SNX27-transfected Jurkat T cells were stimulated with APCs at a 1:1 Jurkat:APC ratio. Cell–cell conjugates were fixed and images acquired by confocal microscopy. (**B**) Top graph shows quantification of cells with GFP–SNX27 polarisation and/or accumulation at the immunological synapse. In the presence of SEE-pulsed APCs, 86% of the cell population show GFP–SNX27 accumulation at the immunological synapse. Of this percentage, 60% of cells also showed polarisation of vesicular compartments (see a representative image in Ae), whereas in the rest there was accumulation at the immunological synapse in the absence of vesicular compartment polarisation (see representative image in Af). Data are presented as the means ± s.e.m. of cell frequency with GFP–SNX27 relocated to the immunological synapse in three independent experiments (n>100 in each experiment) (*P<0.05; Student's t-test). Bottom graph shows quantitative image analysis of GFP–SNX27 accumulated at the immunological synapse compared with total GFP–SNX27. Each dot represents a T-cell–APC conjugate. The bars show the means ± s.e.m. (**P<0.01; Kolmogorov-Smirnov test). (**C**) Jurkat T cells were stimulated with APCs as in A, and endogenous SNX27 was detected with anti-SNX27 and secondary antibody coupled to Alexa Fluor 488. (**D**) Transiently transfected Jurkat T cells were allowed to attach to poly-L-lysine-coated chamber slides. Slides were mounted on heated microscope stage and images were acquired by time-lapse microscopy and SEE-pulsed APCs were added to monitor the formation of conjugates. The figure shows representative images from time 0 to 10 minutes after stimulation. Supplementary material Movie 1 shows all stimulation period images. Scale bars: 3μm.

subcompartments (Blott and Griffiths, 2002; Maxfield and McGraw, 2004). To determine the mechanism of translocation of SNX27 to the immunological synapse, we next stained GFP–SNX27-transfected cells with several markers of vesicular trafficking. We used Tf-Rhod as a marker of the endocytic recycling compartment (Maxfield and McGraw, 2004), SNX2 as an early endosomal marker (Gullapalli et al., 2004) and Lamp1 as a marker of the lysosomal and secretory compartments (Blott and Griffiths, 2002; Chen et al., 1988). A fraction of GFP–SNX27 colocalised with Tf-Rhod- and SNX2-positive vesicles that polarise to the T cell synapse in the presence of SEE-pulsed APCs (Fig. 3A, top and middle rows), further corroborating the presence of SNX27 in recycling/early endosomal compartments, whereas there was no colocalisation between SNX27 and lysosomal/secretory compartments (Fig. 3A, bottom). However, although all the vesicular compartment markers tested polarised towards the cell contact zone, none of them showed direct accumulation at the immunological synapse with GFP–SNX27 (Fig. 3A, arrows).

To further assess whether immunological synapse localisation of GFP–SNX27 required vesicular trafficking, Jurkat cells were pretreated with primaquine, which inhibits secretion and recycling processes through irreversible inactivation of the transport vesicles (donors), but not of final membranes (acceptors) (Hiebsch et al., 1991; Somasundaram et al., 1995; van Weert et al., 2000). When primaquine-treated Jurkat T cells were incubated with SEE-pulsed APCs, we observed a marked reduction of the fluorescence intensity of GFP–SNX27 at the immunological synapse that accumulated in recycling endosomes, and colocalised with the transferrin receptor (TfR) (Fig. 3B). These results, which are similar to those describing primaquine-dependent inhibition of the recycling of TfR (van Weert et al., 2000) and TCR (Das et al., 2004), suggest that trafficking through the endosomal compartment is necessary for SNX27 to reach the T-cell–APC contact zone.

GFP–SNX27 accumulates at central and peripheral SMACs

The experimental systems used, either antibody-coated microspheres or SEE-pulsed B cells, are valid models in which to analyse long-term, stable T cell synapses (Friedl et al., 2005). The mature immunological synapse that originates when T cells contact B cells has been studied extensively, allowing identification and characterisation of various supramolecular activation clusters (SMACs) in the T cell contact area (Fooksman et al., 2010). Early fixed-cell imaging studies revealed the formation of a bull's eye

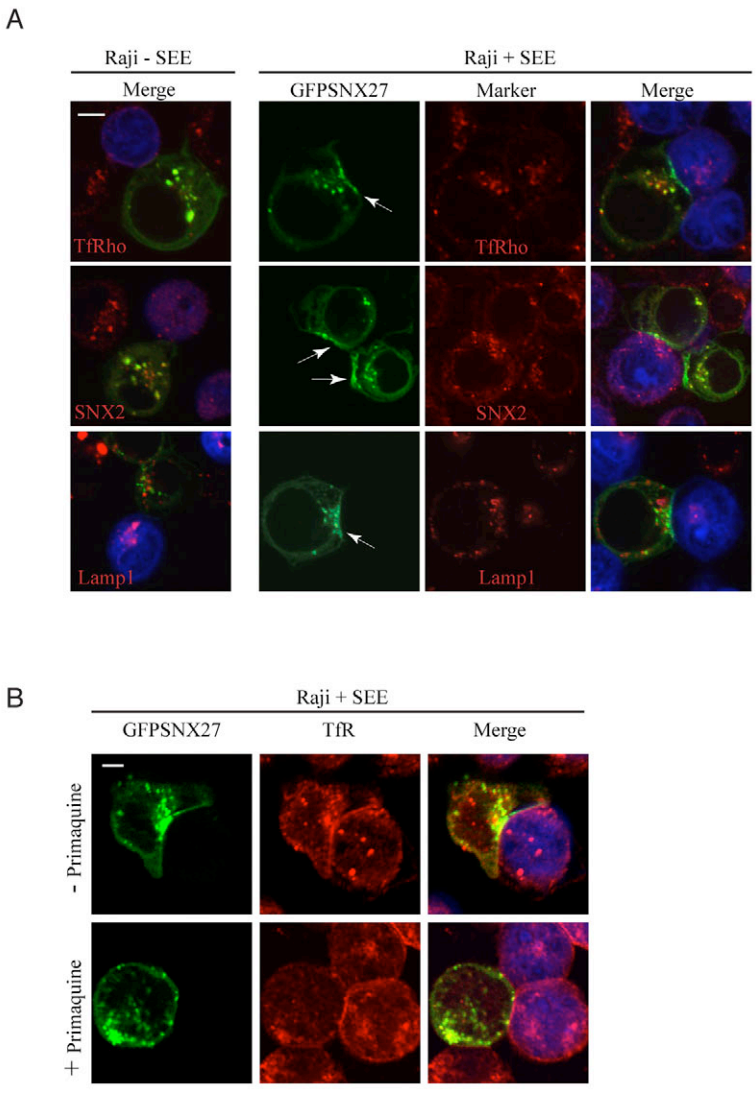

Fig. 3. SNX27 recruitment to the immunological synapse is dependent on early/recycling endosome binding. (**A**) Transiently transfected Jurkat T cells were treated with Tf-Rhod (top), and stimulated with APCs pulsed or not with SEE, as in Fig. 2A. Immunostaining was carried out with anti-SNX2 (middle) or anti-Lamp1 (bottom), followed by Cy3 anti-mouse IgG antibodies and imaged by confocal microscopy. GFP–SNX27 accumulates at the immunological synapse (see arrows). (**B**) GFP–SNX27-transfected cells were incubated with medium alone or with primaquine, then mixed with SEE-pulsed Raji B cells, and protein distribution was analysed by immunostaining with anti-TfR followed by Cy3-anti-mouse IgG antibodies and imaged by confocal microscopy. Scale bars: 3 µm.

pattern with a central cluster of TCR-pMHC (peptide-loaded major histocompatibility complex) defined as the central SMAC (cSMAC), surrounded by a ring that contributes to firm adhesion through accumulation of molecules including LFA-1 (lymphocyte function-associated antigen 1) and talin, named the peripheral SMAC (pSMAC). The region outside the pSMAC, which is rich in CD45, was later named the distal SMAC (dSMAC) (Davis et al., 2003; Fooksman et al., 2010; Monks et al., 1998). To determine whether SNX27 is recruited to a specific SMAC at the immunological synapse, we analysed colocalisation of GFP–SNX27 with CD3 or LFA-1, which are well-characterised markers of cSMAC and pSMAC, respectively. We also detected phosphorylated tyrosine, which is increased at the cell–cell contact zone as a result of tyrosine phosphorylation of scaffolding and signalling molecules. GFP–SNX27 translocated to the contact zone and showed clear colocalisation with LFA-1 (Fig. 4A, top). However, en face (*y*-*z*) reconstruction of the SMAC structures showed a quite homogeneous distribution of GFP–SNX27 areas, which corresponded to both the cSMAC and pSMAC (Fig. 4A, bottom and supplementary material Movie 2).

Planar lipid bilayers supported on glass coverslips have been used to image the immunological synapse at high resolution (Dustin et al., 2007). Dynamic studies using this system have shown that activating TCR clusters form first in the dSMAC and then move to the cSMAC region within a few minutes. The sustained TCR signalling that originates at the immunological synapse appears to be the result of a continuous process of cluster formation and transport from the dSMAC to the cSMAC (Fooksman et al., 2010). More recently, a region in the transition between central and peripheral SMAC has been described, which serves as a platform for costimulatory signalling proteins, such as CD28 (Yokosuka et al., 2008). To assess whether the distribution of GFP–SNX27 observed in fixed cells was the result of a dynamic transport between the different SMACs, we determined the localisation of GFP–SNX27 vesicles in the mature immunological synapse generated when Jurkat cells interacted with supported planar lipid bilayers containing GPI-linked ICAM-1 (intercellular adhesion molecule 1) and tethered anti-CD3 antibodies as surrogate antigen (see the Materials and Methods). We used the accumulated anti-CD3 fluorescent signal as a marker for the cSMAC at the mature immunological synapse; the pSMAC area was estimated as the cell–lipid-bilayer contact region (followed by interference reflection microscopy, IRM) surrounding the cSMAC (CD3-positive region). This analysis showed that GFP–SNX27 vesicles reached both the cSMAC and the pSMAC (Fig. 4B and supplementary material Movie 3). It is noteworthy that the merge between GFP–SNX27, CD3 and IRM images, showed that the localisation of GFPSN27 at the pSMAC appears very close to the boundary with the CD3-

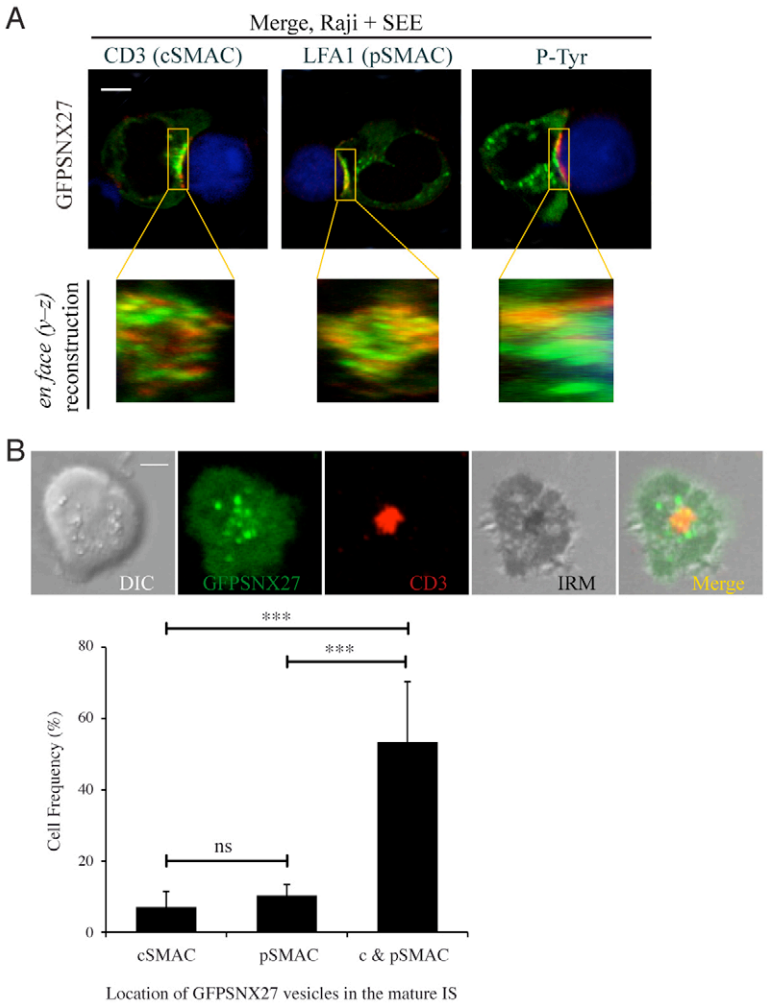

Fig. 4. Distribution of GFP–SNX27 at the Jurkat T cell mature immunological synapse. (**A**) GFP–SNX27-transfected Jurkat T cells were stimulated with APCs as in Fig. 2A. Cell–cell conjugates were fixed, processed for immunofluorescence with anti-CD3 (first column), anti-LFA1 (second column) or anti-phosphorylated-Tyrosine (third column), followed by Cy3-anti-mouse IgG antibodies and imaged by confocal microscopy. Three-dimensional reconstructions of the SMAC structures are shown in the magnified panels and in supplementary material Movie 2. (**B**) DIC, fluorescent anti-CD3 and IRM images of a representative GFP–SNX27 transfected Jurkat T cell forming the immunological synapse after anti-CD3 recognition on an ICAM-1 containing lipid bilayer. Graph shows the frequency of Jurkat T cells that exhibited immunological synapse accumulation of GFP–SNX27 vesicles at the indicated locations. Data are presented as the means ± s.e.m. of four experiments (ns, not significant; ***P<0.001; Student's t-test). Scale bars: 3 µm.

positive region or cSMAC (Fig. 4B, top), suggesting the localisation of a SNX27 pool in the costimulatory platform of the mature immunological synapse (Yokosuka et al., 2008).

GFP–SNX27 recruitment to the T cell synapse requires both PX and PDZ domains

To gain further insight into the nature of the signals regulating SNX27, we next examined the input of the different structural domains of SNX27 on its localisation at the immunological synapse. Visual analysis suggested that deletion of the RA-FERM domains had no apparent effect on vesicular localisation of SNX27 or its recruitment to the immunological synapse (Fig. 5A, right, second row). To analyse the contribution of the PX domain, we generated point mutations in the R196,Y197 sequence. This sequence has been shown to interact with phosphatidylinositol 3-phosphate (PI3P), the most abundant phosphatidylinositol derivative in endosomal membranes (Gillooly et al., 2000), with other PX domain-containing proteins such as $p40^{phox}$ (R58,Y59) (Bravo et al., 2001), PLD1 (K119, which is similar to R196) (Stahelin et al., 2004) and SNX3 (R70,Y71) (Xu, 2001) (Fig. 5A, bottom left shows an alignment of PX sequences). As predicted, the PX domain mutant lost vesicular localisation almost completely, although interestingly, a small pool was still able to localise at the cell contact zone (Fig. 5A, right, third row). Finally, we examined a SNX27 construct bearing a deletion of the PDZ domain. As previously reported, this deletion strongly impaired SNX27 targeting to the endocytic compartment (Rincon et al., 2007). When T cells were challenged with SEE-pulsed APCs, the vesicles positive for SNX27 lacking the PDZ motif (GFP–SNX27ΔPDZ) polarised to the cell contact area; however, they did not accumulate at the immunological synapse (Fig. 5A, right, fourth row). Quantitative analysis of accumulation of the distinct mutants (Fig. 5B, black dots) and exclusion (grey dots) at the immunological synapse confirmed that, albeit much lower than in the full-length protein, GFP–SNX27 mutants defective in PI3P binding retained certain ability to localise to the immunological synapse; deletion of the RA domain did not result in significant differences with respect to the wild-type GFP–SNX27 and GFP–SNX27ΔPDZ was always excluded from the immunological synapse.

We next assessed the capacity of mutants bearing a truncation of the PDZ region or with impaired PIP3 binding to reach the immunological synapse in T cells contacting antigen-loaded lipid bilayers. As for fixed cells, the number of GFP–SNX27 vesicles reaching the synapse was strongly reduced if the PDZ domain was truncated (Fig. 5C and supplementary material Fig. S1). As expected, the GFP–SNX27 mutant defective in PIP3 binding did not show vesicle localisation but there was significant frequency of fluorescence accumulation when it was in contact with lipid bilayers (Fig. 5C and supplementary material Fig. S1).

These experiments suggest that deletion of the PDZ region has an important effect on GFP–SNX27 recruitment to the immunological synapse. To test whether PDZ truncation affected PX domain accessibility and PI3P binding, we used a lipid-binding assay. Recombinant proteins expressing GST-fused wild-type SNX27 (GST–SNX27), the PX domain point mutant [GST–SNX27(R196A,Y197A)], or the PDZ region deleted mutant (GST–SNX27ΔPDZ) were generated, purified and overlaid on lipid strips. Analysis with anti-GST antibodies showed proteins of the predicted molecular weight (not shown). GST–SNX27 showed specific PI3P binding (Fig. 5D). Point mutation of the PX domain resulted in complete loss of PI3P binding, whereas PDZ domain truncation did not affect binding to PI3P (Fig. 5D).

Taken together, these results show that the PDZ region does not participate in PI3P binding, and strongly suggest that SNX27 localisation to the immunological synapse requires synergy between the PX domain, which binds to PI3P, and the PDZ domain, which would bind to an as yet uncharacterised protein(s).

The DGKζ C-terminal region blocks recruitment of SNX27to the immunological synapse

The previous experiments revealed that PDZ-based interaction was essential for SNX27 recruitment to the immunological synapse. Since our proteomic screen revealed that SNX27 is a direct binding partner of DGKζ (Rincon et al., 2007), we next wanted to study the contribution of DGKζ to the recruitment of SNX27 to the immunological synapse. We examined localisation of SNX27 in cells overexpressing the C-terminal region of DGKζ (HA–DGKζCT), which encompasses the ETAV sequence required for the DGKζ–SNX27 interaction and acts as a dominant negative (Rincon et al., 2007). As reported, cells expressing the HA–DGKζCT construct showed fewer GFP–SNX27-positive vesicles, confirming the relevance of the PDZ domain in this localisation (Rincon et al., 2007 and Fig. 6). Moreover, when cells positive for the HA–DGKζCT were in contact with SEE-pulsed APCs, no recruitment of GFP–SNX27 to the immunological synapse was observed. These experiments suggest that SNX27 requires PDZ-mediated interactions with endogenous proteins to localise to endomembrane compartments, which is necessary to drive SNX27 to the immunological synapse.

To determine the role of endogenous DGKζ on SNX27 polarisation and recruitment, we monitored the translocation of GFP–SNX27 in a gene-silencing experiment by short interfering RNA (siRNA). Jurkat T cells transfected with control siRNA and siRNA to knock down DGKζ were compared by immunofluorescence. Although we achieved good silencing efficiency of DGKζ, no significant difference in GFP–SNX27 recruitment was observed (supplementary material Fig. S2).

Role of DGKζ in the regulation of SNX27 translocation in response to antigen presentation

The previous results suggest that DGKζ is not the protein responsible for SNX27 accumulation at the immunological synapse. Moreover, overexpression of the DGKζ sequence responsible for this interaction impairs accumulation of GFP–SNX27 at the contact zone. We coexpressed GFP–SNX27 with DGKζ tagged with the red fluorescent protein (RFP) to check their colocalisation. In basal conditions, DGKζ and SNX27 shared strong overlap in subcellular localisation, which was lost when we coexpressed the mutant of DGKζ deficient in the PDZ binding domain, thus suggesting that this colocalisation requires PDZ-mediated interaction (Fig. 7A). This observation correlated with our previous report showing that both proteins colocalise in internal membranes (Rincon et al., 2007).

To further study whether SNX27 and DGKζ interaction was maintained during T-cell–APC contact, we then followed their redistribution during immunological synapse formation. As expected, GFP–SNX27 translocated to the immunological synapse when cotransfected with empty RFP vector (Fig. 7B, top). GFP–SNX27 recruitment to the immunological synapse was less pronounced when cotransfected with RFP–DGKζ, but instead, we observed a clear relocalisation of SNX27 to the whole plasma

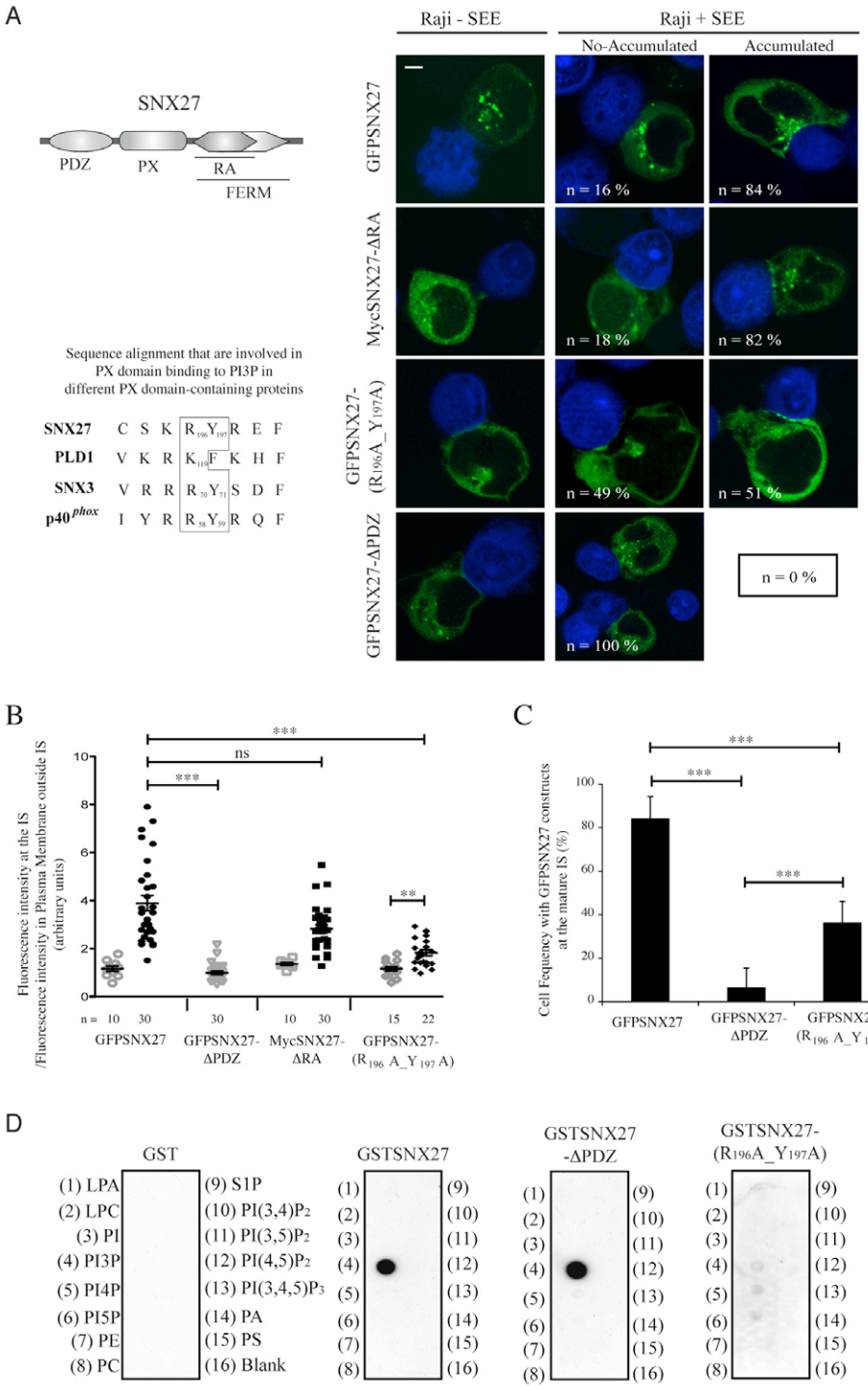

Fig. 5. GFP–SNX27 recruitment to the immunological synapse requires PI3P binding through the PX domain and presence of the PDZ domain. (**A**) Top left drawing shows the SNX27 domains. Micrographs on the right show Jurkat T cells transfected with GFP–SNX27, MycSNX27ΔRA, a construct with RA and FERM domains deleted, GFP–SNX27($R_{196}A,Y_{197}A$), a construct with point mutations to alanine in the residues R196,Y197 and GFP–SNX27ΔPDZ, a mutant in which the PDZ domain is deleted. Cells were stimulated with APCs pulsed or not with SEE, as in Fig. 2A, fixed and imaged by confocal microscopy. MycSNX27ΔRA, was detected with anti-Myc, followed by Cy3-anti-mouse IgG antibody. The frequency of T cells with GFP–SNX27 accumulation at the immunological synapse is shown in each image (n>100 cells). Scale bar: 3 µm. Sequence alignment with other PX-domain-containing proteins is shown on the left. (**B**) Quantitative image analysis of GFP–SNX27 accumulated at the immunological synapse compared with GFP–SNX27 located in plasma membrane regions outside the immunological synapse. Each dot represents a T-cell–APC conjugate: empty grey dots represent cells with no accumulation of GFP–SNX27 constructs at the immunological synapse (representative images are shown in A, middle column); solid black dots represent cells with GFP–SNX27 construct accumulation (representative images shown in A, right column). The bars show the means ± s.e.m. (ns, not significant; **P<0.01; ***P<0.001; Kolmogorov–Smirnov test). (**C**) Frequency of transfected Jurkat T cells that accumulate GFP–SNX27 constructs at the immunological synapse after anti-CD3 recognition on an ICAM-1-containing lipid bilayer. The data show the mean of two experiments ± s.e.m. (***P<0.001; Student's t-test). (**D**) Full-length SNX27, SNX27ΔPDZ and SNX27(R196A,Y197A) fused to GST tag were incubated with PIP strips and detected with anti-GST antibody. LPA, lysophosphatidic acid; LPC, lysophosphatidylcholine; PI, phosphatidylinositol; PI3P, PI4P, PI5P, phosphatidylinositol phosphorylated in positions 3, 4, 5; PE, phosphatidylethanolamine; PC, phosphatidylcholine; S1P, sphingosine-1-phosphate; PA, phosphatidic acid; PS, phosphatidylserine.

membrane, mimicking the behaviour of RFP–DGKζ. Line-scan analysis confirmed that GFP–SNX27 colocalised with RFP–DGKζ to the entire plasma membrane, suggesting that DGKζ overexpression recruited SNX27 to this localisation (Fig. 7B, middle). Interestingly, coexpression with RFP–DGKζΔPDZbm did not affect the subcellular localisation of GFP–SNX27, which remained in vesicles and reached the immunological synapse, similarly to the control condition (Fig. 7B, top), although this PDZ-deficient mutant could translocate to the membrane upon T cell activation (Fig. 7B, bottom). This correlates with our observation that HA-DGKζCT blocked recruitment of SNX27 to the immunological synapse, and suggests that DGKζ can compete for SNX27 interaction with other proteins at the immunological synapse.

SNX27 silencing results in enhanced TCR-mediated Ras–ERK activation

The previous experiments demonstrate that, whereas both proteins colocalise under resting conditions, DGKζ relocates to the plasma membrane following formation of the immunological synapse, and

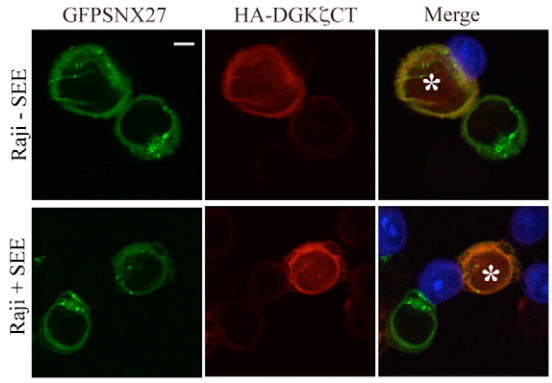

Fig. 6. The DGKζ CT region blocks SNX27 accumulation at the immunological synapse. Jurkat T cells were cotransfected with GFP–SNX27 and a plasmid encoding the DGKζ CT region fused to a HA tag. At 24 hours after transfection, cells were stimulated with APCs as in Fig. 2A, fixed, stained with anti-HA followed by Cy3-anti-mouse IgG antibodies and imaged by confocal microscopy. SNX27 localisation in cells expressing both proteins (asterisk) compared with that in cells not expressing the HA-DGKζ construct showed clear inhibition of GFP–SNX27 accumulation at the immunological synapse in the former. Scale bar: 3 µm.

SNX27 accumulates at the cell–cell contact area. This correlates with the fact that GFP–SNX27 accumulation at the immunological synapse, although it requires intact PX and PDZ regions, is not affected by downmodulation of DGKζ. This somewhat puzzling scenario suggests that, upon T-cell–APC contact, the interaction between the two proteins is disrupted. Localisation studies did not allow us to draw any conclusion regarding a functional relationship between these two proteins.

Studies in Jurkat cells have shown that overexpression of DGKζ limits the threshold of Ras activation by metabolising the DAG that binds to and activates RasGRP1 (Roose et al., 2005). We determined the role of endogenous SNX27 on TCR-mediated activation of Ras by measuring ERK phosphorylation in SNX27-silenced cells using short interfering RNA (siRNA). Jurkat T cells transfected with control siRNA showed marked ERK phosphorylation 15 minutes after TCR triggering (Fig. 8). Silencing of DGKζ resulted in enhanced ERK phosphorylation, confirming the negative function of this lipid kinase in the regulation of this pathway. Longer exposures showed enhanced phosphorylation, even in the absence of TCR triggering, confirming a role for DAG metabolism in the regulation of RasGRP1 (Roose et al., 2007). Downmodulation of SNX27 levels showed a similar increase in ERK phosphorylation both before and after TCR stimulation. (Fig. 8B). These results indicate a functional relationship between the two proteins and suggest that SNX27 is required for adequate downregulation of the Ras–ERK pathway by DGKζ.

Discussion

The sorting nexins are a large family of proteins defined by the presence of a PX domain. Some of these proteins can link endosomal sorting with specific signalling events. SNX27 is suggested to be one such protein, because it contains recognised signalling domains such as the RA and the PDZ (Cullen, 2008). Here we show that SNX27 is transported in early or recycling endosomes that polarise to the T cell synapse, a large signalling molecule platform (Cemerski and Shaw, 2006). In addition, we found that a fraction of SNX27 is recruited to the immunological synapse by a mechanism that depends on vesicle trafficking, and characterised the SNX27 PDZ region as essential in the control of this accumulation.

Our studies show that SNX27-positive endosomes polarise to the immunological synapse in response to TCR activation, similarly to SNX27 polarisation in migrating and tumour-engaged natural killer cells (MacNeil and Pohajdak, 2007). In addition, an SNX27 pool is recruited to the cell–cell contact area within ~2–3 minutes after an encounter with pulsed APCs. These results are reminiscent of studies showing that components of the TCR signalling machinery (including LAT, p56lck and CD3, which similarly to SNX27 codistribute with transferrin) are recruited to the immunological synapse with kinetics similar to that observed here (Anton et al., 2008; Bonello et al., 2004; Das et al., 2004; Ehrlich et al., 2002). The subcellular distribution of GFP–SNX27 resembled that of endogenous SNX27, which excludes artefacts caused by the GFP tag. The results obtained using the planar lipid bilayer approach, show the localisation of GFP–SNX27 at the cSMAC, but also at the pSMAC, where GFP–SNX27-positive vesicles are distributed very close to the transition region with the cSMAC, an area recently described as the costimulation platform for T cell activation (Yokosuka et al., 2008). These data confirm the concentration of SNX27 at the immunological synapse and suggest its participation as a component of some signalling platforms that remain to be fully characterised.

Analysis of several SNX27 mutants confirmed that the SNX27 PX domain is necessary for vesicle localisation, collaborates in immunological synapse accumulation, and binds PI3P lipids, confirming its role in vesicle binding (Gillooly et al., 2000). The PX domain is the signature of the sorting nexin family, but other family members as we show for SNX2, do not accumulate at this site. This is, to our knowledge, the first report of immunological synapse recruitment for a sorting nexin, although studies in T cells by Badour and co-workers show that SNX9 interacts simultaneously with WASp (Wiskott–Aldrich syndrome protein) through its Src homology 3 domain and with PI3-kinase through its PX domain. The formation of this complex regulates internalisation of CD28 and activation of NFAT (nuclear factor of activated T cells) (Badour et al., 2007). SNX27 is the only family member with a PDZ domain (Cullen, 2008) and our analyses show that this region is essential for both its endosomal distribution and its recruitment to the immunological synapse. This is not due to phosphatidylinositol binding, which we have shown is dependent exclusively on the PX region. Together, our data suggest that SNX27 participates in PDZ-mediated protein sorting to the immunological synapse. We searched extensively for SNX27-interacting proteins at the immunological synapse, but have not detected a suitable candidate. Identification of additional SNX27 partners will help to elucidate additional functions of this protein during T cell stimulation.

The PDZ domain is a well-characterised protein–protein interaction module (Sheng and Sala, 2001); in fact, several SNX27 partners containing PDZ binding motifs have been characterised in lymphoid and non-lymphoid cells. Elegant studies in neurons have shown that SNX27 interacts with Kir3.3 and Kir3.2c potassium channels, which promotes their trafficking to endosomes and leads to smaller Kir3 potassium currents (Lunn et al., 2007). SNX27 also targets the $5\text{-HT}_{4(a)}$ receptor to endosomal compartments (Joubert et al., 2004). Studies in the natural killer T cell line YT showed that SNX27 interacts with CASP, a cytokine-inducible protein that associates with members of the GEF

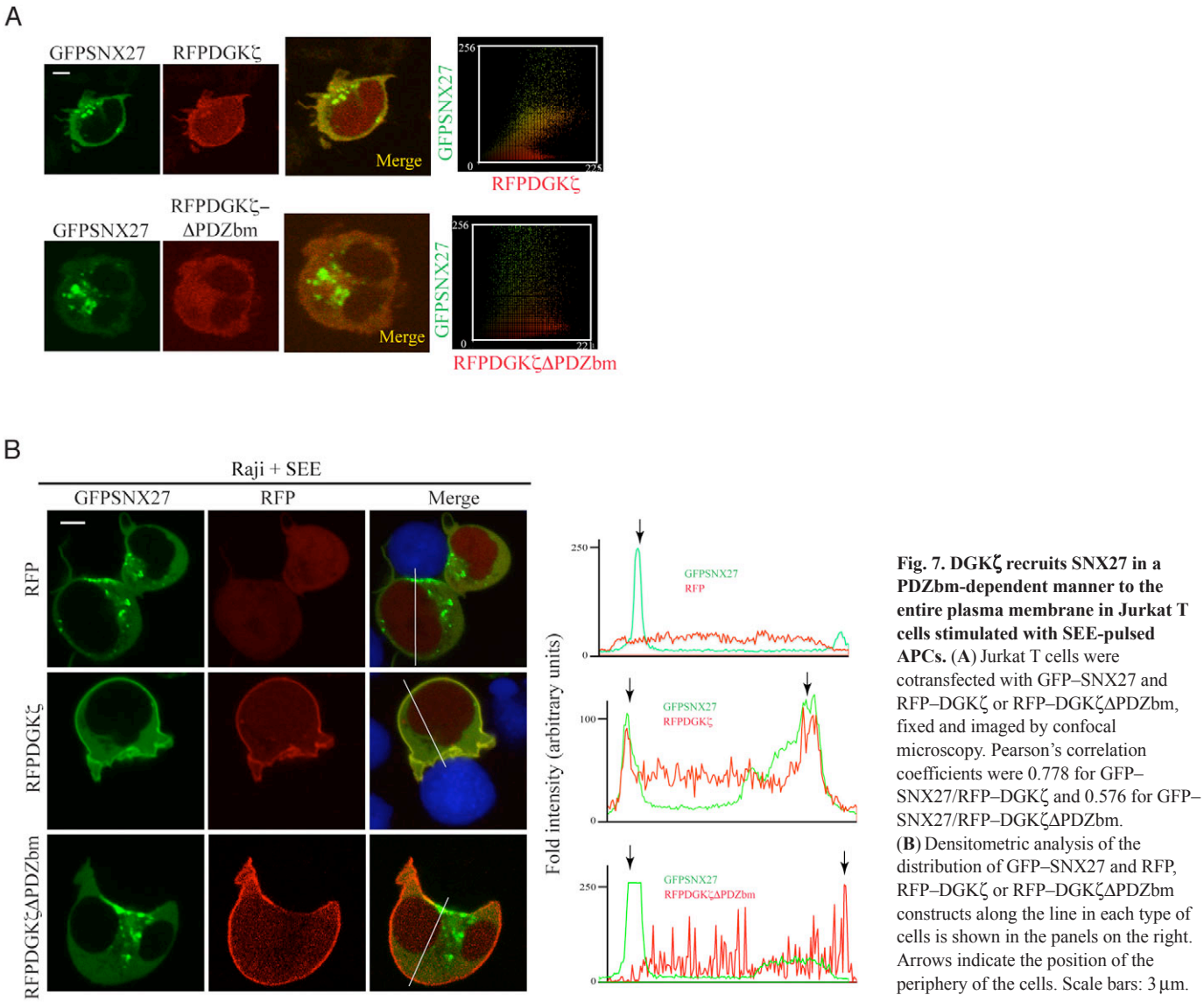

Fig. 7. DGKζ recruits SNX27 in a PDZbm-dependent manner to the entire plasma membrane in Jurkat T cells stimulated with SEE-pulsed APCs. (**A**) Jurkat T cells were cotransfected with GFP–SNX27 and RFP–DGKζ or RFP–DGKζΔPDZbm, fixed and imaged by confocal microscopy. Pearson's correlation coefficients were 0.778 for GFP–SNX27/RFP–DGKζ and 0.576 for GFP–SNX27/RFP–DGKζΔPDZbm. (**B**) Densitometric analysis of the distribution of GFP–SNX27 and RFP, RFP–DGKζ or RFP–DGKζΔPDZbm constructs along the line in each type of cells is shown in the panels on the right. Arrows indicate the position of the periphery of the cells. Scale bars: 3 µm.

cytohesin family. These results suggest that endosomal SNX27 recruits CASP, although there are no further data on the functional role of this interaction (MacNeil et al., 2007). It is noteworthy that all SNX27 partners identified are closely related to the neuronal and immunological systems (MacNeil et al., 2007; Rincon et al., 2007). These two tissues showed specific expression of genes that encode PDZ-containing proteins (Giallourakis et al., 2006). The role of PDZ-containing protein in neuronal tissues is well documented. They are enriched in the neuronal synapse where they regulate synapse composition, thereby determining its size and strength (Kim and Sheng, 2004). Although somewhat unexpected, the large number of PDZ-containing proteins in immune tissue suggests an important function at this site (Giallourakis et al., 2006). Recruitment of hDlg (human Discs large) to the immunological synapse, for example, regulates T cell function and polarity by specific recruitment of PDZbm-containing proteins (Ludford-Menting et al., 2005). Our data identify SNX27 as a PDZ component of the T cell immunological synapse. Immunofluorescence analysis with an anti-hDlg antibody showed no colocalisation with SNX27 at the immunological synapse (not shown), suggesting that SNX27 and hDlg form part of distinct protein complexes.

Our earlier data describing the interaction between SNX27 and DGKζ in T cells (Rincon et al., 2007) prompted us to investigate the functional relationship of these two proteins. Following overexpression of the DGKζ C-terminal region, localisation of SNX27 to the immunological synapse was lost, although it was unaffected by DGKζ downmodulation, confirming the presence of additional SNX27 partners that interact at this site. Microscopy analysis reveals a PDZ-mediated interaction between DGKζ and SNX27. Interestingly, DGKζ shuttles to the plasma membrane in response to T cell engagement and its overexpression was sufficient to dislodge SNX27 from an immunological synapse pool and to send it to the whole plasma membrane. This would suggest that there is a tight regulation between these two proteins and that they can reciprocally alter their localisation and activation. We were not able to detect specific recruitment of DGKζ to the immunological synapse, although it is possible that SNX27 directs localisation of DGKζ to this site. Our silencing estimation showed that, although DGKζ was not necessary to direct SNX27 to the immunological

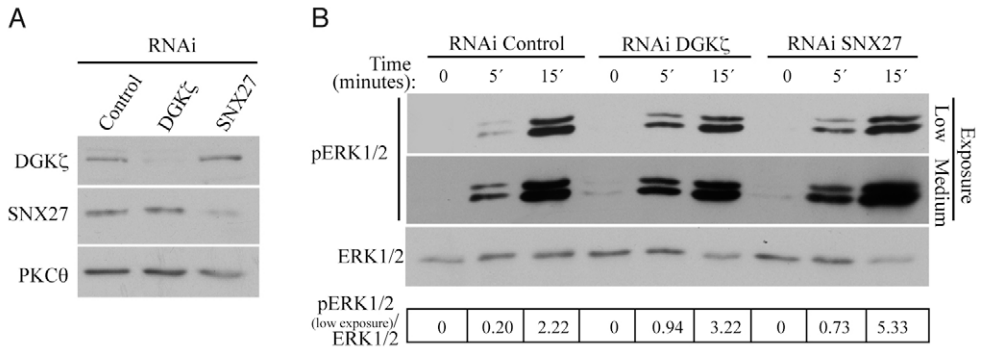

Fig. 8. Enhanced ERK phosphorylation in Jurkat T cells with knockdown of DGKζ or SNX27. Jurkat T cells were transfected with siRNA control, siRNA against SNX27 or DGKζ and collected 3 days after transfection. (**A**) RNAi efficiency was evaluated by western blotting with rabbit anti-DGKζ or anti-SNX27; anti-PKCθ was used as a control. (**B**) Silenced Jurkat cells were stimulated with unpulsed APCs (time 0) or SEE-pulsed APCs (5 and 15 minutes) and phosphorylation of ERK1/2 was evaluated using specific antibody (top and middle panels). Blot was reprobed with anti-ERK1/2 (bottom panel). Normalised values of perk to ERK were quantified using ImageJ program (table). The experiment is representative of three performed with similar results.

synapse, SNX27 itself could be important to attract DGKζ to the immunological synapse and/or to endosomal compartments where it will regulate DAG levels and, ultimately, TCR signals. Indeed, SNX27 silencing mirrors the activation of the ERK pathway that is observed in DGKζ knockdown cells, strongly suggesting that both proteins act in the same pathway. These results are better understood when examined in relation to the mechanisms by which DAG membrane levels modulate Ras activation in T cells. Studies in Jurkat T cells have elegantly shown that DAG-dependent activation of RasGRP1 is important to induce a positive-feedback loop, priming SOS activation (Roose et al., 2007). The interplay between these two RasGEF proteins has been the basis for theoretical models that explain how lymphocytes can adopt specific responses to antigens with different affinities to the TCR (Das et al., 2009).

The regulation of RasGRP1 by a membrane lipid not only provides a sophisticated mechanism that translates affinity of the receptor into signal strength, but could also provide a mechanism for Ras signalling compartmentalisation, a matter that has recently received considerable attention (Mor and Philips, 2006). Whereas SOS activates Ras exclusively at the plasma membrane, RasGRP1 can also function in internal membranes providing a mechanism to activate Ras localised to endosomes (Daniels et al., 2006). DGKζ limits the threshold of T cell activation by metabolising the DAG required to activate RasGRP1 (Roose et al., 2005), but there is no information available regarding the spatial regulation of DGKζ following TCR triggering. Our data not only shows a common role for SNX27 and DGKζ as negative modulators of ERK phosphorylation, but also suggests a role for SNX27 in the complex and still unresolved mechanism by which DGKζ regulates the Ras–ERK pathway.

Our data showing PDZ-independent recruitment of DGKζ to the entire plasma membrane as a consequence of T cell-APC interaction, are reminiscent of the dynamic translocation of this enzyme in response to ectopically expressed muscarinic type I receptors (Santos et al., 2002). Recent studies showed that DAG and proteins bearing DAG-binding motifs have a key role in different steps of immunological synapse formation, including MTOC reorientation, immunological synapse breakdown and granule polarisation (Ma et al., 2008; Quann et al., 2009; Sims et al., 2007). DGKζ dissociation from the endocytic/recycling compartment as a consequence of APC contact would facilitate membrane DAG elevation in this membrane compartment.

Overall, the data presented in this paper support a model in which feedback between SNX27 and DGKζ ensures the spatial recruitment of both proteins to sites of active signalling. The identification of SNX27 as a DGKζ partner and the characterisation of its relocation during immunological synapse formation allow us to postulate a previously unreported function in T cell activation for this member of the sorting nexin family. These data shed new light on the dynamic regulation of SNX27 and DGKζ in T cells and provide additional evidence on the important role of membrane trafficking in the regulation of T cell functions.

Materials and Methods

Antibodies

Anti-DGKζ (N-terminal peptide) was a generous gift from Matthew Topham (University of Utah, Salt Lake City, UT) (Abramovici et al., 2003), anti-SNX27 was previously described (Rincon et al., 2007) anti-phosphorylated MAPK (pERK1+pERK2, Cell Signaling), anti-haemagglutinin (anti-HA; Babco), anti-GST (Santa Cruz Biotechnology), anti-SNX2 and anti-PKCθ (BD Transduction Laboratories), anti-human-CD3 and -CD28 (BD Pharmingen), anti-tubulin (Sigma) and anti-phosphotyrosine (Upstate Biotechnology), anti-human-TfR and -MAPK (ERK1+ERK2) (Zymed Laboratories). Monoclonal antibodies against human Lamp1 (developed by Thomas August and James E. K. Hildreth) was obtained from the Developmental Studies Hybridoma Bank (developed under the auspices of the NICHD and maintained by the Univ. Iowa Dept Biological Sciences, Iowa City, IA). Mouse anti-LFA-1 and -CD3 (clone T3b for lipid planar bilayer assays and clone OKT3 for IF analysis) were a generous gift from Miguel A. Alonso (CBMSO, Madrid, Spain) and Francisco Sánchez-Madrid (Hospital de la Princesa, Madrid, Spain), respectively.

Plasmids and DNA constructs

HA–DGKζCT, GFP–RasGRP1 and human Myc-tagged SNX27ΔRA, mouse green fluorescence protein (GFP)-tagged SNX27 and SNX27ΔPDZ were previously described (Carrasco and Merida, 2004; Rincon et al., 2007; Santos et al., 2002). GFP–PKCθ was from Clontech. To generate GFP–SNX27($R_{196}A$,$Y_{197}A$), the (559)CGGTAC(564) sequence in GFP–SNX27 was mutated to GCGGCC. To generate RFP–DGKζ, pcDNA3MycDGKζ (Santos et al., 2002) was digested with *Kpn*I and *Bgl*II and the 2.9 kb fragment was subcloned into the *Kpn*I–*Bgl*II site of the mRFP expression vector (kindly provided by Santos Mañes, Centro Nacional de Biotecnología, Madrid, Spain). To generate the PDZ-binding motif deletion mutant (RFP–DGKζΔPDZbm), the (2776)GAG(2778) sequence in RFP–DGKζ was mutated to TAG. Site-directed mutagenesis was performed using the QuikChange mutagenesis kit (Stratagene). To generate GST fusion proteins, GFP–SNX27, GFP–SNX27($R_{196}A$,$Y_{197}A$) and GFP–SNX27ΔPDZ were digested with *Sal*I and *Not*I and the 1.7 kb (1.35 kb for SNX27ΔPDZ) fragments were subcloned in the pGEX4T1 vector digested with *Sal*I and *Not*I, generating GST–SNX27, GST–SNX27($R_{196}A$,$Y_{197}A$) and GST–SNX27ΔPDZ. All constructs were confirmed by sequencing.

siRNA knockdown of DGKζ and SNX27

Silencing of DGKζ was performed as reported (Rincon et al., 2007). The mouse DGKα sequence (nucleotides 1153–1173) was used as control (pSUPER-RNAi-

Control). For ERK phosphorylation analysis, we purchased the silencer negative control 1 siRNA and a pre-designed siRNA against human SNX27 (siRNA ID: 131018) from Ambion; for DGKζ knockdown in this analysis, we selected the 21-nucleotide sequence mentioned above.

Cell lines and transient transfection

Jurkat T cells (human acute T cell leukaemia) in logarithmic growth phase were transfected (1.2×10^7 in 400 µl complete medium) with 20 µg plasmid DNA by electroporation with a Gene Pulser (Bio-Rad; 270 V, 975 µF); cells were assayed 24 hours after transfection. For RNAi of DGKζ and SNX27, 1.2×10^7 Jurkat T cells were transfected in 400 µl of OptiMEM (Gibco, Invitrogen Life Technologies) with 5 µg siRNA by electroporation at 250 V, 950 µF) and cells were assayed at 72 hours after transfection. Raji B cells (human B cell lymphoma), used as APCs, were maintained in RPMI 1640 medium (BioWhittaker) with 10% FBS and 2 mM glutamine.

Stimulation with anti-CD3 and anti-CD28 fibronectin-coated plates or CD3 and CD28 beads

Slides were precoated with a 1:1 mixture of anti-CD3 and anti-CD28 (10 µg/ml each) in PBS or with fibronectin (10 µg/ml) in PBS for 1 hour at 37°C and washed three times with PBS. Transfected Jurkat cells were plated onto slides (20 minutes) then examined by confocal microscopy. To stimulate with antibody-coated beads, polystyrene microspheres (15.0 µm, from Polysciences) were pre-coated with anti-CD3 and anti-CD28, as previously described (Carrasco and Merida, 2004). For stimulation, 0.4×10^5 transfected Jurkat cells were mixed with antibody-coated beads at a 1:1 cell:bead ratio and plated on chambered coverslips. After 20 minutes, images were captured by confocal microscopy.

Stimulation with antigen-presenting cells

Raji B cells were stained with 50 µM CMAC and were pulsed with medium alone or with 1 µg/ml bacterial superantigen *Staphylococcus* enterotoxin E (SEE) (Toxin Technology) (Fraser et al., 2000) (1 hour, 37°C); Raji cells were washed in complete medium and then mixed 1:1 with Jurkat T cells. For primaquine treatment, Jurkat T cells were incubated with medium alone or with 300 µM primaquine (15 minute, 37°C) before mixing with Raji cells. Cell–cell conjugates were imaged by confocal microscopy or processed for immunofluorescence analysis. For MAPK activation analysis, Jurkat T cells transiently transfected with selected siRNA, were stimulated with Raji B cells (1:1) unpulsed (time 0) or pulsed (times 5 and 15 minutes). After treatment, cells were pelleted and lysed for western blot analysis.

Western blot

Jurkat cells, transiently transfected with selected plasmids or siRNA, were lysed in NP40 buffer (150 mM NaCl, 10 mM NaF, 10 mM $Na_4P_2O_7$, 50 mM Tris-HCl, pH 7.5, 1% Igepal CA-630 and 0.5 mM PMSF/protease inhibitor cocktail); lysates were incubated (15 minutes, on ice) and centrifuged (20,800 ***g***, 10 minutes, 4°C). Following protein assay (DC protein assay, Bio-Rad), equivalent protein amount per sample was analysed by SDS-PAGE. Proteins were transferred to nitrocellulose membrane, incubated with specified antibodies, and detected using the ECL detection kit (Amersham Bioscience).

Lipid-binding assay

GST-tagged SNX27 constructs were produced in *Escherichia coli* strain BL21(De3)pLysS by standard procedures. GST alone was used as control. Protein-rich fractions were collected and concentrated using Amicon Ultra-4 centrifugal filter devices (Millipore). Protein concentration was determined and the GST-recombinant proteins were used for lipid-binding studies. PIP Strips (Molecular Probes) were probed with 0.5 µg/ml GST-tagged fusion protein following the manufacturer's instructions.

Immunofluorescence analysis

Cells were transferred to poly-DL-lysine-coated coverslips and allowed to attach (30 minutes). Where indicated, attached cells were serum-starved (30 minutes) and incubated with transferrin–Rhodamine (Tf-Rhod) (20 µg/ml, 15–30 minutes, 37°C). Cells were fixed for 4 minutes in cold methanol (10 minutes in 2% paraformaldehyde to visualise RFP–DGKζFL or RFP–GDKζΔPDZbm), then washed with phosphate-buffered saline (PBS) and blocked in PBS, 3% FBS for 15 minutes at room temperature. Primary antibodies (diluted 1:100 in PBS with 3% FBS) were incubated (1 hour, 37°C) and washed with PBS; the same procedure was followed for secondary antibodies. Cells mounted on glass slides were imaged with an Olympus Fluoview FV-1000 laser-scanning confocal microscope. Images were processed using ImageJ (National Institutes of Health; http://rsb.info.nih.gov/ij/index.html) and Adobe Photoshop software. For quantitative analysis of SNX27 and DGKζ distribution at the plasma membrane, fluorescence signals were profiled along a line at the equatorial plane of the cell using the ImageJ program. The colocalisation plots and the Pearson´s correlation coefficients (Bolte and Cordelieres, 2006) were also produced with ImageJ. Three-dimensional (3D) reconstructions of confocal sections (0.250 µm separation in the vertical axis, acquired on a Zeiss Axiovert LSM 510-META inverted microscope) were assembled with Imaris 6.0 software (Bitplane).

Time-lapse microscopy imaging

At 24 hours after transfection, cells were transferred to chambered coverslips coated with poly-DL-lysine, fibronectin or anti-CD3 and anti-CD28 (Nunc LabTek), allowed to attach for at least 20 minutes at 37°C, washed and maintained in HEPES-buffered Hanks' balanced salt solution (HBSS; 25 mM HEPES-KOH, pH 7.4, 1 mM $MgCl_2$, 1 mM $CaCl_2$, 132 mM NaCl, 0.1% BSA) supplemented with 2% FBS. Cells were placed on a heated plate and were time-lapse imaged every 20 seconds with an Olympus confocal microscope; pulsed and stained APCs were added during acquisition. Images were processed using ImageJ and Adobe Photoshop.

Analysis of protein accumulation at the T-cell–APC contact area

To quantify the amount of GFP–SNX27 accumulated at the immunological synapse compared with the total GFP–SNX27, *Z*-series optical sections (0.2 µm) were recorded. Four or five contiguous optical sections were stacked and contained all the three-dimensional fluorescence information. To analyse these stacks, we devised a plug-in for ImageJ that allows us to measure the average fluorescent intensity in the background (Bg), at the whole cell (Cell) and in the region of interest (ROI). Then, we compute the intensity ratio as Z=(ROI–Bg)/(Cell–Bg). To quantify protein accumulation at the immunological synapse compared with other regions of plasma membrane of the T cell, we designed another plugin for ImageJ, which measures the average intensity value of the image in small circles at the background (Bg), the plasma membrane of the T cell outside the immunological synapse (T) and the synapse (S) when the fluorescent protein is expressed by only one of the two cells. For each measurement (Bg, T and S) the average pixel value was computed. From these observed values, we separated the contribution of each one of the components (background, constitutive T cell and T cell at the synapse). Finally, we computed the ratio between the fluorescence at the synapse and outside the synapse. Ratio values were represented as dot plots, with each dot representing the value of an individual cell.

Planar lipid bilayers

The planar lipid bilayers were formed on FCS2 flow chambers as previously described (Grakoui et al., 1999). Briefly, unlabeled GPI-linked ICAM-1 (intercellular adhesion molecule 1) liposomes and biotinylated lipids were mixed with 1,2-dioleoyl-PC (DOPC) lipids (Avanti Polar Lipids) at different ratios to get the molecular density required. Once the planar bilayers formed, the chambers were blocked with PBS 2% FBS for 1 hour at room temperature, followed by antigen loading in PBS 0.5% FBS. Monobiotinylated anti-human CD3 antibody (clone T3b) was tethered on the lipid bilayers as surrogate antigen, previous incubation with Alexa Fluor 647 streptavidin (Molecular Probes). T cells were injected into the warmed (37°C) chamber at time zero, and then followed over the time by confocal fluorescence microscopy. The assays were done in PBS with 0.5% FBS, 2 mM Mg^{2+}, 0.5 mM Ca^{2+}, 1 g/l D-glucose at 37°C. Images were acquired on a Zeiss Axiovert LSM 510-META inverted microscope with a 40× oil-immersion objective and analysed by LSM 510 software (Zeiss, Germany) and Imaris 6.0 software (Bitplane). To quantify the frequency of cells that exhibit protein accumulation at the immunological synapse, we acquired images 25 minutes after cell injection.

Statistical analysis

To analyse the fluorescence intensity data of SNX27 at the immunological synapse, we used a two-sample Kolmogorov-Smirnov test to compare pairs of distributions of ratios from different cells. We applied a Bonferroni correction to the confidence thresholds to account for the multiple comparisons performed. Differences between two cell frequency means were tested by Student's *t*-tests using PRISM software. Differences were considered not significant (ns) when $P>0.05$, significant (*) when $P<0.05$, very significant (**) when $P<0.01$ and extremely significant (***) when $P<0.001$.

We are grateful to colleagues who generously provided reagents. We thank I.M. group members for stimulating discussion, especially M. Almena and A. Ávila for unconditional support to this work and critical assessment of the manuscript, C. Andradas Arias for technical assistance, A. Checa and R. Villares for confocal assistance and C. Mark for excellent editorial assistance. E.R. receives a fellowship from the Comunidad de Madrid. This work was supported in part by grants RD067002071035 from the Spanish Ministry of Health (Instituto de Salud Carlos III), BFU2007-62639 from the Spanish Ministry of Education and S-SAL-0311 from Comunidad de Madrid to I.M.

Supplementary material available online at
http://jcs.biologists.org/cgi/content/full/124/5/776/DC1

References

Abramovici, H., Hogan, A., Obagi, C., Topham, M. and Gee, S. (2003). Diacylglycerol kinase-zeta localization in skeletal muscle is regulated by phosphorylation and interaction with syntrophins. *Mol. Biol. Cell* **14**, 4499-4511.

Anton, O., Batista, A., Millan, J., Andres-Delgado, L., Puertollano, R., Correas, I. and Alonso, M. A. (2008). An essential role for the MAL protein in targeting Lck to the plasma membrane of human T lymphocytes. *J. Exp. Med.* **205**, 3201-3213.

Badour, K., McGavin, M. K., Zhang, J., Freeman, S., Vieira, C., Filipp, D., Julius, M., Mills, G. B. and Siminovitch, K. A. (2007). Interaction of the Wiskott-Aldrich syndrome protein with sorting nexin 9 is required for CD28 endocytosis and cosignaling in T cells. *Proc. Natl. Acad. Sci. USA* **104**, 1593-1598.

Billadeau, D. D., Nolz, J. C. and Gomez, T. S. (2007). Regulation of T cell activation by the cytoskeleton. *Nat. Rev. Immunol.* **7**, 131-143.

Blott, E. J. and Griffiths, G. M. (2002). Secretory lysosomes. *Nat. Rev. Mol. Cell Biol.* **3**, 122-131.

Bolte, S. and Cordelieres, F. P. (2006). A guided tour into subcellular colocalization analysis in light microscopy. *J. Microsc.* **224**, 213-232.

Bonello, G., Blanchard, N., Montoya, M. C., Aguado, E., Langlet, C., He, H. T., Nunez-Cruz, S., Malissen, M., Sanchez-Madrid, F., Olive, D. et al. (2004). Dynamic recruitment of the adaptor protein LAT: LAT exists in two distinct intracellular pools and controls its own recruitment. *J. Cell Sci.* **117**, 1009-1016.

Bravo, J., Karathanassis, D., Pacold, C., Pacold, M., Ellson, C., Anderson, K. E., Butler, P., Lavenir, I., Perisic, O., Hawkins, P. T. et al. (2001). The crystal structure of the PX domain from p40(phox) bound to phosphatidylinositol 3-phosphate. *Mol. Cell* **8**, 829-839.

Carlton, J., Bujny, M., Rutherford, A. and Cullen, P. (2005). Sorting nexins- unifying trends and prespectives. *Traffic* **6**, 75-82.

Carrasco, S. and Merida, I. (2004). Diacylglycerol-dependent binding recruits PKCtheta and RasGRP1 C1 domains to specific subcellular localizations in living T lymphocytes. *Mol. Biol. Cell* **15**, 2932-2942.

Cemerski, S. and Shaw, A. (2006). Immune synapses in T-cell activation. *Curr. Opin. Immunol.* **18**, 298-304.

Chen, J. W., Cha, Y., Yuksel, K. U., Gracy, R. W. and August, J. T. (1988). Isolation and sequencing of a cDNA clone encoding lysosomal membrane glycoprotein mouse LAMP-1. Sequence similarity to proteins bearing onco-differentiation antigens. *J. Biol. Chem.* **263**, 8754-8758.

Cullen, P. J. (2008). Endosomal sorting and signalling: an emerging role for sorting nexins. *Nat. Rev. Mol. Cell Biol.* **9**, 574-582.

Daniels, M. A., Teixeiro, E., Gill, J., Hausmann, B., Roubaty, D., Holmberg, K., Werlen, G., Hollander, G. A., Gascoigne, N. R. and Palmer, E. (2006). Thymic selection threshold defined by compartmentalization of Ras/MAPK signalling. *Nature* **444**, 724-729.

Das, J., Ho, M., Zikherman, J., Govern, C., Yang, M., Weiss, A., Chakraborty, A. K. and Roose, J. P. (2009). Digital signaling and hysteresis characterize ras activation in lymphoid cells. *Cell* **136**, 337-351.

Das, V., Nal, B., Dujeancourt, A., Thoulouze, M. I., Galli, T., Roux, P., Dautry-Varsat, A. and Alcover, A. (2004). Activation-induced polarized recycling targets T cell antigen receptors to the immunological synapse; involvement of SNARE complexes. *Immunity* **20**, 577-588.

Davis, M. M., Krogsgaard, M., Huppa, J. B., Sumen, C., Purbhoo, M. A., Irvine, D. J., Wu, L. C. and Ehrlich, L. (2003). Dynamics of cell surface molecules during T cell recognition. *Annu. Rev. Biochem.* **72**, 717-742.

Dustin, M. L., Starr, T., Varma, R. and Thomas, V. K. (2007). Supported planar bilayers for study of the immunological synapse. *Curr. Protoc. Immunol.* **Chapter 18**, Unit 18.13.

Ehrlich, L. I., Ebert, P. J., Krummel, M. F., Weiss, A. and Davis, M. M. (2002). Dynamics of p56lck translocation to the T cell immunological synapse following agonist and antagonist stimulation. *Immunity* **17**, 809-822.

Fabre, S., Reynaud, C. and Jalinot, P. (2000). Identification of functional PDZ domain binding sites in several human proteins. *Mol. Biol. Rep.* **27**, 217-224.

Fooksman, D. R., Vardhana, S., Vasiliver-Shamis, G., Liese, J., Blair, D. A., Waite, J., Sacristan, C., Victora, G. D., Zanin-Zhorov, A. and Dustin, M. L. (2010). Functional anatomy of T cell activation and synapse formation. *Annu. Rev. Immunol.* **28**, 79-105.

Fraser, J., Arcus, V., Kong, P., Baker, E. and Proft, T. (2000). Superantigens-powerful modifiers of the immune system. *Mol. Med. Today* **6**, 125-132.

Friedl, P. and Gunzer, M. (2001). Interaction of T cells with APCs: the serial encounter model. *Trends Immunol.* **22**, 187-191.

Friedl, P. and Storim, J. (2004). Diversity in immune-cell interactions: states and functions of the immunological synapse. *Trends Cell Biol.* **14**, 557-567.

Friedl, P., den Boer, A. T. and Gunzer, M. (2005). Tuning immune responses: diversity and adaptation of the immunological synapse. *Nat. Rev. Immunol.* **5**, 532-545.

Giallourakis, C., Cao, Z., Green, T., Wachtel, H., Xie, X., Lopez-Illasaca, M., Daly, M., Rioux, J. and Xavier, R. (2006). A molecular-properties-based approach to understanding PDZ domain proteins and PDZ ligands. *Genome Res.* **16**, 1056-1072.

Gillooly, D. J., Morrow, I. C., Lindsay, M., Gould, R., Bryant, N. J., Gaullier, J. M., Parton, R. G. and Stenmark, H. (2000). Localization of phosphatidylinositol 3-phosphate in yeast and mammalian cells. *EMBO J.* **19**, 4577-4588.

Grakoui, A., Bromley, S. K., Sumen, C., Davis, M. M., Shaw, A. S., Allen, P. M. and Dustin, M. L. (1999). The immunological synapse: a molecular machine controlling T cell activation. *Science* **285**, 221-227.

Gullapalli, A., Garrett, T. A., Paing, M. M., Griffin, C. T., Yang, Y. and Trejo, J. (2004). A role for sorting nexin 2 in epidermal growth factor receptor down-regulation: evidence for distinct functions of sorting nexin 1 and 2 in protein trafficking. *Mol. Biol. Cell* **15**, 2143-2155.

Hiebsch, R. R., Raub, T. J. and Wattenberg, B. W. (1991). Primaquine blocks transport by inhibiting the formation of functional transport vesicles. Studies in a cell-free assay of protein transport through the Golgi apparatus. *J. Biol. Chem.* **266**, 20323-20328.

Hogan, A., Shepherd, L., Chabot, J., Quenneville, S., Prescott, S. M., Topham, M. K. and Gee, S. H. (2001). Interaction of gamma 1-syntrophin with diacylglycerol kinase-zeta. Regulation of nuclear localization by PDZ interactions. *J. Biol. Chem.* **276**, 26526-26533.

Huse, M., Lillemeier, B. F., Kuhns, M. S., Chen, D. S. and Davis, M. M. (2006). T cells use two directionally distinct pathways for cytokine secretion. *Nat. Immunol.* **7**, 247-255.

Huse, M., Quann, E. J. and Davis, M. M. (2008). Shouts, whispers and the kiss of death: directional secretion in T cells. *Nat. Immunol.* **9**, 1105-1111.

Joubert, L., Hanson, B., Barthet, G., Sebben, M., Claeysen, S., Hong, W., Marin, P., Dumuis, A. and Bockaert, J. (2004). New sorting nexin (SNX27) and NHERF specifically interact with the 5-HT4a receptor splice variant: roles in receptor targeting. *J. Cell Sci.* **117**, 5367-5379.

Kim, E. and Sheng, M. (2004). PDZ domain proteins of synapses. *Nat. Rev. Neurosci.* **5**, 771-781.

Kim, K., Yang, J., Zhong, X. P., Kim, M. H., Kim, Y. S., Lee, H. W., Han, S., Choi, J., Han, K., Seo, J. et al. (2009). Synaptic removal of diacylglycerol by DGKzeta and PSD-95 regulates dendritic spine maintenance. *EMBO J.* **28**, 1170-1179.

Lee, K. H., Dinner, A. R., Tu, C., Campi, G., Raychaudhuri, S., Varma, R., Sims, T. N., Burack, W. R., Wu, H., Wang, J. et al. (2003). The immunological synapse balances T cell receptor signaling and degradation. *Science* **302**, 1218-1222.

Ludford-Menting, M. J., Oliaro, J., Sacirbegovic, F., Cheah, E. T., Pedersen, N., Thomas, S. J., Pasam, A., Iazzolino, R., Dow, L. E., Waterhouse, N. J. et al. (2005). A network of PDZ-containing proteins regulates T cell polarity and morphology during migration and immunological synapse formation. *Immunity* **22**, 737-748.

Lunn, M. L., Nassirpour, R., Arrabit, C., Tan, J., McLeod, I., Arias, C. M., Sawchenko, P. E., Yates, J. R., III and Slesinger, P. A. (2007). A unique sorting nexin regulates trafficking of potassium channels via a PDZ domain interaction. *Nat. Neurosci.* **10**, 1249-1259.

Ma, J. S., Haydar, T. F. and Radoja, S. (2008). Protein kinase C delta localizes to secretory lysosomes in CD8+ CTL and directly mediates TCR signals leading to granule exocytosis-mediated cytotoxicity. *J. Immunol.* **181**, 4716-4722.

MacNeil, A. J. and Pohajdak, B. (2007). Polarization of endosomal SNX27 in migrating and tumor-engaged natural killer cells. *Biochem. Biophys. Res. Commun.* **361**, 146-150.

MacNeil, A. J., Mansour, M. and Pohajdak, B. (2007). Sorting nexin 27 interacts with the Cytohesin associated scaffolding protein (CASP) in lymphocytes. *Biochem. Biophys. Res. Commun.* **359**, 848-853.

Maxfield, F. R. and McGraw, T. E. (2004). Endocytic recycling. *Nat. Rev. Mol. Cell Biol.* **5**, 121-132.

Monks, C. R., Kupfer, H., Tamir, I., Barlow, A. and Kupfer, A. (1997). Selective modulation of protein kinase C-theta during T-cell activation. *Nature* **385**, 83-86.

Monks, C. R., Freiberg, B. A., Kupfer, H., Sciaky, N. and Kupfer, A. (1998). Three-dimensional segregation of supramolecular activation clusters in T cells. *Nature* **395**, 82-86.

Mor, A. and Philips, M. R. (2006). Compartmentalized Ras/MAPK signaling. *Annu. Rev. Immunol.* **24**, 771-800.

Olenchock, B. A., Guo, R., Carpenter, J. H., Jordan, M., Topham, M. K., Koretzky, G. A. and Zhong, X. P. (2006). Disruption of diacylglycerol metabolism impairs the induction of T cell anergy. *Nat. Immunol.* **7**, 1174-1181.

Quann, E. J., Merino, E., Furuta, T. and Huse, M. (2009). Localized diacylglycerol drives the polarization of the microtubule-organizing center in T cells. *Nat. Immunol.* **10**, 627-635.

Rincon, E., Santos, T., Avila-Flores, A., Albar, J. P., Lalioti, V., Lei, C., Hong, W. and Merida, I. (2007). Proteomics identification of sorting nexin 27 as a diacylglycerol kinase zeta-associated protein: new diacylglycerol kinase roles in endocytic recycling. *Mol. Cell. Proteomics* **6**, 1073-1087.

Roose, J. P., Mollenauer, M., Gupta, V. A., Stone, J. and Weiss, A. (2005). A diacylglycerol-protein kinase C-RasGRP1 pathway directs Ras activation upon antigen receptor stimulation of T cells. *Mol. Cell. Biol.* **25**, 4426-4441.

Roose, J. P., Mollenauer, M., Ho, M., Kurosaki, T. and Weiss, A. (2007). Unusual interplay of two types of Ras activators, RasGRP and SOS, establishes sensitive and robust Ras activation in lymphocytes. *Mol. Cell. Biol.* **27**, 2732-2745.

Sanjuan, M. A., Pradet-Balade, B., Jones, D. R., Martinez, A. C., Stone, J. C., Garcia-Sanz, J. A. and Merida, I. (2003). T cell activation in vivo targets diacylglycerol kinase alpha to the membrane: a novel mechanism for Ras attenuation. *J. Immunol.* **170**, 2877-2883.

Santos, T., Carrasco, S, Jones, D. R., Merida, I. and Eguinoa, A. (2002). Dynamics of DGKzeta translocation in living T cells. Study of the structural domain requirements for translocation and activity. *J. Biol. Chem.* **277**, 30300-30309.

Sheng, M. and Sala, C. (2001). PDZ domains and the organization of supramolecular complexes. *Annu. Rev. Neurosci.* **24**, 1-29.

Sims, T. N., Soos, T. J., Xenias, H. S., Dubin-Thaler, B., Hofman, J. M., Waite, J. C., Cameron, T. O., Thomas, V. K., Varma, R., Wiggins, C. H. et al. (2007). Opposing effects of PKCtheta and WASp on symmetry breaking and relocation of the immunological synapse. *Cell* **129**, 773-785.

Somasundaram, B., Norman, J. C. and Mahaut-Smith, M. P. (1995). Primaquine, an inhibitor of vesicular transport, blocks the calcium-release-activated current in rat megakaryocytes. *Biochem. J.* **309**, 725-729.

Stahelin, R. V., Digman, M. A., Medkova, M., Ananthanarayanan, B., Rafter, J. D., Melowic, H. R. and Cho, W. (2004). Mechanism of diacylglycerol-induced

membrane targeting and activation of protein kinase Cdelta. *J. Biol. Chem.* **279**, 29501-29512.

van der Merwe, P. A. (2002). Formation and function of the immunological synapse. *Curr. Opin. Immunol.* **14**, 293-298.

van Weert, A. W., Geuze, H. J., Groothuis, B. and Stoorvogel, W. (2000). Primaquine interferes with membrane recycling from endosomes to the plasma membrane through a direct interaction with endosomes which does not involve neutralisation of endosomal pH nor osmotic swelling of endosomes. *Eur. J. Cell Biol.* **79**, 394-399.

Wang, H., Lim, D. and Rudd, C. E. (2010). Immunopathologies linked to integrin signalling. *Semin. Immunopathol.* **32**, 173-182.

Worby, C. A. and Dixon, J. E. (2002). Sorting out the cellular functions of sorting nexins. *Nat. Rev Mol. Cell Biol.* **3**, 919-931.

Xu, Y., Hortsman, H., Seet, L., Wong, S. H. and Hong, W. (2001). SNX3 regulates endosomal function trough its PX-domain-mediated interaction with PtdIns(3)P. *Nat. Cell Biol.* **3**, 658-667.

Yokosuka, T., Kobayashi, W., Sakata-Sogawa, K., Takamatsu, M., Hashimoto-Tane, A., Dustin, M. L., Tokunaga, M. and Saito, T. (2008). Spatiotemporal regulation of T cell costimulation by TCR-CD28 microclusters and protein kinase C theta translocation. *Immunity* **29**, 589-601.

Zhong, X., Hainey, E. A., Olenchock, B. A., Jordan, M. S., Maltzman, J. S., Nichols, K. E., Shen, H. and Koretzky, G. A. (2003). Enhanced T cell responses due to diacylglycerol kinase zeta deficiency. *Nat. Immunol.* **4**, 882-890.

Zhong, X. P., Hainey, E. A., Olenchock, B. A., Zhao, H., Topham, M. K. and Koretzky, G. A. (2002). Regulation of T cell receptor-induced activation of the Ras-ERK pathway by diacylglycerol kinase zeta. *J. Biol. Chem.* **277**, 31089-31098.

Janus kinases 1 and 2 regulate chemokine-mediated integrin activation and naïve T cell homing

Gema Pérez-Rivero[1], Graciela Cascio[1], Silvia Fernández Soriano[2], Álvaro Gil Sanz[3], Julia Sáez de Guinoa[1], José Miguel Rodríguez-Frade[1], Rosa P. Gomariz[4], Borja L. Holgado[1], Carlos Cabañas[3], Yolanda R. Carrasco[1], Jens V. Stein[2] and Mario Mellado[1*]

[1]Department of Immunology and Oncology, Centro Nacional de Biotecnología/CSIC, Campus de Cantoblanco, E-28049, Madrid, Spain, [2]Theodor Kocher Institute, University of Bern, Freiestrasse 1, 3012 Bern, Switzerland, [3]Centro de Biología Molecular Severo Ochoa/CSIC-UAM, Campus de Cantoblanco, E-28049, Madrid, Spain, [4]Departament of Cell Biology, Faculty of Biology, UCM, José Antonio Novais, 2. E-28040, Madrid

Key words: lymphocyte homing, chemokine receptor, integrin, Janus kinase

*Corresponding author: Mario Mellado, Dept. Immunology and Oncology, CNB/CSIC, Darwin 3, Cantoblanco, E-28049 Madrid Spain. Tel: (+34) 91/585-4852; Fax: (+34) 91/372-0493; e-mail: mmellado@cnb.csic.es

Abbreviations

CMFDA, 5-chloromethylfluorescein diacetate; CMTMR, 5-(and-6)-(((4-chloromethyl) benzoyl)amino)tetramethylrhodamine; ERM, ezrin/radixin/moesin; GPCR, G protein-coupled receptors; HEV, high endothelial venules; LFA-1, lymphocyte function-associated antigen-1; VLA-4, very late antigen-4

Abstract

Janus kinases (JAK) are central signaling molecules in cytokine receptor cascades. Although they have also been implicated in chemokine receptor signaling, this function continues to be debated. To address this issue, we established a nucleofection model in primary, non-activated mouse T lymphocytes to silence JAK expression and to evaluate the ability of these cells to home to lymph nodes. Reduced JAK1 and JAK2 expression impaired naïve T cell migration in response to gradients of the chemokines CXCL12 and CCL21. *In vivo* homing of JAK1/JAK2-deficient cells to lymph nodes decreased, whereas intranodal localization and motility were unaffected. JAK1 and JAK2 defects altered CXCL12- and CCL21-triggered ERM (ezrin/radixin/moesin) dephosphorylation and F-actin polymerization, as well as activation of lymphocyte function-associated antigen-1 and very late antigen-4 integrins. As a result, the cells did not adhere firmly to integrin substrates in response to these chemokines. The results demonstrate that JAK1/JAK2 participate in chemokine-induced integrin activation and might be considered a target for modulation of immune cell extravasation and therefore, control of inflammatory reactions.

Introduction

The JAK/STAT pathway is crucial in the control of cell responses to cytokines. The cytokine receptors bind Janus kinases, a small family of protein tyrosine kinases with four members, JAK1, JAK2, JAK3, and Tyk2 [1, 2]. Once activated by transphosphorylation [2], the JAKs phosphorylate cytokine receptors on cytosolic tyrosine residues to form docking sites for the STAT (signal transducer and activator of transcription) factors; these are then recruited and phosphorylated by JAK. This allows STAT dimerization, which leads to their nuclear accumulation [3].

Chemokines are a family of low molecular weight proteins that were first recognized to orchestrate lymphocyte polarization and migration [4]; they act by binding specific seven-transmembrane domain GPCR (G protein-coupled receptors) on the cell surface. Among other functions, chemokines organize naïve T cell migration to lymph nodes (homing) and their interstitial motility within them. By binding to CCR7, the ligands CCL19 and CCL21 are essential for lymphocyte homing to lymph nodes (LN) [5]. CCL19/CCL21-deficient *plt/plt* mice show greatly reduced lymphocyte homing and morphological alterations in LN; CCR7-deficient mouse LN have markedly lower cell numbers than those of wild-type mice [6]. CXCL12 and its receptor, CXCR4, also participate in T lymphocyte homing, as CXCL12 cooperates with CCR7 ligands to promote migration, facilitating efficient lymphocyte trafficking across the HEV (high endothelial venules) into LN and Peyer's patches [7]. CXCL12 also directs T central memory cell (T_{CM}) homing to LN [8].

Several reports implicate JAK proteins in signaling pathways elicited by chemokine receptors, both in primary cells and in cell lines [9-12]. Chemokine receptors exist as dimeric entities at the cell membrane; ligand binding triggers JAK recruitment, with subsequent STAT activation [13]. Adoptively transferred lymphocytes treated with the pharmacological JAK inhibitor AG490 show

less adhesion to HEV than untreated controls [14]; in contrast, studies using overexpressed wild-type or catalytically inactive JAK2 showed that CXCL12 signaling is JAK2-independent [15]. There are two potential problems that complicate the interpretation of these conflicting results. First, pharmacological inhibitors often exert non-specific effects on distinct tyrosine kinases or other intracellular signaling modules. Second, at difference from their specificity in cytokine receptor signaling, JAK proteins might be redundant during signal transduction in other signaling pathways.

Here we used naïve T cells nucleofected with specific siRNA to knock down JAK, and found that cells deficient in JAK1 (siJAK1) or JAK2 (siJAK2) migrate almost normally to the homeostatic chemokines CXCL12 and CCL21. In contrast, cells nucleofected simultaneously with siJAK1 and siJAK2 (siJAK1,2) showed altered migration towards both chemokines and their *in vivo* LN homing was impaired. In siJAK1,2 cells, CXCL12- and CCL21-triggered ERM dephosphorylation and F-actin polymerization were reduced, as were LFA-1 (lymphocyte function-associated antigen-1) and VLA-4 (very late antigen-4) activation. As a result, cells did not adhere firmly to their respective ligands, ICAM-1 (intercellular adhesion molecule 1) or VCAM-1 (vascular cell adhesion protein 1), in response to these chemokines. Our data show that JAK1/JAK2 inhibition modulates not only cytokine responses [2], but also chemokine-mediated integrin activation and cell extravasation, and might be considered a target for modulation of inflammatory reactions.

Results

JAK1 and JAK2 reduction in naïve T cells causes chemokine-mediated migration defects

JAK3 has a role in CCR7-mediated lymphocyte homing [11], although other JAK proteins have not been studied in this context. As $JAK1^{-/-}$ mice die within 24 h after birth [16] and $JAK2^{-/-}$ mice die in midgestation due to failure of erythropoiesis [17], we designed a nucleofection-based strategy to analyze the effect of JAK on chemokine-mediated T cell homing (Fig. 1A). We obtained naïve T cells from spleen and peripheral LN (PLN) of C57BL/6 mice by negative selection. Cell preparations were >97% pure, as shown by flow cytometry with anti-CD3, -B220 and -GR1 mAb (Fig. 1B).

To knock down JAK proteins using specific siRNA sequences, we first determined optimal siRNA nucleofection conditions using siGLO Green, a fluorescent oligonucleotide that localizes to the nucleus and permits unambiguous visual assessment of uptake. At 24 h post-nucleofection in cells cultured in RMPI medium with 10% FCS and mIL7 (25 IU/ml), we found a single cell population expressing the fluorescent oligonucleotide, indicating that all cells incorporated siRNA (not shown). To test whether nucleofection of JAK siRNA pools or control (ON-TARGETplus Non-targeting Pool) altered cell viability, we used propidium iodide (PI) incorporation as a marker of dead cells; at 24 h post-nucleofection, the number of viable siRNA-nucleofected naïve T cells was similar for all JAK siRNA pools and controls (~63% viable cells). Viable lymphocytes were recovered by density gradient centrifugation, after which viability was ~98% for all samples (not shown). Flow cytometry analysis using specific antibodies confirmed that nucleofection did not alter the CD4/CD8 ratio or expression of naïve T cell markers ($CD44^{low}$ and $CD62L^{high}$), trigger cell activation (CD69 and CD25), or affect CXCR4 and CCR7 levels (Fig. 1C-E, Table 1). In extracts from naïve T cells nucleofected with siRNA pools for JAK1/2 or controls, Western blot analysis confirmed a sharp reduction in protein levels for each

of the kinases (>60%; Fig. 2A, B). These data indicate that nucleofected naïve T cells can be used to determine the effect of these JAK proteins on chemokine-mediated T cell signaling.

In view of the role of JAK3 in transmitting IL7R-dependent survival signals [18], we assessed cells nucleofected with siRNA pools for JAK1 (siJAK1), JAK2 (siJAK2), JAK1 + JAK2 (siJAK1,2) or control siRNA pools (sicontrol) for *in vitro* migration towards CXCL12 or CCL21 gradients in ICAM-1-coated chemotaxis chambers. CXCL12- and CCL21-induced migration of siJAK1,2 cells was significantly reduced compared to sicontrol cells (Fig. 2C). Cells lacking only JAK1 (siJAK1 cells) or JAK2 (siJAK2 cells) migrated normally. These results confirm previous observations that implicate JAK kinases in chemokine-mediated signaling [9-12]. At difference from siJAK1 and siJAK2 cells, simultaneous downregulation of JAK1 and JAK2 reduced naïve T cell migration, suggesting a compensatory effect between these two JAK proteins.

Naïve T cells with reduced JAK1 and JAK2 levels show altered homing to lymph nodes

We tested whether these *in* vitro migration effects also altered naïve T cell homing. siJAK1 and siJAK2 cells were fluorescently labeled with cell tracker orange CMTMR (5-(and-6)-(((4-Chloromethyl)Benzoyl)Amino)Tetramethylrhodamine) and sicontrol cells with cell tracker green CMFDA (5-Chloromethylfluorescein Diacetate), and siJAK1 or siJAK2 cells were mixed with sicontrol cells at a 1:1 ratio and each mixture injected intravenously (i.v.) into C57BL/6 mice. Mice were killed after 6 h, and axillary, inguinal and mesenteric LN extracted and cells isolated. Cell accumulation in spleen, a chemokine-independent process, was determined as control [8]. Flow cytometry analysis indicated a slight reduction in naïve T cell homing after JAK1 or JAK2 knockdown, with no differences between cells in spleen (Fig. 3A).

We simultaneously nucleofected naïve T cells with siRNA pools for JAK1 and JAK2 (siJAK1,2) or with siRNA control, and determined their ability to home to LN. siJAK1,2 and sicontrol cells were fluorescently labeled with CMTMR and CMFDA, respectively. A 1:1 siJAK1,2:sicontrol cell mixture was injected i.v. into C56BL/6 mice; after 6 h, mice were killed, spleen and LN extracted, and cells isolated. Flow cytometry analysis showed a siJAK1,2:sicontrol ratio of 33.53 ± 0.2% to 66.46 ± 0.2%, indicating a siJAK1,2 cell defect in reaching LN (Fig. 3B). Results were similar when siJAK1,2 cells were labeled with CMFDA and sicontrols with CMTMR (not shown). As homing data at 6 h might be altered by cell proliferation, death or lymphocyte egress [19], we repeated the experiment at 3 h post-cell injection. Flow cytometry analysis showed a siJAK1,2:sicontrol ratio of 30.12 ± 0.1% to 69.87 ± 0.2%, confirming the siJAK1,2 cell defect in LN homing (Fig. 3B). When cells in the spleen were evaluated, the initial ratio was unchanged (47.1 ± 0.3% to 52.9 ± 0.2% at 6 h; 48.3 ± 0.1% to 51.7 ± 0.3% at 3 h), indicating similar siJAK1,2 and sicontrol cell accumulation (Figure 3B). The data indicated that simultaneous downregulation of JAK1 and JAK2 specifically reduced naïve T cell homing to LN, suggesting redundancy between these two kinases, as observed in the *in vitro* migration experiments.

Using RT-PCR analysis, we tested whether the siJAK1,2 cell fraction in LN continued to express reduced JAK levels. siJAK1,2 and sicontrol cells were labeled, mixed and injected into recipient mice as above. LN were extracted after 6 h, cells isolated, the siJAK1,2:sicontrol mixture separated by cell sorting, and JAK1 and JAK2 levels analyzed by RT-PCR and compared to those of cells before injection. siJAK1,2 cells showed reduced JAK1 and JAK2 mRNA levels compared to controls (Fig. 3C), while CXCR4 or JAK3 mRNA levels (control) did

not differ significantly between cell types. The data indicate that reduction of JAK1/2 levels alters the ability of naïve T cells to enter LN.

Naïve T cells with reduced JAK1 and JAK2 levels show normal intranodal localization and dynamics

We tested whether reduction of JAK levels altered intranodal localization of naïve T cells. A 1:1 mixture of green-labeled siJAK1,2:orange-sicontrol cells was injected i.v. into recipient mice; after 6 h, LN were isolated and cryopreserved for immunohistological analysis. Evaluation confirmed lower siJAK1,2 cell numbers compared to sicontrols, with no difference between the two cell types in intranodal cell localization (Fig. 4A, B). These findings indicate that combined reduction of JAK1 and JAK2 affects homing of naïve T cells, but not their intranodal localization.

We studied siJAK1,2 cell dynamics in LN using two-photon microscopy. Adoptive transfer of a 1:1:1 mixture of wt (non-nucleofected) naïve T cells with siJAK1,2 and sicontrol T cells into C56BL/6 mice was followed after 45 min by i.v. injection of Alexa633-Meca-79 to identify HEV (supplemental video 1). After 15 min, mice were anesthetized and PLN exposed for two-photon laser scanning microscopy. Cells were tracked within the lymphoid parenchyma for 30-min periods. Data evaluation indicated that siJAK1,2 and sicontrol cell dynamics were indistinguishable, as shown by determination of meandering index (displacement/path length; 0.50 ± 0.01 siJAK1,2; 0.45 ± 0.01 sicontrol; 0.46 ± 0.01 wt) and mean velocity values (9.71 ± 0.2 μm/min siJAK1,2; 9.07 ± 0.2 μm/min sicontrol; 9.19 ± 0.2 μm/min wt) (Fig. 4C, D).

The results indicate that although JAK1 and JAK2 reduction altered the ability of naïve T cells to enter LN, once inside, reduced levels of these kinases did not alter cell dynamics.

JAK1 and JAK2 contribute to chemokine-mediated naïve T cell adhesion

Extravasation from the bloodstream is initiated by selectin-mediated cell rolling [20], followed by chemokine-mediated integrin activation [21, 22]. Integrin binding to ligands expressed at the endothelium [23] triggers firm adhesion of rolling lymphocytes to HEV. We thus tested siJAK1,2 and sicontrol cell resistance to shear stress using ICAM-1+CXCL12- or ICAM-1+CCL21-coated fluid chambers. On ICAM-1+CXCL12-coated plates, siJAK1,2 cells detached more readily than sicontrols at increased shear stress (0.5 dyne/cm^2) (75% siJAK1,2 vs. 40% sicontrol; Fig. 5A, left). The effect was similar on ICAM-1+CCL21-coated plates (50% siJAK1,2 vs. 30% sicontrol; Fig. 5A, right). These findings suggest that under shear stress, JAK1/JAK2 reduction affected chemokine-induced integrin activation in naïve T cells, although the extent of this effect depended on the chemokine tested.

As naïve T cells respond to CXCL12 and CCL21 in *in vitro* cell adhesion assays [8], we performed static adhesion assays to test the ability of siJAK1,2 cells to adhere to recombinant ICAM-1-Fc-coated plates, alone or with CXCL12 or CCL21. The sicontrol cells adhered to ICAM-1 in response to either ligand, whereas siJAK1,2 cell adhesion was severely impaired after CXCL12 or CCL21 stimulation (Fig. 5B). Both siJAK1,2 and sicontrol cells showed similar membrane LFA-1 expression levels in flow cytometry studies (Fig. 5C) and adhered similarly to ICAM-1 in response to the integrin activator $MnCl_2$ (Fig. 5B). Combined JAK1 and JAK2 reduction thus affected neither cell surface LFA-1 levels nor its activation by non-specific stimuli, but severely reduced its chemokine-mediated activation.

We confirmed these results by interference reflection microscopy (IRM), using a model based on artificial planar lipid bilayers containing ICAM-1 and coated with chemokines [24]. Whereas sicontrol cells adhered normally to ICAM-1 in the presence of CXCL12 or CCL21, siJAK1,2 cell adhesion was significantly reduced; there were no marked differences in basal adhesion between sicontrol and siJAK1,2 cells (Fig. 5D). To determine whether this effect is dependent on integrin

type, we performed a similar experiment using membranes coated with VCAM-1, the ligand for VLA-4. The data showed that siJAK1,2 cell adhesion was also reduced in the presence of either chemokine compared to sicontrol cells (Fig. 5E). As for ICAM-1, basal adhesion to VCAM-1 was similar for both cell types.

These results indicated a defect in the chemokine-triggered signaling cascade that activates integrins in siJAK1,2 cells. To confirm this observation, we evaluated whether siJAK1,2 and sicontrol cells adhered to ICAM-1 in response to a TCR (T cell receptor) signal, and found that after pretreatment with anti-CD3ε mAb, both cell types adhered similarly to ICAM-1-containing planar lipid bilayers (Fig. 5D). Our results confirm JAK1/2 involvement in chemokine signaling, and suggest a role for JAK in the chemokine-mediated integrin activation necessary for naïve T cell extravasation across HEV.

JAK1 and JAK2 participate in chemokine-induced actin polymerization in naïve T cells

The actin cytoskeleton is an essential structure for cell adhesion. CXCR4-mediated integrin activation involves proteins that participate in actin polymerization, including talin [25]. To test whether chemokine-mediated actin polymerization is affected by reduced JAK1 and JAK2 levels, we activated siJAK1,2 and sicontrol cells with CXCL12 or CCL21 and analyzed F-actin polymerization by phalloidin staining and flow cytometry. In controls, F-actin polymerization induced by both chemokines was rapid and transient, whereas in siJAK1,2 cells it was reduced (Fig. 6A, B); this reduction was not significant in siJAK1 or siJAK2 cells (Fig. 6A, B). These results confirm a compensatory mechanism between JAK1 and JAK2, and suggest that their reduction alters chemokine-mediated actin polymerization.

ERM proteins link the actin cytoskeleton directly to the plasma membrane [26]. Evidence shows that chemokine stimulation of human peripheral blood T lymphocytes induces rapid, transient dephosphorylation of ERM, facilitating loss of cell microvilli and polarization [27]. We

examined ERM phosphorylation in siJAK1,2 and sicontrol cells activated with CXCL12 (50 nM) or CCL21 (100 nM) at various times before lysis. Lysates were studied by Western blot using specific anti-P-ERM antibodies. Whereas chemokines triggered rapid, transient ERM dephosphorylation in sicontrol cells (maximum at 1 min), they did not alter ERM phosphorylation in siJAK1,2 cells (Fig. 6C, Supporting Fig. 1). The data indicate JAK1 and JAK2 involvement in chemokine-mediated actin cytoskeleton remodeling, which in turn facilitates integrin activation.

Although polarized structures can differ from cell to cell, there is evidence that cell polarization depends on the actin cytoskeleton and involves the ERM proteins [28]. In view of the differences in chemokine-mediated ERM activation and actin polymerization in siJAK1,2 cells, we evaluated uropod formation in these cells. siJAK1,2 and sicontrol cells were activated in suspension with CXCL12 (50 nM, 15 min, 37ºC) and immediately plated on fibronectin-coated chamber slides (30 min, 37ºC) and fixed. Quantitation of cells labeled with biotinylated-CD44 mAb showed significantly less CXCL12-mediated uropod formation in siJAK1,2 cells than in controls (Fig. 6D).

To rule out a general defect in chemokine signaling pathways due to JAK1 and JAK2 reduction, siJAK1,2 and sicontrol cells were activated with CXCL12 (50 nM) or CCL21 (100 nM) and lysed, and cell extracts analyzed in Western blot using anti-P-ERK1/2 antibodies. Reduced JAK kinase levels did not affect ERK1/2 activation (Fig. 6E, Supporting Fig. 2). The results showed that JAK blockade does not interfere with all signaling cascades, but is specific for chemokine-mediated integrin activation.

Discussion

The JAK/STAT pathway is crucial for type I and II cytokine receptor function, but also participates in the signaling triggered by growth factors and protein tyrosine kinase receptors [29], and by GPCR [30, 31]. Studies using chemical inhibitors, mutant cell lines, primary cells and JAK3-deficient mice report JAK involvement in many chemokine-mediated functions [12, 14, 32]. We studied combined reduction of JAK1 and JAK2 expression in naïve T cells and found impaired *in vitro* cell migration in response to CXCL12 and CCL21; migration was unaffected when JAK1 or JAK2 levels were altered independently. This JAK1 and JAK2 redundancy in the case of chemokine receptors contrasts with the JAK specificity observed for cytokine receptors.

Chemokine activation of JAK has long been debated. Whereas some groups show that JAK have an important role in chemokine function [9, 10, 12], others suggest that chemokine signaling is JAK-independent [15]. These differences were initially attributed to the use of distinct cell systems or to non-specific chemical antagonists. Several reports nonetheless indicate that other GPCR, including those for thyrotropin-secreting hormone [31], serotonin [33], and angiotensin [34] also activate the JAK/STAT pathway. In contrast to the effect of cytokine receptors, GPCR-triggered JAK activation is transient, and JAK/GPCR association takes place through non-specific amino acid sequences on the receptor [30, 31].

Naïve T cells with silenced JAK1/JAK2 expression (~60% reduction compared to controls) showed markedly reduced homing to LN, which correlated with defects in *in vitro* CCL21-mediated siJAK1,2 cell migration. Lymphocyte homing is CCR7-dependent; mice lacking CCR7 ($CCR7^{-/-}$) or its specific ligands CCL19 and CCL21 (*plt/plt* mice) show severe defects in cell homing to LN and in intranodal organization [6, 35-37]. CCR7 ligands are necessary and

sufficient to induce LFA-1-dependent arrest of T cells at the HEV, as LFA-1-mediated T cell arrest is restored in *plt/plt* PLN injected intracutaneously with CCL21 [38].

In *in vitro* assays, we also observed impaired CXCL12-mediated siJAK1,2 cell migration. CXCL12 is expressed by stromal cells, is found in the lumen of some HEV, and participates in B cell homing to LN [39]. It nonetheless has no direct role in naïve T cell homing to LN, but facilitates CCL21-mediated homing [7]. In LN from C57BL/6 mice adoptively transferred with nucleofected naïve T cells, we detected fewer siJAK1,2 than control cells, which continued to show low JAK1 and JAK2 mRNA levels. Although reduced JAK1 and JAK2 levels altered the ability of naïve T cells to enter LN, some of these cells were able to extravasate. Other JAK proteins might participate in CCR7-mediated responses; for example, JAK3-deficient T lymphocytes have an intrinsic defect in CCR7-mediated homing to PLN [32], although a defect in very early T cell development in these mice [40] render interpretation of these findings difficult.

The intranodal dynamics of siJAK1,2 cells was normal in the adoptively transferred mice. Intranodal movement is in part CCR7-dependent, and CCR7 signaling affects T lymphocyte basal velocity within the T cell area of non-inflamed LN [41, 42]. These observations and our finding of altered *in vitro* CCR7-triggered chemotaxis of siJAK1,2 cells suggest that other molecules might also participate in intranodal motility. Similar loss-of-function strategies were used to determine that LFA-1 is not necessary for leukocyte migration in the LN interstitial space [43, 44]. In *in vitro* chemotaxis experiments performed in the absence of the ICAM-1 integrin substrate, we found that siJAK1,2 cells migrated normally towards CCL21 (Supporting Fig. 3). JAK pathway involvement in chemokine-mediated integrin activation is thus plausible.

Studies using LFA-1-blocking antibody [45] and LFA-1-deficient mice [46] showed that lymphocyte homing to LN is critically dependent on LFA-1, and intravital microscopy analyses

indicated that LFA-1 inhibitors block intravascular lymphocyte arrest on HEV [47, 48]. Our static adhesion experiments and artificial planar lipid bilayer assays showed that whereas control cells responded equally to CCL21 or CXCL12 stimulation, chemokine-mediated LFA-1 and VLA-4 activation was significantly reduced in siJAK1,2 cells. The effect on chemokine signaling is specific, as siJAK1,2 cells adhere normally after TCR stimulation using an anti-CD3ε mAb. The sicontrol cell resistance to shear stress induced by CXCL12- or CCL21-mediated adhesion was greatly reduced in siJAK1,2 cells. These data indicate JAK1 and JAK2 involvement in the chemokine-mediated signaling cascade that leads to integrin activation, although we cannot completely discard other possibilities; for example, these kinases also participate in the integrin-triggered signaling [49]. Chemokine involvement in triggering integrin activation is studied extensively [50], and there is evidence of a role for tyrosine kinases in this process [51].

Chemokines modulate actin cytoskeleton polymerization/depolymerization [52], a process implicated not only in cell migration, but also in chemokine-mediated integrin activation [25, 53]. In our sicontrol cells, CCL21 and CXCL12 promoted F-actin polymerization, which was greatly reduced in siJAK1,2 cells. JAK1/JAK2 thus link chemokine signaling with the actin cytoskeleton, suggesting a connection between both signaling events in integrin activation. In Drosophila, the JAK/STAT pathway controls actomyosin network assembly [54]. Talin and kindlins, two cytoskeletal proteins involved in CXCR4-mediated integrin activation and/or chemotaxis [53, 55], have a FERM domain with binding sites for several integrin beta subunits [56]. JAK proteins also have a FERM motif [57], associating these tyrosine kinases to the ERM complex and thus to the actin cytoskeleton. In siJAK1,2 cells, we also found that activation of either CXCL12 or CCL21 impaired ERM dephosphorylation, a signaling event that facilitates cytoskeletal reorganization and lymphocyte recruitment [27]. We observed defective CXCL2-

mediated uropod formation in siJAK1,2 cells, in accordance with the active role of ERM proteins and actin cytoskeleton in cell polarization [28]. Direct interaction between the JAK FERM domain and integrins is also possible, however, as the FERM domains are implicated in focal adhesion kinase (FAK) and JAK increase at contact points between the cell and the extracellular matrix [58].

Chemokines participate in many cell functions, including integrin activation, cell polarization, migration and survival, as well as in T cell co-stimulation, by activating a plethora of signaling molecules such as G proteins, MAPK, PI3K, small GTPases, PLC [59] and, as we show here, JAK proteins. At difference from the strong dependence of cytokine signaling on JAK, we found that some chemokine responses are JAK-dependent, whereas others are JAK-independent. CXCL12- and CCL21-triggered ERK1/2 activation was unaffected in siJAK1,2 cells. Specific blockade of JAK binding to chemokine receptors might thus be a means of interfering with immune cell recruitment to inflamed areas without inhibiting cytokine-mediated functions; such a strategy could bypass the undesirable effects associated with systemic JAK blockade.

Materials and methods

Mice

Male and female 4- to 6-week-old C57BL/6 mice were purchased from Harlan Laboratories. Mice were housed in pathogen-free conditions at the animal facility of the Centro Nacional de Biotecnología/CSIC. All animal experiments were approved by the appropriate Ethics Committees and carried out according to national and European Union guidelines.

Cell culture and siRNA nucleofection

Naïve T cells were obtained from C57BL/6 mouse spleen and LN, and purified by negative selection using a mouse T cell negative isolation kit (Dynal); T cell purity was routinely >97%. Freshly isolated murine T cells were nucleofected with a mixture (2 μM/3 x 10^6 cells/100 μl) of four individual duplexes siRNA (ON-TARGETplus SMARTpool siRNA; Dharmacon) for the target sequences on JAK1 (GAAAAUGAAUUGAGUCGAU; GAAAUCACCCACAUUGUAA; CGCAUGAGGUUCUACUUUA; GCACAGGGACAGUAUGAUU), JAK2 (AAUAGGAGAC UUCGGAUUA; GAAUUGUAACUGUCCAUAA; GAACUUAGCUCAUUAAAAG; GAAUU UAUGCGAAUGAUUG), or siRNA control (ON-TARGETplus Non-targeting Pool D-001810-10; Dharmacon), to ensure silencing specificity, using the mouse T cell Nucleofector Kit (Amaxa). Nucleofection efficiency was controlled with fluorescent labeled siRNA duplex siGLO Green indicator (Dharmacon) as a positive control. Nucleofected naïve T cells were incubated (24 h, 37ºC) in complete RPMI 1640 medium containing mIL7 (25 U/ml; Cell Signaling).

Antibodies and reagents

For western blot assays, the following antibodies were used: anti-JAK1 antibody (Ab) (Santa Cruz), -JAK2 Ab (Upstate Biotechnology), anti-P-ERM and -ERM antibodies (Cell Signaling), anti-P-ERK1/2 and -ERK1/2 Ab (Santa Cruz) and anti-β-tubulin mAb (Sigma). Horseradish peroxidase (HRP)-labeled anti-mouse and -rabbit Ig (Dako) and Alexa647-goat anti-mouse

(Invitrogen) were used as secondary antibodies in Western blot assays. The anti-PNAd antibody (Alexa-633-Meca-79) was purified from hybridoma supernatant (Nanotools) and fluorescent-labeled in our laboratory. Purity of naïve T cells was assessed by flow cytometry using anti-B220 mAb and -Gr1 (BD Pharmingen), and chemokine receptor expression using biotin-anti-mouse CXCR4 (CD184, fusin) and CCR7 (CD197, EBI-1) (BD Biosciences). Surface marker expression was determined by flow cytometry using fluorochrome-labeled antibodies to CD3, CD4, CD8, CD62L, CD44 and CD69 (Beckman Coulter), CD25 (BD Pharmingen) and LFA-1 (BioLegend). Anti-CD3ε mAb was used for cell adhesion experiments (2C11, BD Pharmingen). CCL21 and CXCL12 were purchased from Peprotech.

Adoptive transfer and in vivo T cell homing

Naïve T cells from C57BL/6 mice (20 x10^6 $CD3^+$ cells/mouse) were nucleofected as above with siRNA pools for JAK1, JAK2, a mixture of siRNA pools for JAK1+JAK2, or siRNA pool control (Dharmacon). Viable lymphocytes (~63% of initial cells) were recovered 24 h after density gradient centrifugation (Cedarlane Laboratories). Cells (10^7 cells/ml) were then stained with CMFDA (0.3 μM) or CMTMR (1.5 μM; both 45 min, 37ºC; Invitrogen) and cell mixtures (1:1 green:orange; total 10^7 cells/200 μl) were injected intravenously into 3-month-old C57BL/6 mice. Mice were killed after 3 h or 6 h for spleen, inguinal (ILN), axillary (ALN) and mesenteric lymph node (MLN) removal, and fluorophore-labeled cells counted by flow cytometry. For 3 h analysis, cells from all LN were pooled. Some ILN and ALN were snap-frozen in Tissue-Tek (Sakura) for immunohistological analysis. Flow cytometry was performed on a Cytomics FC500 (Beckman Coulter).

Lymphocyte polarization assay

Sicontrol or siJAK1,2 cells (5 x 10^6 cells/ml) were stimulated in suspension with 50 nM CXCL12 (15 min, 37ºC), plated on fibronectin-coated chamber slides and incubated (30 min, 37ºC). Cells

where then fixed with 4% paraformaldehyde (5 min, 37ºC) and stained with biotinylated anti-CD44 mAb (BD Pharmingen) followed by Cy3-streptavidin (Jackson ImmunoRes.). Fluorescence was visualized on a confocal Zeiss Axiovert LSM 510-META inverted microscope with a 40x oil immersion objective. T cell polarization was determined and expressed as the percentage of the ratio of $CD44^+$ staining at the uropod vs. total cells counted.

Two-photon laser scanning microscopy of popliteal lymph nodes

Freshly isolated murine T cells were nucleofected with siRNA pools for JAK1 and JAK2 (siJAK1,2 cells) target sequences or siRNA pool control (sicontrol cells) as above. siJAK1,2 cells were then stained with CMTMR, wild-type cells (untreated) with CMAC (Cell Tracker Blue; Invitrogen) and sicontrol cells with CFSE (green; Invitrogen). Cells were mixed (1:1:1 green:orange:blue; total 2 x 10^7 cells/200 μl) and injected into 6-12-weeks-old C57BL/6 mice as above. After 6 h, a PLN in an anesthetized mouse was prepared essentially as described [60]. At 20 min before recording, 15-20 μg Alexa633-Meca-79 was injected intravenously to label the HEV network. Two-photon laser scanning microscopy was performed with an Olympus BX50WI fluorescence microscope equipped with a 20X objective and a TrimScope 2PM system controlled by Imspector software (LaVision Biotec). For two-photon excitation, a Ti:sapphire laser (Mai Tai HP; Spectra-Physics) was tuned to 780 or 840 nm and 200 x 200 x 40-60 μm stacks recorded with 4 μm z-steps at 20 sec intervalls. For T cell tracking experiments, cell motility parameters were calculated from x, y and z coordinates of cell centroids using Volocity software (Improvision).

Adhesion assay on artificial planar lipid bilayers

Planar lipid bilayers of 1,2-dioleoyl-PC (DOPC) lipids (Avanti Polar Lipids) containing unlabeled GPI (glycosylphosphatidyl inositol)-linked ICAM-1 or GPI-linked VCAM-1 (150

molecules/μm^2) were formed as described [24, 61], blocked (PBS-2% FCS, 1 h), followed by coating with recombinant murine CCL21 or CXCL12 (both at 100 nM; Peprotech) at room temperature. Nucleofected naïve T cells (2×10^6) were injected into the warmed (37ºC) chamber; after 10 min incubation, DIC and IRM images were acquired on a Zeiss Axiovert LSM 510-META inverted microscope with a 40x oil immersion objective. When required, nucleofected naïve T cells were pre-incubated with anti-CD3ε mAb (1μm/ml, 2C11, BD Pharmingen) for 30 min at 37ºC, washed, and allowed to settle on ICAM-1-containing planar lipid bilayers in absence of chemokine. Assays were performed in PBS 0.5% FCS, 2 mM Mg^{2+}, 0.5 mM Ca^{2+}, 1 g/l D-glucose at 37ºC. Images were analyzed with ImageJ software to determine T cell adhesion frequency (IRM-positive cells).

Statistical analysis

Statistical analysis was performed with Prism software (GraphPad) by applying the non-parametric Mann-Whitney test, or when necessary, the One-way ANOVA, Kruskal-Wallis test.

ACKNOWLEDGMENTS

We thank Dr M Thelen for critical reading of the manuscript, L Gómez for animal handling, MC Moreno-Ortíz and S Escudero for help with flow cytometry analysis, R Villares for help with microscope images, and C Bastos and C Mark for secretarial and editorial assistance, respectively. GP is supported by a contract from the Spanish Ministry of Health Fondo de Investigaciones Sanitarias de la Seguridad Social (FISS). This work was supported in part by grants from the Spanish Ministry of Science and Innovation (SAF 2011-27370 for MM and BFU2011-30097 for YRC), the FISS (RD08/0075/0010 and RD12/0009/0009), the Comunidad de Madrid (S2010/BMD-2350), Fundación Genoma España and the European Union (FP7-integrated project Masterswitch 223404).

References

1 **Ihle, J.N.,** Cytokine receptor signalling. *Nature* 1995. **377**: 591-594.

2 **O'Shea, J.J., Gadina, M. and Schreiber, R.D.,** Cytokine signaling in 2002: new surprises in the Jak/Stat pathway. *Cell* 2002. **109 Suppl**: S121-131.

3 **Levy, D.E. and Darnell, J.E., Jr.,** Stats: transcriptional control and biological impact. *Nature reviews. Mol Cell Biol* 2002. **3**: 651-662.

4 **Rot, A. and von Andrian, U.H.,** Chemokines in innate and adaptive host defense: basic chemokinese grammar for immune cells. *Ann Rev Immunol* 2004. **22**: 891-928.

5 **Campbell, J.J. and Butcher, E.C.,** Chemokines in tissue-specific and microenvironment-specific lymphocyte homing. *Curr Opin Immunol* 2000. **12**: 336-341.

6 **Forster, R., Schubel, A., Breitfeld, D., Kremmer, E., Renner-Muller, I., Wolf, E. and Lipp, M.,** CCR7 coordinates the primary immune response by establishing functional microenvironments in secondary lymphoid organs. *Cell* 1999. **99**: 23-33.

7 **Bai, Z., Hayasaka, H., Kobayashi, M., Li, W., Guo, Z., Jang, M.H., Kondo, A., Choi, B.I., Iwakura, Y. and Miyasaka, M.,** CXC chemokine ligand 12 promotes CCR7-dependent naive T cell trafficking to lymph nodes and Peyer's patches. *J Immunol* 2009. **182**: 1287-1295.

8 **Scimone, M.L., Felbinger, T.W., Mazo, I.B., Stein, J.V., Von Andrian, U.H. and Weninger, W.,** CXCL12 mediates CCR7-independent homing of central memory cells, but not naive T cells, in peripheral lymph nodes. *Journal Exp Med* 2004. **199**: 1113-1120.

9 **Wong, M., Uddin, S., Majchrzak, B., Huynh, T., Proudfoot, A.E., Platanias, L.C. and Fish, E.N.,** Rantes activates Jak2 and Jak3 to regulate engagement of multiple signaling pathways in T cells. *J Biol Chem* 2001. **276**: 11427-11431.

10 **Wong, M. and Fish, E.N.,** RANTES and MIP-1alpha activate stats in T cells. *J Biol Chem* 1998. **273**: 309-314.

11 **Soldevila, G., Licona, I., Salgado, A., Ramirez, M., Chavez, R. and Garcia-Zepeda, E.,** Impaired chemokine-induced migration during T-cell development in the absence of Jak 3. *Immunology* 2004. **112**: 191-200.

12 **Vila-Coro, A.J., Rodriguez-Frade, J.M., Martin De Ana, A., Moreno-Ortiz, M.C., Martinez, A.C. and Mellado, M.,** The chemokine SDF-1alpha triggers CXCR4 receptor dimerization and activates the JAK/STAT pathway. *FASEB J* 1999. **13**: 1699-1710.

13 **Soriano, S.F., Serrano, A., Hernanz-Falcon, P., Martin de Ana, A., Monterrubio, M., Martinez, C., Rodriguez-Frade, J.M. and Mellado, M.,** Chemokines integrate JAK/STAT and G-protein pathways during chemotaxis and calcium flux responses. *Eur J Immunol* 2003. **33**: 1328-1333.

14 **Stein, J.V., Soriano, S.F., M'Rini, C., Nombela-Arrieta, C., de Buitrago, G.G., Rodriguez-Frade, J.M., Mellado, M., Girard, J.P. and Martinez, A.C.,** CCR7-mediated physiological lymphocyte homing involves activation of a tyrosine kinase pathway. *Blood* 2003. **101**: 38-44.

15 **Moriguchi, M., Hissong, B.D., Gadina, M., Yamaoka, K., Tiffany, H.L., Murphy, P.M., Candotti, F. and O'Shea, J.J.,** CXCL12 signaling is independent of Jak2 and Jak3. *J Biol Chem* 2005. **280**: 17408-17414.

16 **Rodig, S.J., Meraz, M.A., White, J.M., Lampe, P.A., Riley, J.K., Arthur, C.D., King, K.L., Sheehan, K.C., Yin, L., Pennica, D., Johnson, E.M., Jr. and Schreiber, R.D.,** Disruption of the Jak1 gene demonstrates obligatory and nonredundant roles of the Jaks in cytokine-induced biologic responses. *Cell* 1998. **93**: 373-383.

17 **Neubauer, H., Cumano, A., Muller, M., Wu, H., Huffstadt, U. and Pfeffer, K.,** Jak2 deficiency defines an essential developmental checkpoint in definitive hematopoiesis. *Cell* 1998. **93**: 397-409.

18 **O'Shea, J.J., Husa, M., Li, D., Hofmann, S.R., Watford, W., Roberts, J.L., Buckley, R.H., Changelian, P. and Candotti, F.,** Jak3 and the pathogenesis of severe combined immunodeficiency. *Mol Immunol* 2004. **41**: 727-737.

19 **Cyster, J.G. and Schwab, S.R.,** Sphingosine-1-phosphate and lymphocyte egress from lymphoid organs. *Annu Rev Immunol* 2012. **30**: 69-94.

20 **Alon, R. and Dustin, M.L.,** Force as a facilitator of integrin conformational changes during leukocyte arrest on blood vessels and antigen-presenting cells. *Immunity* 2007. **26**: 17-27.

21 **Ley, K., Laudanna, C., Cybulsky, M.I. and Nourshargh, S.,** Getting to the site of inflammation: the leukocyte adhesion cascade updated. *Nat Rev Immunol* 2007. **7**: 678-689.

22 **Shamri, R., Grabovsky, V., Gauguet, J.M., Feigelson, S., Manevich, E., Kolanus, W., Robinson, M.K., Staunton, D.E., von Andrian, U. H. and Alon, R.,** Lymphocyte arrest requires instantaneous induction of an extended LFA-1 conformation mediated by endothelium-bound chemokines. *Nat Immunol* 2005. **6**: 497-506.

23 **Anthis, N.J. and Campbell, I.D.,** The tail of integrin activation. *Trends Biochem Sci* 2011. **36**: 191-198.

24 **Saez de Guinoa, J., Barrio, L., Mellado, M. and Carrasco, Y.R.,** CXCL13/CXCR5 signaling enhances BCR-triggered B-cell activation by shaping cell dynamics. *Blood* 2011. **118**: 1560-1569.

25 **Burkhardt, J.K., Carrizosa, E. and Shaffer, M.H.,** The actin cytoskeleton in T cell activation. *Ann Rev Immunol* 2008. **26**: 233-259.

26 **Bretscher, A., Edwards, K. and Fehon, R.G.,** ERM proteins and merlin: integrators at the cell cortex. *Nature reviews. Mol Cell Biol* 2002. **3**: 586-599.

27 **Brown, M.J., Nijhara, R., Hallam, J.A., Gignac, M., Yamada, K.M., Erlandsen, S. L., Delon, J., Kruhlak, M. and Shaw, S.,** Chemokine stimulation of human peripheral blood T lymphocytes induces rapid dephosphorylation of ERM proteins, which facilitates loss of microvilli and polarization. *Blood* 2003. **102**: 3890-3899.

28 **Gautreau, A., Louvard, D. and Arpin, M.,** ERM proteins and NF2 tumor suppressor: the Yin and Yang of cortical actin organization and cell growth signaling. *Curr Opin Cell Biol* 2002. **14**: 104-109.

29 **Nicolas, C.S., Peineau, S., Amici, M., Csaba, Z., Fafouri, A., Javalet, C., Collett, V.J., et al.,** The Jak/STAT pathway is involved in synaptic plasticity. *Neuron* 2012. **73**: 374-390.

30 **Ali, M.S., Sayeski, P.P., Dirksen, L.B., Hayzer, D.J., Marrero, M.B. and Bernstein, K.E.,** Dependence on the motif YIPP for the physical association of Jak2 kinase with the intracellular carboxyl tail of the angiotensin II AT1 receptor. *J Biol Chem* 1997. **272**: 23382-23388.

31 **Park, E.S., Kim, H., Suh, J.M., Park, S.J., You, S.H., Chung, H.K., Lee, K.W., et al.,** Involvement of JAK/STAT (Janus kinase/signal transducer and activator of transcription) in the thyrotropin signaling pathway. *Mol Endocrinol* 2000. **14**: 662-670.

32 **Garcia-Zepeda, E.A., Licona-Limon, I., Jimenez-Solomon, M.F. and Soldevila, G.,** Janus kinase 3-deficient T lymphocytes have an intrinsic defect in CCR7-mediated homing to peripheral lymphoid organs. *Immunology* 2007. **122**: 247-260.

33 **Guillet-Deniau, I., Burnol, A.F. and Girard, J.,** Identification and localization of a skeletal muscle secrotonin 5-HT2A receptor coupled to the Jak/STAT pathway. *The J Biol Chem* 1997. **272**: 14825-14829.

34 **Marrero, M.B., Venema, V.J., Ju, H., Eaton,D. C. and Venema, R.C.,** Regulation of angiotensin II-induced JAK2 tyrosine phosphorylation: roles of SHP-1 and SHP-2. *Am J Physiol* 1998. **275**: C1216-1223.

35 **Gunn, M.D., Kyuwa, S., Tam, C., Kakiuchi, T., Matsuzawa, A., Williams, L.T. and Nakano, H.,** Mice lacking expression of secondary lymphoid organ chemokine have defects in lymphocyte homing and dendritic cell localization. *J Exp Med* 1999. **189**: 451-460.

36 **Mori, S., Nakano, H., Aritomi, K., Wang, C.R., Gunn, M.D. and Kakiuchi, T.,** Mice lacking expression of the chemokines CCL21-ser and CCL19 (plt mice) demonstrate delayed but enhanced T cell immune responses. *J Exp Med* 2001. **193**: 207-218.

37 **Ohl, L., Henning, G., Krautwald, S., Lipp, M., Hardtke, S., Bernhardt, G., Pabst, O. and Forster, R.,** Cooperating mechanisms of CXCR5 and CCR7 in development and organization of secondary lymphoid organs. *J Exp Med* 2003. **197**: 1199-1204.

38 **Stein, J.V., Rot, A., Luo, Y., Narasimhaswamy, M., Nakano, H., Gunn, M.D., Matsuzawa, A., et al.,** The CC chemokine thymus-derived chemotactic agent 4 (TCA-4, secondary lymphoid tissue chemokine, 6Ckine, exodus-2) triggers lymphocyte function-associated antigen 1-mediated arrest of rolling T lymphocytes in peripheral lymph node high endothelial venules. *J Exp Med* 2000. **191**: 61-76.

39 **Okada, T., Ngo, V.N., Ekland, E.H., Forster, R., Lipp, M., Littman, D.R. and Cyster, J.G.,** Chemokine requirements for B cell entry to lymph nodes and Peyer's patches. *J Exp Med* 2002. **196**: 65-75.

40 **Baird, A.M., Lucas, J.A. and Berg, L.J.,** A profound deficiency in thymic progenitor cells in mice lacking Jak3. *J Immunol* 2000. **165**: 3680-3688.

41 **Worbs, T., Mempel, T.R., Bolter, J., von Andrian, U.H. and Forster, R.,** CCR7 ligands stimulate the intranodal motility of T lymphocytes in vivo. *J Exp Med* 2007. **204**: 489-495.

42 **Cyster, J.G.,** Chemokines, sphingosine-1-phosphate, and cell migration in secondary lymphoid organs. *Ann Rev Immunol* 2005. **23**: 127-159.

43 **Woolf, E., Grigorova, I., Sagiv, A., Grabovsky, V., Feigelson, S. W., Shulman, Z., Hartmann, T., Sixt, M., Cyster, J.G. and Alon, R.,** Lymph node chemokines promote sustained T lymphocyte motility without triggering stable integrin adhesiveness in the absence of shear forces. *Nat Immunol* 2007. **8**: 1076-1085.

44 **Lammermann, T., Bader, B.L., Monkley, S.J., Worbs, T., Wedlich-Soldner, R., Hirsch, K., Keller, M., Forster, R., Critchley, D.R., Fassler, R. and Sixt, M.,** Rapid leukocyte migration by integrin-independent flowing and squeezing. *Nature* 2008. **453**: 51-55.

45 **Hamann, A., Jablonski-Westrich, D., Duijvestijn, A., Butcher, E.C., Baisch, H., Harder, R. and Thiele, H.G.,** Evidence for an accessory role of LFA-1 in lymphocyte-high endothelium interaction during homing. *J Immunol* 1988. **140**: 693-699.

46 **Berlin-Rufenach, C., Otto, F., Mathies, M., Westermann, J., Owen, M. J., Hamann, A. and Hogg, N.,** Lymphocyte migration in lymphocyte function-associated antigen (LFA)-1-deficient mice. *J Exp Med* 1999. **189**: 1467-1478.

47 **Warnock, R.A., Askari, S., Butcher, E.C. and von Andrian, U.H.,** Molecular mechanisms of lymphocyte homing to peripheral lymph nodes. *J Exp Med* 1998. **187**: 205-216.

48 **Shimaoka, M., Lu, C., Palframan, R.T., von Andrian, U.H., McCormack, A., Takagi, J. and Springer, T.A.,** Reversibly locking a protein fold in an active conformation with a disulfide bond: integrin alphaL I domains with high affinity and antagonist activity in vivo. *Proc Nat Acad Sci USA* 2001. **98**: 6009-6014.

49 **Brizzi, M.F., Defilippi, P., Rosso, A., Venturino, M., Garbarino, G., Miyajima, A., Silengo, L., Tarone, G. and Pegoraro, L.,** Integrin-mediated adhesion of endothelial cells induces JAK2 and STAT5A activation: role in the control of c-fos gene expression. *Mol Biol Cell* 1999. **10**: 3463-3471.

50 **Kliche, S., Worbs, T., Wang, X., Degen, J., Patzak, I., Meineke, B., Togni, M., et al.,** CCR7-mediated LFA-1 functions in T cells are regulated by 2 independent ADAP/SKAP55 modules. *Blood* 2012. **119**: 777-785.

51 **Garcia-Bernal, D., Parmo-Cabanas, M., Dios-Esponera, A., Samaniego, R., Hernan, P. de la Osa D. and Teixido, J.,** Chemokine-induced Zap70 kinase-mediated dissociation of the Vav1-talin complex activates alpha4beta1 integrin for T cell adhesion. *Immunity* 2009. **31**: 953-964.

52 **Cotton, M. and Claing, A.,** G protein-coupled receptors stimulation and the control of cell migration. *Cell Signall* 2009. **21**: 1045-1053.

53 **Smith, A., Carrasco, Y.R., Stanley, P., Kieffer, N., Batista, F.D. and Hogg, N.,** A talin-dependent LFA-1 focal zone is formed by rapidly migrating T lymphocytes. *J Cell Biol* 2005. **170**: 141-151.

54 **Bertet, C., Rauzi, M. and Lecuit, T.,** Repression of Wasp by JAK/STAT signalling inhibits medial actomyosin network assembly and apical cell constriction in intercalating epithelial cells. *Development* 2009. **136**: 4199-4212.

55 **Malinin, N.L., Plow, E.F. and Byzova, T.V.,** Kindlins in FERM adhesion. *Blood* 2010. **115**: 4011-4017.

56 **Ziegler, W.H., Gingras, A.R., Critchley, D.R. and Emsley, J.,** Integrin connections to the cytoskeleton through talin and vinculin. *Biochem Soc transactions* 2008. **36**: 235-239.

57 **Yamaoka, K., Saharinen, P., Pesu, M., Holt, V.E., 3rd, Silvennoinen, O. and O'Shea, J.J.,** The Janus kinases (Jaks). *Genome Biol* 2004. **5**: 253.

58 **Girault, J. A., Labesse, G., Mornon, J.P. and Callebaut, I.,** Janus kinases and focal adhesion kinases play in the 4.1 band: a superfamily of band 4.1 domains important for cell structure and signal transduction. *Mol Med* 1998. **4**: 751-769.

59 **Thelen, M. and Stein, J.V.,** How chemokines invite leukocytes to dance. *Nat Immunol* 2008. **9**: 953-959.

60 **Soriano, S.F., Hons, M., Schumann, K., Kumar, V., Dennier, T.J., Lyck, R., Sixt, M. et al.,** In vivo analysis of uropod function during physiological T cell trafficking. *J Immunol* 2011. **187**: 2356-2364.

61 **Grakoui, A., Bromley, S.K., Sumen, C., Davis, M.M., Shaw, A.S., Allen, P.M. and Dustin, M.L.,** The immunological synapse: a molecular machine controlling T cell activation. *Science* 1999. **285**: 221-227.

Figure legends

Figure 1. siJAK1,2 cells have a naïve T cell phenotype. **(A)** Scheme for siJAK cell preparation. **(B)** Freshly isolated naïve T cells from C57BL6 mouse spleen and lymph nodes (LN) were purified by negative selection and analyzed by flow cytometry with anti-CD3 (blue), -B220 (red) and -Gr1 (green) mAb. As control, an isotype-matched mAb (grey) was used. A representative experiment is shown (n = 7). **(C)** Nucleofected naïve T cells with JAK1 and JAK2 siRNA pools were analyzed by flow cytometry using anti-CD3, -CD44 and -CD62L mAb as naïve T cell markers. A representative experiment is shown (n = 7). **(D)** Cells as in C) were stained with anti-CD3, -CD69 and -CD25 mAb as activated T cell markers. A representative experiment is shown (n = 7). **(E)** sicontrol (blue) and siJAK1,2 (pink) cells were stained with anti-CCR7 (left) or -CXCR4 mAb (right) and analyzed by flow cytometry. As control, we used an isotype-matched mAb. A representative experiment is shown (n = 3).

Figure 2. siJAK1,2 cells show reduced JAK1 and JAK2 protein expression and chemokine-induced migration. **(A)** Naïve T cells (untreated), mock-nucleofected (MOCK), sicontrol, and siJAK1,2 cells were lysed and analyzed in Western blot with anti-JAK1 and -JAK2 antibodies; anti-β tubulin mAb were used as loading control. A representative experiment is shown (n = 3). (**B)** Densitometry analysis of data from western blots as in A). Data show mean ± SD of three independent experiments (*p ≤0.05 nonparametric test). **(C)** Naïve T cells nucleofected with siRNA pools for JAK1, JAK2, and JAK1+JAK2 or siRNA pool control were allowed to migrate on ICAM-1-coated chemotaxis chambers toward CXCL12 or CCL21. The migration index was calculated (see Methods). Data show mean ± SD (n = 4), (***p<0.001, One-way ANOVA).

Figure 3. Naïve siJAK1,2 T cells show reduced homing to lymph nodes. **(A)** siJAK1 or siJAK2 were fluorescently labeled with CellTracker Orange (CMTMR) and sicontrol cells with Green (CMFDA), then mixed at a 1:1 ratio, injected intravenously into mice, and their accumulation in

LN and spleen were analyzed by flow cytometry. Results are expressed as the percentage of orange- and green-stained cells (mean ± SD, *n* = 3), calculated as indicated in Methods. **(B)** siJAK1,2 and sicontrol cells were fluorescently labeled, mixed and injected into mice as in A) and their accumulation 3 or 6 h later in LN (ALN, ILN, MLN) and spleen were analyzed by flow cytometry. Results are expressed as the percentage of orange- and green-stained cells (mean ± SD, *n* = 3), as above (** $p \leq 0.01$ nonparametric test). **(C)** Relative mRNA content of JAK1, JAK2, JAK3 and CXCR4 in siJAK1,2 and sicontrol cells before injection into mice (left) and after cell sorting analysis of LN cells from mice in B) (right). As control, target gene mRNA content was normalized to that of β-actin. Data show mean ± SD (*n* = 5, * $p \leq 0.05$ nonparametric test).

Figure 4. Intranodal localization and movement of siJAK1,2 cells are similar to controls. **(A)** Immunohistological analysis of LN from mice in Fig. 3B, showing siJAK1,2 (green) and sicontrol cells (orange). LN B follicles were identified using anti-B220 mAb (blue). A representative image is shown. (**B**) Immunohistological analysis as in A; HEV were identified using anti-MECA79 mAb (blue). A representative image is shown. (**C,D**) Motility coefficients for meandering index D) and velocity C) of siJAK1,2 and control (None and sicontrol) cell migration into WT PLN. Data are pooled from 7 videos obtained from three independent experiments. Dots represent individual cells; red bars indicate mean values.

Figure 5. siJAK1,2 cells show reduced chemokine-mediated adhesion on ICAM-1 and on VCAM-1. **(A)** In an adhesion-under-flow assay using siJAK1,2 and sicontrol cells on plates coated with recombinant ICAM1-Fc and CXCL12 (left) or CCL21 (right), the number of cells adhered at different shear forces was determined and expressed as a percentage of total adhered cells. A representative experiment is shown (*n* = 3). **(B)** Static adhesion assay using siJAK1,2 and sicontrol cells on microplates coated with recombinant ICAM-1-Fc alone or with CXCL12 or

CCL21. Results are expressed as a percentage of cell input. Mean ± SD (n = 3) (**p ≤0.01, ***p ≤0.001; nonparametric test). As positive control, $MnCl_2$-stimulated cells were allowed to adhere to recombinant ICAM-1-Fc. **(C)** siJAK1,2 and sicontrol cells were stained with anti-LFA-1 mAb and analyzed by flow cytometry. As control, an isotype-matched control was used. A representative experiment is shown (n = 3). **(D)** Adhesion frequency of siJAK1,2 and sicontrol cells to ICAM-1-containing lipid bilayers, alone or coated with CXCL12 or CCL21, or cells pretreated with anti-CD3ε mAb exposed to ICAM-1-containing lipid bilayers. Each dot represents an image field with 20-40 T cells. Data shown from two independent experiments (*p ≤0.05, ***p ≤0.001; n.s. not significant; nonparametric test). **(E)** Adhesion frequency of siJAK1,2 and sicontrol cells to VCAM-1-containing lipid bilayers, alone or coated with CXCL12 or CCL21. Each dot represents an image field with 20-40 T cells. Data shown from two independent experiments (***p ≤0.001, ****p ≤0.0001; nonparametric test).

Figure 6. siJAK1,2 cells showed reduced chemokine-mediated actin polymerization. **(A)** siJAK1, siJAK2, siJAK1,2 and sicontrol cells were stimulated with CXCL12 at times indicated, and actin polymerization determined by phalloidin-FITC staining and flow cytometry. Results show mean ± SD of mean fluorescence index (MFI) for five experiments. Bar graph shows MFI values for phalloidin staining at 15 sec post-activation (**p≤0.01; nonparametric test). **(B)** siJAK1, siJAK2, siJAK1,2 and sicontrol cells were CCL21-stimulated at times indicated, actin polymerization determined and expressed as in A). Bar graph shows MFI values for phalloidin staining at 15 sec post-activation (***p≤0.001; nonparametric test). **(C)** sicontrol and siJAK1,2 cells were activated with CCL21 (top) or CXCL12 (bottom) and cell extracts analyzed by Western blot using anti-pERM antibody. As protein loading control, the membrane was reblotted with anti-ERM antibody. A representative experiment is shown (n = 3). (**D**) Polarity index of sicontrol and siJAK1,2 cells treated in suspension with CXCL12 and adhered to fibronectin-

coated plates (see Methods). The data are from one experiment (three slides/condition). We analyzed 120 sicontrol cells and 183 siJAK1,2 cells (***p<0.001 nonparametric test). **(E)** sicontrol and siJAK1,2 cells activated as in C) were lysed and cell extracts analyzed in Western blot with anti-pERK1/2 antibody. To control protein loading, the membrane was reblotted with anti-ERK1/2 antibody. A representative experiment is shown (*n* = 3).

Table 1. Flow cytometry characterization of isolated naïve T cells and sicontrol- and siJAK1,2-transfected T cells

	CD3	**CD4**	**CD8**	**LFA1**	**CD25**	**CD44^{low}**	**CD62L^{high}**	**CD69**	**CCR7**	**CXCR4**
Naïve T cells	93.8 ± 3	53.4 ± 2	38.8 ± 3	97.1 ± 1	3.1 ± 0.2	35.9 ± 2	81.3 ± 7	2.6 ± 0.9	80.6 ± 2	86.9 ± 2
sicontrol	95.8 ± 2	52.9 ± 7	40.3 ± 3	98.3 ± 2	2.4 ± 1.3	45.6 ± 1	85.9 ± 4	1.6 ± 0.1	80.9 ± 3	84.1 ± 2
siJAK1,2	94.0 ± 6	51.2 ± 3	40.1 ± 6	97.9 ± 7	2.3 ± 0.1	38.6 ± 1	86.4 ± 7	1.6 ± 0.1	84.8 ± 4	85.5 ± 3

Naïve T cells immediately after isolation and after nucleofection with siJAK1 + siJAK2 (siJAK1,2) or with control siRNA (sicontrol) were incubated with IL-7 (24 h), stained for the indicated markers and evaluated by flow cytometry. The percentage of cells expressing the markers are shown. Data correspond to the mean ± SD of seven independent experiments.

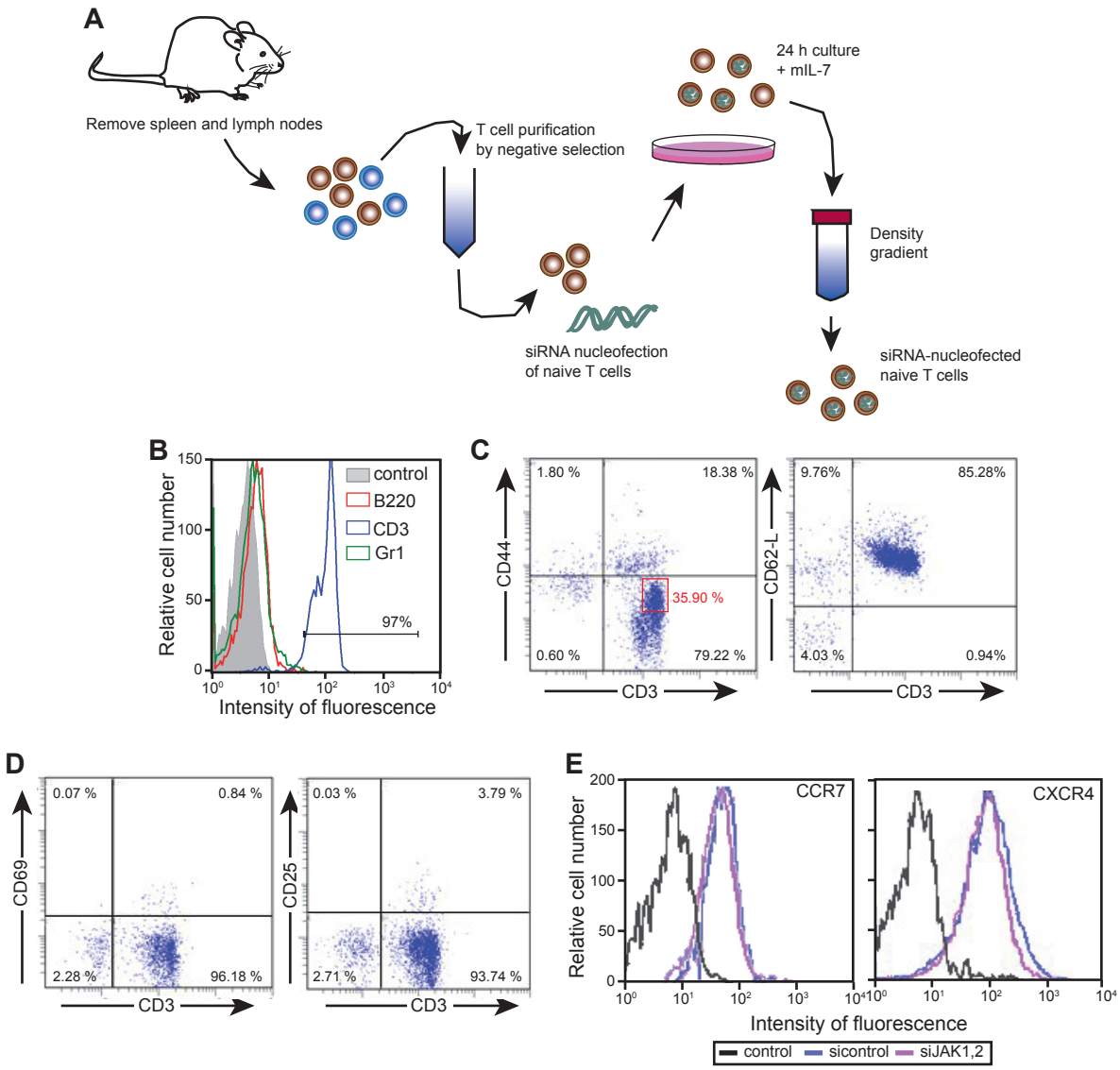

Figure 1
G Perez et al

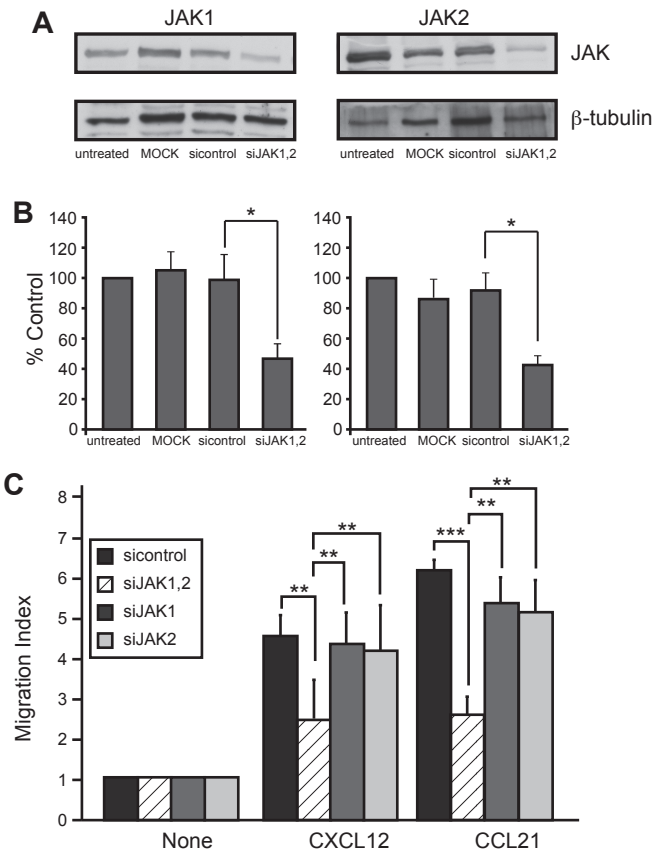

Figure 2
G Perez et al

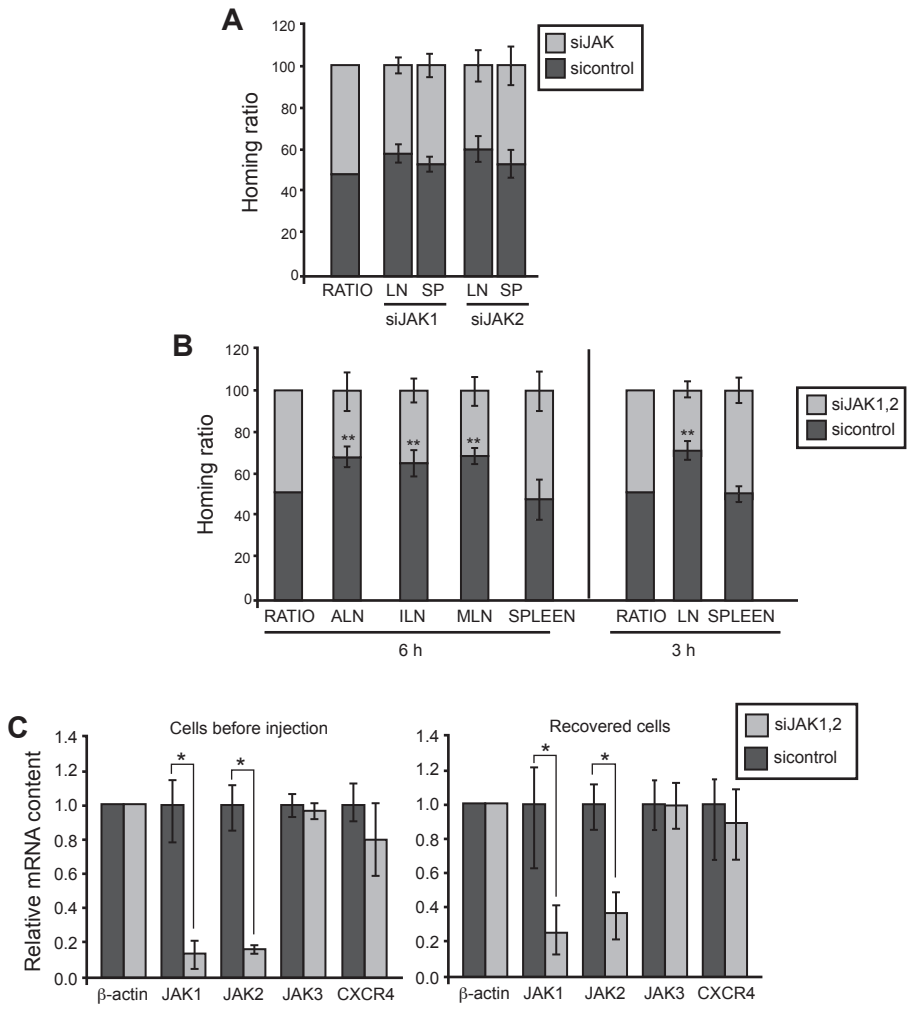

Figure 3
G Perez et al

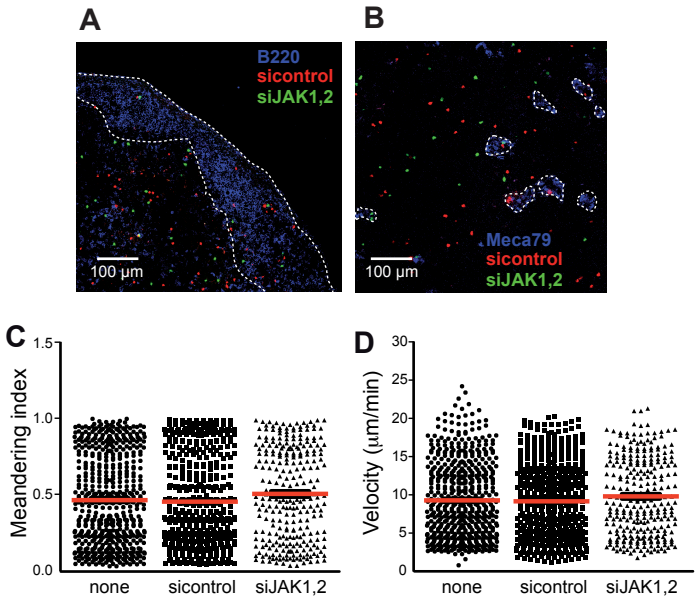

Figure 4
G Perez et al

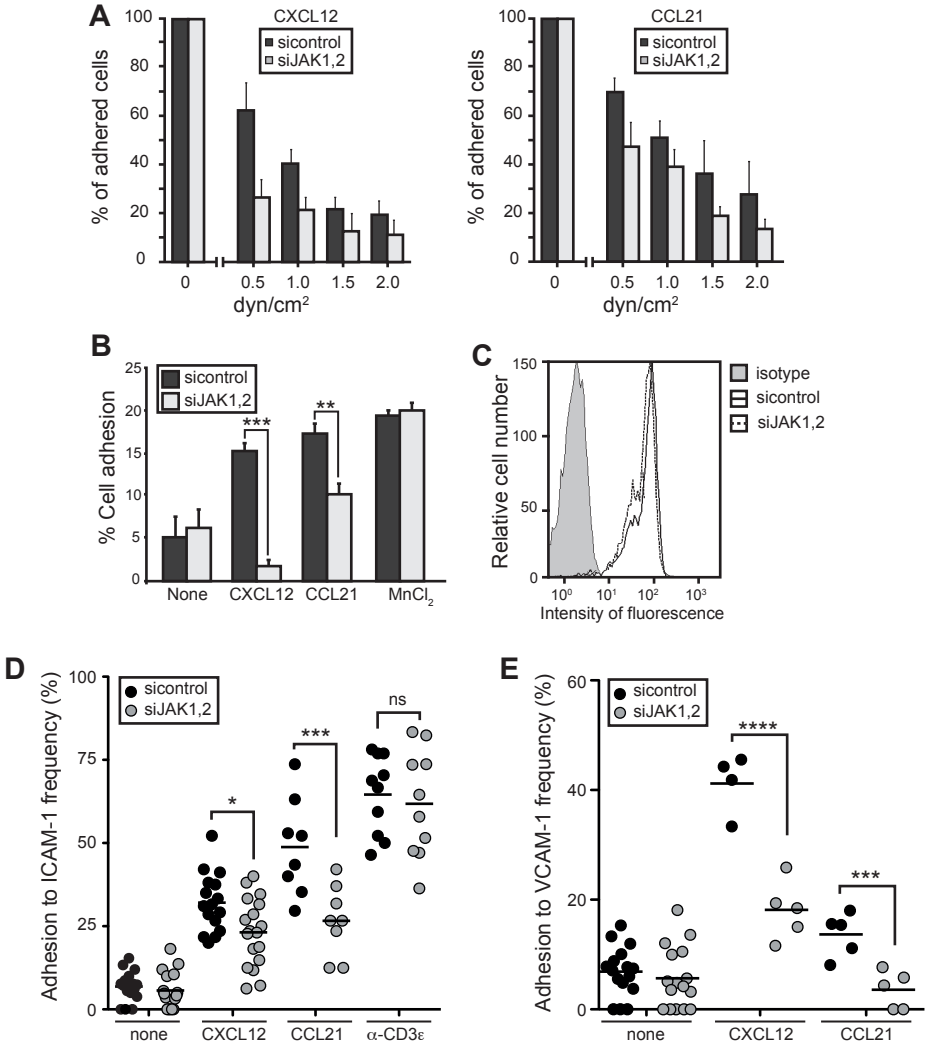

Figure 5
G Perez et al

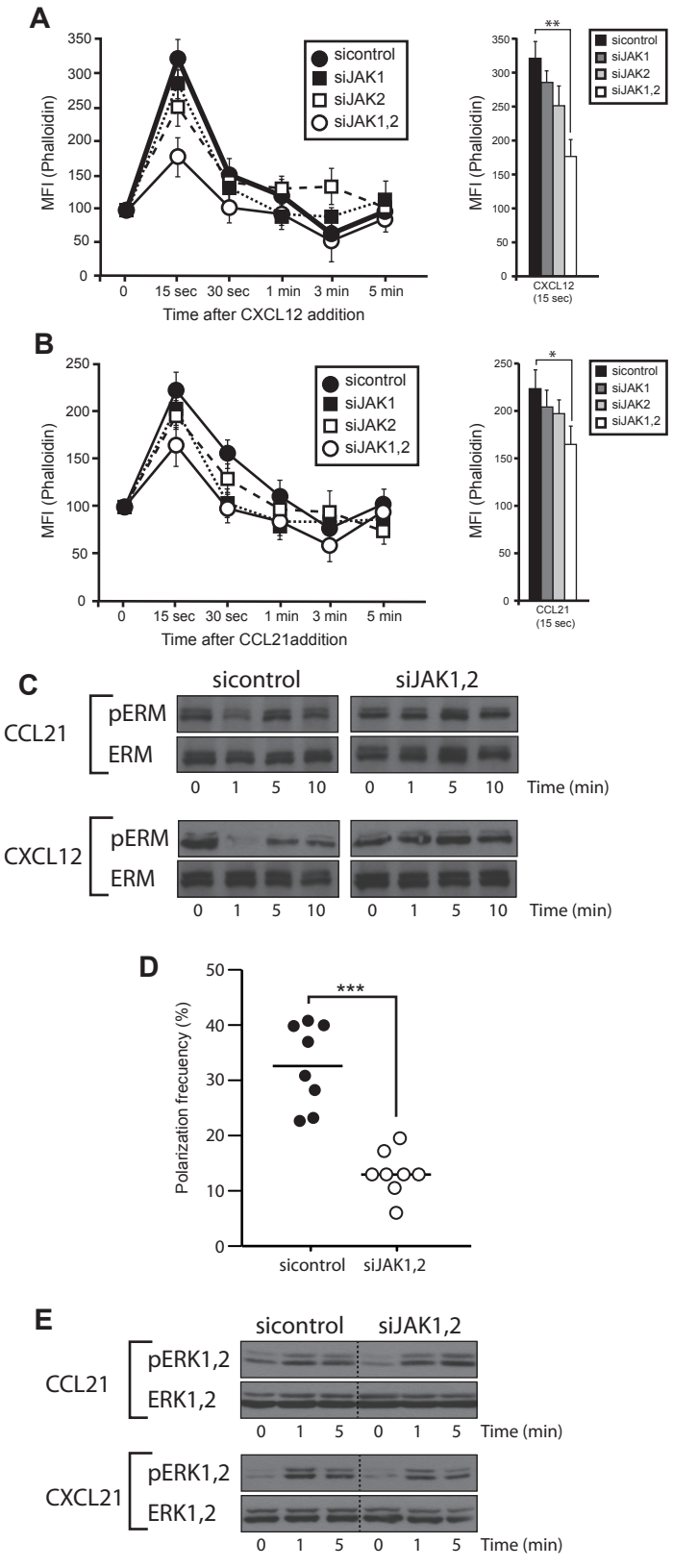

Figure 6
G Perez et al

Supporting materials and methods

Flow cytometry analysis

Cells were plated in V-bottom 96-well plates (2.5 x 10^5 cells/well) and incubated with specific antibodies (30 min, 4°C), followed by flow cytometry. Cell-bound fluorescence was determined in a Profile XL or Gallios flow cytometer (Beckman Coulter).

Western blot analysis

T cells were lysed in triethanolamine buffer (20 mM triethanolamine pH 8.0, 300 mM NaCl, 2 mM EDTA, 20% glycerol, 1% digitonin, with 10 μM sodium orthovanadate, 10 μg/ml each leupeptin and aprotinin) (30 min, 4ºC, with continuous rocking), then centrifuged (15,000 xg, 15 min, 4ºC). Protein extracts were resolved in SDS-PAGE and transferred to nitrocellulose membranes. Western blot analysis was performed as described [1], using 3% non-fat dry milk in TBS as a blocking agent. Protein loading was controlled with a protein detection kit (Pierce) and, when necessary, by reprobing the membrane with anti-β tubulin Ab.

To determine signal pathway activation, cells were starved in serum-free RPMI (2 h, 37ºC), resuspended (5 x 10^6 cells/ml) in RPMI with 10% FBS (fetal bovine serum) and 10 mM HEPES, then activated with 50 nM CXCL12 or 100 nM CCL21 for the times indicated. Cells were lysed in 200 μl detergent buffer (1% Nonidet-P40, 50 mM Tris HCl pH 8.0, 150 mM NaCl, 0.5 mM EDTA, 10 mM sodium pyrophosphate, 1 mM PMSF, 10 μg/ml each leupeptin and aprotinin, 10 μM sodium orthovanadate) (30 min, 4ºC), and analyzed in Western blot as above. Densitometry analyses were performed using ImageJ software (NIH).

Transwell migration assay

Cells (2.5 x 10^5 cells in 0.1 ml) were placed in the upper well of ICAM-1 (recombinant mouse ICAM-1/Fc chimera, 6 μg/ml; R&D Systems)-coated 24-well transmigration chambers (3 μm pore; Transwell, Costar). CXCL12 or CCL21 in 0.6 ml RPMI with 0.25% BSA was added to the lower well. Plates were incubated (120 min, 37ºC) and cells that migrated to the lower chamber were counted in a flow cytometer [1]. Cell migration was calculated as the *x*-fold increase in migration observed relative to the medium control. When needed cell migration was assayed in the absence of ICAM-1.

Flow chamber assays

Petri dishes were precoated with protein A (20 μg/ml, 90 min, 37ºC), alone or with CXCL12 or CCL21 (2 μM) and blocked with PBS/2.5% BSA (60 min, 37ºC), then coated with ICAM-1-Fc (6 μg/ml). After incubation (overnight, 4ºC in a humidified chamber), coated spots were washed twice with PBS and blocked with 200 μl FCS (15 min, 37ºC). Substrate-coated petri dishes were incorporated as the cover wall of a parallel flow chamber (IQUUM) and mounted on an inverted microscope (Olympus) connected to a CCD camera (Cohu). Cells (10^6/ml) were infused (2 min, 37ºC) at 1 dyne/cm^2 (0.204 ml/min). Flow was stopped, cells were allowed to adhere to the plate (10 min), after which flow was restored at 0.5 dyne/cm^2 and increased by 0.5 dyne/cm^2/min to 2.0 dyne/cm^2. Events were recorded on a VHS videocassette recorder for off-line analysis. Cells adhered in each field in each flow condition were counted and expressed as a percentage of cells initially adhered in that field.

Real-time polymerase chain reaction

To determine JAK1 and JAK2 mRNA expression in naïve T cells that home to LN, cells were labeled and injected into 3-month-old C57BL/6 mice as above; 6 h later, mice were killed and LN removed. Cells were harvested, and green- and orange-labeled

cells separated by sorting on an Epics Altra Hypersort System (Beckman Coulter). JAK1 and JAK2 mRNA levels were analyzed by RT-PCR with specific primers. As control JAK3 and CXCR4 mRNA levels were also determined. Cells (3 x 10^5) were lysed and RNA extracted using the RNeasy micro Kit (Qiagen), with DNase treatment to digest residual genomic DNA. Equal amounts of RNA were reverse transcribed using a reverse transcription system (Promega). Relative quantification of cDNA was done by semi-quantitative RT-PCR with the LightCycler480 SybrGreen I Master kit (Roche Diagnostics) using specific primer pairs (JAK1 5'-TGAGCTTTGATCGGATCCTT-3' and 5'-GCAGGGTCCCAGAATAGATATG-3'; JAK2 5'-GAACCTACAGATACGGAGTGTCC-3' and 5'-CAAAATCATGCCGCCACT-3'; JAK3 5'-CACAGTGCATGGCCTATGAT-3' and 5'-AGGTGTGGGTCTGAGAGG-3'; CXCR4 5'-CCATGGAACCGATCAGTGTG-3' and 5'-TTTTCATCCCGGAAGCAGG-3'; β-actin 5'-GGCACCACACCTTCTACAATG-3' and 5'-TGGATGGCTACGTACATGGCTG-3'). Samples were analyzed in duplicate and normalized to β-actin using ABI 7900HT SDS 2.3 software.

Immunohistochemistry

Frozen LN sections (8 μm) were fixed (2% paraformaldehyde, 10 min), washed with PBS, blocked with PBS containing 1% BSA and 10% goat serum, and stained with anti-B220 mAb followed by Alexa-647-goat anti-mouse Ab and Alexa633-anti-PNAd mAb. Lymphocytes in PLN sections were visualized on a confocal Leica TCS SP5 microscope (Leica Microsystems).

Actin polymerization

Nucleofected naïve T cells were starved in serum-free RPMI (2 h, 37ºC) and resuspended (5 x 10^6 cells/ml) in RPMI with 10% FBS and 10 mM HEPES. Cells were

activated with 50 nM CXCL12 or 100 nM CCL21 for different times, fixed in 4% paraformaldehyde (10 min), stained with FITC-phalloidin (Molecular Probes), and analyzed by flow cytometry (Cytomics FC 500).

Adhesion assay

Nucleofected naïve T cells were loaded with the fluorescent probe BCECF-AM (2',7'-Bis-(2-Carboxyethyl)-5-(and-6)-Carboxyfluorescein, Sigma). Cells were plated (2 x 10^5 cells/well in adhesion buffer: 20 mM Hepes, 149 mM NaCl, 2 mg/ml glucose, pH 7.4, supplemented with 0.5 mM $CaCl_2$ + 1 mM $MgCl_2$ to simulate physiological conditions, or with 0.2 mM $MnCl_2$ to induce LFA-1 activation), in 96-microwell plates precoated with mouse ICAM-1-Fc (1.75 μg/well; R&D Systems), alone or with appropriate chemokines (10 nM CXCL12 or 20 nM CCL21). Cells were allowed to adhere (15 min, 37°C), after which plates were submerged in warm PBS and inverted to allow detachment of non-adherent cells by gravity (20 min, 37°C). Adherent cell fluorescence was determined in a GENios plate reader (Tecan) and background adhesion to BSA was subtracted. Cell adhesion is expressed relative to control siRNA-nucleofected cells in the absence of chemokines.

1 **Vila-Coro, A.J., Rodriguez-Frade, J.M., Martin De Ana, A., Moreno-Ortiz, M.C., Martinez, A.C. and Mellado, M.,** The chemokine SDF-1alpha triggers CXCR4 receptor dimerization and activates the JAK/STAT pathway. *FASEB J* 1999. **13**: 1699-1710.

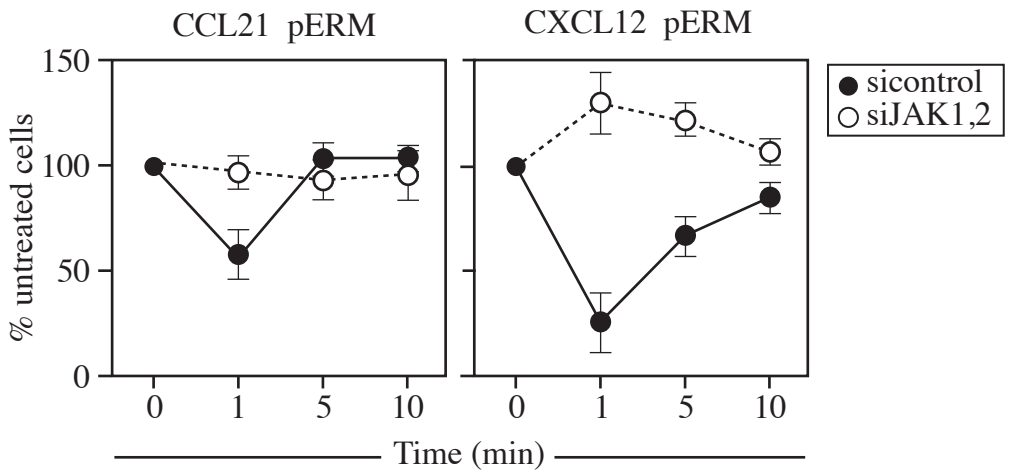

Supporting Fig 1. Effect of JAK1,2 blockade on CCL21 and CXCL12-induced ERM dephosphorylation Naïve T cells nucleofected with siRNA pools for JAK1+JAK2 or siRNA pool control were stimulated with CCL21 or CXCL12, ERM phosphorylation was analyzed by western blot using specific antibodies, and quantified by densitometry using ImageJ. Data show mean ± SD (n = 3).

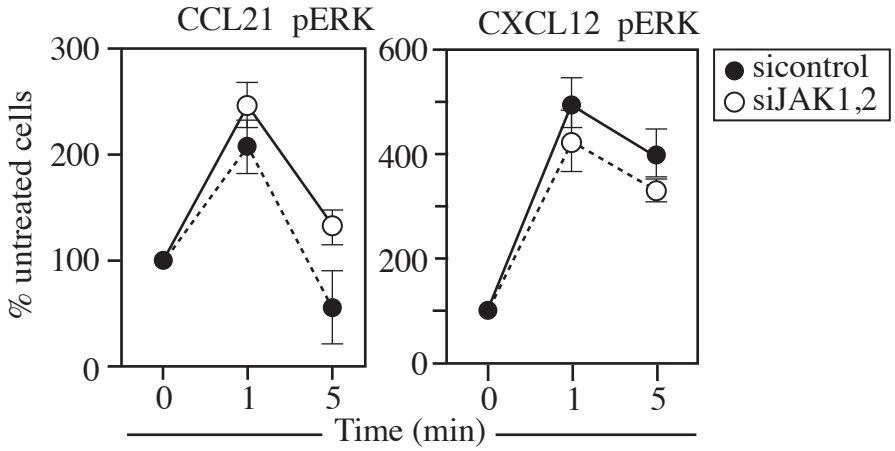

Supporting Fig 2. Effect of JAK1,2 blockade on CCL21 and CXCL12-induced ERK phosphorylation. Naïve T cells nucleofected with siRNA pools for JAK1+JAK2 or siRNA pool control were stimulated with CCL21 or CXCL12, ERK phosphorylation was analyzed by western blot using specific antibodies and quantified by densitometry using ImageJ. Data show mean ± SD (n = 3).

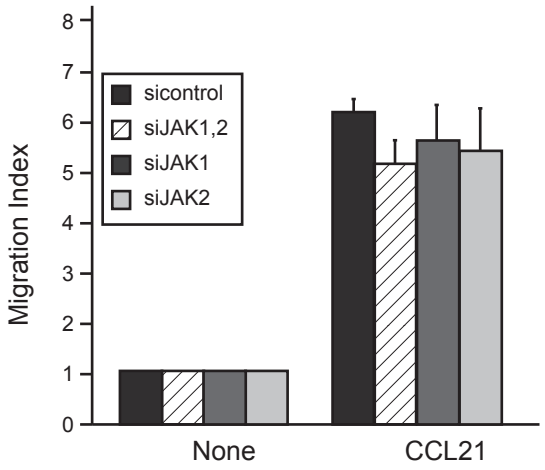

Supporting Fig 3. siJAK1,2 T cells migrate normally in the absence of integrin substrates. Naïve T cells nucleofected with siRNA pools for JAK1, JAK2, and JAK1+JAK2 or siRNA pool control were allowed to migrate after CXCL12 or CCL21 stimulation in the absence of integrin substrates (ICAM-1 or VCAM-1). The migration index was calculated (see Methods). Data show mean ± SD (n = 4). One-way Anova.

Supplemental Movie 1. Interstitial movement of JAK1/2^{low} naïve T cells in lymph node. Fluorescently labeled untreated, siControl- and JAK1/JAK2-nucleofected T cells were injected intravenously into C57BL/6 mice; after 40 min, cells in the popliteal LN were imaged by multiphoton intravital microscopy every 20 s for 30 min. Videos show wt T cells (blue), siControl (green)- and JAK1/JAK2-nucleofected T cells (orange). HEV are identified by anti-PNAD (gold). Time indicated in seconds. Scale bar = 45 μm.

WIP regulates persistence of cell migration and ruffle formation in both mesenchymal and amoeboid modes of motility

Inmaculada Bañón-Rodríguez[1,^], Julia Sáez de Guinoa[2], Alejandra Bernardini[1], Chiara Ragazzini[1], Estefanía Fernández[1], Yolanda R. Carrasco[2], Gareth E. Jones[3], Francisco Wandosell[4], Inés M. Antón[1,*].

[1] Department of Molecular and Cell Biology, [2]Department of Immunology and Oncology, Centro Nacional de Biotecnología (CNB-CSIC), Darwin 3, 28049 Madrid, Spain

[3] The Randall Division of Cell & Molecular Biophysics, King's College London, London SE1 1UL, UK

[4] Centro de Biología Molecular "Severo Ochoa", CBM-UAM, Nicolás Cabrera 1, 28049 Madrid, Spain.

[^] Present address: Centro de Biología Molecular "Severo Ochoa", CBM-UAM, Nicolás Cabrera 1, 28049 Madrid, Spain.

* Corresponding author:
Dr. Inés M. Antón, Centro Nacional de Biotecnología (CNB-CSIC), Darwin 3, 28049 Madrid, Spain.
Ph. +34 915855312; Fax +34 915854506. E-mail: ianton@cnb.csic.es.

Running title

WIP regulates persistence of cell migration

SUMMARY

The spatial distribution of signals downstream from receptor tyrosine kinases (RTKs) or G-protein coupled receptors (GPCR) regulates fundamental cellular processes that control cell migration and growth. Both pathways rely significantly on actin cytoskeleton reorganization mediated by nucleation-promoting factors such as the WASP-(Wiskott-Aldrich Syndrome Protein) family. WIP (WASP Interacting Protein) is essential for the formation of a class of polarised actin microdomain, namely dorsal ruffles, downstream of the RTK for PDGF (platelet-derived growth factor) but the underlying mechanism is poorly understood. Using lentivirally-reconstituted WIP-deficient murine fibroblasts we define the requirement for WIP interaction with N-WASP and Nck for efficient dorsal ruffle formation and of WIP-Nck binding for fibroblast chemotaxis towards PDGF-AA. The formation of both circular dorsal ruffles in PDGF-AA-stimulated primary fibroblasts and lamellipodia in CXCL13-treated B lymphocytes are also compromised by WIP-deficiency. We provide data to show that a WIP-Nck signalling complex interacts with RTK to promote polarised actin remodelling in fibroblasts and provide the first evidence for WIP involvement in the control of migratory persistence in both mesenchymal and amoeboid motility.

INTRODUCTION

Dynamic remodeling of the actin cytoskeleton plays an essential role in cell motility [1]. Many actin-binding proteins that organise actin filaments into functionally specialized arrays such as filopodia, lamellipodia or ruffles are involved in cell displacement, contributing to individual amoeboid (rounded) or mesenchymal (elongated) migration [2]. It is often found that cytoskeletal proteins regulate the switch between both types of locomotion (e.g. GTPases [3]) or regulate one type but not the other (e.g. the actin filament crosslinker filamin is necessary for macrophage mesenchymal migration but dispensable for amoeboid migration [4]). Amoeboid locomotion is driven by the force generated via actin-mediated forward flow of the cell front, followed by actomyosin-mediated contraction of the mid region and rear uropod [5]. Mesenchymal movement is supported by strong integrin-mediated attachment at or just behind the leading edge and cell contractility that generates movement in a polarised morphology [6].

Platelet-derived growth factor (PDGF) is a chemotactic cytokine that induces rapid changes in cell shape associated with mesenchymal cell motility and migration [7]. PDGF exists as separate isoforms consisting of homo- or hetero-dimeric proteins of A- and B-polypeptide chains, which bind in a differential manner to two structurally related cell surface receptors, PDGFRα and PRGFRβ [8]. The homodimer PDGF-AA binds exclusively the transmembrane tyrosine kinase receptor PDGFRα (PDGFRαα) whereas PDGF-BB (B chain homodimer) activates PDGFRαα, PDGFRαβ and PDGFRββ [6]. Ligand binding induces dimerization of the receptors and subsequent transphosphorylation on specific tyrosine residues [7] that then become docking sites for proteins containing Src homology 2 (SH2) domains. These SH2-containing proteins either possess intrinsic enzymatic activity (e.g. phosphatidyl-inositol-3 kinase, PI3K) or act as adaptor proteins (e.g. Grb and Nck) that recruit other catalytically active signal transduction molecules to the receptor environment. Several distinct signalling cascades specific for the activated receptor tyrosine kinase (RTK), are then initiated that predominately converge on actin cytoskeleton remodelling pathways. The end point of these actin-linked cascades lead to the generation of filopodia, lamellipodia, peripheral membrane ruffles and circular dorsal ruffles. Circular dorsal ruffles, (also called waves, ring ruffles or actin ribbons), are highly dynamic surface structures that form transiently on the dorsal plasma membrane of adherent cells in 2D cultures and contribute to cytoplasmic remodelling, the establishment of polarity in motile cells, preparation of a

stationary cell for subsequent movement, macropinocytosis and the internalization of cell surface receptors [9-11].

One of the pathways that regulate the formation of dorsal ruffles involves the Wiskott–Aldrich Syndrome protein (WASP) family proteins and the Arp2/3 (actin-related protein) complex that is activated by WASP proteins [12, 13]. The WASP family member N-WASP (neural WASP) has been localized to dorsal ruffles along with WIP (WASP Interacting Protein), dynamin 2, and cortactin after PDGF BB stimulation [10, 14]. N-WASP involvement in dorsal ruffle formation in mouse embryonic fibroblasts (MEFs) has been demonstrated through chemical inhibition with wiskostatin, siRNA treatment, or genetic depletion [15]. In addition, the expression of an N-WASP truncation mutant that cannot bind the Arp2/3 complex blocks the formation of these structures. The N-WASP/WIP complex is known to form a functional unit that contributes to actin cytoskeletal reorganisation and cell migration [16] but its contribution to ruffle formation has not been addressed. WIP is ubiquitously expressed and can independently bind filamentous actin (F-actin) [16], regulating at different levels the formation of most cellular actin-rich structures described to date including filopodia, lamellipodia, dorsal ruffles, stress fibres, podosomes and invadopodia [17, 18]. WIP overexpression in murine fibroblasts enhances dorsal ruffle formation in response to PDGF-BB stimulation [14]. Conversely, microinjection of anti-WIP antibody or the absence of WIP in murine null fibroblasts results in decreased ruffle formation in response to PDGF-BB treatment. Additionally overexpression of a modified form of WIP lacking the actin-binding site blocks PDGF-BB-induced membrane ruffling [14]. WIP also interacts with other cytoskeletal-related proteins involved in dorsal ruffle formation such as cortactin, mAbp1 (murine actin-binding protein-1), and Nck [18].

Chemokines trigger amoeboid forms of cell movement in lymphocytes. This diverse family of small proteins all signal through G-protein coupled receptors (GPCR); the activated signalling cascades lead to actin cytoskeleton rearrangements and integrin activation to induce cell polarization and motility. WASP, exclusively expressed in immune cells, is involved in chemokine-mediated migration of distinct type of leukocytes. The lack of WASP impairs macrophage and dendritic cell adhesion and migration [19-21]. T cell and B cell migration in response to a chemokine gradient and lymphocyte trafficking in vivo are also affected by WASP deficiency [22-24]. The B cell immune response is delayed and reduced in the absence

of WASP [25]; in addition, a role for WASP in B cell-mediated autoimmunity has been reported [26]. WIP is highly expressed in lymphoid tissue and protects WASP from degradation in resting cells [27, 28]. In fact, WIP null mice develop immune disorders that mimic Wiskott-Aldrich syndrome [29]. WIP deficient lymphocytes show defects in the subcortical actin filament network and in the normal responses to chemokines in vivo and in vitro [22, 30]. Nevertheless, the role of WIP in leukocyte amoeboid motility is poorly understood and the mechanisms underlying WIP function in cell movement remain elusive.

Here we demonstrate that WIP regulates the persistence of cell movement during both mesenchymal and amoeboid chemotactic migration whilst cell speed is only affected in amoeboid B lymphocytes and not in fibroblasts using the mesenchymal mode of migration. Moreover we show that WIP binding to Nck is essential for fibroblast chemotaxis towards PDGF-AA.

RESULTS

WIP deficiency impairs amoeboid cell motility

To investigate the role of WIP in amoeboid migration, we studied B lymphocyte behaviour in response to the most specific B cell chemokine CXCL13 (C-X-C motif chemokine 13). We isolated B cells from spleens of control ($WIP^{+/+}$) and $WIP^{-/-}$ mice. B cell phenotypic analysis showed no significant differences in cell size, cell complexity, or surface expression of typical markers for these lymphocytes (CD19, IgM) (supplemental Fig. 1A). We detected low WASP level in $WIP^{-/-}$ B cells, as predicted from the reported role of WIP in protecting WASP from degradation [27, 28] (supplemental Fig. 1B). More surprisingly, low Nck levels were also recorded in $WIP^{-/-}$ B cells (supplemental Fig. 1B).

We evaluated the B cell chemotactic response to a gradient of CXCL13 in Boyden chambers; the absence of WIP reduced by half the percentage of migratory B cells, independently of the chemokine dose used (400 nM Fig. 1A; 40 nM data not shown). To track B cell motility in real time, we used a 2D system based on the use of artificial planar lipid bilayers containing the adhesion molecule ICAM-1 (intercellular adhesion molecule-1) and CXCL13 coating [31]. The presence of adhesion molecules and a homogeneous chemokine coating results in a haptokinesis system, where B cells move by random migration. We labelled control and $WIP^{-/-}$ purified B cells with distinct fluorescent probes (CFSE, SNARF-1), and seeded cell aliquots onto the haptokinetic substratum. CXCL13 signalling promoted B cell polarization, as measured by the formation of dynamic membrane protrusions from the cell body over time (detected by Differential Interference Contrast, DIC, microscopy) (Movie 1 **S1?**). The chemokine activated LFA-1 integrin/ICAM-1 interaction that supports cell migration was followed by Internal Reflection Microscopy, IRM) (Movie 1 **S1?**). $WIP^{-/-}$ B cells showed a significant reduction in polarization and migration compared with wild-type B cells (Fig. 1B). They displayed lower mean velocity and directionality (measured as a persistence index using Imaris software, Bitplane) than $WIP^{+/+}$ counterparts (Fig. 1C). In addition, $WIP^{-/-}$ B cells displayed more restricted tracks than control B cells (Fig. 1D).

The defects in B cell migration due to the lack of WIP may be related to alterations in actin polymerization. We evaluated F-actin rich lamellipodia by phalloidin staining in fixed B cells attached to the 2D substratum. $WIP^{-/-}$ B cells had fewer F-actin rich lamellipodia than $WIP^{+/+}$ counterparts (Fig. 1E). We tracked WIP localization at the B cell-substratum contact plane in real time by expression of a WIP-GFP fusion protein in the B cell line 2PK3. We observed

that WIP accumulated at the lamella of new forming membrane ruffles, where nascent adhesion points also appeared (detected by IRM) (supplemental Fig. 2; Movie 2 **S2?**).

To confirm the relevance of WIP function in amoeboid cell motility, we reconstituted purified $WIP^{-/-}$ B cells with full length WIP as GFP fusion protein by transduction with recombinant lentivirus; we used GFP-expressing recombinant lentivirus as a transduction control (Fig. 2A). We observed that lentiviral infected B cells displayed enhanced basal migration and also CXCL13-mediated chemotaxis in Boyden chambers when compared with freshly isolated B cells (Fig. 1A and Fig. 2B). The reconstitution of $WIP^{-/-}$ B cells with full length WIP recovered chemotaxis, mean velocity values and F-actin-rich lamellipodium frequency to the levels of GFP-transduced control B cells (Fig. 2B-D); the tracks were similar to those seen in GFP-transduced control B cells (Fig. 2E). In contrast, $WIP^{-/-}$ B cells transduction with GFP lentivirus did not rescue chemotaxis, mean speed or lamellipodium production frequency; these B cells still showed restricted tracks (Fig. 2B-E).

These findings stress the importance of WIP function in F-actin-rich lamellipodium formation and amoeboid motility where it regulates polarization, speed and directional persistence of migration.

WIP-null fibroblasts retain a normal phenotype.

In order to address the role of WIP in mesenchymal cell movement, we examined fibroblast migration in response to growth factors. Primary lung fibroblasts were derived from control ($WIP^{+/+}$) or $WIP^{-/-}$ adult mice and maintained in complete medium with foetal calf serum (FCS) up to a maximum of 12 passages to prevent undesired cell selection. Absence of WIP was confirmed by Western blot analysis of soluble cell lysates (Fig. 3A). Neither the levels of WIP- associated proteins such as N-WASP or Nck, nor those of unrelated cytoskeleton-associated proteins such as GAPDH, were affected by the absence of WIP. Similarly, no significant differences were observed between cell size or cell surface rugosity of control and $WIP^{-/-}$ cells when both populations were analysed by flow cytometry (Fig. 3B). In order to confirm that WIP deficiency did not alter cell morphology, we performed image comparison of growing fibroblasts in 2D culture. Control and $WIP^{-/-}$ fibroblasts showed comparable morphologies in vitro (Fig. 3C). These results indicate that WIP deficiency is not sufficient to modify fibroblast morphology or the levels of N-WASP and Nck.

WIP controls fibroblast chemotaxis through controlling directional persistence.

WIP is known to be required for lymphocyte chemotaxis to CXCL12 both *in vitro* and *in vivo* [22]. More recently, WIP's contribution to fibroblast chemotaxis has been reported [32]. However, the mechanism by which WIP modulates cellular responses to chemotactic stimuli remains largely unsolved. To address this question, we loaded Dunn chemotaxis chambers with 15% FCS in the external ring and imaged by phase contrast time-lapse microscopy the displacement of fibroblasts derived from control or $WIP^{-/-}$ murine lungs [33]. An in-house (Dunn & Jones) Mathematica 6.0 (Wolfram Research Institute) workbook analysis of cell tracks over time demonstrated that $WIP^{+/+}$ fibroblasts (n = 167) migrated preferentially towards the chemoattractant source while $WIP^{-/-}$ fibroblasts (n = 154) showed random motility (Fig. 4A, supplemental Fig. 3A and supplemental videos $WIP^{+/+}$ (**Movie 3**) and $WIP^{-/-}$ (**Movie 4**)). Interestingly, both cell types had similar mean velocity: 0.44 ± 0.01 μm/min for control fibroblasts and 0.41 ± 0.01 μm/min for $WIP^{-/-}$ fibroblasts (supplemental Fig. 3B). In contrast, WIP deficiency significantly decreased cell persistence during chemotaxis (Fig. 4B and supplemental Figure 3C). These results indicate that WIP does not regulate fibroblast displacement velocity but it is necessary to maintain directional persistence during fibroblast movement towards a source of serum-derived chemoattractants, as also observed for amoeboid cell migration.

To confirm the function of WIP in fibroblast chemotaxis towards serum, we performed Boyden chamber (Transwell) analyses with control and $WIP^{-/-}$ fibroblasts. Following the pattern seen in the Dunn chamber, migration towards the serum loaded into the lower chamber was significantly decreased in $WIP^{-/-}$ fibroblasts compared to control cells (Fig. 5A). Significantly, chemotaxis was restored in $WIP^{-/-}$ fibroblasts rescued by exogenous WIP-GFP expression but not by GFP alone (Fig. 5A). This result supports the conclusion that the diminished chemotaxis observed in $WIP^{-/-}$ fibroblasts was due to the absence of WIP and not to potential secondary effects derived from genetic manipulation.

WIP is necessary for fibroblast chemotaxis towards PDGF-AA

Serum contains an array of lipid and peptide chemoattractants, with LPA (lysophosphatidic acid), EGF (epidermal growth factor), FGF, (fibroblast growth factor) and PDGF (platelet-derived growth factor) being some of the well-known constituents [34]. To determine whether the contribution of WIP to the observed chemotaxis was exclusively induced as a response to

a combination of chemotactic cues or was specific to some of them, we independently tested the responses of WIP$^{-/-}$ fibroblasts to each of the above mention chemoattractants (Fig. 5B to E). WIP-deficiency did not modify fibroblast chemotaxis towards LPA (5μM; 2μM, data not shown), EGF (50 ng/ml), FGF (20 ng/ml) (Fig. 5B-D) or a combination of the two latter proteins (data not shown). In contrast, WIP$^{-/-}$ fibroblasts showed a significantly reduced capacity to migrate towards PDGF-AA (Fig. 5E, 50 ng/ml; 10 ng/ml, data not shown). This deficiency was recovered by exogenous expression of WIP-GFP but not of control GFP (Fig. 5E). We then posed the question of whether WIP overexpression would increase the chemotactic response. Control murine fibroblasts were transduced with lentivirus directing GFP (control) or WIP-GFP expression (4- to 6-fold endogenous WIP expression; data not shown) and their migration towards PDGF-AA was quantified (Fig. 5F). WIP overexpression led to a significantly reduced capability of the murine lung fibroblasts to reach the bottom well of the Transwell. These results indicate that WIP is necessary for fibroblast chemotaxis induced by serum and PDGF-AA, and that fine-tuned WIP levels are required for proper control of the process since both reduced and increased WIP expression impair chemotaxis.

WIP expression is required for dorsal ruffle formation.

Having identified a role for WIP in PDGF-AA chemotaxis in fibroblasts we subsequently studied whether WIP contributes to dorsal ruffle formation after PDGF-AA stimulation. Dorsal ruffles were identified as dynamic and transient circular structures enriched in cortactin (Fig. 6A) and polymerized actin (supplemental Fig. 4A). Serum-starved WIP-null fibroblasts showed impaired dorsal ruffle formation in the presence of PDGF-AA at all times tested, decreasing by twofold after 15 min exposure to the cytokine (Fig. 6B). The decreased ability of WIP-deficient fibroblasts to form dorsal ruffles after PDGF-AA exposure was restored after lentiviral expression of WIP-m**C**herry in WIP$^{-/-}$ fibroblasts but not after lentiviral expression of a control **C**herry construct (Fig. 6C,D). Moreover, WIP-mCherry redistribution to dorsal ruffles after PDGF-AA treatment (supplemental Fig. 4B) emphasizes the crucial role of WIP in dorsal ruffle dynamics.

The receptor for PDGF-AA is not affected by the absence of WIP

Of the different homo- or heterodimeric PDGFRs expressed on the cell surface, PDGF-AA exclusively activates the homodimeric PDGFRαα isoform as shown *in vitro* and *in vivo* [35]. One possible explanation of the limited responses we observed in WIP$^{-/-}$ cells would be a

reduction in PDGFRα levels in WIP$^{-/-}$ fibroblasts. To test this hypothesis we performed Western blot analysis of total protein extracts obtained from WIP$^{+/+}$ and WIP$^{-/-}$ fibroblasts (Fig. 6E) and performed real time PCR and microarray analyses from RNA samples (data not shown). We found no differences in the levels of PDGFRα in any of the assays. As measured by FACS, there was also no significant difference in the cell surface levels of PDGFRα between WIP$^{+/+}$ and WIP $^{-/-}$ cells, neither in the presence of serum (Fig. 6F, left panel) nor after serum starvation (Fig. 6F, right panel).

PDGFRα is known to undergo endocytosis upon treatment with PDGF–AA [35] so we speculated that WIP could instead have a role in regulating PDGF-mediated signalling at this level. Analyses of surface levels of PDGFRα over a time course of treatment with PDGF–AA revealed that WIP$^{-/-}$ cells showed no difference to control ones in their endocytic capacity for PDGFRα (Fig. 6F right panel). These results rule out the possibility that WIP could modify PDGFRα expression, surface distribution or endocytosis rate at the times tested. These data suggest an alternative downstream role for WIP as a scaffolding/signalling molecule.

WIP binding to Nck and N-WASP is required for dorsal ruffle formation.

WIP binds to proteins involved in dorsal ruffle formation such as actin, cortactin, mAbp1, Nck and N-WASP [14, 32, 36]. The interaction between WIP and actin [14] or mAbp1 is important to dorsal ruffle formation but the WIP-cortactin interaction is dispensable [36]. There remains a gap in our understanding of the contribution of the WIP-Nck-N-WASP complex to ruffle generation. To gain further insight into how WIP interactions regulate dorsal ruffle formation, WIP$^{-/-}$ fibroblasts were transduced with recombinant lentivirus expressing GFP, full length WIP-GFP or WIP mutants deleted of the Nck-binding site domain (a.a. 321-415; WIPΔNBD) or N-WASP-binding domain (a.a. 450-503; WIPΔWBD) [37] also fused to GFP. Equivalent expressed protein was confirmed by Western blot analysis (Fig 7A) and infected cells were treated with PDGF-AA to induce dorsal ruffle formation (Fig. 7B). Deficient dorsal ruffle formation in WIP-null cells was seen to be restored by expression of wild-type WIP-GFP but not by the WIP mutants WIPΔNBD or WIPΔWBD, suggesting that WIP binding to Nck and N-WASP is essential for this process (Fig. 7B). These results show that WIP complexes with Nck and N-WASP to contribute to dorsal ruffle formation after PDGF-AA stimulation.

WIP binding to Nck but not to N-WASP is required for chemotaxis towards PDGF-AA

Dorsal ruffle formation has been linked to fibroblast migration [38]. In this report we demonstrate that WIP deficiency perturbs both fibroblast chemotaxis and dorsal ruffle generation. To discover whether WIP domains involved in chemotaxis overlapped with those whose contribution to ruffle formation was identified, we quantified the percentage of cells translocating to the PDGF-AA-enriched lower chamber of a Transwell after $WIP^{-/-}$ fibroblasts were transduced with recombinant lentivirus expressing GFP, full length WIP-GFP, WIPΔNBD or WIPΔWBD (Fig. 8). Chemotactic response to PDGF-AA by WIP-deficient cells was rescued after expression of wild-type WIP-GFP and WIP-ΔWBD but not by WIP mutants lacking the capability to bind Nck (WIP-ΔNBD). These data strongly ppoint to Nck binding to WIP being essential for the chemotactic response (Fig. 8). These findings indicate that dorsal ruffle formation is not a pre-requisite for proper chemotactic responses since WIP binding to N-WASP contributes to dorsal ruffle formation but is not essential for chemotaxis of primary fibroblasts towards PDGF-AA.

DISCUSSION

In this study we identify WIP as an essential component for cell persistence during mesenchymal migration of lung fibroblasts and amoeboid migration of splenic B lymphocytes. We also show that WIP localizes to and regulates lamellipodium formation in CXCL13-treated B cells and circular dorsal ruffle formation in PDFG-AA-stimulated fibroblasts. Moreover, we conclude that WIP-dependent signals required for dorsal ruffle formation and efficient fibroblast chemotaxis towards PDGF-AA involve WIP binding to Nck, an adaptor protein and N-WASP activator.

B cells lacking WIP have defects in the actin cytoarchitecture [30], though they do not show distinct morphology from control cells in the steady state (supplemental Fig. 1). However, the absence of WIP diminishes chemokine-triggered cell polarization, migration, and F-actin-rich lamellipodium formation in B cells. These alterations may be related to low WASP levels due to its degradation in the absence of WIP with a knock-on effect on the activation of the Arp2/3 complex [39]. In addition, other WASP-independent WIP functions on the actin cytoskeleton may be implicated [40]. The decreased B cell chemotactic response to a gradient of CXCL13 chemokine together with the lower values of the persistence index obtained in the planar membranes, where random migration takes place, point to an important role for WIP in regulating directional persistence in amoeboid motility. In support of our findings, it has been shown that WASP-deficient macrophages have reduced directional migration [20]. The defects in cell behaviour derived from WIP deficiency may compromise B cell localization and pathogen searching, thus, B cell function. In fact, defective B cell migration may underline the severe reduction of the area containing follicular B cells ($B220^{+}$) observed in the spleen of WIP-/- mice [29]. It is important to point out the immune disorder that WIP null mice develop [29] and also the recent identification of an immunedeficient patient due to WIP mutations [41].

Our previous results have shown that actin distribution in serum-starved primary lung fibroblasts from $WIP^{-/-}$ mice was similar to control fibroblasts from $WIP^{+/+}$ mice [14]. In this report we have compared the morphology of growing fibroblasts and our study indicates that in the presence of serum WIP does not contribute to gross differences in overall cellular size, rugosity or shape (Fig. 3B-C), confirming that no significant morphological differences are detected in growing fibroblasts (up to 12 passages) in the absence of WIP. These results

demonstrate that WIP is not essential for cell architecture in primary murine fibroblasts. Our data also support previous reports [28, 42] indicating that WIP does not regulate N-WASP stability since, in contrast to WASP in hematopoietic cells, N-WASP levels are not modified in WIP$^{-/-}$ fibroblasts (Fig. 3A). A recent report described that siRNA-mediated reduction of WIP levels in mouse embryonic fibroblasts (MEFs) decreases N-WASP levels [32]. This disagreement may be due to differences in cell type (murine fibroblasts versus MEFs) or to an adaptative response favored by permanent and total loss of WIP expression in WIP-deficient lung fibroblasts compared to the partial loss of WIP in interfered MEFs.

Fibroblasts migrate on 2D surfaces by forming actin-rich lamellipodia at the leading edge of the cell [43]. Lamellipodia and ruffles are widely believed to be critical for directional cell motility and their generation depends on Arp2/3 activity [44]. However, conflicting data on the contribution of Arp2/3 to directional migration appears in the literature: Whereas some publications support the argument that the Arp2/3 complex is required for lamellipodia extension and directional fibroblast cell migration [45], other reports indicate that Arp2/3-depleted fibroblast respond normally to shallow gradients of PDGF, indicating that lamellipodia are not required for chemotaxis [46]. Our results support the latter idea: actin-rich membrane protrusions such as circular dorsal ruffles are dispensable for PDGF-AA-induced chemotaxis since fibroblasts reconstituted with a WIP mutant that does not bind N-WASP (WIP-ΔWBD) have significantly decreased formation of dorsal ruffles but intact chemotactic capability (Figs. 7 and 8). Many reports describe PDGF-BB stimulation as a first step for dorsal ruffle formation [47]. However, to our knowledge, this is the first work defining a specific role for PDGF-AA (and by extension PDGFRα stimulation) in the formation of actin-rich dorsal ruffles. Endocytosis of the PDGFR promotes actin remodelling and cell migration. PDGFR uptake has been shown to be delayed in WIP KD cells 60-120 min after PDGF-BB stimulation and not affected at earlier times (15 min) [32]. Similarly, PDGFRα endocytosis in WIP$^{-/-}$ fibroblasts is not modified 15 min after stimulation (Fig. 6F), time points that match with the dorsal ruffle response. Therefore, the abnormal dorsal ruffling is unlikely to be due to reduced PDGFRα uptake following ligand binding.

In this report, we provide the first evidence for WIP/Nck/N-WASP participation in PDGF-AA-mediated ruffle generation and of WIP/Nck, but not N-WASP, in PDGF-AA-mediated chemotaxis in 2D. The latter results are in accordance with previous reports showing that N-WASP contributes to dorsal ruffle formation but not to 2D migration [48]. N-WASP($^{-/-}$) fibroblast-like cells generate aberrant dorsal ruffles; highly unstable, severely depleted of

Arp2/3 complex, and diminished in size [15]. In addition, expression of an N-WASP truncation mutant that cannot bind Arp2/3 complex block the formation of these structures [15]. These results suggest that N-WASP and Arp2/3 complex are part of a multiprotein assembly important for the generation of PDGFAA-induced dorsal ruffles. A similar correlation between Nck and the formation of dorsal ruffles has been observed [49]. These observations clearly put Nck and its binding partners in a common pathway in the formation of dorsal ruffles. Our data support this idea and add N-WASP interaction with WIP as an essential step in the process. Moreover, WIP and Nck appear as essential components of the complex that regulates dorsal ruffle formation. These results place WIP within a biochemical pathway (PDGFR/Nck-WIP-N-WASP/Arp2/3-actin) that links growth factor stimulation to dynamic actin changes that are involved in cell motility and morphological plasticity. Moreover, these and previous results support the hypothesis that WIP might function as a scaffolding molecule, with the potential to influence both actin polymerization and the assembly of actin filaments into higher-order arrays involved in adhesion and migration. Our data fits well with a recently proposed model arising from both computational simulations and experimentation, in which the density of Nck molecules in multicomponent aggregates is a critical determinant of actin polymerization with a Nck/N-WASp/Arp2/3 stoichiometry of 4:2:1 [50]. The two N-WASP molecules would provide two Nck molecules and the other two Nck proteins required to reach a total of four, would come from binding to WIP. Finally, we have confirmed WIP-mCherry location in dorsal ruffles in reconstituted $WIP^{-/-}$ murine lung fibroblasts (Fig. 6C) in agreement with previous studies showing endogenous WIP in dorsal ruffles and overexpressed in 3T3 fibroblasts [14, 36]. Moreover, we describe the preferential distribution of WIP at the lamellipodial protrusions formed by B lymphocytes during their amoeboid migration.

MATERIAL AND METHODS

Reagents and antibodies

Anti-GFP was purchased from Roche, anti-βactin from Sigma, anti-GAPDH from AbD Serotec and anti-cortactin from Millipore. PDGFRα, WASP and N-WASP rabbit antibodies and monoclonal antibody to Nck were obtained from Santa Cruz Biotech. Rabbit anti-WIP was generated by ProteinTools [27]. Horseradish peroxidase (HRP)-labelled anti-mouse, anti-rat and anti-rabbit antibodies were purchased from Dako.

Derivation of murine primary fibroblasts

Animal experimentation was approved by the CNB-CSIC Bioethics Committee and conforms to institutional and national regulations. Lung pieces of wild-type or $WIP^{-/-}$ SV129/BL6 mice were washed with PBS, minced and deposit into multi-6-well plates. Each small piece was squashed with a coverslip to favor tissue disaggregation and cell release, and cultured in fibroblast growth medium (DMEM medium supplemented with 10% FCS, penicillin and streptomycin (50U/ml), 1X non essential aminoacids and 50μM β-mercaptoethanol) for 5 to 10 days. After removal of unattached debris, adherent cells were trypsinized and maintained in culture up to passage 12.

B cells

Naïve B cells were freshly isolated from spleens of $WIP^{+/+}$ and $WIP^{-/-}$ mice, 2.5 months old, by negative immunoselection, as previously described (>95% purity; [31]. Purified B cells were labeled when indicated with 0.1μm CFSE or SNARF-1 long-term dyes (Molecular Probes) for 10 minutes at 37ºC before use. The murine 2PK3 B cell line was transiently transfected with the WIP-GFP construct, cloned in the pLV lentiviral vector, by electroporation. Cells were used for the experiments 24 hours after electroporation.

Transwell chemotaxis assay

Fibroblasts were incubated for 6-8 h with DMEM without serum. For transwell assays, 5 x 10^5 starved cells in 500μl of DMEM (Sigma-Aldrich) were added to the upper chamber of the transwell (Costar; 6,5mm diameter, 8,0μm pore size). The lower chamber was filled with 500μl of DMEM supplemented with the indicated chemoattractant (15 % FCS, 5μM LPA, 50 ng/ml EGF, 20 ng/ml FGF, 1 ng/ml PDGF-BB or 50 ng/ml PDGF-AA). The cells were incubated overnight at 37ºC. The upper chamber remaining cells were mechanically removed, and migrated cells through the membrane to the lower chamber were fixed with paraformaldehyde (PFA) 4%, and stained with DAPI. For the control transwells (without chemottractant added), the cells that were mechanically removed were the cells that migrate

through the membrane. The chemotactic frequency, a measure of the specificity of migration, was calculated as follows: [(Number of cells migrating to the chemokines)/(Number of cells that stayed in the upper chamber in the control transwell)] x 100.

Freshly isolated or transduced B cells, 2.5 x 10^5 cells in 100μls of RPMI 10% FCS, were added to the upper insert of the Boyden chamber (Costar; 6,5 mm diameter, 3,0 μm pore size). The recombinant murine CXCL13 chemokine (Peprotech) was added at the indicated concentrations to the lower chamber filled with 600 μls of RPMI 10% FCS. After 2h 30min incubation at 37ºC, we collected the volume of the lower chamber and counted the cells by flow cytometry. Migration frequency was estimated as the [(B cell nº at the lower chamber / the initial B cell input in the upper chamber) x 100] in each condition.

Dunn chamber chemotaxis assays

Fibroblasts (6-8 x 10^4 cells) were seeded on 18-mm square glass coverlips in fibroblast growth medium. Chemotaxis assays were carried out 12-24 h after seeding the cells; cells were starved of serum for 8 h prior to exposure to a serum gradient. Dunn chambers were set up as previously described [51] with DMEM 15 % serum in the outer well. Cells were filmed at 37ºC on Olympus IX50 Inverted microscopes fitted with phase-contrast optics, heated stages, and heated chambers. Frames were filmed using a CCD camera (Hitachi) every 5 min for 8 h using Acquisition Manager software from Kinetic Imaging (Wirral, UK) as previously described [51]. Cell tracks were generated from the time-lapse images using the image-processing program Lucida (kinetic Imaging), and the resulting tracks were analysed with the software Mathematica. The mean migration speed or persistence for each tracked cell was calculated, and then the mean migration speed or persistence of the population derived. Cells that translocated less than 20μm from their point of origin[34] were excluded from this analysis.

B cell migration on planar lipid bilayers

The two-dimensional substrates based on the use of planar lipid bilayers containing GPI-linked ICAM-1 protein was prepared and assembled in FCS2 chambers (Bioptechs) as previously described [31]. Before imaging, the membranes were coated with 100μM CXCL13 (Peprotech) for 30 min at RT. CFSE labeled $WIP^{+/+}$ and SNARF-1 labeled $WIP^{-/-}$ B cells in 1:1 ratio were injected into the warmed (37ºC) chamber; DIC, IRM and fluorescent images were acquired sequentially every 30 s for 20 min. All assays were done in PBS 0.5% FCS, 0.5 g/L D-glucose, 2mM $MgCl_2$, and 0.5mM $CaCl_2$. Images were acquired on a Zeiss Axiovert LSM 510-META inverted microscope with a 40x oil-immersion objective, and analysed with

Imaris 6.0 software (Bitplane). Graphs and statistical analysis were done with Prism 4.0 software (GraphPad).

Western blot analysis

Growing or infected fibroblats plated in p100 dishes were washed in PBS, lysed in cold lysis buffer containing 0.2% Triton X-100, 150 mM NaCl, 50 mM Tris-HCl pH 7.4, 1 mM EDTA, 1 mM EGTA, with protease (Complete from Merck) and phosphatase inhibitors (50 mM NaF, 1 mM Sodium orthovanadate and 1 mM okadaic acid), and scraped off. Lysates were centrifuged at 13,000 rpm to spin down cell debris. Similarly, freshly isolated and transduced B cells were lysed in cold lysis buffer for 30 min and spinned at 13,000 rpm for 30 min; the fractions of soluble proteins were collected. Soluble proteins were analysed by SDS-PAGE and Western blot. In brief, proteins were separated by gel electrophoresis under denaturing and reducing conditions, then, separated proteins were electrophoretically transferred to nitrocellulose or PVDF membranes using a Bio-Rad Mini protein II transfer apparatus. Blots were blocked with 5% dried milk solution diluted in TBS-T (10 mM Tris-HCl, pH 7.5, 100 mM NaCl, 0.1% Tween 20) containing NaF 5μM for 1h at room temperature (RT), and incubated overnight at 4ºC with the primary antibody diluted in the same buffer. Labeling was detected by incubation with HRP-conjugated secondary antibodies (diluted in TBS-T) for 1h at RT and enhanced chemiluminiscence (ECL) detection system.

Infection using lentiviral vectors

Recombinant lentiviral stocks were produced in 293T cells by co-transfecting the transfer vector (GFP, WIP-eGFP, WIPΔNBD or WIPΔWBD,) the envelope plasmid pMD.2G, and the packaging plasmid pCMVR8.91, as previously described [52]. Cells ($1.5x10^7$) were seeded onto 150 cm^2 flasks and transfected with 10 μg DNA envelope, 30 μg DNA packaging and 40 μg DNA transfer vector by precomplexing with 0.125 mM PEI (22 kDa) for 15 min at RT in OptiMEM. After 4 h at 37°C the medium was replaced with fresh DMEM 10% FCS and virus particles were harvested 48 and 72 h post transfection. After filtering through a 0.45 μm-pore-size filter, the virus suspension was concentrated by centrifugation at 50,000 g for 2 h at 4°C. The resulting pellet was resuspended in RPMI (Sigma, UK) and stored at –80°C until used. The desired number of fibroblasts were plated in complete culture medium and concentrated lentivirus was added to the cells at a multiplicity of infection (MOI) of 10 and incubated for 72 h to allow maximal expression of recombinant proteins before being used for experiments. For B cell transduction, 2 x 10^6 purified B cells (none-labelled or SNARF-1 labelled) were infected with concentrated lentivirus (MOI of 1-10) in 500μls of RPMI with 10% FCS and

LPS (2.5 μg/ml; Sigma) for 6 h at 37ºC; then, the medium was replaced and the infected B cells were cultured for 24 or 48 hours to allow protein expression.

Immunofluorescence

The cells were fixed in 4% PFA in PBS, permeabilised with 0.5% Triton X-100 in PBS, blocked with 3% bovine serum albumin (BSA) in PBS+0.1% Tween-20 and incubated with appropriate primary and secondary antibodies or fluorescent phalloidin diluted in PBS+0.1% Tween-20. Coverslips were mounted onto slides using Vectashield mounting medium (Vector Laboratories, UK) and visualised using a Zeiss LSM 510 Meta confocal laser scanning head attached to a Zeiss Axioplan 2 microscope. LSM 510 software was used to obtain merged confocal images.

In the case of B cells, they were fixed in 4% PFA (10 min, 37ºC) after 30 mins in contact with the planar membranes, permeabilized with 0.2% Triton X-100 in PBS (5 min, RT), blocked with PBS with 2% BSA and 2% FCS, stained with Alexa-Fluor647-Phalloidin (20 min), and imaged on a Zeiss Axiovert LSM 510-META inverted microscope with a 40x oil-immersion objective. Data analysis was done with Imaris 6.0 software (Bitplane).

Flow cytometry

The cells were either grown on complete medium or starved for 24 h and stimulated with 50 ng/ml of PDGF-AA for different periods of time. After stimulation, cells were washed once with PBS, trypsinised and resuspended at 10^6 cells/100 μl. Cells were centrifuged, fixed with 4% PFA for 20 min and resuspended in PBS staining (PBS with 3% FCS and EDTA 2mM). The antibody specific for the extracellular region of PDGFRα was diluted in PBS staining, and cells were incubated for 1h with the primary antibody and for 30 min with the secondary. Finally, cells were resuspended again in PBS staining and analysed by flow cytometry in a FACScalibur cytometer (Becton Dickinson).

Freshly isolated B cells (2×10^5) were stained with fluorescently conjugated rat anti-mouse CD19 and rat anti-mouse IgM (Pharmingen) for 30 min on ice, washed, and analysed by flow cytometry as above.

Statistical analysis

The unpaired Student *t* test was applied to calculate statistical significance, except for the determination of the confidence interval of mean direction of migration (where the Rayleigh´s test was applied) and for comparision of ruffle formation in transduced populations (where the ANOVA test and test of Tukey were applied).

ACKNOWLEDGEMENTS

This work was supported by grants from Spanish Ministry of Science and Innovation (BFU2010-21374/BMC) and CIBERNED (Instituto de Salud Carlos III) to IMA. IB held a contract from the CAM (Comunidad Autónoma de Madrid), AB a "La Caixa" fellowship and EF a JAE-pre fellowship. Work in the laboratory of GEJ is supported by the MRC (G1100041) IMA and an EU FP7 award (237946, T3Net). In the laboratory of YRC, JS held a contract from the CAM and the work is supported by grants from the Spanish Ministry of Science (BFU2011-30097) and from the EU (FP7-integrated project Masterswicht 223404 FP7).

FIGURE LEGENDS

Fig. 1. The lack of WIP reduces B cell amoeboid motility. (A) Chemotactic response of freshly isolated $WIP^{+/+}$ and $WIP^{-/-}$ B cells to CXCL13 (400nM) in Boyden chambers. (B) Polarization and migration frequencies of $WIP^{+/+}$ and $WIP^{-/-}$ B cells settled on ICAM-1-containing planar membranes coated with CXCL13. In (A) and (B) each dot corresponds to one experiment; black thick bar, averaged value. (C) Mean speed values (left panel) and Straightness index (right panel) of $WIP^{+/+}$ and $WIP^{-/-}$ B cells in the same conditions than in (B); each dot corresponds to a single cell. (D) Tracks of representative $WIP^{+/+}$ and $WIP^{-/-}$ B cells migrating on the planar membranes; each line corresponds to a single cell track. (E) DIC and F-actin images of representative $WIP^{+/+}$ (left panels) and $WIP^{-/-}$ (middle panel) B cells; right panel, lamellipodium frequency in control and deficient B cells. Data on B, C and E is the merge of three experiments. *, $p<0.05$; **, $p<0.001$; ***, $p<0.0001$.

Fig. 2. WIP re-expression recovers amoeboid motility in $WIP^{-/-}$ B cells. Purified $WIP^{+/+}$ and $WIP^{-/-}$ B cells were transduced with recombinant lentivirus expressing GFP (GFP) or full-length WIP-GFP (WIP) as described in Materials and Methods; 24h later, they were used for the different assays. (A) Total lysates of the indicated transduced B cells were used to detect the expression of the WIP construct by western-blot with anti-GFP. (B) Migration frequency of the indicated transduced B cells in response to 400 nM CXCL13 in Boyden chambers; data merged from two experiments are shown. (C) Mean speed values, (D) F-actin-rich lamellipodium frequency, and (E) representative tracks of the specified transduced B cells migrating on the planar membranes; each dot is a single cell in C; data from a representative experiment are shown in D and E. *, $p<0.05$; **, $p<0.001$.

Fig. 3. WIP deficiency does not affect fibroblast morphology or protein content. (A) Representative western blot of WIP, N-WASP and Nck expression in soluble lysates of lung-derived fibroblasts from $WIP^{+/+}$ and $WIP^{-/-}$ mice. Numbers indicate relative expression levels of each protein to GAPDH content and control fibroblasts determined by densitometry. GAPDH labeling confirmed equivalent protein loading control. (B) FACS analysis of forward and side scatter in control ($WIP^{+/+}$) and $WIP^{-/-}$ fibroblasts. (C) Phase-contrast images from plated control ($WIP^{+/+}$) and $WIP^{-/-}$ murine fibroblasts do not show evident morphological differences between both populations. Scale bar 50 μm.

Fig. 4. Reduced persistence in chemotacting $WIP^{-/-}$ fibroblasts towards serum. Control ($WIP^{+/+}$) and $WIP^{-/-}$ murine fibroblasts were assayed for chemotaxis towards 15% serum in Dunn chambers. (A) Circular rose plots show the proportion of cells with migratory direction lying within each 20º interval (serum source at bottom of histogram). The arrow represents the mean direction of migration; the grey segment represents the 95% confidence interval determined by the Rayleigh´s test ($p<5{,}67x10^{-12}$) between $WIP^{+/+}$ and $WIP^{-/-}$ murine fibroblasts. (B) Representation of mean persistence values.

Fig. 5. Reduced chemotaxis towards serum or PDGF-AA of $WIP^{-/-}$ murine fibroblasts. Control ($WIP^{+/+}$) and $WIP^{-/-}$ murine fibroblasts were loaded onto the upper chamber of the Transwell and the percentage of cells chemotacting to the lower well was calculated. Cells were assayed for chemotaxis towards 15% serum (A), 5 μM LPA (B), 50 ng/ml EGF (C), 20 ng/ml FGF (D) and 50 ng/ml PDGF-AA (E and F). Reconstitution assays were performed by lentiviral-mediated expression of WIP-GFP or control GFP in $WIP^{-/-}$ cells and overexpression assays by transduction of control ($WIP^{+/+}$) fibroblasts with GFP or WIP-GFP. * $p<0{,}05$; ** $p<0{,}001$.

Fig. 6. PDGF-AA-induced dorsal ruffle formation is diminished in $WIP^{-/-}$ fibroblasts. (A) Control ($WIP^{+/+}$) and $WIP^{-/-}$ primary murine fibroblasts were serum starved over night (0 min) or serum starved and stimulated with PDGF-AA for increasing times (8 and 15 min). Fixed and permeabilised cells were stained with anti-cortactin and FITC-secondary antibody and imaged in a Zeiss microscope to identify dorsal ruffles (white arrow). (B) The percentage of $WIP^{+/+}$(black) and $WIP^{-/-}$ (white) cells forming dorsal ruffles after PDGF-AA stimulation is

plotted against incubation times. (C) $WIP^{-/-}$ primary fibroblasts were lentivirally transduced to express control cherry or WIP-cherry, starved and incubated with PDGF-AA for 8 or 15 min. Fixed cells were imaged. (D) The percentage of $WIP^{-/-}$ cells expressing cherry (white) or WIP-cherry (black) and forming dorsal ruffles after PDGF-AA stimulation is plotted against incubation times. (E) Representative western blot of PDGFRα expression in soluble lysates of lung-derived fibroblasts from $WIP^{+/+}$ and $WIP^{-/-}$ mice. Numbers indicate relative expression levels of the protein to control fibroblasts determined by densitometry. β-actin labeling confirmed equivalent protein loading control. (F) $WIP^{+/+}$ and $WIP^{-/-}$ primary fibroblasts were grown in the presence of serum (left panel) or starved and stimulated with PDGF-AA (right panel) and stained with anti-PDGFRα plus labeled secondary antibody and analysed by FACS. The percentage of fluorescence intensity in control $WIP^{+/+}$ (black) or $WIP^{-/-}$ (white) populations is represented. * p<0,05.

Fig. 7. Nck and N-WASP binding to WIP contribute to dorsal ruffle formation induced by PDGF-AA stimulation. (A) $WIP^{-/-}$ primary murine fibroblasts were transduced with recombinant lentivirus coding for GFP, WIP-GFP, WIPΔNBD-GFP (missing the Nck binding domain) or WIPΔWBD-GFP (missing the N-WASp binding site). Soluble protein extracts were subjected to western blot analysis, using anti-GFP as probe, and developed with ECL detection kit. (B) Transduced $WIP^{-/-}$ murine fibroblasts were serum starved and stimulated with PDGF-AA for increasing times (8 and 15 min). Fixed and permeabilised cells were stained with anti-cortactin and FITC-secondary antibody and imaged in a Zeiss microscope. The percentage of GFP-positive cells forming dorsal ruffles after PDGF-AA stimulation is plotted against incubation times. One way ANOVA test and Test of Tukey * p<0,05; ** p<0,001.

Fig. 8. Nck binding to WIP contributes to chemotaxis towards PDGF-AA. $WIP^{-/-}$ murine fibroblasts were transduced with recombinant lentivirus engineered to express control GFP or fusion constructs including WIP, WIPΔNBD or WIPΔWBD. Fibroblasts were loaded onto the upper chamber of the Transwell and the percentage of GFP-expressing cells chemotacting towards 50 ng/ml PDGF-AA was calculated. * p<0,05.

LEGENDS TO SUPPLEMENTAL FIGURES AND VIDEOS

Figure S1. Phenotypic analysis of WIP$^{-/-}$ B cells. (A) Freshly isolated B cells from WIP$^{+/+}$ and WIP$^{-/-}$ mice were analysed for cell size (Forward scatter), cell complexity (Side scatter), and expression of the cell surface markers CD19 and IgM by flow cytometry. Profiles of a representative experiment are shown; the purity of the purified B cell fraction was 95% for WIP$^{+/+}$ and 85% for WIP$^{-/-}$. (B) Lysates of WIP$^{+/+}$ and WIP$^{-/-}$ B cells were assessed for WIP, WASP, Nck and tubulin protein expression levels by western-blot; numerical values below bands correspond to expression levels for each protein in WIP$^{-/-}$ B cells in comparison to WIP$^{+/+}$ B cells.

Figure S2. Predominant localization of WIP at the lamella of migratory B cells. 2PK3 B cell line was transiently transfected with full-length WIP-GFP expression vector; 24h after, cells were settled on planar membranes and monitored for migration by real-time microscopy. DIC, WIP-GFP and IRM time-frame images at the contact plane of a representative B cell with the 2D substrate are shown; white arrow, accumulation of WIP-GFP at the lamella of the cell.

Figure S3. WIP deficiency reduces persistence but not velocity during chemotaxis towards serum. Control (WIP$^{+/+}$) and WIP$^{-/-}$ murine fibroblasts were assayed for chemotaxis towards 15% serum in Dunn chambers. (A) Individual cell track with black dots at the end point of cell displacement. (B) Individual cell velocity profile (upper) and mean velocity values (lower) calculated by Mathematica software. (C) Persistence profiles of individual cells (each line represents a single cell) calculated by Mathematica software.

Figure S4. PDGF-AA-induced dorsal ruffle formation is diminished in WIP$^{-/-}$ fibroblasts. (A) Control (WIP$^{+/+}$) and WIP$^{-/-}$ primary murine fibroblasts were serum starved over night (0 min) or serum starved and stimulated with PDGF-AA for increasing times (8 and 15 min). Fixed and permeabilised cells were stained with TRITC-phalloidin to label actin filaments and imaged in a Zeiss microscope. Dorsal ruffles are indicated by white arrows. (B) WIP$^{-/-}$ primary fibroblasts were lentivirally transduced to express control cherry or WIP-cherry, starved and incubated with PDGF-AA for 8 or 15 min. Fixed and permeabilised cells were stained with FITC-phalloidin to label actin filaments and imaged in a Zeiss microscope.

Movie 1. Migration of wild type and WIP-deficient B cells.

Purified $WIP^{+/+}$ (CFSE-labeled; green) and $WIP^{-/-}$ (SNARF-1 labeled; red) B cells, mixed in a 1:1 ratio, migrating on ICAM-1-containing planar membranes coated with CXCL13. Fluorescence (CFSE, SNARF-1; left panel) and IRM (right panel) images over time (6 frames/second) are shown. The tracks followed by migratory B cells (IRM positive) are highlighted with the dragon tails (green/red lines).

Movie 2. WIP localization in motile B cells.

Migration of a representative 2PK3 B cell transfected with WIP-GFP construct on ICAM-1-containing planar membranes coated with CXCL13. DIC (left panel), WIP-GFP fluorescence (middle panel) and IRM (right panel) images at the contact plane of the 2PK3 B cell with the target membrane over time (2 frames/second) are shown.

Movie 3. Directional migration towards serum of murine fibroblasts in Dunn chambers.

Murine lung fibroblasts were seeded onto 18-mm square glass coverlips and grown for 12-24 h. Cells were serum starved for 8 h and exposed to a serum gradient (15% FCS in the outer well). Cells were filmed at 37ºC on Olympus IX50 Inverted microscopes fitted with phase-contrast optics, heated stages, and heated chambers. Frames were filmed using a CCD camera (Hitachi) every 5 min for 8 h using Acquisition Manager software from Kinetic Imaging (Wirral, UK).

Movie 4. Directional migration towards serum of $WIP^{-/-}$ murine fibroblasts in Dunn chambers. $WIP^{-/-}$ murine lung fibroblasts were seeded onto 18-mm square glass coverslips and grown for 12-24 h. Cells were serum starved for 8 h and exposed to a serum gradient (15% FCS in the outer well). Cells were filmed at 37ºC on Olympus IX50 Inverted microscopes fitted with phase-contrast optics, heated stages, and heated chambers. Frames were filmed using a CCD camera (Hitachi) every 5 min for 8 h using Acquisition Manager software from Kinetic Imaging (Wirral, UK).

REFERENCES

1. **Rottner, K., and Stradal, T.E. (2011). Actin dynamics and turnover in cell motility. Curr Opin Cell Biol *23*, 569-578.**
2. **Sanz-Moreno, V., and Marshall, C.J. (2010). The plasticity of cytoskeletal dynamics underlying neoplastic cell migration. Curr Opin Cell Biol *22*, 690-696.**
3. **Parri, M., and Chiarugi, P. (2010). Rac and Rho GTPases in cancer cell motility control. Cell communication and signaling : CCS *8*, 23.**
4. **Guiet, R., Verollet, C., Lamsoul, I., Cougoule, C., Poincloux, R., Labrousse, A., Calderwood, D.A., Glogauer, M., Lutz, P.G., and Maridonneau-Parini, I. Macrophage mesenchymal migration requires podosome stabilization by filamin A. J Biol Chem *287*, 13051-13062.**
5. **Lammermann, T., and Sixt, M. (2009). Mechanical modes of 'amoeboid' cell migration. Curr Opin Cell Biol *21*, 636-644.**
6. **Friedl, P., and Wolf, K. (2010). Plasticity of cell migration: a multiscale tuning model. J Cell Biol *188*, 11-19.**
7. **Seppa, H., Grotendorst, G., Seppa, S., Schiffmann, E., and Martin, G.R. (1982). Platelet-derived growth factor in chemotactic for fibroblasts. J Cell Biol *92*, 584-588.**
8. **Eriksson, A., Siegbahn, A., Westermark, B., Heldin, C.H., and Claesson-Welsh, L. (1992). PDGF alpha- and beta-receptors activate unique and common signal transduction pathways. Embo J *11*, 543-550.**
9. **Itoh, T., and Hasegawa, J. (2013). Mechanistic insights into the regulation of circular dorsal ruffle formation. Journal of biochemistry *153*, 21-29.**
10. **Krueger, E.W., Orth, J.D., Cao, H., and McNiven, M.A. (2003). A dynamin-cortactin-Arp2/3 complex mediates actin reorganization in growth factor-stimulated cells. Mol Biol Cell *14*, 1085-1096.**
11. **Orth, J.D., Krueger, E.W., Weller, S.G., and McNiven, M.A. (2006). A novel endocytic mechanism of epidermal growth factor receptor sequestration and internalization. Cancer research *66*, 3603-3610.**
12. **Machesky, L.M., and Insall, R.H. (1999). Signaling to actin dynamics. J Cell Biol *146*, 267-272.**
13. **Suetsugu, S., Yamazaki, D., Kurisu, S., and Takenawa, T. (2003). Differential roles of WAVE1 and WAVE2 in dorsal and peripheral ruffle formation for fibroblast cell migration. Dev Cell *5*, 595-609.**
14. **Anton, I.M., Saville, S.P., Byrne, M.J., Curcio, C., Ramesh, N., Hartwig, J.H., and Geha, R.S. (2003). WIP participates in actin reorganization and ruffle formation induced by PDGF. J Cell Sci *116*, 2443-2451.**
15. **Legg, J.A., Bompard, G., Dawson, J., Morris, H.L., Andrew, N., Cooper, L., Johnston, S.A., Tramountanis, G., and Machesky, L.M. (2007). N-WASP involvement in dorsal ruffle formation in mouse embryonic fibroblasts. Mol Biol Cell *18*, 678-687.**
16. **Martinez-Quiles, N., Rohatgi, R., Anton, I.M., Medina, M., Saville, S.P., Miki, H., Yamaguchi, H., Takenawa, T., Hartwig, J.H., Geha, R.S., et al. (2001). WIP regulates N-WASP-mediated actin polymerization and filopodium formation. Nat Cell Biol *3*, 484-491.**
17. **Anton, I.M., Jones, G.E., Wandosell, F., Geha, R., and Ramesh, N. (2007). WASP-interacting protein (WIP): working in polymerisation and much more. Trends Cell Biol *17*, 555-562.**

18. Garcia, E., Jones, G.E., Machesky, L.M., and Anton, I.M. (2012). WIP: WASP-interacting proteins at invadopodia and podosomes. Eur J Cell Biol *91*, 869-877.
19. Bouma, G., Mendoza-Naranjo, A., Blundell, M.P., de Falco, E., Parsley, K.L., Burns, S.O., and Thrasher, A.J. (2011). Cytoskeletal remodeling mediated by WASp in dendritic cells is necessary for normal immune synapse formation and T-cell priming. Blood *118*, 2492-2501.
20. Ishihara, D., Dovas, A., Park, H., Isaac, B.M., and Cox, D. (2012). The chemotactic defect in wiskott-Aldrich syndrome macrophages is due to the reduced persistence of directional protrusions. PLoS One *7*, e30033.
21. Monypenny, J., Chou, H.C., Banon-Rodriguez, I., Thrasher, A.J., Anton, I.M., Jones, G.E., and Calle, Y. (2010). Role of WASP in cell polarity and podosome dynamics of myeloid cells. Eur J Cell Biol *90*, 198-204.
22. Gallego, M.D., de la Fuente, M.A., Anton, I.M., Snapper, S., Fuhlbrigge, R., and Geha, R.S. (2006). WIP and WASP play complementary roles in T cell homing and chemotaxis to SDF-1{alpha}. Int Immunol *18*, 221-232.
23. Meyer-Bahlburg, A., Becker-Herman, S., Humblet-Baron, S., Khim, S., Weber, M., Bouma, G., Thrasher, A.J., Batista, F.D., and Rawlings, D.J. (2008). Wiskott-Aldrich syndrome protein deficiency in B cells results in impaired peripheral homeostasis. Blood *112*, 4158-4169.
24. Westerberg, L., Larsson, M., Hardy, S.J., Fernandez, C., Thrasher, A.J., and Severinson, E. (2005). Wiskott-Aldrich syndrome protein deficiency leads to reduced B-cell adhesion, migration, and homing, and a delayed humoral immune response. Blood *105*, 1144-1152.
25. Westerberg, L.S., Dahlberg, C., Baptista, M., Moran, C.J., Detre, C., Keszei, M., Eston, M.A., Alt, F.W., Terhorst, C., Notarangelo, L.D., et al. (2012). Wiskott-Aldrich syndrome protein (WASP) and N-WASP are critical for peripheral B-cell development and function. Blood *119*, 3966-3974.
26. Becker-Herman, S., Meyer-Bahlburg, A., Schwartz, M.A., Jackson, S.W., Hudkins, K.L., Liu, C., Sather, B.D., Khim, S., Liggitt, D., Song, W., et al. (2011). WASp-deficient B cells play a critical, cell-intrinsic role in triggering autoimmunity. J Exp Med *208*, 2033-2042.
27. Chou, H.C., Anton, I.M., Holt, M.R., Curcio, C., Lanzardo, S., Worth, A., Burns, S., Thrasher, A.J., Jones, G.E., and Calle, Y. (2006). WIP regulates the stability and localization of WASP to podosomes in migrating dendritic cells. Curr Biol *16*, 2337-2344.
28. de la Fuente, M.A., Sasahara, Y., Calamito, M., Anton, I.M., Elkhal, A., Gallego, M.D., Suresh, K., Siminovitch, K., Ochs, H.D., Anderson, K.C., et al. (2007). WIP is a chaperone for Wiskott-Aldrich syndrome protein (WASP). Proc Natl Acad Sci U S A *104*, 926-931.
29. Curcio, C., Pannellini, T., Lanzardo, S., Forni, G., Musiani, P., and Anton, I.M. (2007). WIP null mice display a progressive immunological disorder that resembles Wiskott-Aldrich syndrome. J Pathol *211*, 67-75.
30. Anton, I.M., de la Fuente, M.A., Sims, T.N., Freeman, S., Ramesh, N., Hartwig, J.H., Dustin, M.L., and Geha, R.S. (2002). WIP deficiency reveals a differential role for WIP and the actin cytoskeleton in T and B cell activation. Immunity *16*, 193-204.
31. Saez de Guinoa, J., Barrio, L., Mellado, M., and Carrasco, Y.R. (2011). CXCL13/CXCR5 signaling enhances BCR-triggered B-cell activation by shaping cell dynamics. Blood *118*, 1560-1569.

32. King, S.J., Worth, D.C., Scales, T.M., Monypenny, J., Jones, G.E., and Parsons, M. beta1 integrins regulate fibroblast chemotaxis through control of N-WASP stability. Embo J *30*, 1705-1718.
33. Zicha, D., Dunn, G., and Jones, G. (1997). Analyzing chemotaxis using the Dunn direct-viewing chamber. Methods Mol Biol *75*, 449-457.
34. van der Valk, J., Brunner, D., De Smet, K., Fex Svenningsen, A., Honegger, P., Knudsen, L.E., Lindl, T., Noraberg, J., Price, A., Scarino, M.L., et al. (2010). Optimization of chemically defined cell culture media--replacing fetal bovine serum in mammalian in vitro methods. Toxicology in vitro : an international journal published in association with BIBRA *24*, 1053-1063.
35. Andrae, J., Gallini, R., and Betsholtz, C. (2008). Role of platelet-derived growth factors in physiology and medicine. Genes & development *22*, 1276-1312.
36. Cortesio, C.L., Perrin, B.J., Bennin, D.A., and Huttenlocher, A. (2010). Actin-binding protein-1 interacts with WASp-interacting protein to regulate growth factor-induced dorsal ruffle formation. Mol Biol Cell *21*, 186-197.
37. Anton, I.M., Lu, W., Mayer, B.J., Ramesh, N., and Geha, R.S. (1998). The Wiskott-Aldrich syndrome protein-interacting protein (WIP) binds to the adaptor protein Nck. J. Biol. Chem. *273*, 20992-20995.
38. Hoon, J.L., Wong, W.K., and Koh, C.G. (2012). Functions and regulation of circular dorsal ruffles. Mol Cell Biol *32*, 4246-4257.
39. Machesky, L., and Gould, K. (1999). The Arp2/3 complex: a multifunctional actin organizer. Curr. Opin. cell Biol. *11*, 117-121.
40. Anton, I.M., and Jones, G.E. (2006). WIP: A multifunctional protein involved in actin cytoskeleton reorganization. Eur. J. Cell Biol. *85*, 295-304.
41. Lanzi, G., Moratto, D., Vairo, D., Masneri, S., Delmonte, O., Paganini, T., Parolini, S., Tabellini, G., Mazza, C., Savoldi, G., et al. (2012). A novel primary human immunodeficiency due to deficiency in the WASP-interacting protein WIP. J Exp Med *209*, 29-34.
42. Konno, A., Kirby, M., Anderson, S.A., Schwartzberg, P.L., and Candotti, F. (2007). The expression of Wiskott-Aldrich syndrome protein (WASP) is dependent on WASP-interacting protein (WIP). Int Immunol *19*, 185-192.
43. Sixt, M. (2012). Cell migration: fibroblasts find a new way to get ahead. J Cell Biol *197*, 347-349.
44. Bailly, M., Ichetovkin, I., Grant, W., Zebda, N., Machesky, L.M., Segall, J.E., and Condeelis, J. (2001). The F-actin side binding activity of the Arp2/3 complex is essential for actin nucleation and lamellipod extension. Curr Biol *11*, 620-625.
45. Suraneni, P., Rubinstein, B., Unruh, J.R., Durnin, M., Hanein, D., and Li, R. (2012). The Arp2/3 complex is required for lamellipodia extension and directional fibroblast cell migration. J Cell Biol *197*, 239-251.
46. Wu, C., Asokan, S.B., Berginski, M.E., Haynes, E.M., Sharpless, N.E., Griffith, J.D., Gomez, S.M., and Bear, J.E. (2012). Arp2/3 is critical for lamellipodia and response to extracellular matrix cues but is dispensable for chemotaxis. Cell *148*, 973-987.
47. Mellstrom, K., Heldin, C.H., and Westermark, B. (1988). Induction of circular membrane ruffling on human fibroblasts by platelet-derived growth factor. Exp Cell Res *177*, 347-359.
48. Yu, X., Zech, T., McDonald, L., Gonzalez, E.G., Li, A., Macpherson, I., Schwarz, J.P., Spence, H., Futo, K., Timpson, P., et al. (2012). N-WASP coordinates the delivery and F-actin-mediated capture of MT1-MMP at invasive pseudopods. J Cell Biol *199*, 527-544.

49. Rivera, G.M., Antoku, S., Gelkop, S., Shin, N.Y., Hanks, S.K., Pawson, T., and Mayer, B.J. (2006). Requirement of Nck adaptors for actin dynamics and cell migration stimulated by platelet-derived growth factor B. Proc Natl Acad Sci U S A *103*, 9536-9541.

50. Ditlev, J.A., Michalski, P.J., Huber, G., Rivera, G.M., Mohler, W.A., Loew, L.M., and Mayer, B.J. (2012). Stoichiometry of Nck-dependent actin polymerization in living cells. J Cell Biol *197*, 643-658.

51. Monypenny, J., Zicha, D., Higashida, C., Oceguera-Yanez, F., Narumiya, S., and Watanabe, N. (2009). Cdc42 and Rac family GTPases regulate mode and speed but not direction of primary fibroblast migration during platelet-derived growth factor-dependent chemotaxis. Mol Cell Biol *29*, 2730-2747.

52. Zufferey, R., Nagy, D., Mandel, R.J., Naldini, L., and Trono, D. (1997). Multiply attenuated lentiviral vector achieves efficient gene delivery in vivo. Nature biotechnology *15*, 871-875.

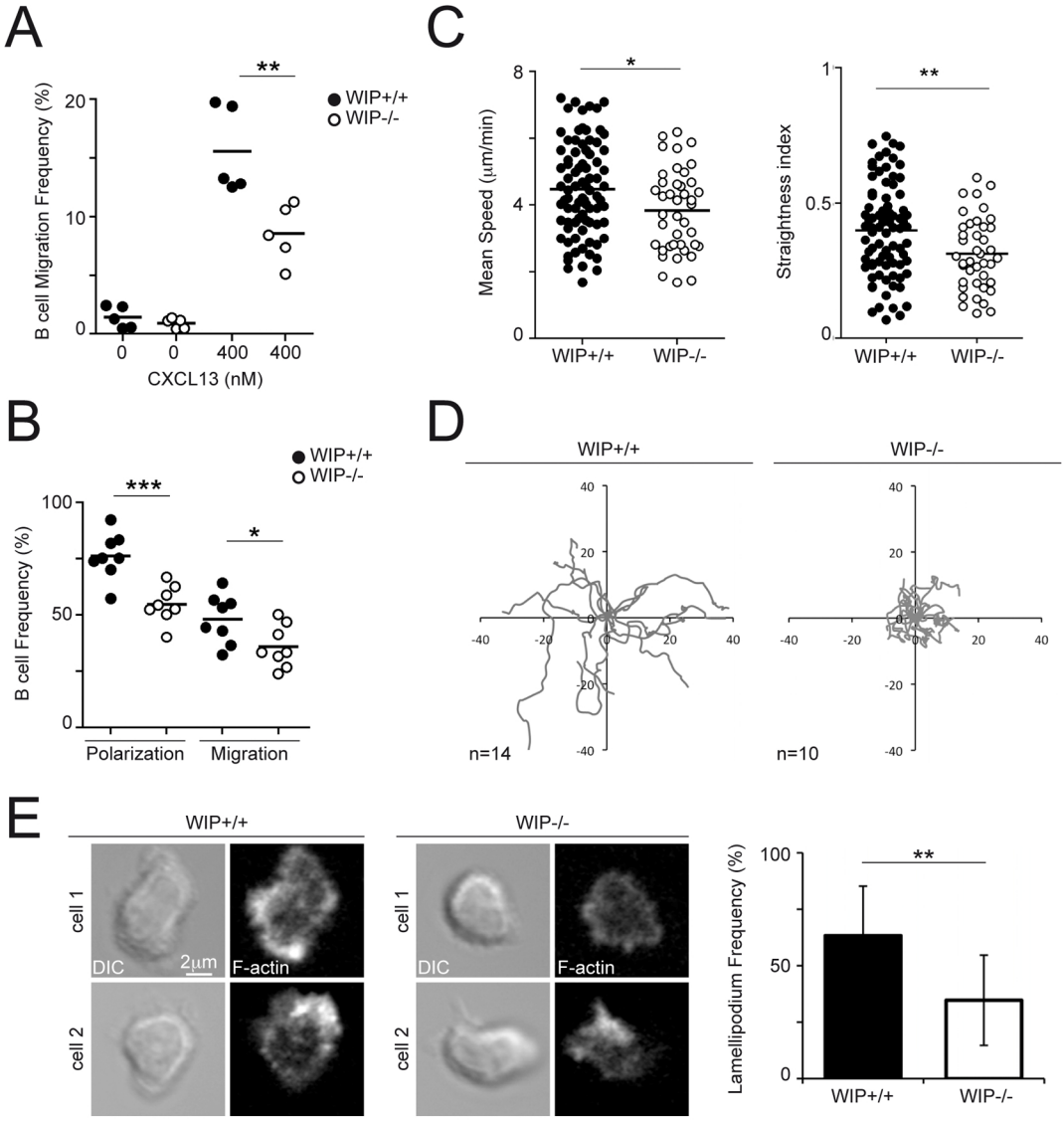
A
B cell Migration Frequency (%)
20
10
0
**
WIP+/+
WIP-/-
0
0
400
400
CXCL13 (nM)
B
B cell Frequency (%)
100
50
0
***
*
WIP+/+
WIP-/-
Polarization
Migration
C
Mean Speed (μm/min)
8
4
0
*
WIP+/+
WIP-/-
Straightness index
1
0.5
0
**
WIP+/+
WIP-/-
D
WIP+/+
WIP-/-
40
20
0
-20
-40
n=14
n=10
E
WIP+/+
WIP-/-
cell 1
cell 2
DIC
2μm
F-actin
Lamellipodium Frequency (%)
100
50
0
**
WIP+/+
WIP-/-

Figure 1

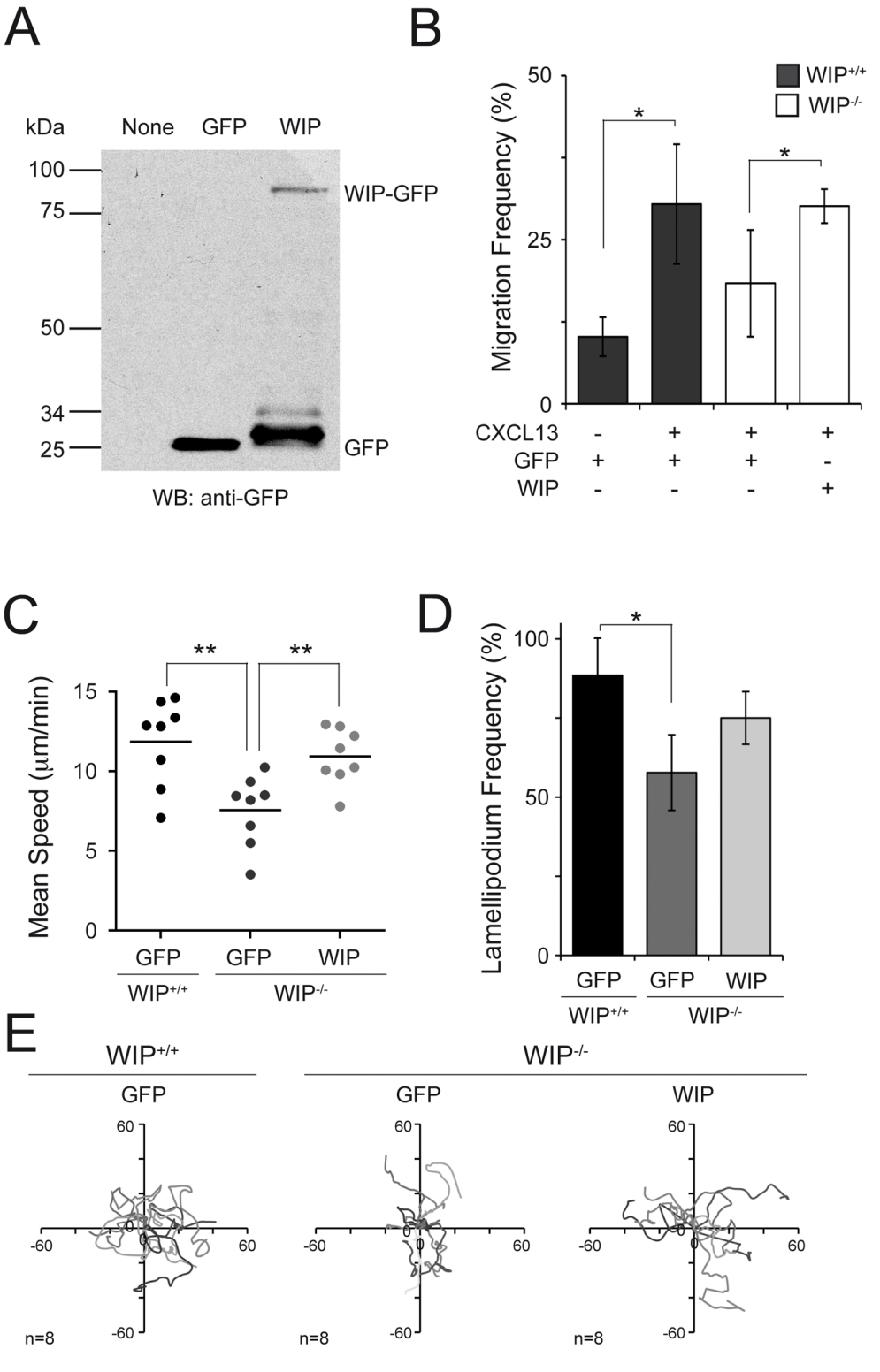
A
kDa
None
GFP
WIP
100
75
50
34
25
WIP-GFP
GFP
WB: anti-GFP
B
Migration Frequency (%)
50
25
0
WIP+/+
WIP-/-
*
*
CXCL13 - + + +
GFP + + + -
WIP - - - +
C
Mean Speed (μm/min)
15
10
5
0
**
**
GFP
GFP
WIP
WIP+/+
WIP-/-
D
Lamellipodium Frequency (%)
100
50
0
*
GFP
GFP
WIP
WIP+/+
WIP-/-
E
WIP+/+
WIP-/-
GFP
GFP
WIP
60
-60
0
n=8
n=8
n=8

Figure 2

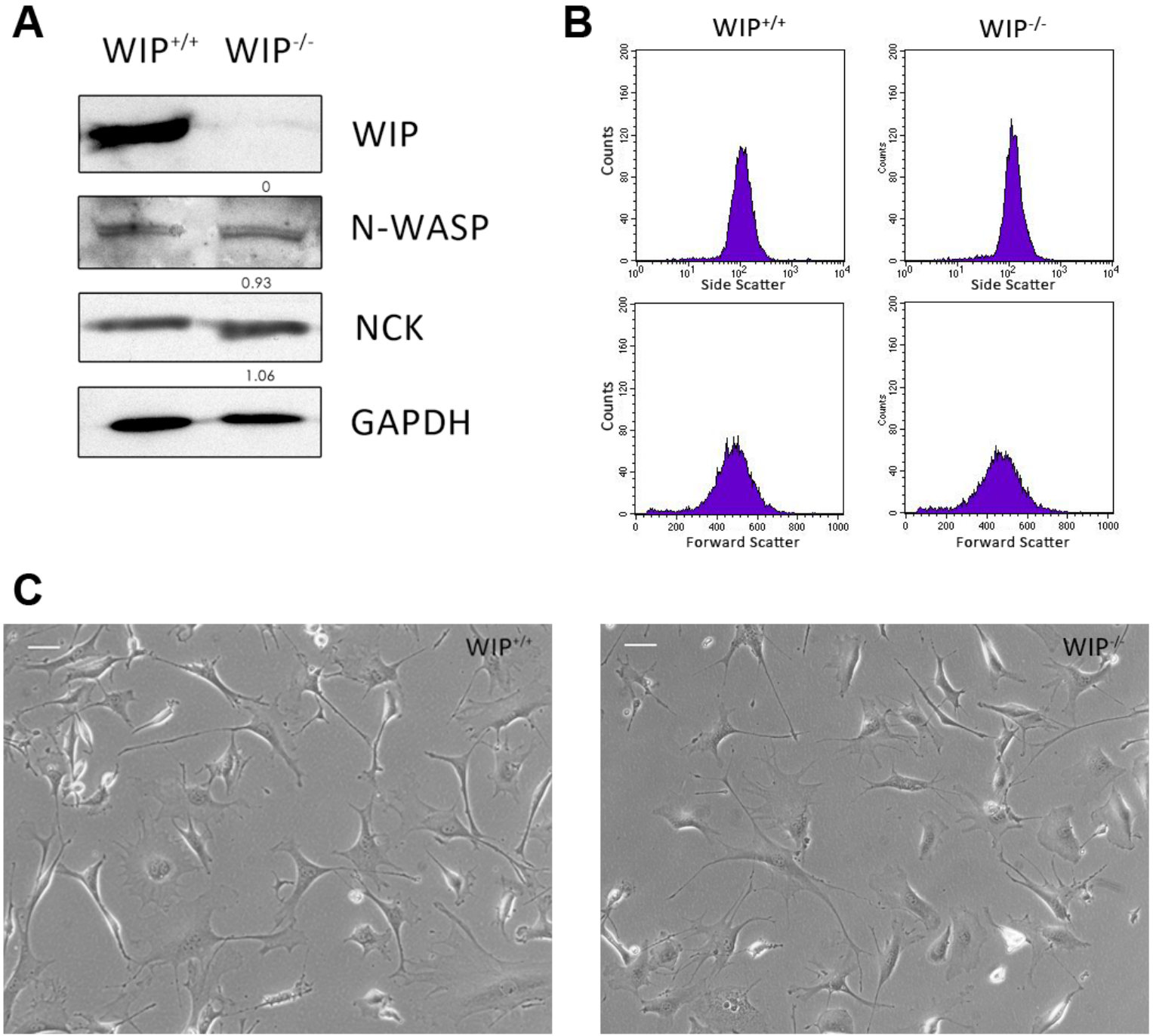
A
WIP+/+
WIP-/-
WIP
0
N-WASP
0.93
NCK
1.06
GAPDH
B
WIP+/+
WIP-/-
Counts
Side Scatter
Forward Scatter
C
WIP+/+
WIP-/-

Figure 3

A

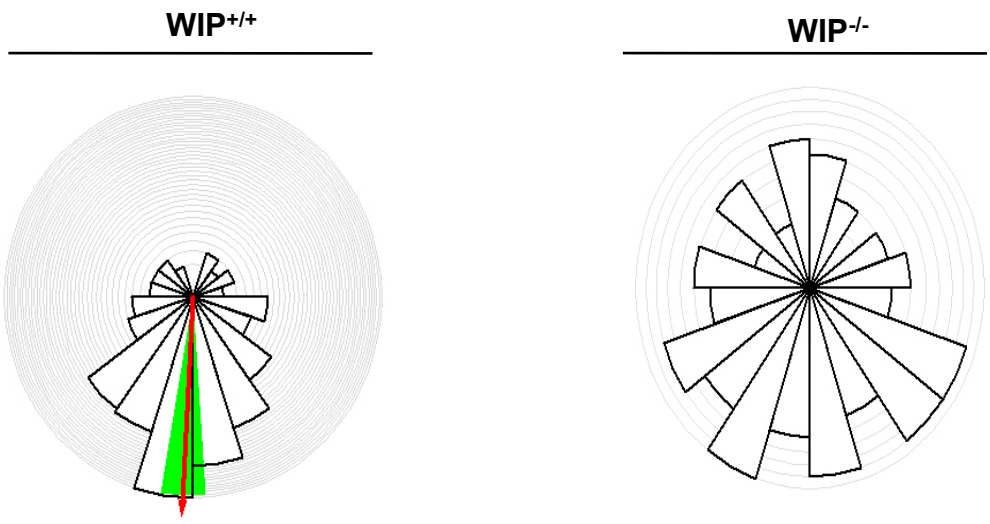
WIP+/+
WIP-/-
15% SERUM
15% SERUM

B

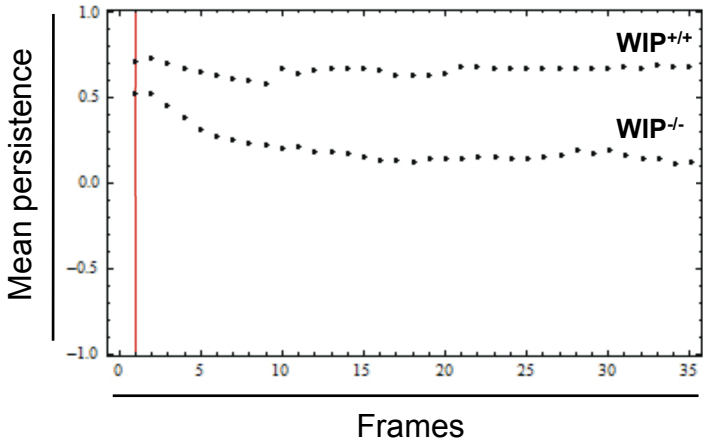
Mean persistence
1.0
0.5
0.0
−0.5
−1.0
0
5
10
15
20
25
30
35
Frames
WIP+/+
WIP-/-

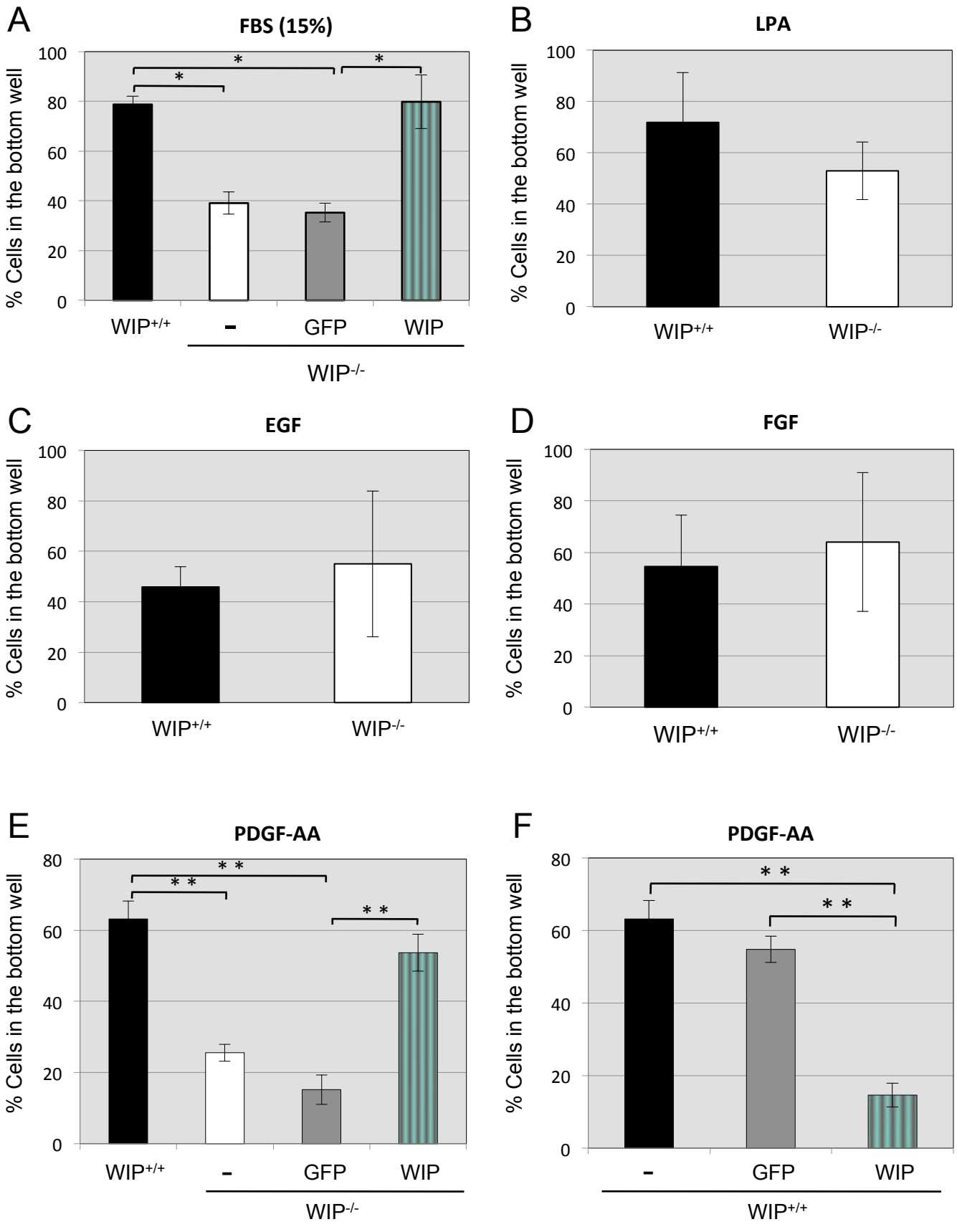
A
FBS (15%)
% Cells in the bottom well
100
80
60
40
20
0
*
*
*
WIP+/+
-
GFP
WIP
WIP-/-
B
LPA
% Cells in the bottom well
WIP+/+
WIP-/-
C
EGF
% Cells in the bottom well
WIP+/+
WIP-/-
D
FGF
% Cells in the bottom well
WIP+/+
WIP-/-
E
PDGF-AA
% Cells in the bottom well
80
60
40
20
0
* *
* *
* *
WIP+/+
-
GFP
WIP
WIP-/-
F
PDGF-AA
% Cells in the bottom well
* *
* *
-
GFP
WIP
WIP+/+

Figure 5

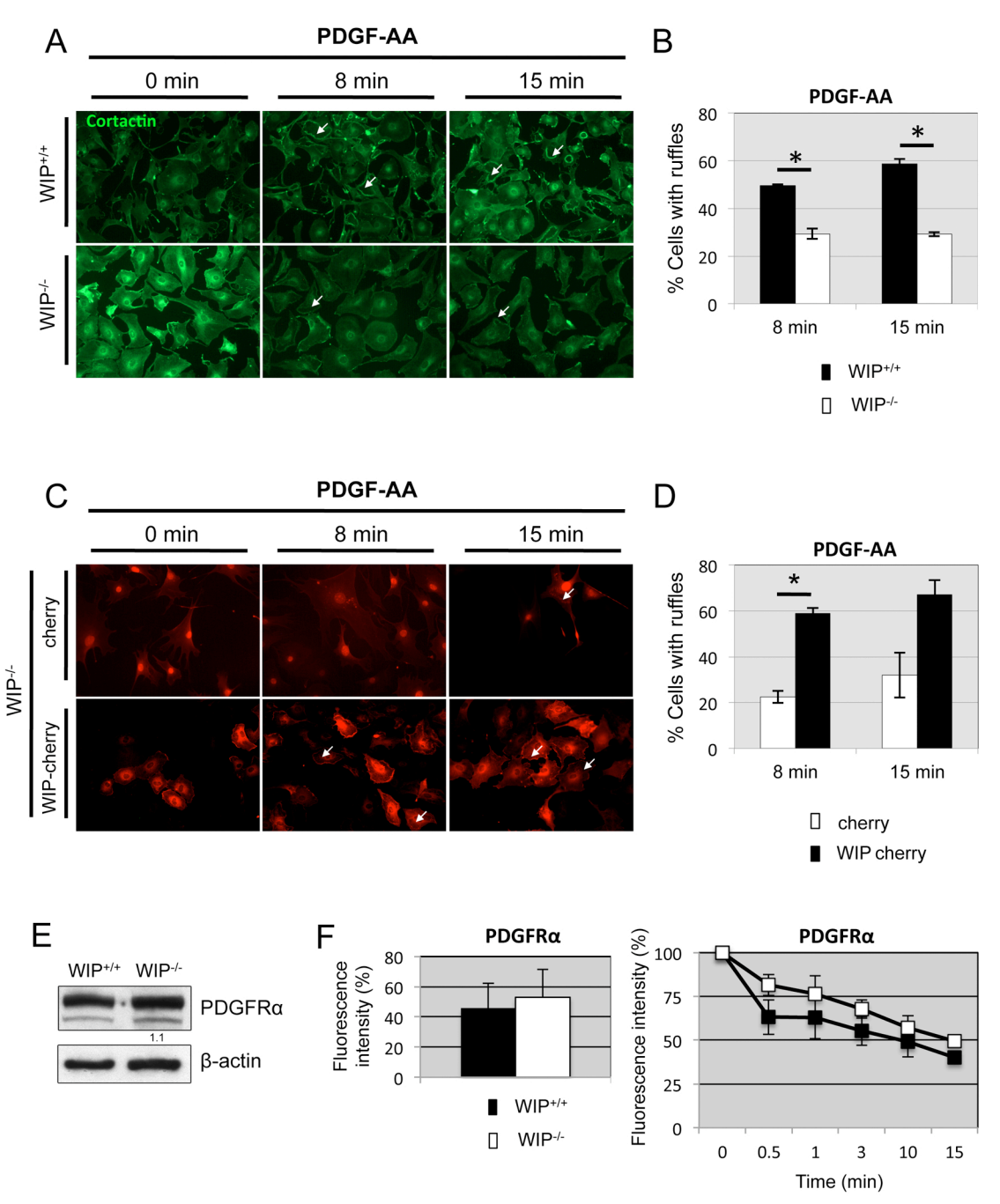
A
PDGF-AA
0 min
8 min
15 min
Cortactin
WIP+/+
WIP-/-
B
PDGF-AA
% Cells with ruffles
80
60
40
20
0
*
*
8 min
15 min
WIP+/+
WIP-/-
C
PDGF-AA
0 min
8 min
15 min
WIP-/-
cherry
WIP-cherry
D
PDGF-AA
% Cells with ruffles
80
60
40
20
0
*
8 min
15 min
cherry
WIP cherry
E
WIP+/+
WIP-/-
PDGFRα
1.1
β-actin
F
PDGFRα
Fluorescence intensity (%)
80
60
40
20
0
WIP+/+
WIP-/-
PDGFRα
Fluorescence intensity (%)
100
75
50
25
0
0
0.5
1
3
10
15
Time (min)

Figure 6

A

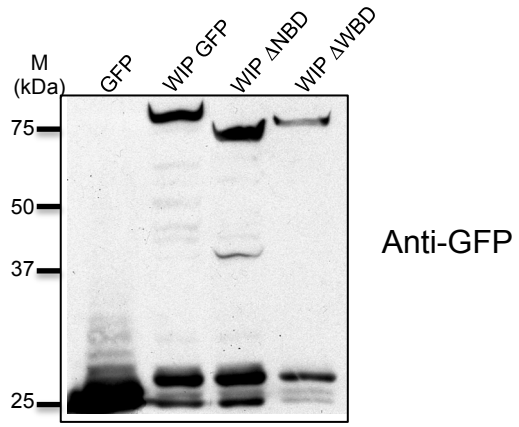
M
(kDa)
GFP
WIP GFP
WIP ΔNBD
WIP ΔWBD
75
50
37
25
Anti-GFP

B

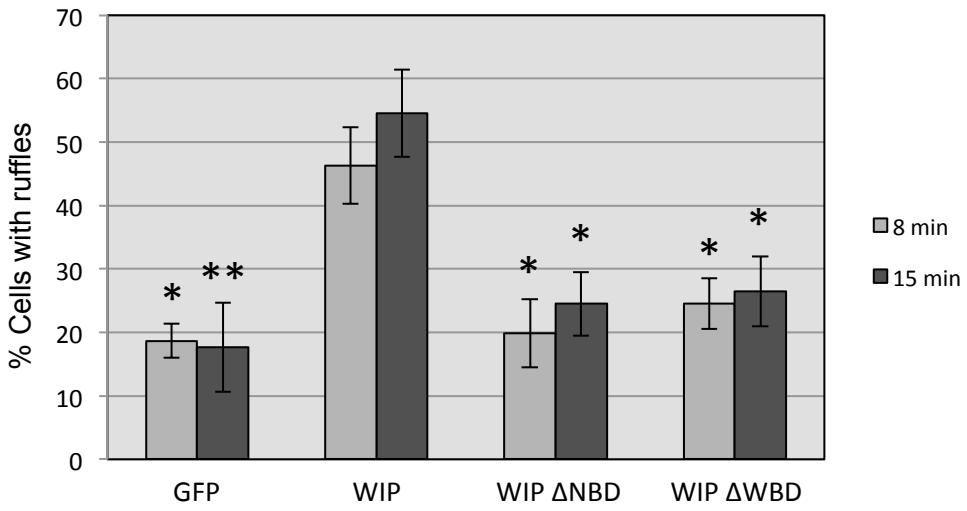
% Cells with ruffles
70
60
50
40
30
20
10
0
*
**
*
*
*
*
GFP
WIP
WIP ΔNBD
WIP ΔWBD
8 min
15 min

Figure 7

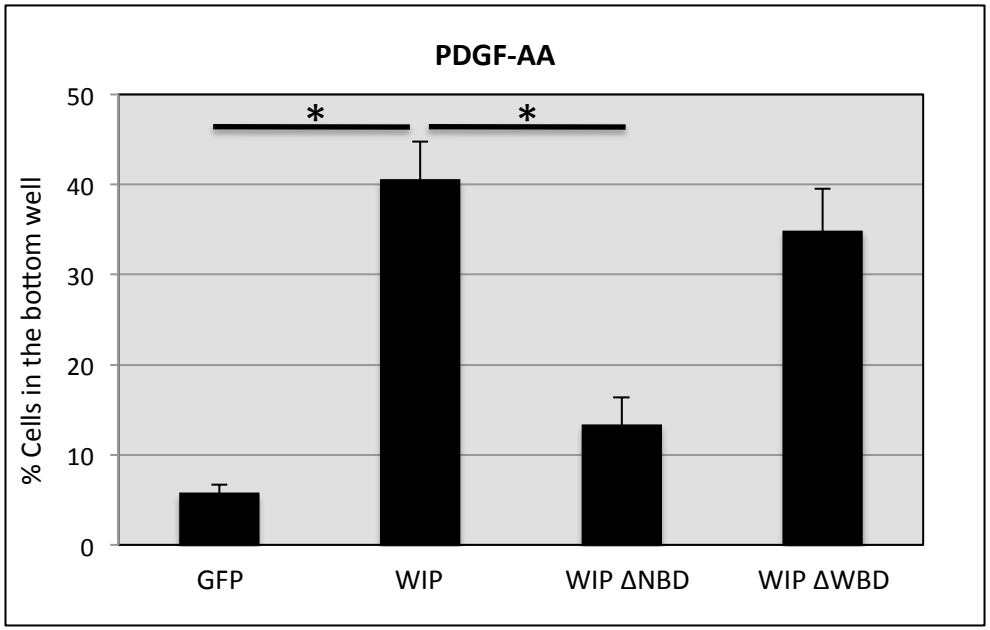
PDGF-AA
% Cells in the bottom well
50
40
30
20
10
0
*
*
GFP
WIP
WIP ΔNBD
WIP ΔWBD

Figure 8

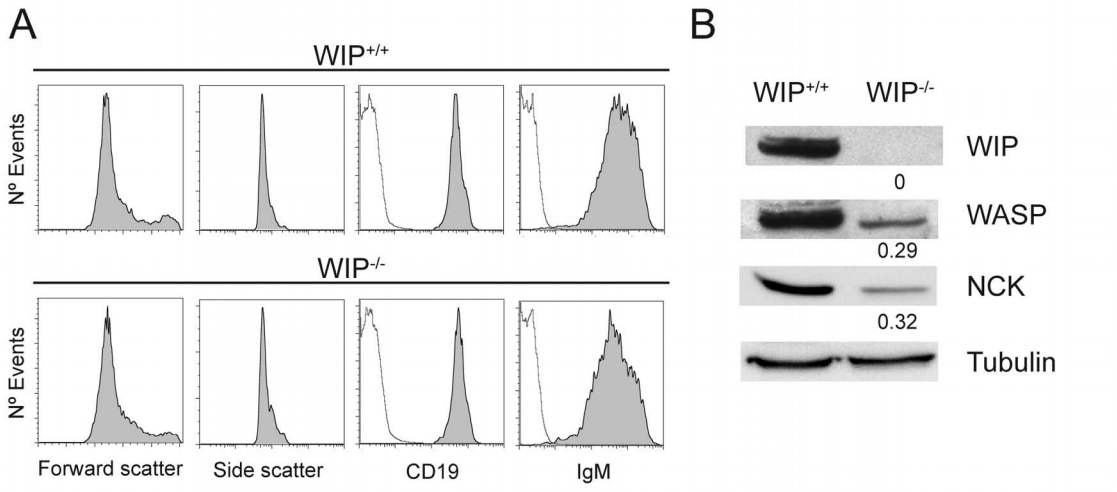
A
WIP+/+
Nº Events
WIP-/-
Nº Events
Forward scatter
Side scatter
CD19
IgM
B
WIP+/+
WIP-/-
WIP
0
WASP
0.29
NCK
0.32
Tubulin

Figure S1

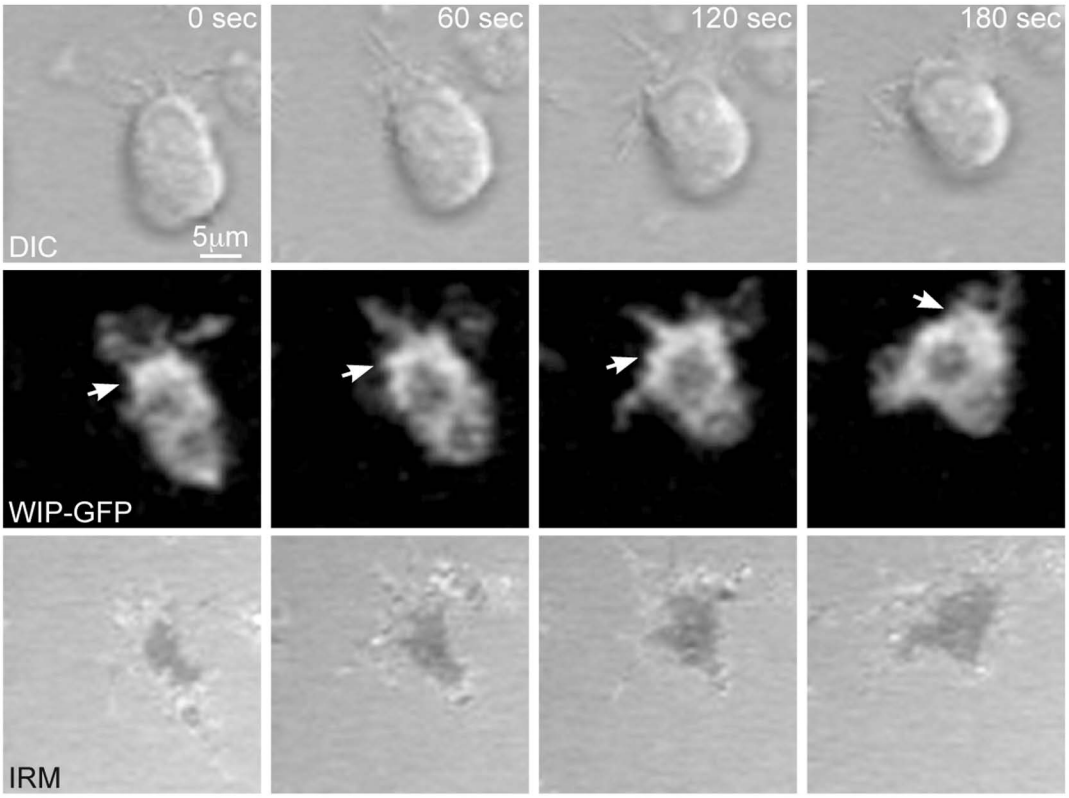

Figure S2

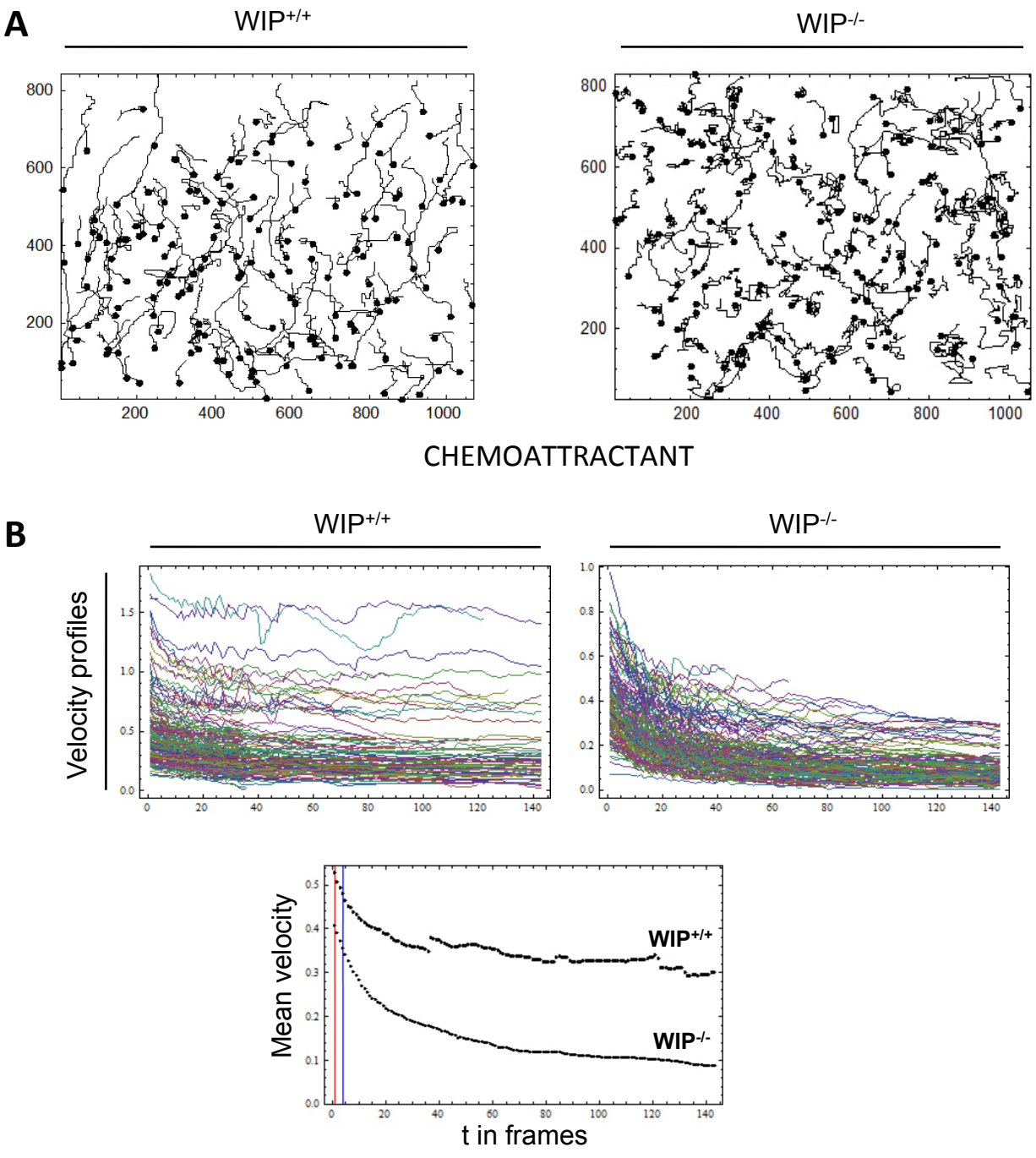
A
WIP+/+
WIP-/-
800
600
400
200
200
400
600
800
1000
CHEMOATTRACTANT
B
WIP+/+
WIP-/-
Velocity profiles
Mean velocity
WIP+/+
WIP-/-
t in frames
C
WIP+/+
WIP-/-
Persistence profiles

Figure S3

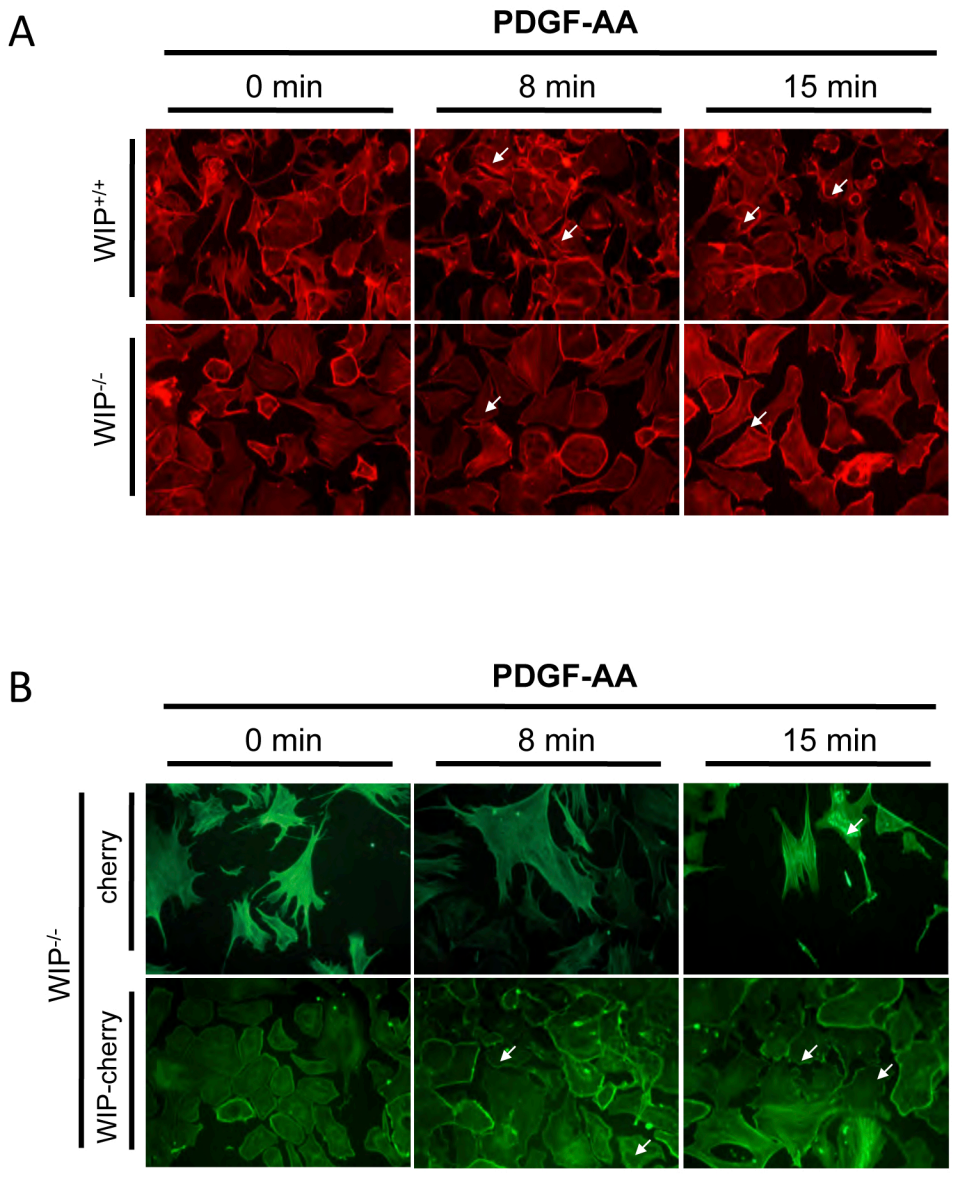
A
PDGF-AA
0 min
8 min
15 min
WIP+/+
WIP-/-
B
PDGF-AA
0 min
8 min
15 min
WIP-/-
cherry
WIP-cherry

Figure S4